NASA TECHNICAL NOTE

NASA TN D-1585

LATERAL CONTROL CHARACTERISTICS OF A POWERED MODEL OF A TWIN-PROPELLER DEFLECTED SLIPSTREAM STOL AIRPLANE CONFIGURATION

by Richard J. Margason and Alexander D. Hammond

Langley Research Center
Langley Station, Hampton, Va.

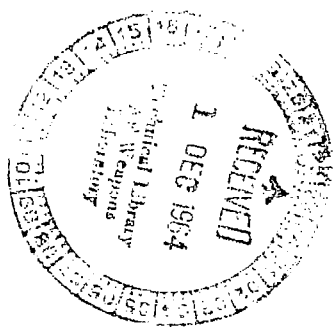

NATIONAL AERONAUTICS AND SPACE ADMINISTRATION • WASHINGTON, D. C. • NOVEMBER 1964

LATERAL CONTROL CHARACTERISTICS OF A POWERED MODEL OF A TWIN-PROPELLER DEFLECTED SLIPSTREAM STOL AIRPLANE CONFIGURATION

By Richard J. Margason and Alexander D. Hammond

Langley Research Center
Langley Station, Hampton, Va.

NATIONAL AERONAUTICS AND SPACE ADMINISTRATION

For sale by the Office of Technical Services, Department of Commerce,
Washington, D.C. 20230 -- Price $3.50

LATERAL CONTROL CHARACTERISTICS OF A POWERED MODEL OF A TWIN-PROPELLER DEFLECTED SLIPSTREAM STOL AIRPLANE CONFIGURATION

By Richard J. Margason and Alexander D. Hammond
Langley Research Center

SUMMARY

Results are presented of a wind-tunnel investigation on the static lateral and directional control capabilities of a two-propeller deflected-slipstream STOL airplane in the take-off and landing speed range.

The results show that neither the ailerons nor differential propeller thrust alone provide adequate lateral-directional control but they indicate that the lateral-directional control characteristics of the aileron were good when used in conjunction with differential propeller thrust as expected. The results also indicate that rolling moments which are large enough for lateral control even with the single engine-out condition can be obtained from a full-span slot lip aileron (spoiler), but that some adverse yawing moment is produced.

INTRODUCTION

Most short take-off and landing (STOL) airplanes which use large flaps to deflect the propeller slipstream to achieve the high-lift coefficients required for flight at low speed use the differential thrust of the propellers (differential blade angle) combined with differential flap deflection to provide lateral and directional control at low speeds. (For example, see refs. 1 and 2.) This method of obtaining control was originally conceived for use with VTOL configurations (refs. 3, 4, and 5) and STOL airplanes which achieve a large part of their lift by deflecting the propeller slipstream and must therefore obtain their control by modulating and vectoring the deflected slipstream. Little attention has been paid to alternate means of obtaining control.

The present investigation was undertaken to investigate the possible use of slot lip ailerons (spoilers) for lateral control of a deflected slipstream STOL configuration.

The investigation was conducted in the 17-foot test section of the Langley 300-MPH 7- by 10-foot tunnel and covered a range of flap deflections and power conditions representing the take-off, cruise (flaps retracted), and landing

regions of flight. Data on the effectiveness of differential thrust and differential deflection of the rear-flap element as lateral-control devices are included for comparison.

SYMBOLS

b	wing span, ft
c	wing chord, 1.29 ft
C_D	drag coefficient, $\frac{\text{Drag}}{qS}$
C_L	lift coefficient, $\frac{\text{Lift}}{qS}$
C_T	propeller thrust coefficient based on free-stream velocity and wing area T/qS
$C_{T,s}$	propeller thrust coefficient based on slipstream velocity and propeller disk area, $T/q_s NS_p$
C_l	rolling-moment coefficient, $\frac{\text{Rolling moment}}{qSb}$
C_n	yawing-moment coefficient, $\frac{\text{Yawing moment}}{qSb}$
$\Delta C_l, \Delta C_n$	coefficient due to control deflection $\left(\text{For example, } \Delta C_l = C_{l_{(\text{spoiler deflected})}} - C_{l_{(\text{no spoiler deflection})}}\right)$
ΔC_T	difference in propeller thrust due to asymmetric power, $\Delta C_T = C_{T_{(\text{left motor})}} - C_{T_{(\text{right motor})}}$
D	propeller diameter, ft
h_t	height of horizontal-tail chord above wing chord, ft
l_t	tail length measured from wing quarter chord to horizontal-tail quarter chord, ft
N	number of propellers
q	dynamic pressure, $\frac{\rho}{2}V^2$, lb/sq ft

q_s slipstream dynamic pressure, $q + \frac{T}{NS_p}$, sq ft

S wing area, sq ft

S_p propeller disk area, $\frac{\pi D^2}{4}$, sq ft

T total propeller thrust, lb

V free-stream velocity, ft/sec

α angle of attack, deg

β propeller pitch angle, deg

δ deflection of movable surface (with subscript to denote surface deflected), deg

δ_s spoiler deflection measured normal to upper surface of wing in fraction of wing chord

ρ air density, slugs/cu ft

Subscripts:

a aileron

f flap (see fig. 3)

l lower

t tail

u upper

v vane (see fig. 3)

w wing

MODEL AND APPARATUS

A three-view drawing and photographs of the model are presented in figures 1 and 2, respectively. The wing had an NACA 4415 airfoil section, a 15.50-inch chord, was unswept, and had a span of either 5 feet or 7 feet with a corresponding aspect ratio of either 3.87 or 5.42. The variation of the wing span was accomplished by removable outboard-wing panels on each side of the model. The wing contour was formed with faired wooden blocks fastened to a metal spar which supported the two motor nacelles and the fuselage spine as well as the brackets which held the spoiler and flap system. The wing was

equipped with a full-span slot lip aileron (spoiler) having a chord equal to 15.5 percent of the wing chord which was tested over a range of spoiler projections from 0- to 8-percent wing chord on the basic wing as well as on the wing with high-lift flaps.

The double slotted high-lift flap system consisted of a 20-percent wing-chord vane and a 40-percent wing-chord flap. The vane had a St. Cyr 156 airfoil section and the flap had a modified Rhode St. Genese 35 airfoil section over the forward 30 percent of its chord which faired into the wing airfoil section over the rear 70 percent of the flap chord. The flap and vane ordinates, as well as the flap and vane positions, when deflected, are given in figure 3. The flap was used as a full-span aileron for some of the tests and was deflected differentially about the 45° and 75° flap deflections.

The horizontal tail had an NACA 4415 airfoil section which was modified to have a 9-percent maximum thickness and was mounted inverted to provide an inverse camber on the horizontal tail. A tail incidence of -7° was used for the tail-on lateral control tests presented in this report.

Since no directional stability tests were included in the investigation, the vertical tail served only as a support for the horizontal tail. The vertical surface consisted of a sheet of 1/2-inch aluminum with a rounded leading edge and a beveled trailing edge.

The three-blade propellers were made of balsa covered with glass fiber cloth and were driven by water-cooled variable-frequency electric motors operated in parallel from a variable-frequency power supply, which kept the motor speeds matched within 20 revolutions per minute. The speed of rotation of each propeller was determined by a stroboscopic indicator which received the output frequency of small alternators connected to each motor shaft. For all the tests the right propeller rotated in a clockwise direction and the left propeller rotated in a counterclockwise direction when viewed from the rear of the model. During most of the tests the speed of rotation was maintained at 6,000 revolutions per minute. The thrust coefficient was varied by changing the wind-tunnel speed.

The motors were mounted inside aluminum-alloy nacelles by means of strain-gage beams so that the propeller thrust could be measured. The total lift, longitudinal force, rolling moment, yawing moment, and side force were measured by a strain-gage balance mounted to the fuselage at the wing quarter chord. However, the sensitivity of the balance to side force was such that this component could not be obtained with sufficient accuracy; therefore, no side-force data are presented.

TESTS AND CORRECTIONS

The investigation was made in the 17-foot test section of the Langley 300-MPH 7- by 10-foot tunnel. The free-stream dynamic pressure varied from about 1.5 to 5.3 pounds per square foot depending on the desired thrust coefficient. The slipstream dynamic pressure was relatively constant at about 7.5

for all thrust coefficients. A free-stream dynamic pressure of about 6.0 pounds per square foot was used for the propeller-off tests. For the powered tests the Reynolds number in the slipstream based on wing chord averaged about 0.65×10^6; for the propeller-off tests the Reynolds number in the free stream averaged about 0.58×10^6. Since errors due to blockage, slipstream contraction, and tunnel wall effects have not been determined exactly but have been found to be small for models of this size in the 17-foot test section (ref. 6), no corrections for these errors have been applied to the data.

The propeller thrust data have been presented as conventional thrust coefficients nondimensionalized by the product of free-stream dynamic pressure and wing area $\left(C_T = \frac{T}{qS}\right)$. In some cases it is desirable to use the propeller thrust coefficient based on slipstream velocity and propeller disk area. Figure 4 presents a plot of the relation between these two thrust coefficients for the two wing areas used in this investigation.

PRESENTATION OF RESULTS

The results of the investigation are grouped either by control devices or by the appropriate test variable; within each group complete data for a particular model configuration are presented. The seven model configurations for which data are presented are described in the following table:

Configuration	Span, b, ft	Vane deflection, δ_v, deg	Flap deflection, δ_f, deg
A	7	0	0
B	7	0	32.5
C	7	20	45.0
D	7	20	75.0
E	5	0	0
F	5	20	45.0
G	5	20	75.0

These flap deflections can be interpreted as representations of the following flight conditions. Configurations A and E ($\delta_f = 0^\circ$) represent cruise configurations; configuration B ($\delta_f = 32.5^\circ$) represents a transition configuration from the take-off configuration or to the landing configuration; configurations C and F ($\delta_f = 45^\circ$) represent possible take-off or landing configurations; and configurations D and G ($\delta_f = 75^\circ$) represent a landing configuration.

The data are presented in the following figures:

All the data presented on rolling moment and yawing moment represent the increments due to the control device. For these data, the small amount of asymmetry present in the appropriate zero control deflection configuration has been subtracted from the data obtained for the various lateral-directional control devices.

DISCUSSION OF RESULTS

This report contains a discussion of the more significant results of a wind-tunnel investigation of a two-propeller deflected-slipstream STOL airplane model. No attempt has been made to analyze the data completely. The lateral and directional control produced by the flap deflected differentially as an aileron, by differential propeller thrust, and by a slot-lip aileron (spoiler) are shown.

A preliminary investigation of the effectiveness of the flap system at several thrust coefficients was undertaken to provide a basis for choosing the flap deflections to be used in the lateral control investigation. This preliminary investigation was conducted with the short-span configuration. The results are presented in figure 5 and summarized in figure 6.

Effect of Aileron Deflection

The effects of aileron deflection on configurations C and D (long span, $\delta_f = 45°$ and $\delta_f = 75°$) and configurations F and G (short span, $\delta_f = 45°$ and $\delta_f = 75°$) are presented in figures 7 to 10. The summary plots are presented in figure 11; the change to a larger scale as compared with figures 7 to 10 should be noted. These figures show that the rolling moment obtained by deflection of ailerons on the left wing was small and that the yawing moments created were as large as the rolling moments. They also show for configurations C and F ($\delta_f = 45°$) that the rolling moment increases with increasing

differential flap deflection and for configurations D and G ($\delta_f = 75^\circ$) that the rolling moment decreases with increasing differential flap deflection.

Effect of Differential Propeller Thrust

The basic data for configurations C and D (long span, $\delta_f = 45^\circ$ and $\delta_f = 75^\circ$) showing the effect of differential propeller thrust are presented in figures 12 and 13. A comparison of the effects of differential thrust at several thrust coefficients is presented in figures 14 and 15. (Note that the scale is larger than that in figs. 12 and 13.) The data were obtained by making tests with a speed of 6,000 rpm with the left motor and with speeds of 7,000 rpm, 6,000 rpm, 5,000 rpm, and 0 rpm (propeller off) with the right motor on successive runs. Moderate values of rolling moment and yawing moment are obtained by configuration C ($\delta_f = 45^\circ$), whereas configuration D ($\delta_f = 75^\circ$) produces moderate rolling moments but only negligible yawing moments.

Combination of Aileron and Differential Propeller Thrust for Control

The investigation of the effectiveness of ailerons and differential thrust indicates that neither of these, when used alone, produces satisfactory control. The large yaw due to roll and the relatively low roll effectiveness of the differentially deflected flap make it necessary to couple this control with the propeller pitch control to provide for a good lateral-directional control system.

An example of the lateral and directional control effectiveness which can be realized from coupling the aileron and propeller pitch together for the long span configuration with 45° flap deflection can be determined from the data of figures 7(c) and 12(c). The effectiveness of this combination as a roll control is shown in figure 16(a) which shows a comparison of the rolling and yawing moments resulting from 20° of aileron deflection compared with a combination of this aileron deflection with the equivalent to approximately 10° total ($\pm 5^\circ$) propeller pitch. The use of $\pm 5^\circ$ blade angle in this example is high when compared with the airplanes in references 1 and 2 which use only about half this amount for control during normal take-off and landing conditions. The results indicate a large increase in roll, when compared with the aileron alone, and a very small net yaw due to roll with the combined lateral control system. Similarly, the effectiveness of the combination when used as a yaw control is shown in figure 16(b) which again shows a comparison of the yawing and rolling moments of the combination of the aileron and differential propeller pitch with the aileron alone. The combination of the aileron and differential propeller pitch as a yaw control results in a substantial increase in yaw, when compared with the aileron alone and results in very small levels of roll due to yaw at low angles of attack with an increase in roll due to yaw in the high angle-of-attack range.

This example indicates the type of lateral-directional control characteristics obtained by a particular combination of the moments due to aileron deflection and due to differential propeller thrust at a given basic flap deflection of 45°. The results for the 75° flap deflections (figs. 8, 10, and 13) show that similar levels of roll and yaw control must be obtained by a different combination of these moments. This change in combination can be achieved in a practical application by a mechanical device which mixes the various amounts of aileron deflection and differential propeller thrust at different flap deflections to obtain the necessary control throughout the required range.

Effect of Spoiler Projection

The basic data for all the configurations showing the effect of spoiler projection on the longitudinal and lateral aerodynamic characteristics are presented in figures 17 to 23 for all the configurations investigated (configurations A to G). Summary plots showing the variation of the rolling and yawing moments with spoiler projection at an angle of attack of 4° for several thrust coefficients are presented in figures 24 to 30 for the configurations investigated. The tests were made with the spoiler projected on the left wing. The data indicate that for the cruise conditions ($\delta_f = 0°$) on both the short and long span configurations (figs. 17 and 21), the roll effectiveness was relatively small when compared with that for the take-off and landing configurations. However, it is felt that the roll effectiveness obtained on both of the cruise configurations is of an acceptable level. The increased roll effectiveness obtained with the double slotted flap deflected will be required at the take-off and landing approach speeds to provide adequate lateral control in these critical flight areas.

In addition, there was some yawing moment produced which must be trimmed by the directional control system with an additional increment left over in order to provide an adequate level of directional control. The yawing moment produced by spoiler projection was somewhat less for the long-span configurations (configurations A to D) than for the corresponding short-span configurations (configurations E to G).

In order to compare more easily the levels of rolling and yawing moment developed by spoiler projection with those obtained by each of the two control devices discussed previously, a summary of the data obtained for the control settings tested is presented in figure 31. These summary plots show, for an angle of attack of 4°, the variation of rolling and yawing moments due to differential flap deflections (aileron deflection), differential propeller thrust, and spoiler projection. It should be noted that the data for spoiler projection have been plotted for a spoiler located on the right wing. Since the model was tested by projecting the spoiler on the left wing, this procedure changes the sign of the rolling and yawing moments from that for the data previously presented. This was done so that most of the rolling moments in figure 31 would have the same sign and could then be more easily compared. These results are not intended as a complete presentation of the control capabilities of these devices. For example, the differential flap deflections presented do not cover the entire range available although the differential propeller thrust settings

include the maximum possible range. This maximum range is obtained by removing one of the propellers and operating the remaining propeller at full power. These single-engine-out cases are represented for each thrust coefficient by the solid data points. The values at these points represent the maximum rolling moments which can be obtained by differential propeller thrust for each thrust coefficient. It should be noted in figure 31 by comparing the rolling moments described with those presented for spoiler projection that these single-engine-out rolling moments can be trimmed by spoiler projections. For example, in figure 31(a) for a thrust coefficient of 1.6, the engine-out rolling moment can be trimmed by a spoiler projection of 0.046c.

SUMMARY OF RESULTS

The wind-tunnel investigation of the lateral-directional control characteristics of a 1/5-scale model of a two-propeller deflected slipstream STOL airplane indicates the following results:

1. Neither the ailerons nor differential propeller thrust alone provide adequate lateral-directional control but they indicate that the lateral-directional control characteristics of the aileron were good when used in conjunction with differential propeller thrust.

2. Rolling moments which are large enough for lateral control even with the single-engine-out condition can be obtained from a full-span slot lip aileron (spoiler), but some adverse yawing moment is produced.

Langley Research Center,
National Aeronautics and Space Administration,
Langley Station, Hampton, Va., June 29, 1964.

REFERENCES

1. James, Harry A., Wingrove, Rodney C., Holzhauser, Curt A., and Drinkwater, Fred J., III: Wind-Tunnel and Piloted Flight Simulator Investigation of a Deflected-Slipstream VTOL Airplane, the Ryan VZ-3RY. NASA TN D-89, 1959.

2. Quigley, Hervey C., Innis, Robert C., and Holzhauser, Curt A.: A Flight Investigation of the Performance, Handling Qualities, and Operational Characteristics of a Deflected Slipstream STOL Transport Airplane Having Four Interconnected Propellers. NASA TN D-2231, 1964.

3. Tosti, Louis P., and Davenport, Edwin E.: Hovering Flight Tests of a Four-Engine-Transport Vertical Take-Off Airplane Model Utilizing a Large Flap and Extensible Vanes for Redirecting the Propeller Slipstream. NACA TN 3440, 1955.

4. Lovell, Powell M., Jr., and Parlett, Lysle P.: Hovering-Flight Tests of a Model of a Transport Vertical-Take-Off Airplane With Tilting Wing and Propellers. NACA TN 3630, 1956.

5. Lovell, Powell M., Jr., and Parlett, Lysle P.: Transition-Flight Tests of a Model of a Low-Wing Transport Vertical-Take-Off Airplane With Tilting Wing and Propellers. NACA TN 3745, 1956.

6. Staff of Powered-Lift Aerodynamics Section, NASA Langley Research Center: Wall Effects and Scale Effects in V/STOL Model Testing. AIAA Aerodynamic Testing Conference (Washington, D.C.), Mar. 1964.

Wing:	
Airfoil section	NACA 4415
Chord, ft	1.29
Short span:	
Area, sq ft	6.46
Span, ft	5.00
Aspect ratio	3.87
Long span:	
Area, sq ft	9.04
Span, ft	7.00
Aspect ratio	5.42
Horizontal tail:	
Area, sq ft	2.88
Span, ft	3.00
Chord, ft	.96
Aspect ratio	3.13
l_t/wing chord	2.67
h_t/wing chord	.94
Propellers:	
Diameter, ft	2.00
Nacelle diameter, ft	.33
Number of blades (each)	3

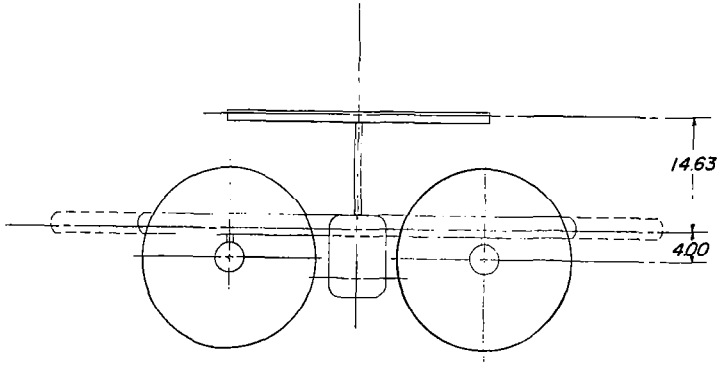

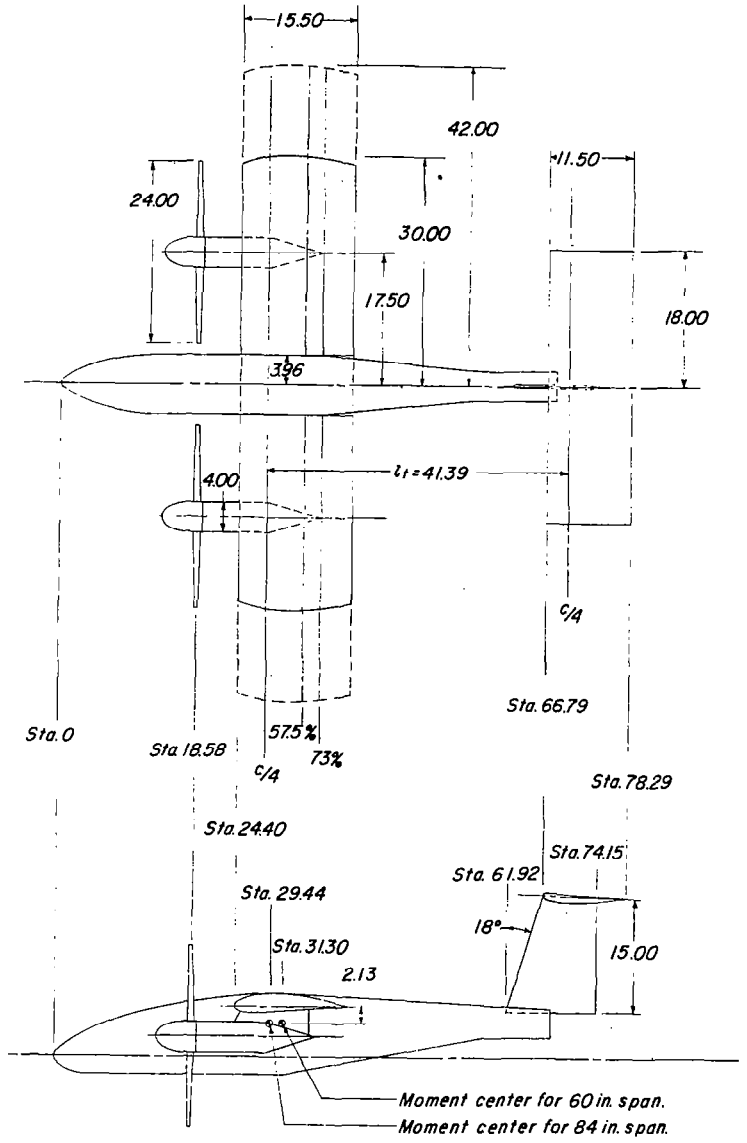

Figure 1.- Three-view drawing of 1/5-scale model and table of geometric characteristics. All dimensions are in inches unless otherwise noted.

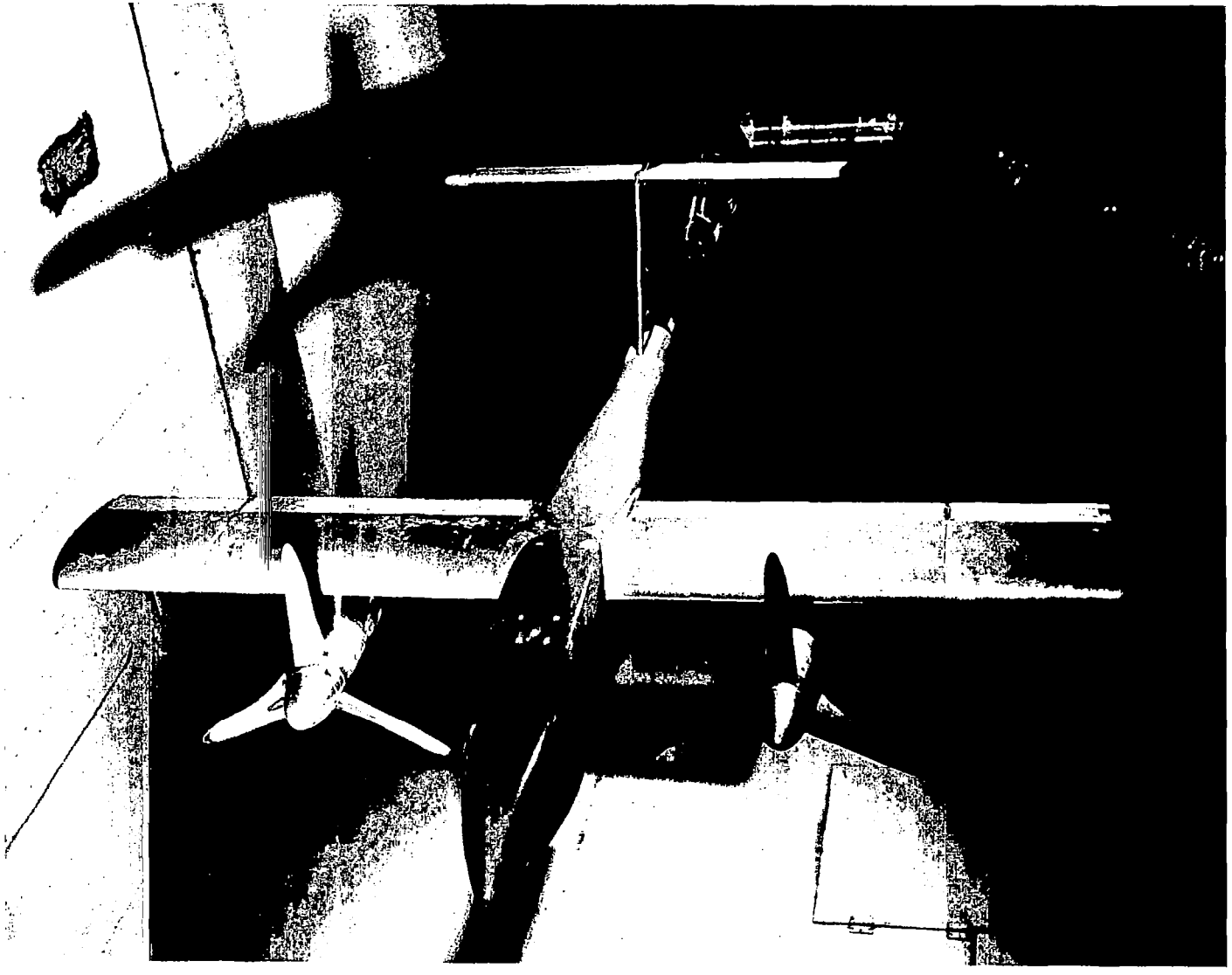

(a) Top quarter front view. L-63-9676

Figure 2.- Photograph of the model in the wind tunnel.

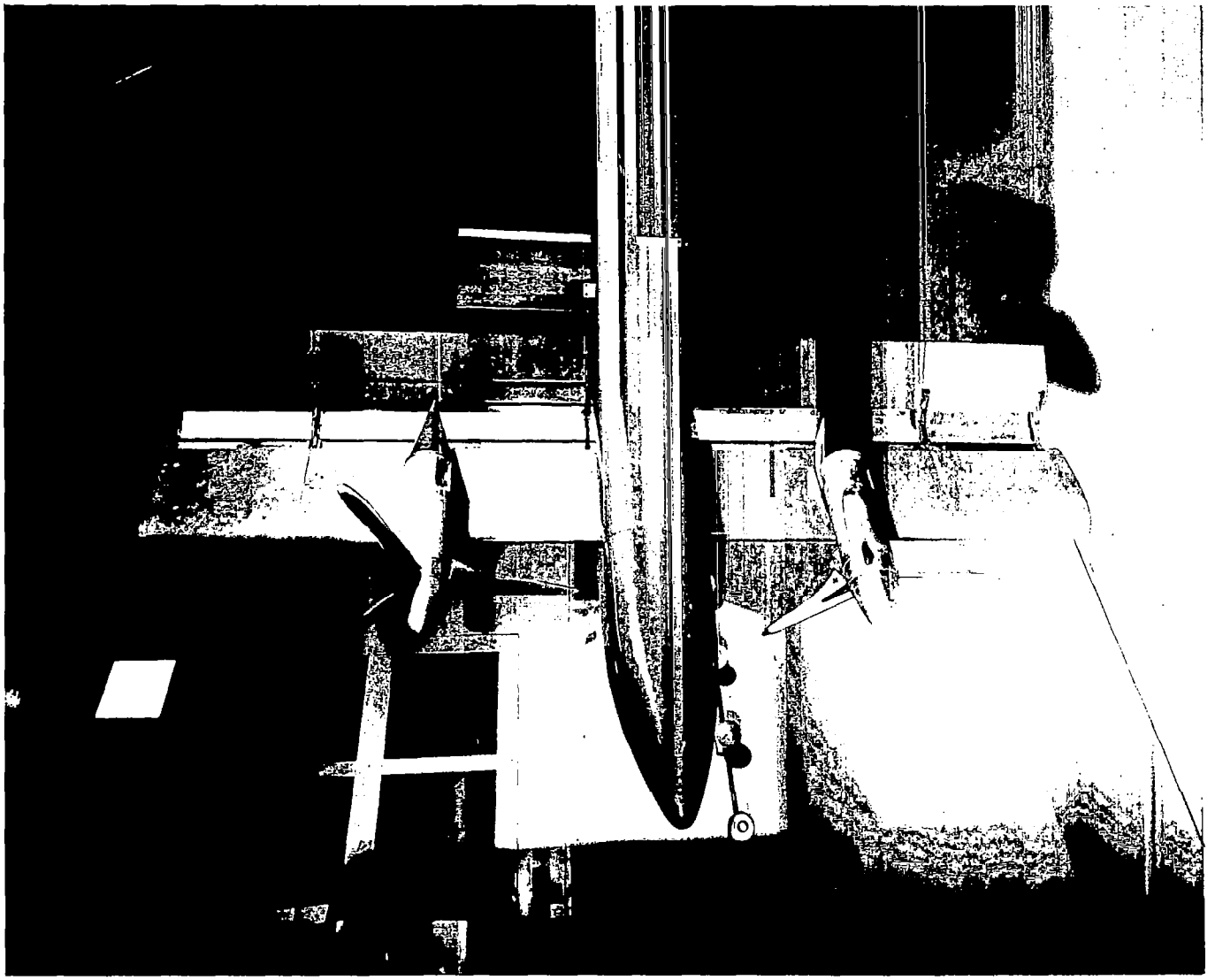

(b) Lower quarter front view.

L-63-9677

Figure 2.- Concluded.

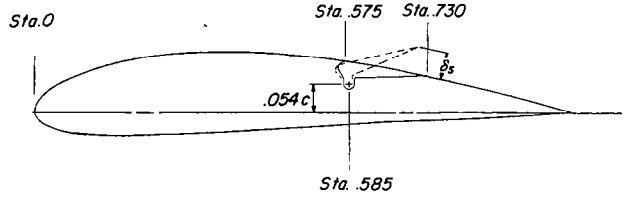

(a) Plain wing (NACA 4415 airfoil).

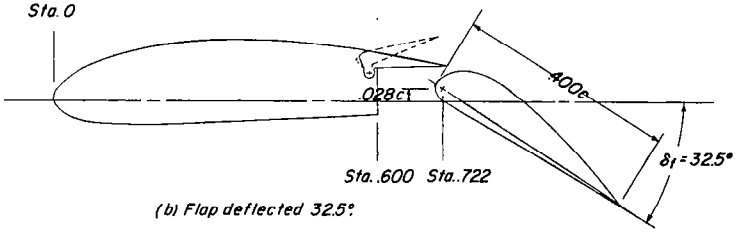

(b) Flap deflected 32.5°.

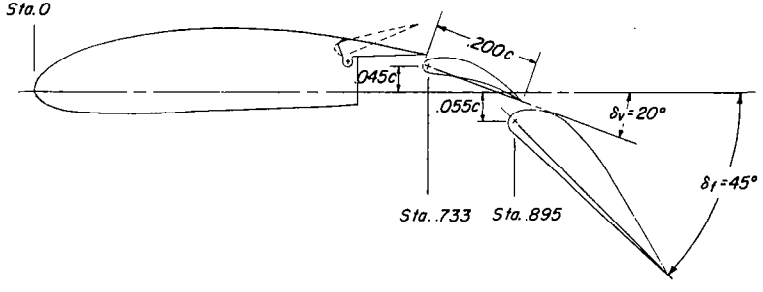

(c) Flap deflected 45°.

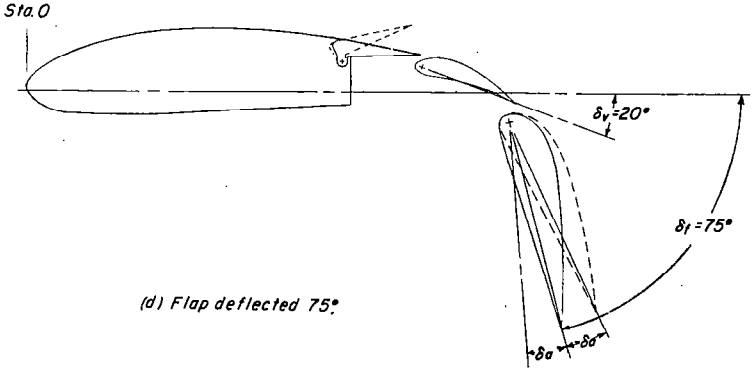

(d) Flap deflected 75°.

Vane ordinates St. Cyr 156 section		
x/c	y_u/c	y_l/c
.0000	.0000	-.0000
.0125	.0381	-.0268
.0250	.0522	-.0339
.0500	.0739	-.0409
.0750	.0905	-.0446
.1000	.1039	-.0448
.1500	.1269	-.0409
.2000	.1440	-.0300
.3000	.1630	-.0140
.4000	.1660	.0010
.5000	.1600	.0180
.6000	.1440	.0300
.7000	.1170	.0320
.8000	.0830	.0300
.9000	.0484	.0180
.9500	.0274	.0107
1.0000	.0065	.0000

Flap ordinates		
x/c	y_u/c	y_l/c
.0000	.0000	-.0000
.0125	.0460	-.0290
.0250	.0645	-.0387
.0500	.0919	-.0435
.0750	.1145	-.0460
.1000	.1306	-.0468
.1500	.1516	-.0444
.2000	.1621	-.0420
.3000	.1677	-.0373
.4275	.1532	-.0312
.5000	.1387	-.0278
.6275	.1065	-.0217
.7500	.0769	-.0159
.8750	.0435	-.0100
1.0000	.0040	-.0040

Figure 3.- Geometric characteristics of wing section showing flap deflection. All dimensions are in fraction of wing chord unless otherwise noted.

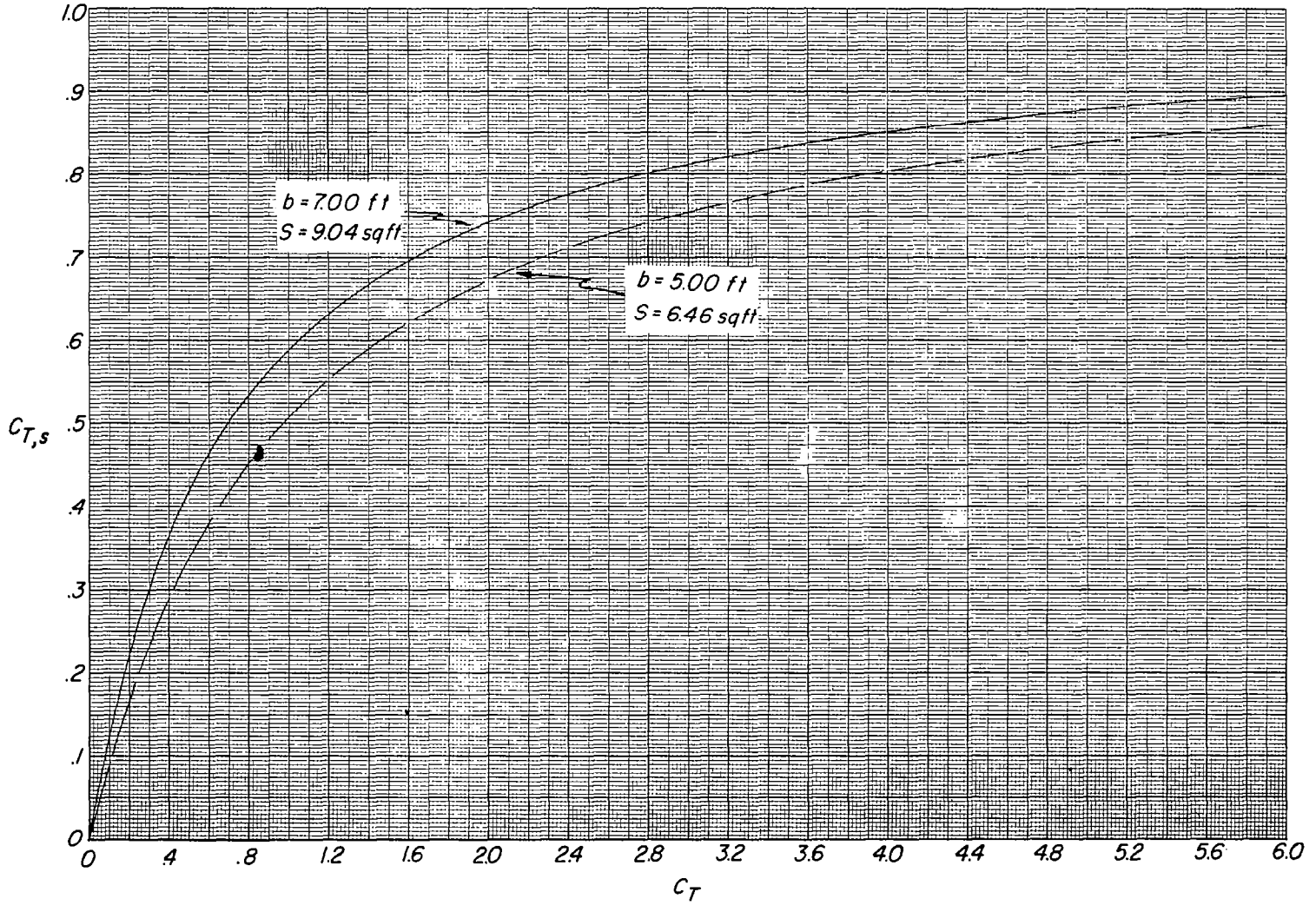

Figure 4.- Slipstream thrust coefficient plotted as a function of free-stream thrust coefficient for the two wing spans. $C_{T,s} = \frac{C_T}{C_T - \frac{NS_p}{S}}$.

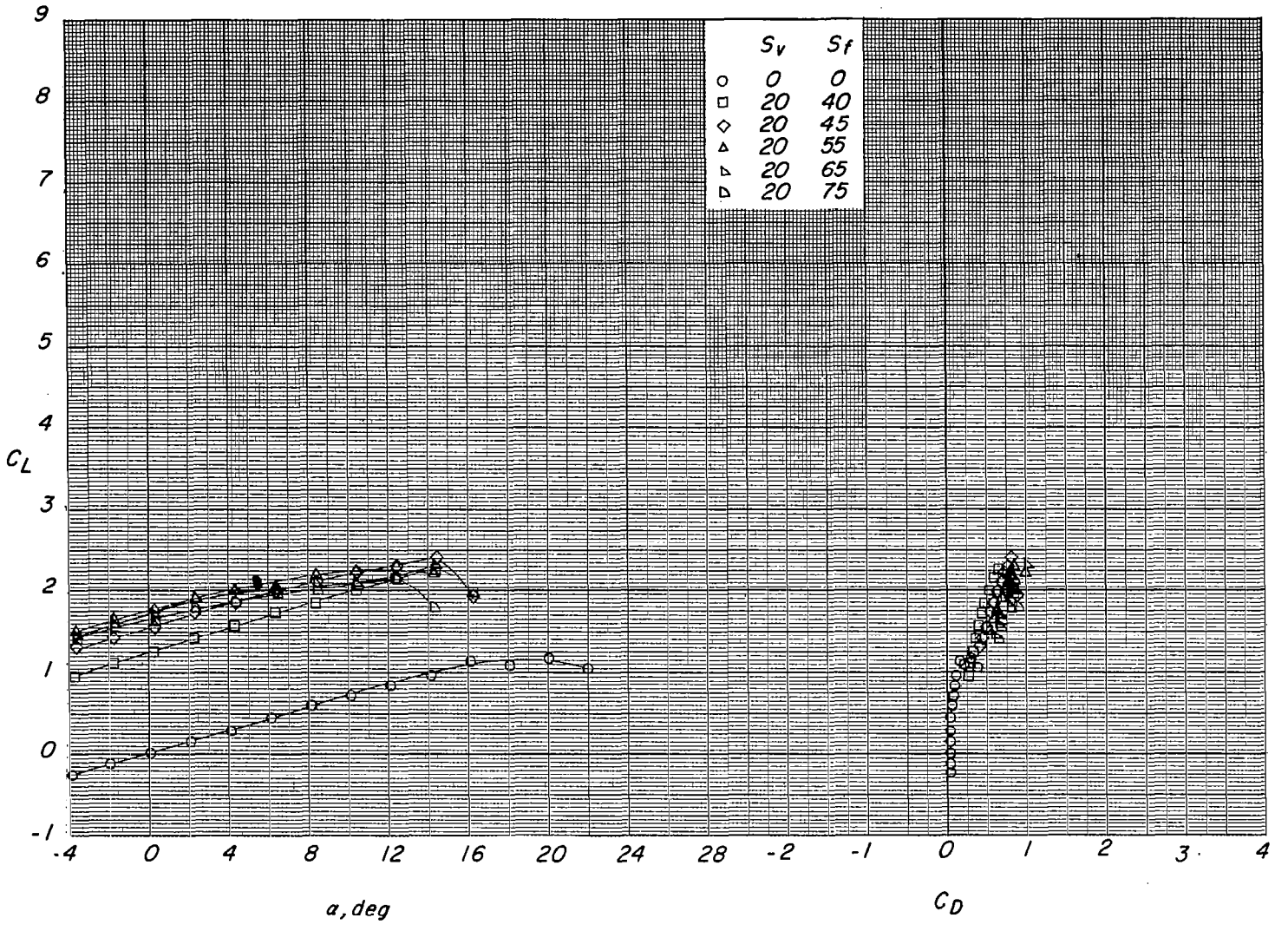

(a) $C_T = 0$ (propellers off).

Figure 5.- Effect of flap deflection on longitudinal characteristics for the short-span model at several thrust coefficients and at two vane deflections.

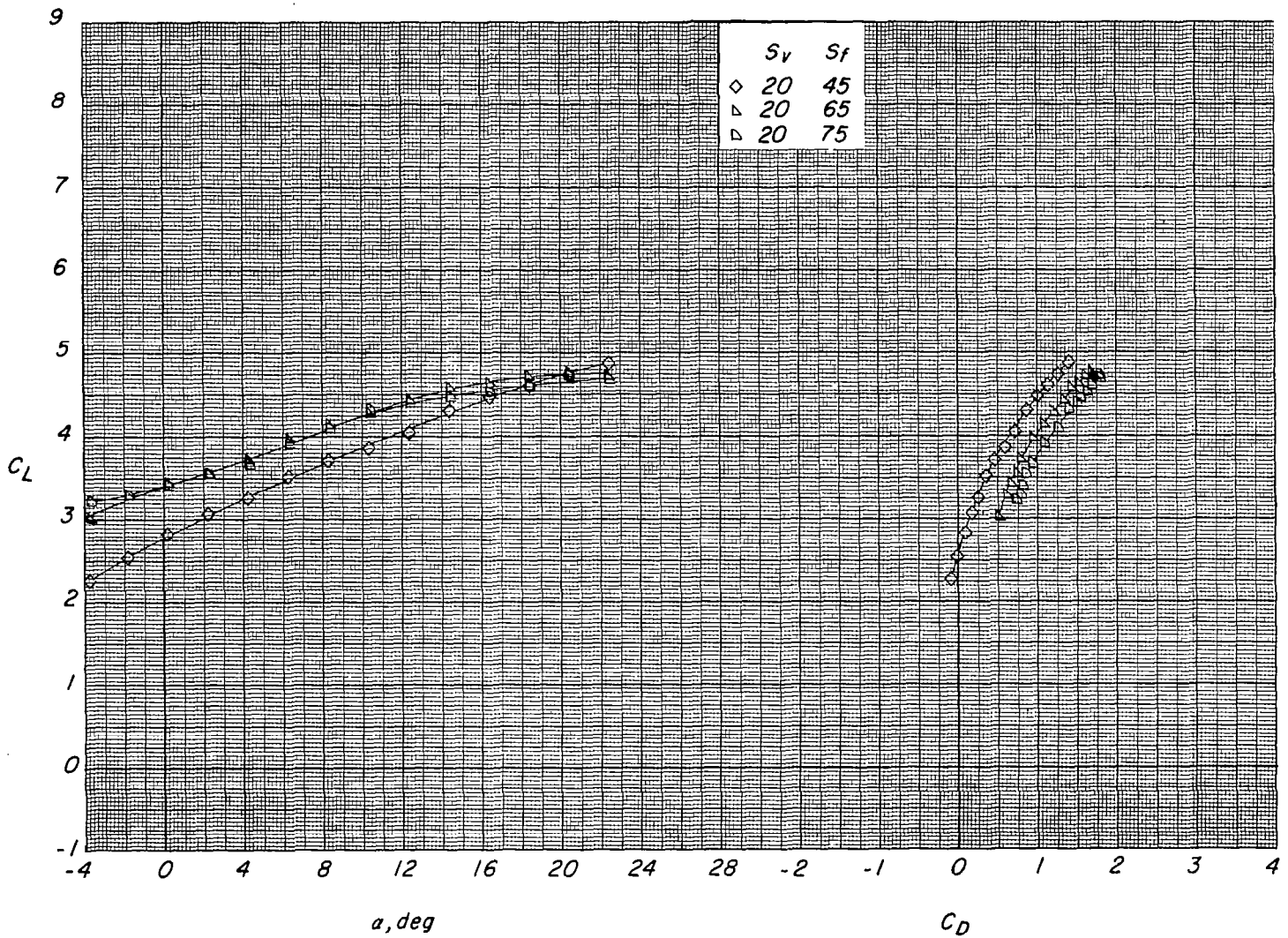

(b) $C_T \approx 1.0$.

Figure 5.- Continued.

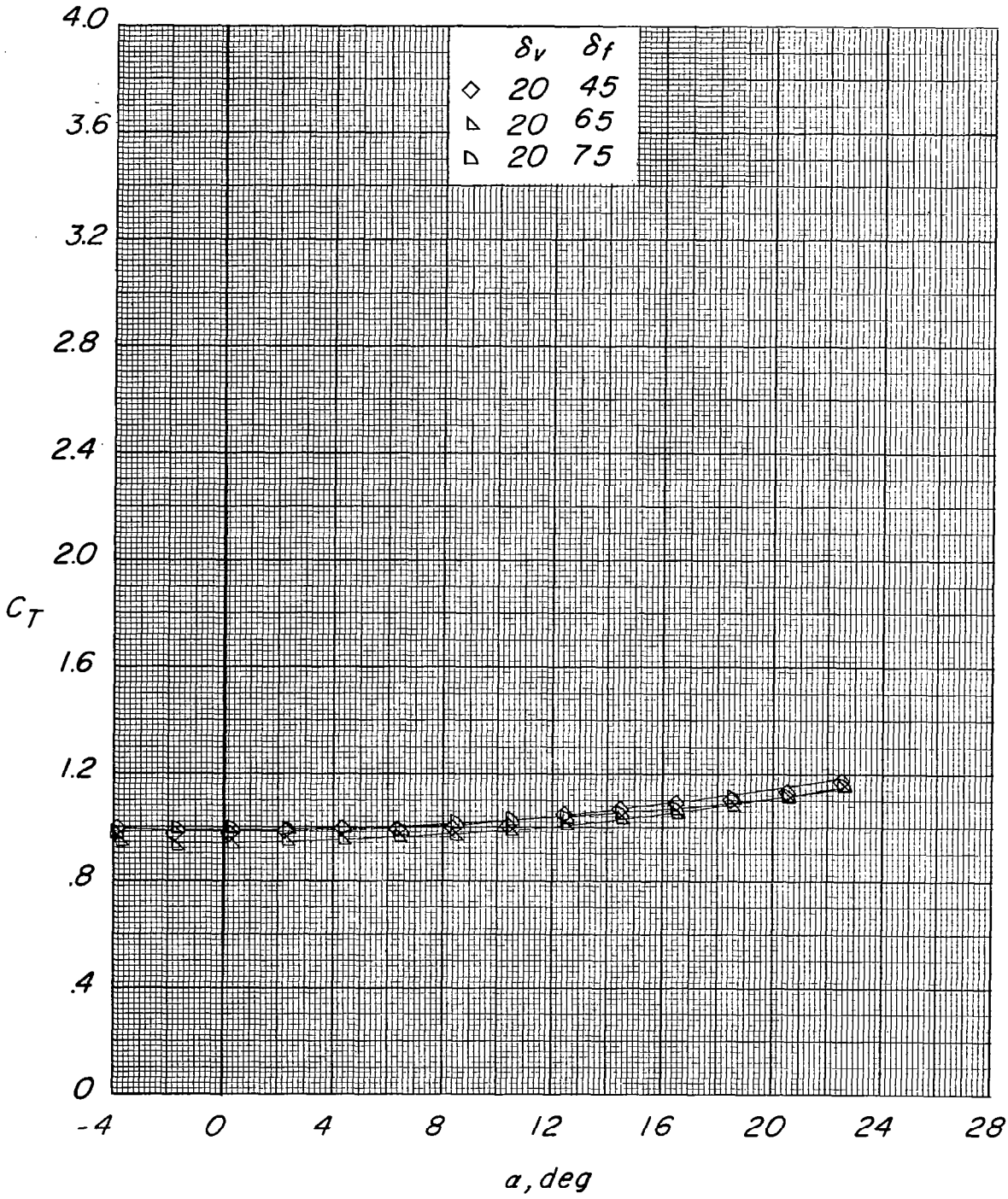

(b) Concluded.

Figure 5.- Continued.

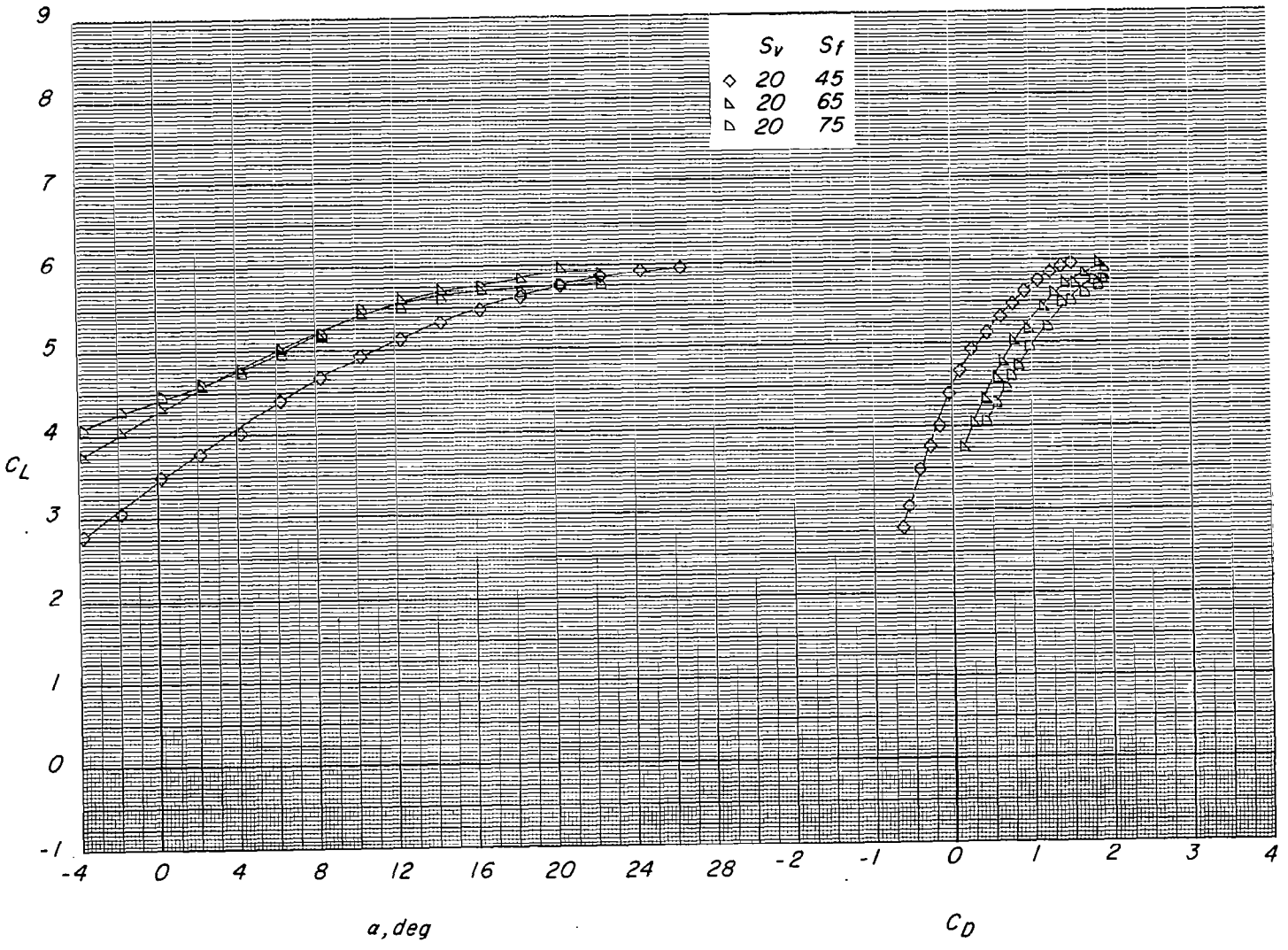

(c) $C_T \approx 1.9$.

Figure 5.- Continued.

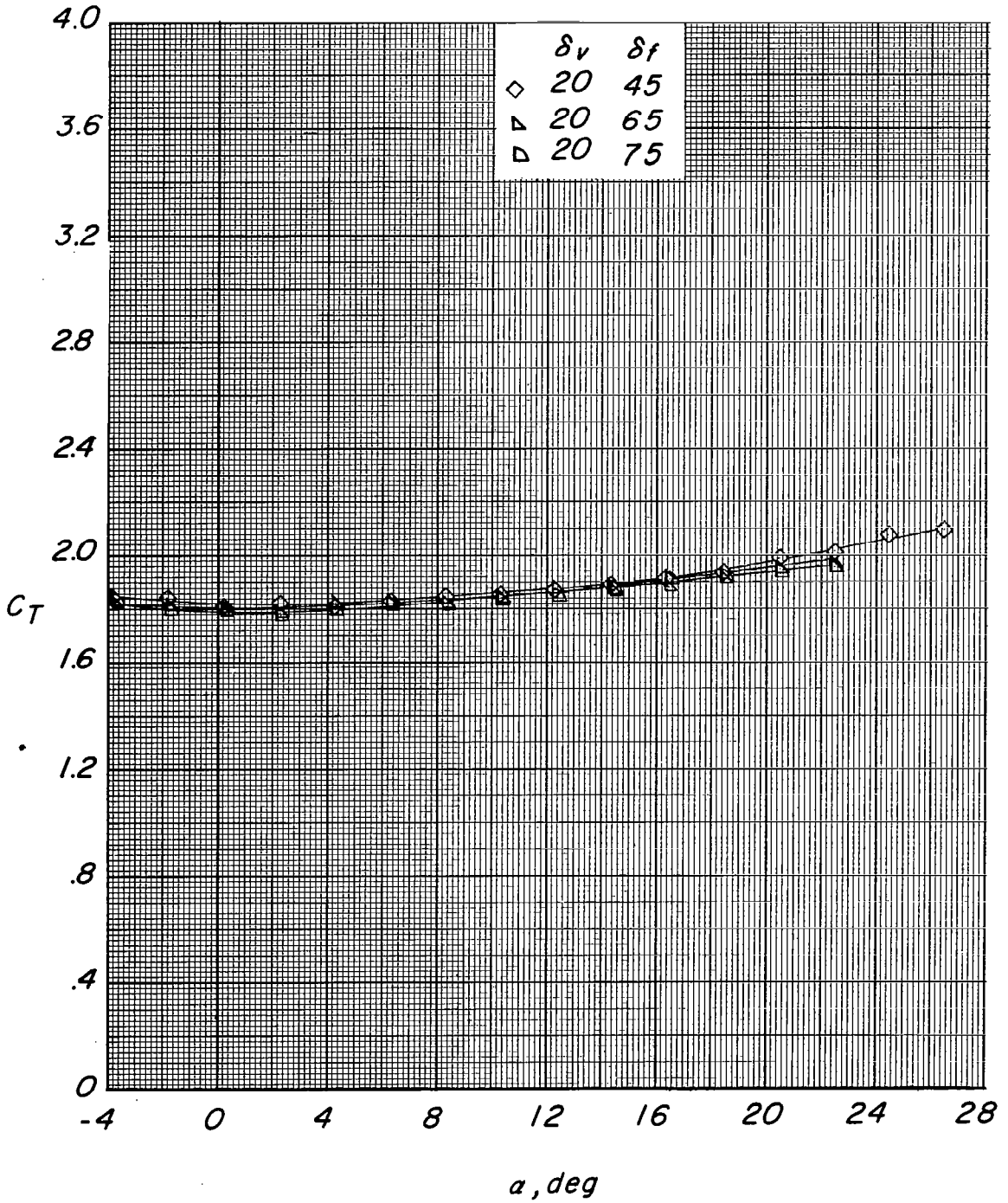

(c) Concluded.

Figure 5.- Continued.

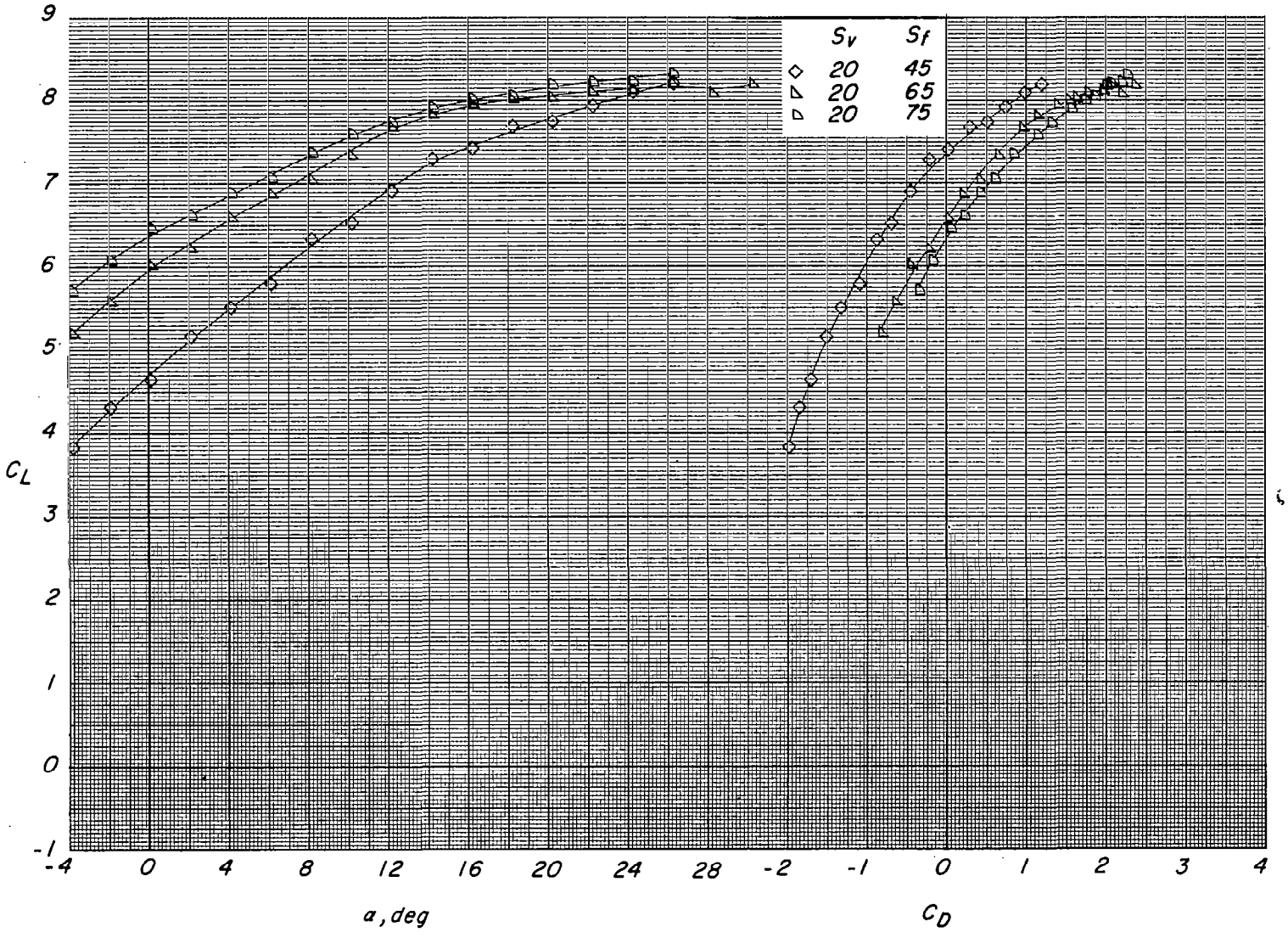

(d) $C_T \approx 3.7$.

Figure 5.- Continued.

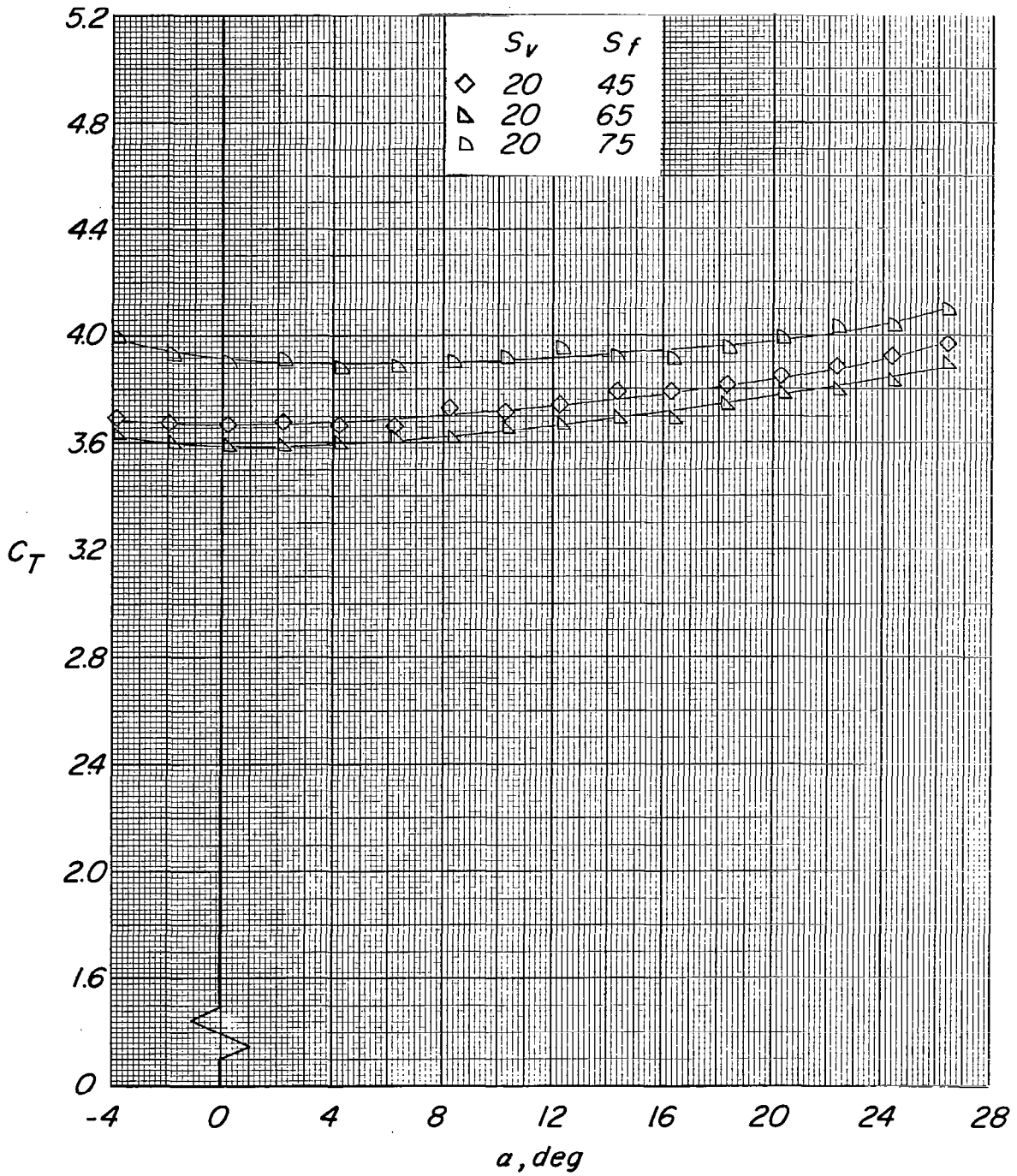

(d) Concluded.

Figure 5.- Continued.

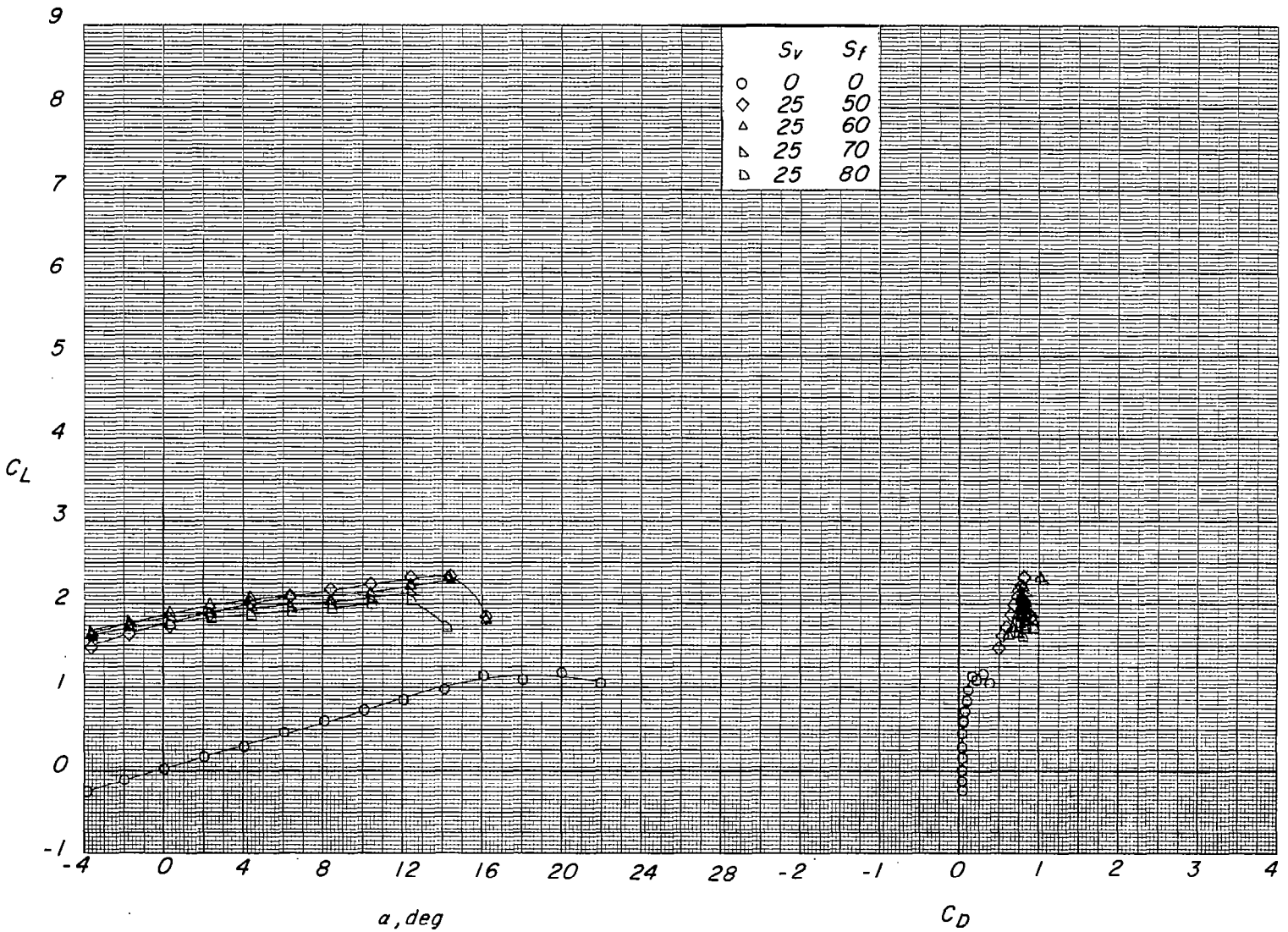

(e) $C_T = 0$ (propellers off).

Figure 5.- Continued.

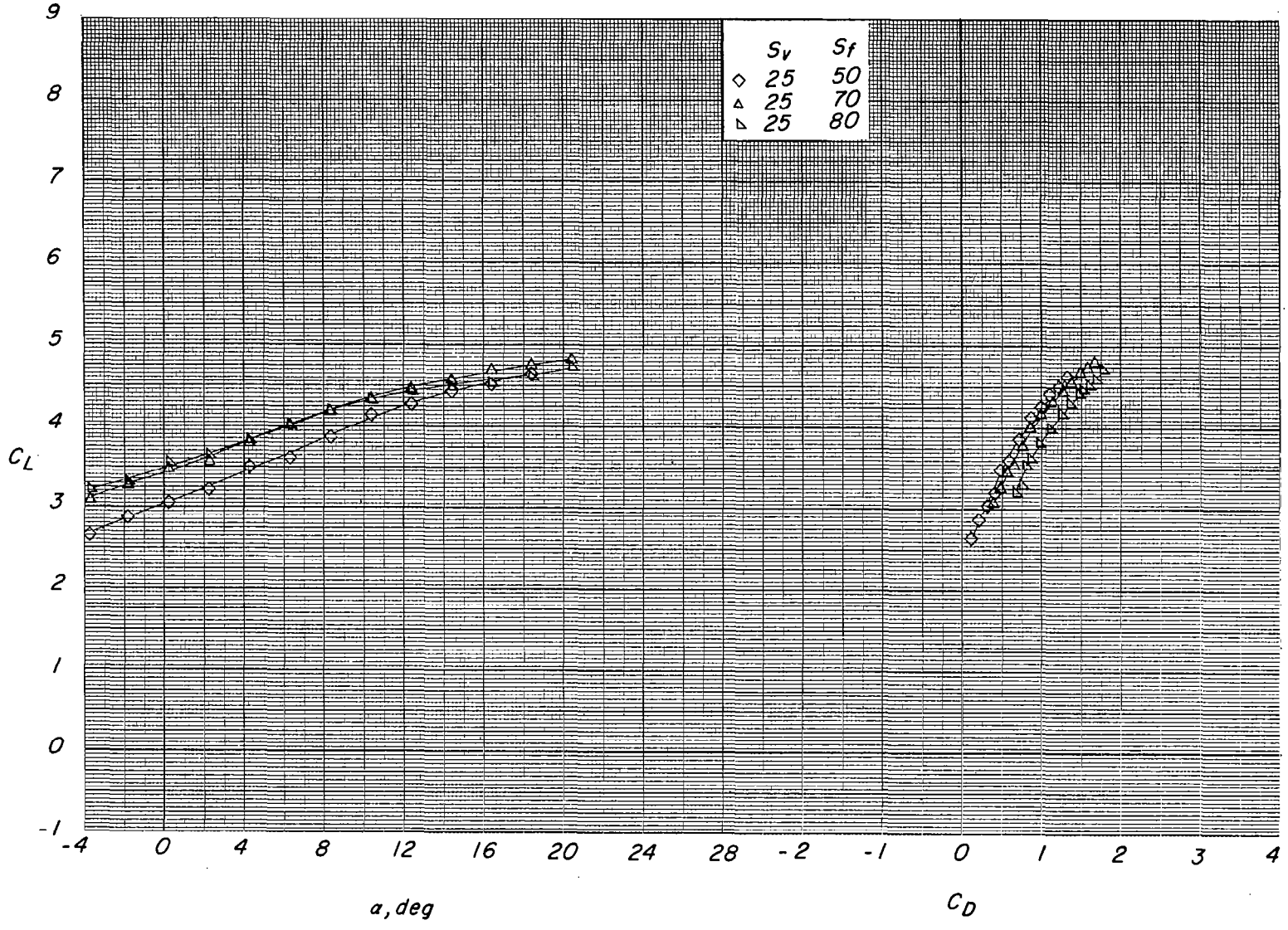

(f) $C_T \approx 1.0$.

Figure 5.- Continued.

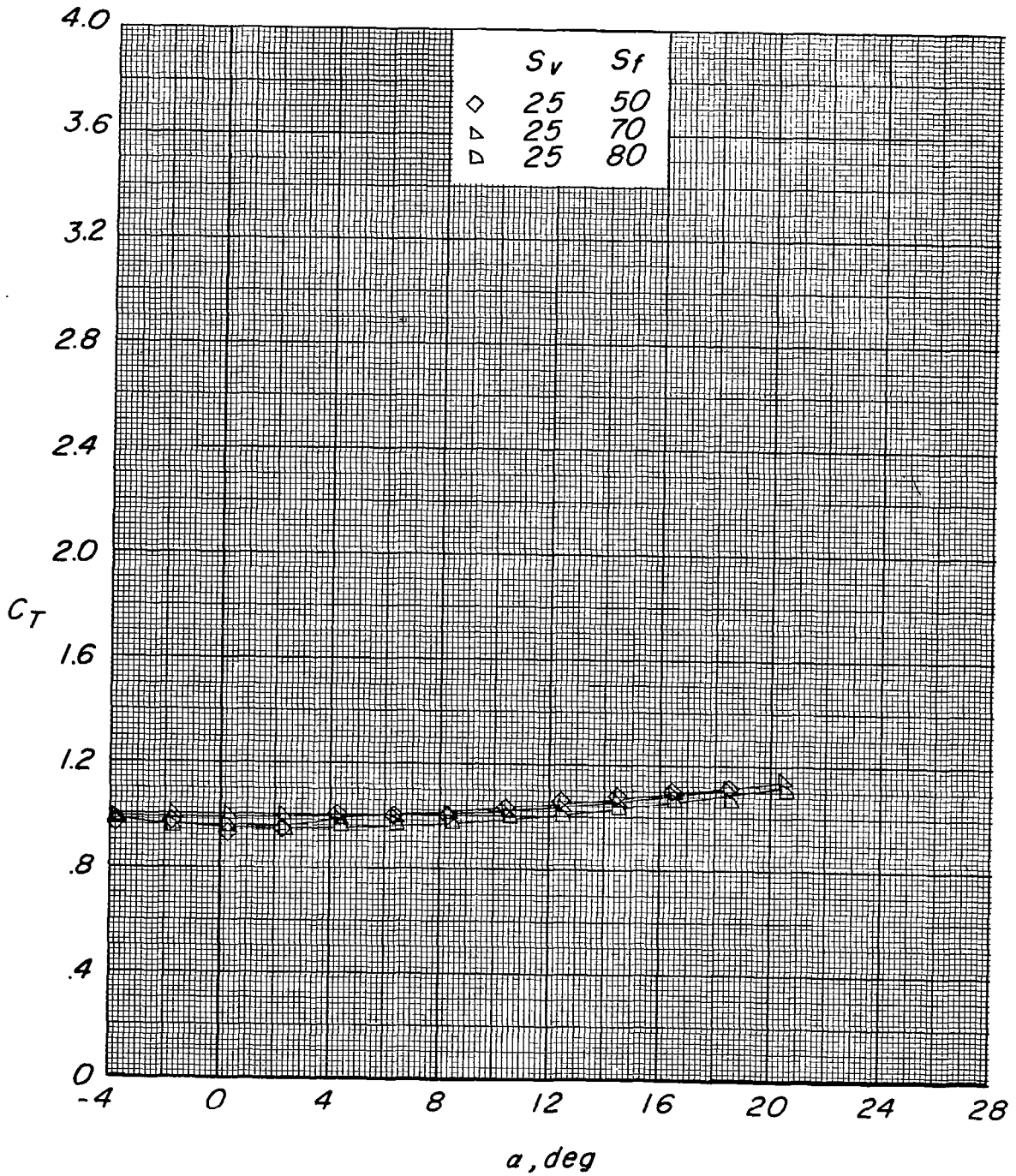

(f) Concluded.

Figure 5.- Continued.

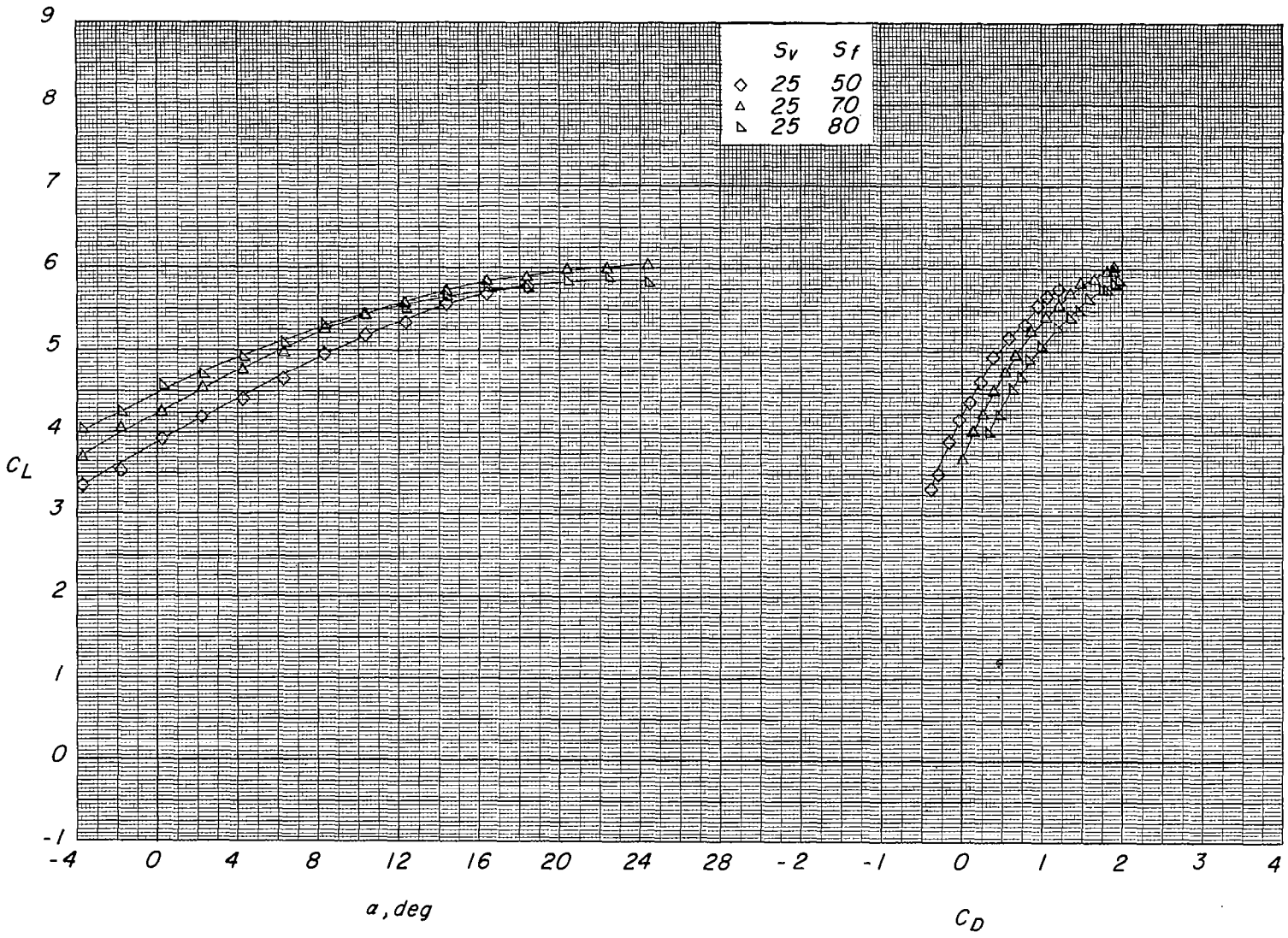

(g) $C_T \approx 1.9$.

Figure 5.- Continued.

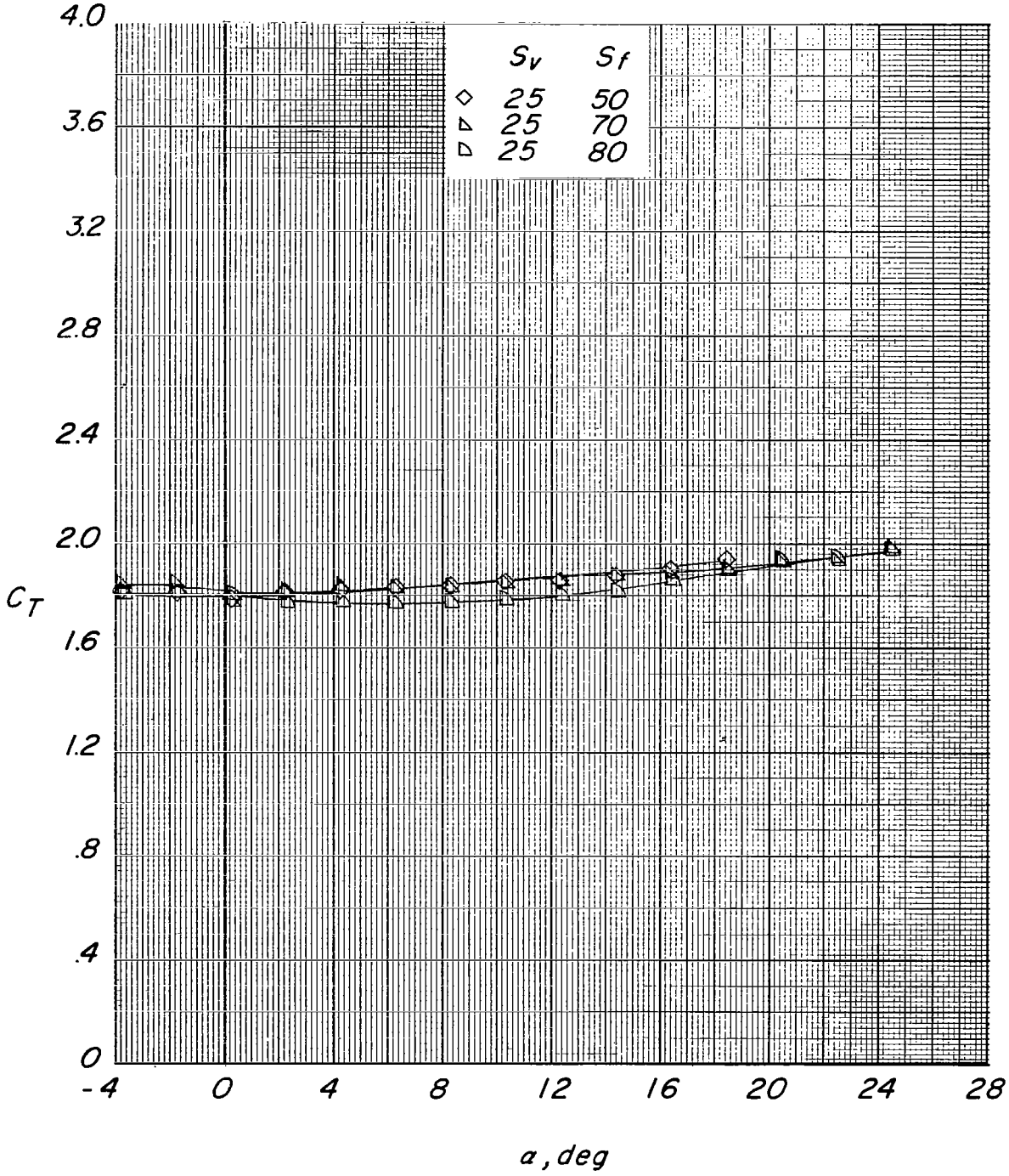

(g) Concluded.

Figure 5.- Continued.

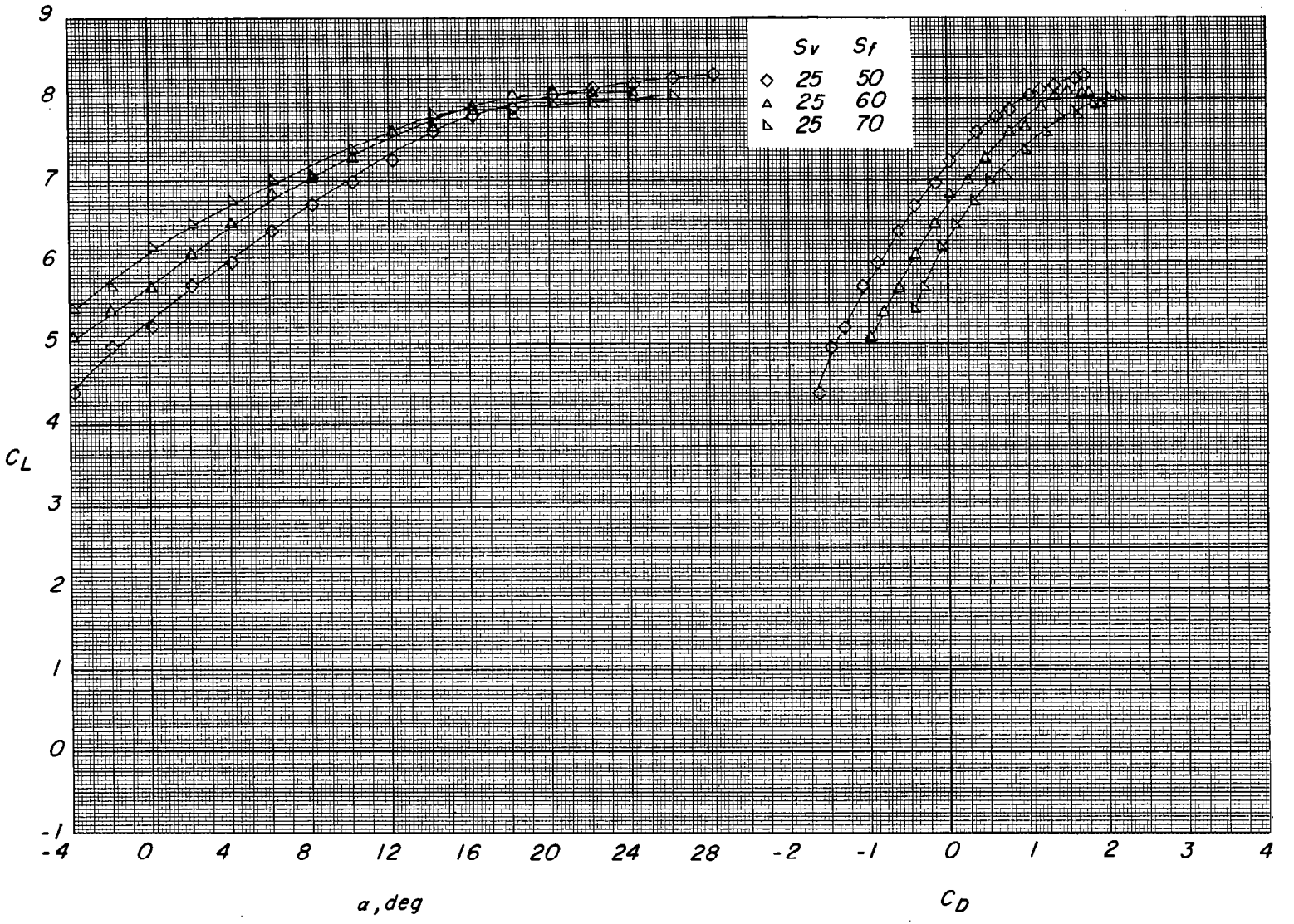

(h) $C_T \approx 3.7$.

Figure 5.- Continued.

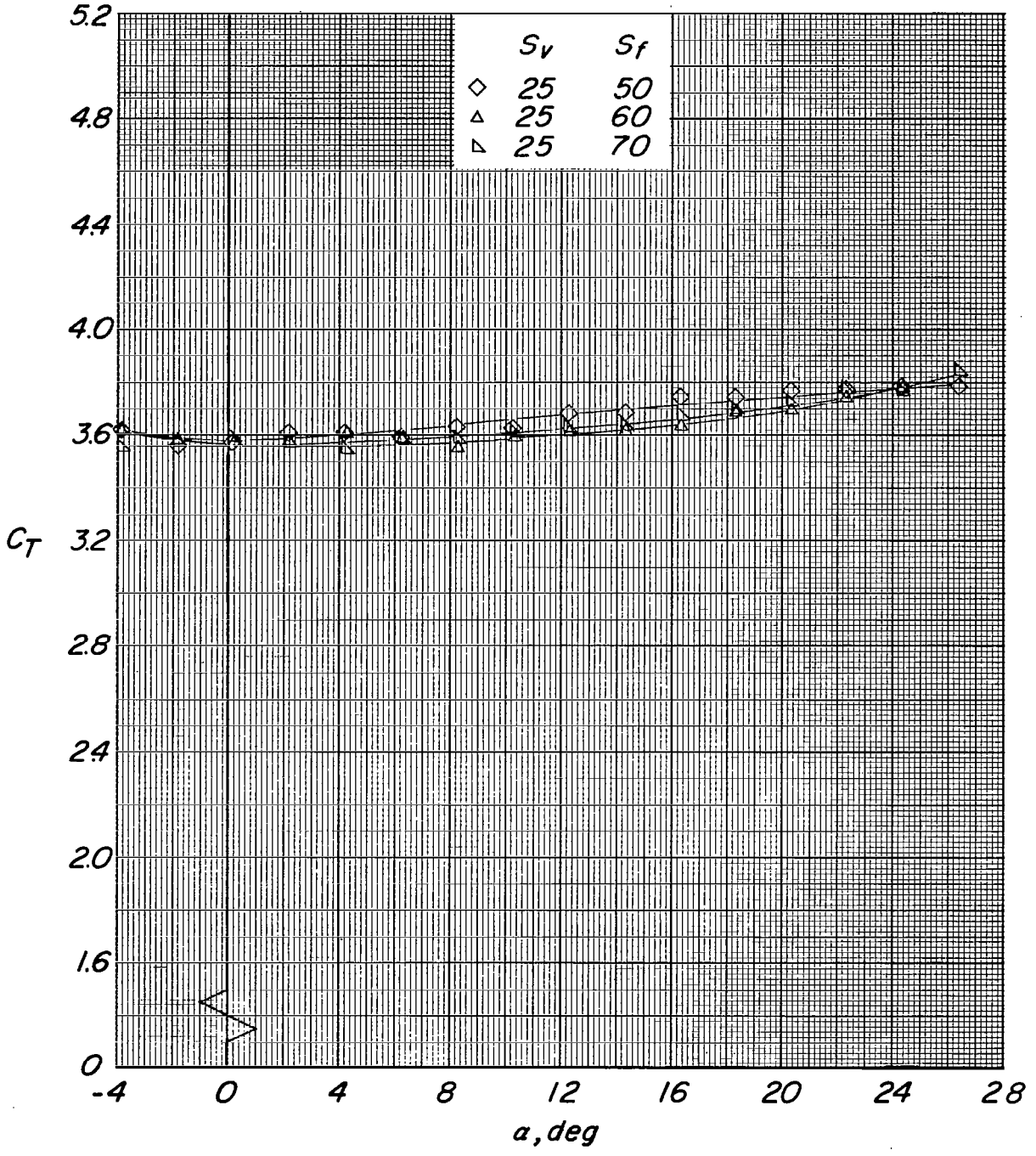

(h) Concluded.

Figure 5.- Concluded.

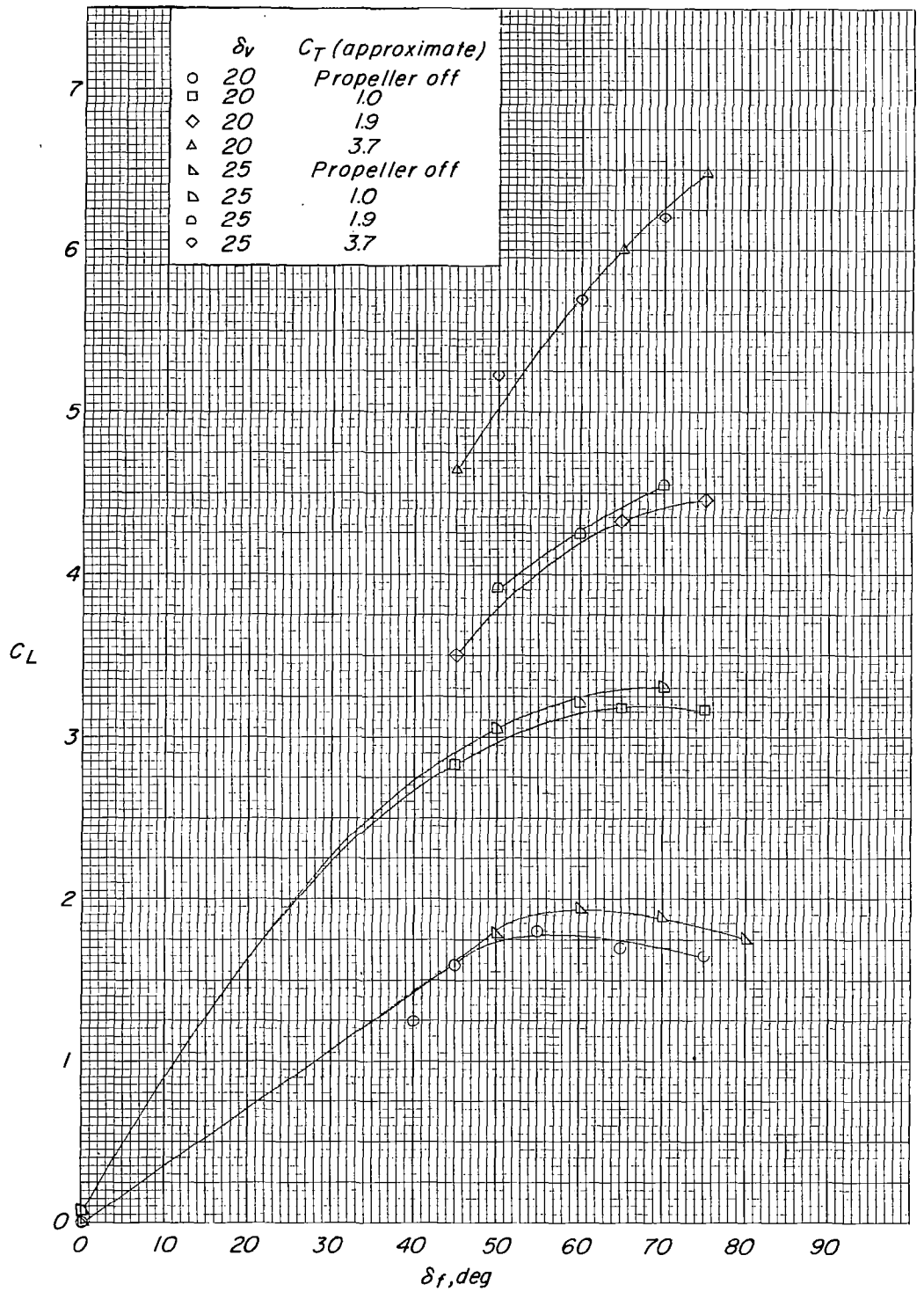

Figure 6.- Variation of lift coefficient with flap deflection for the short-span wing at $\alpha = 0^{\circ}$.

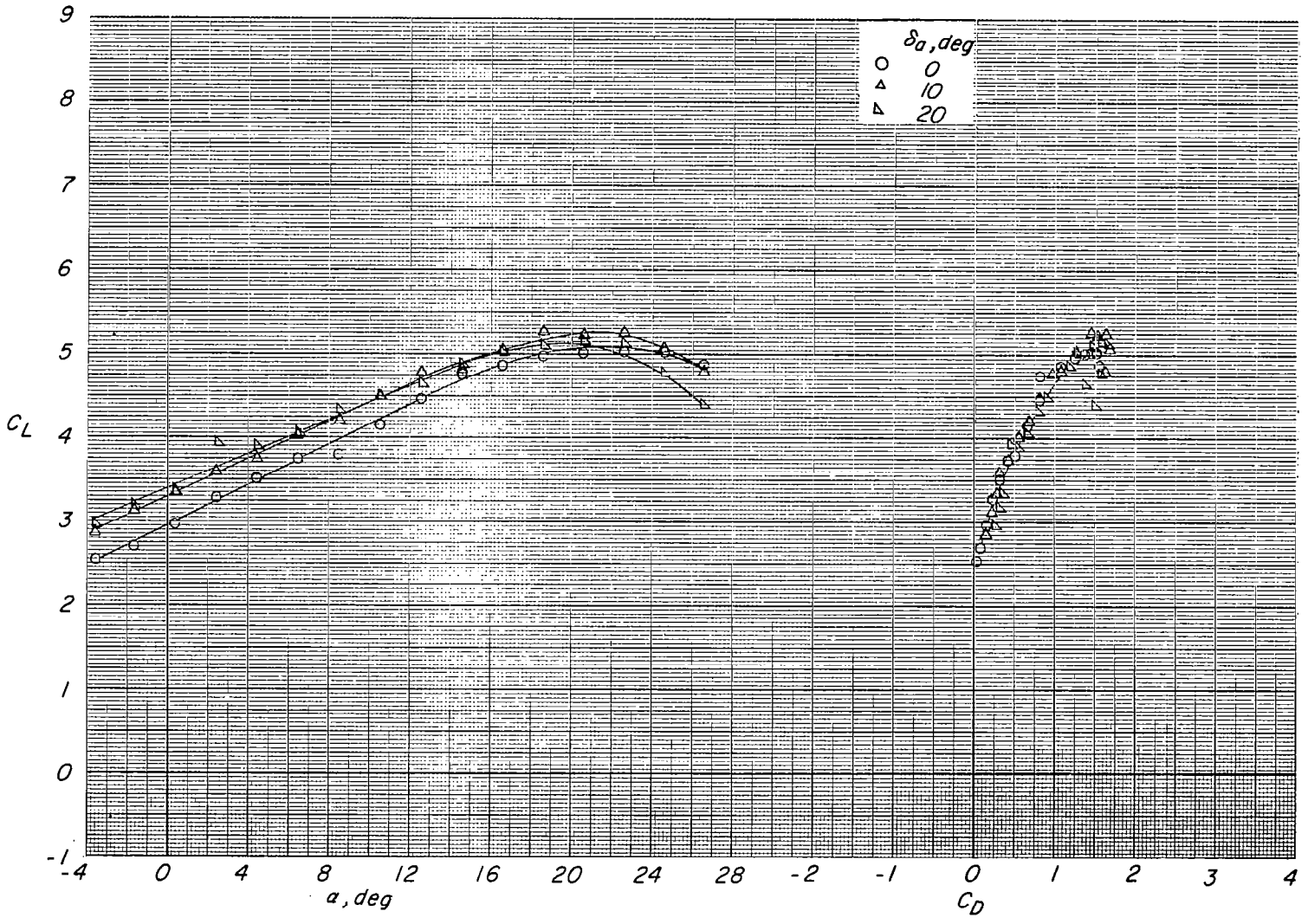

(a) $C_T \approx 0.9$.

Figure 7.- Effect of aileron deflection on configuration C (long span, $\delta_f = 45^\circ$) at several thrust coefficients.

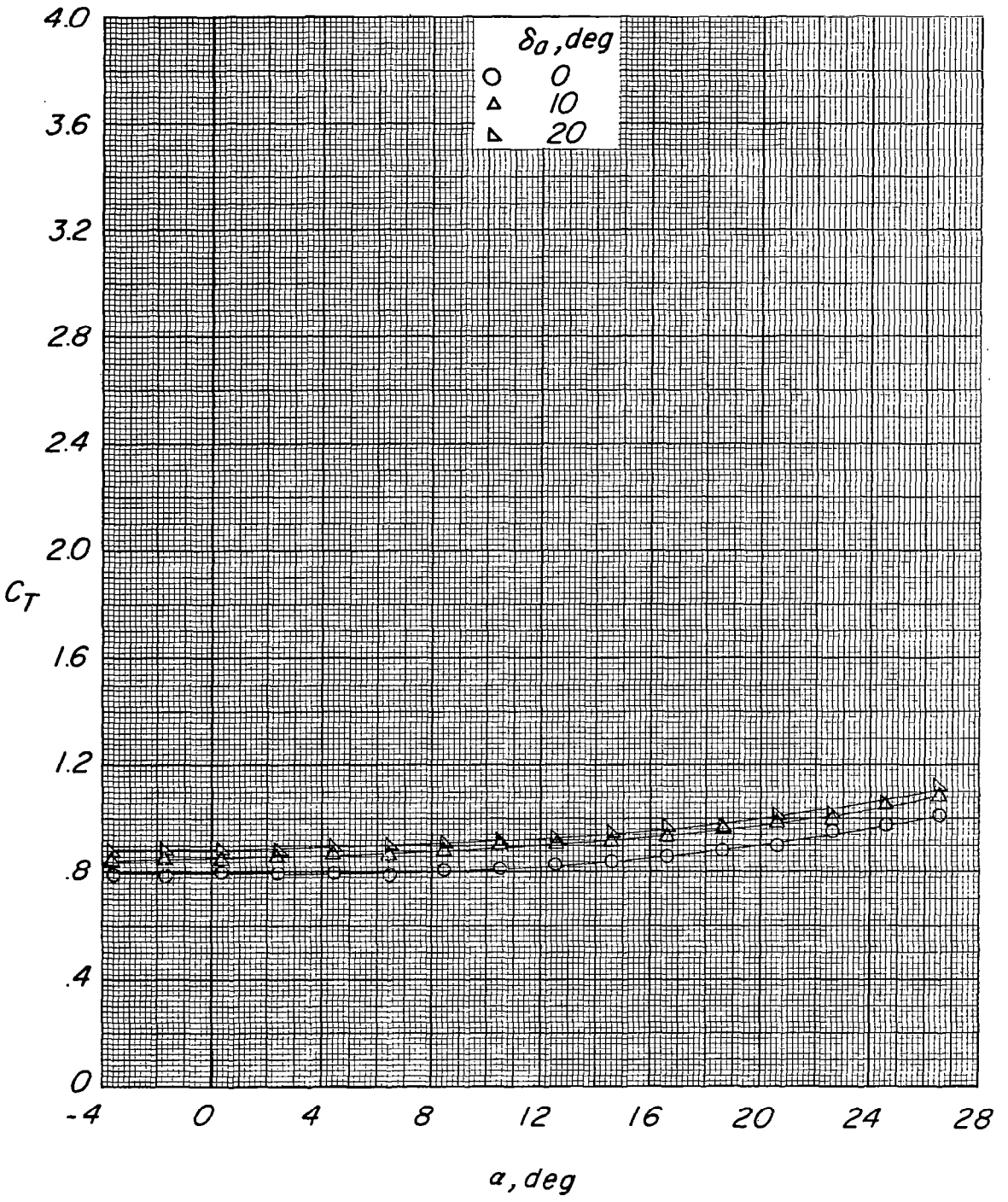

(a) Continued.

Figure 7.- Continued.

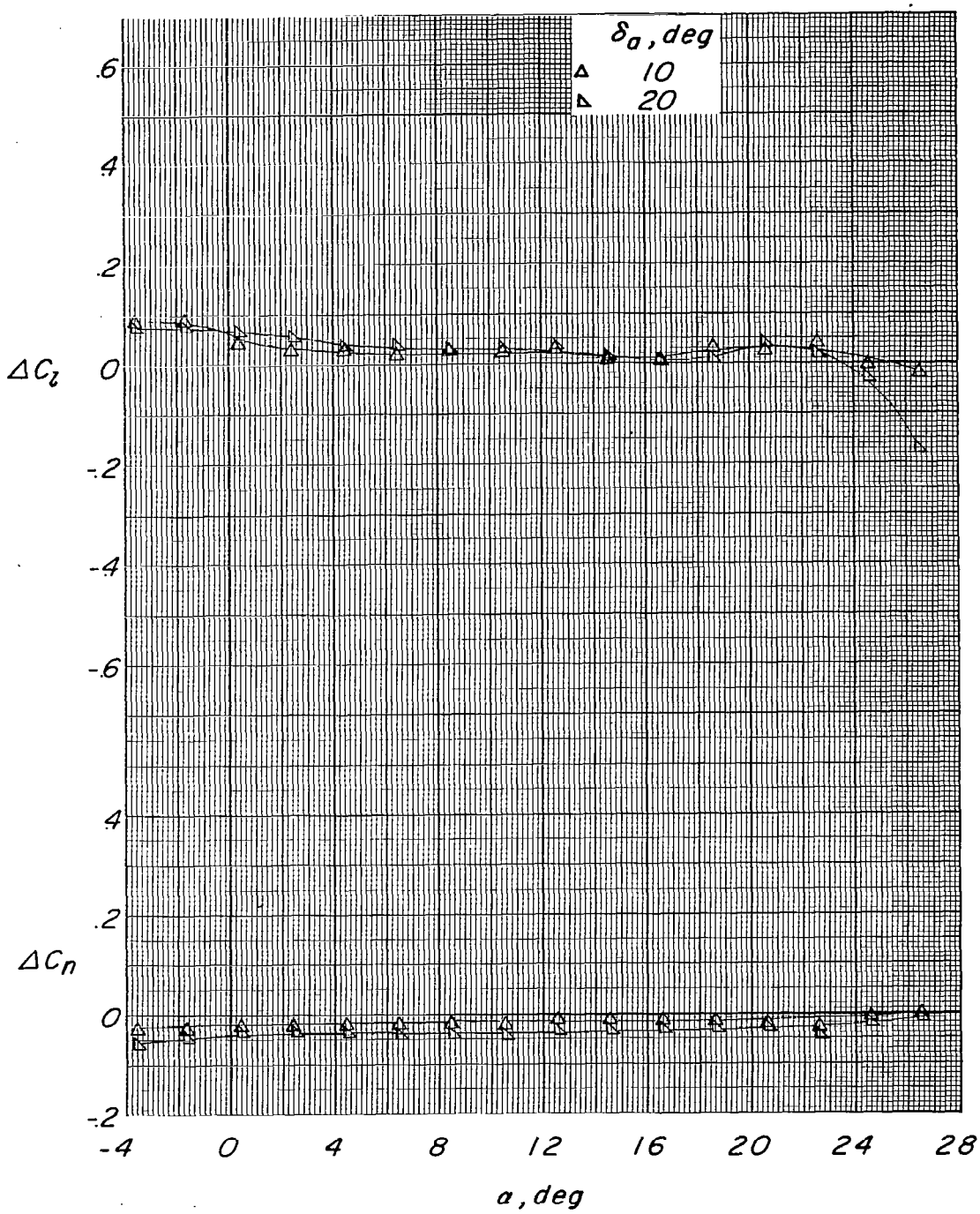

(a) Concluded.

Figure 7.- Continued.

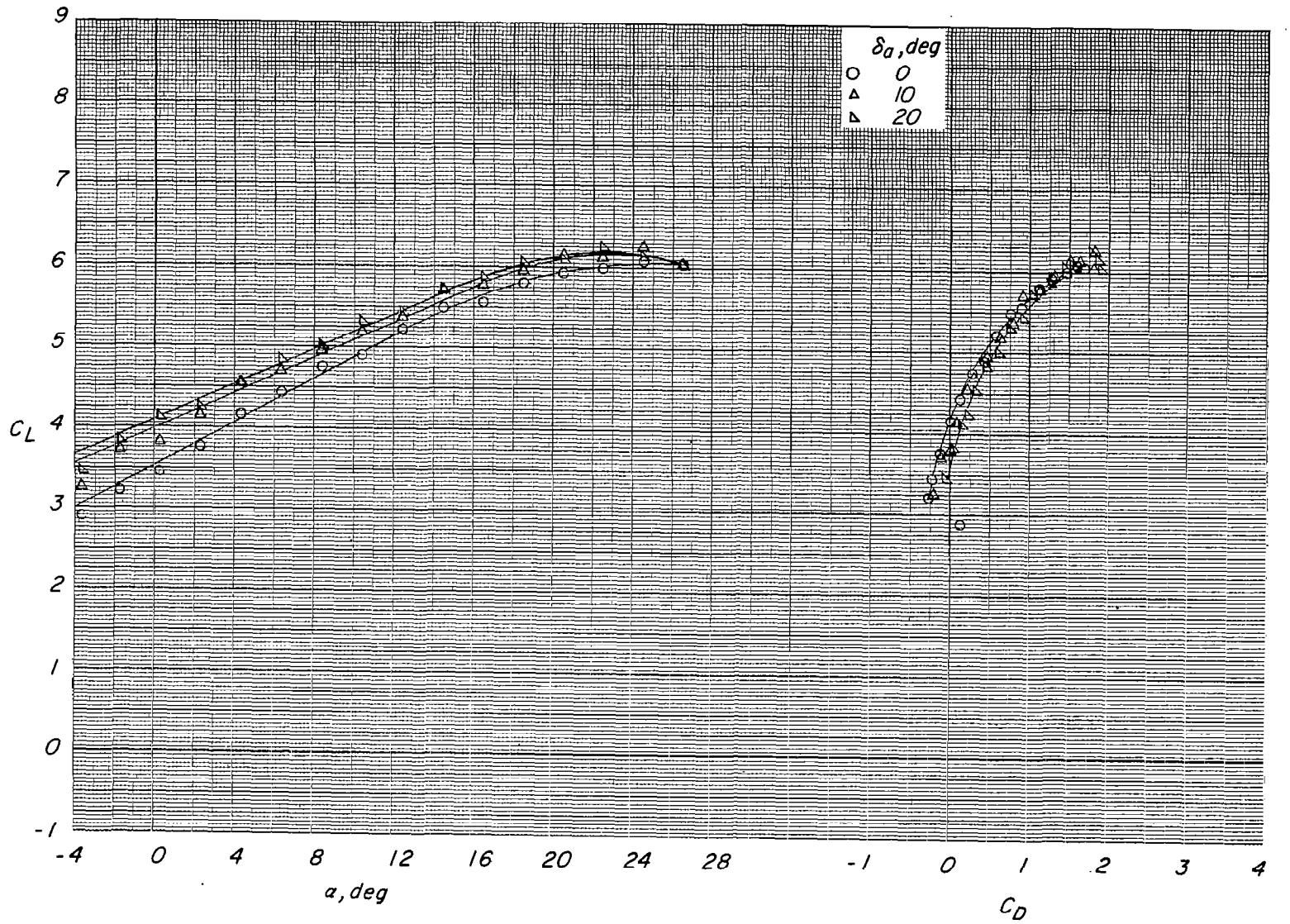

(b) $C_T \approx 1.6$.

Figure 7.- Continued.

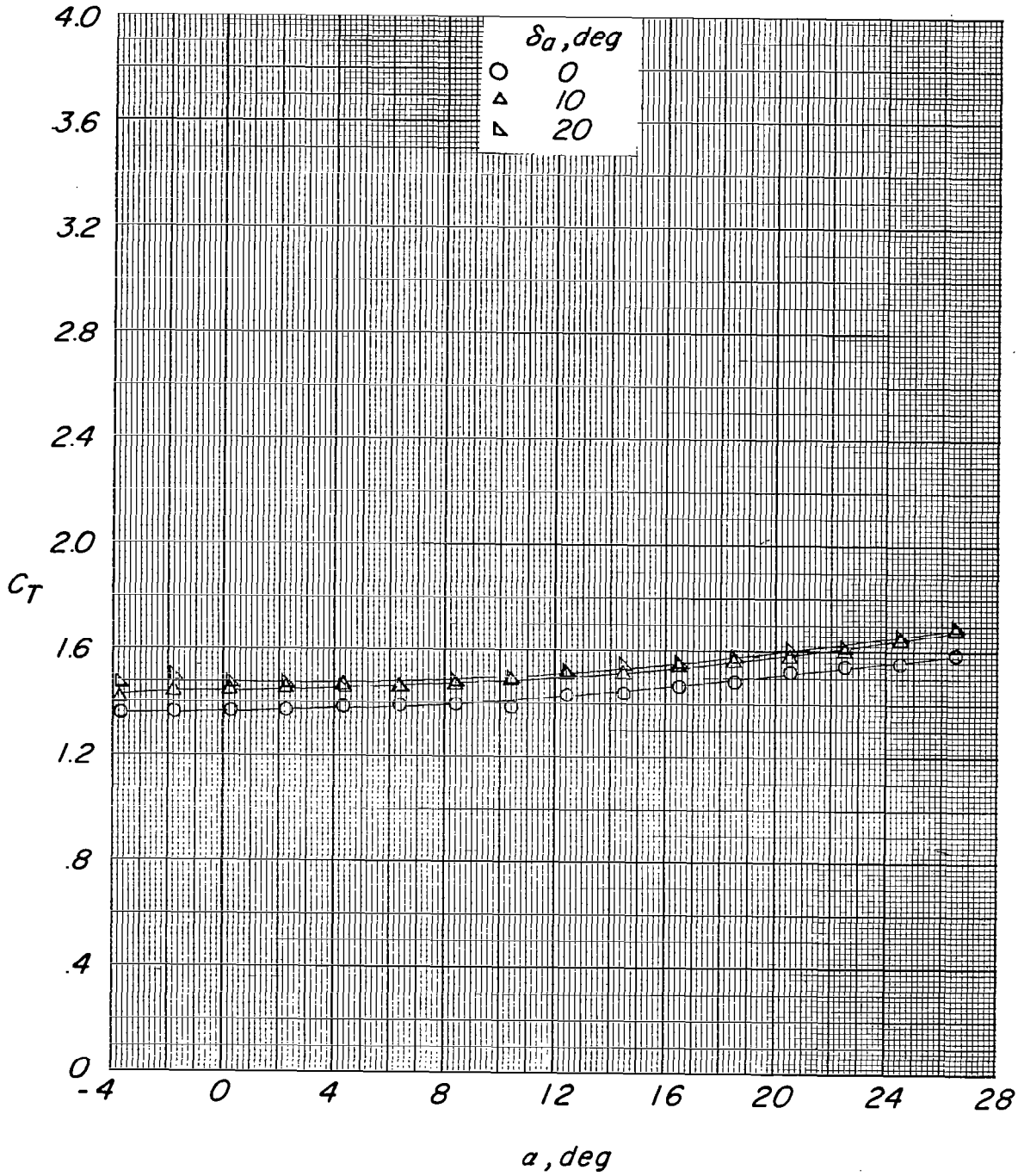

(b) Continued.

Figure 7.- Continued.

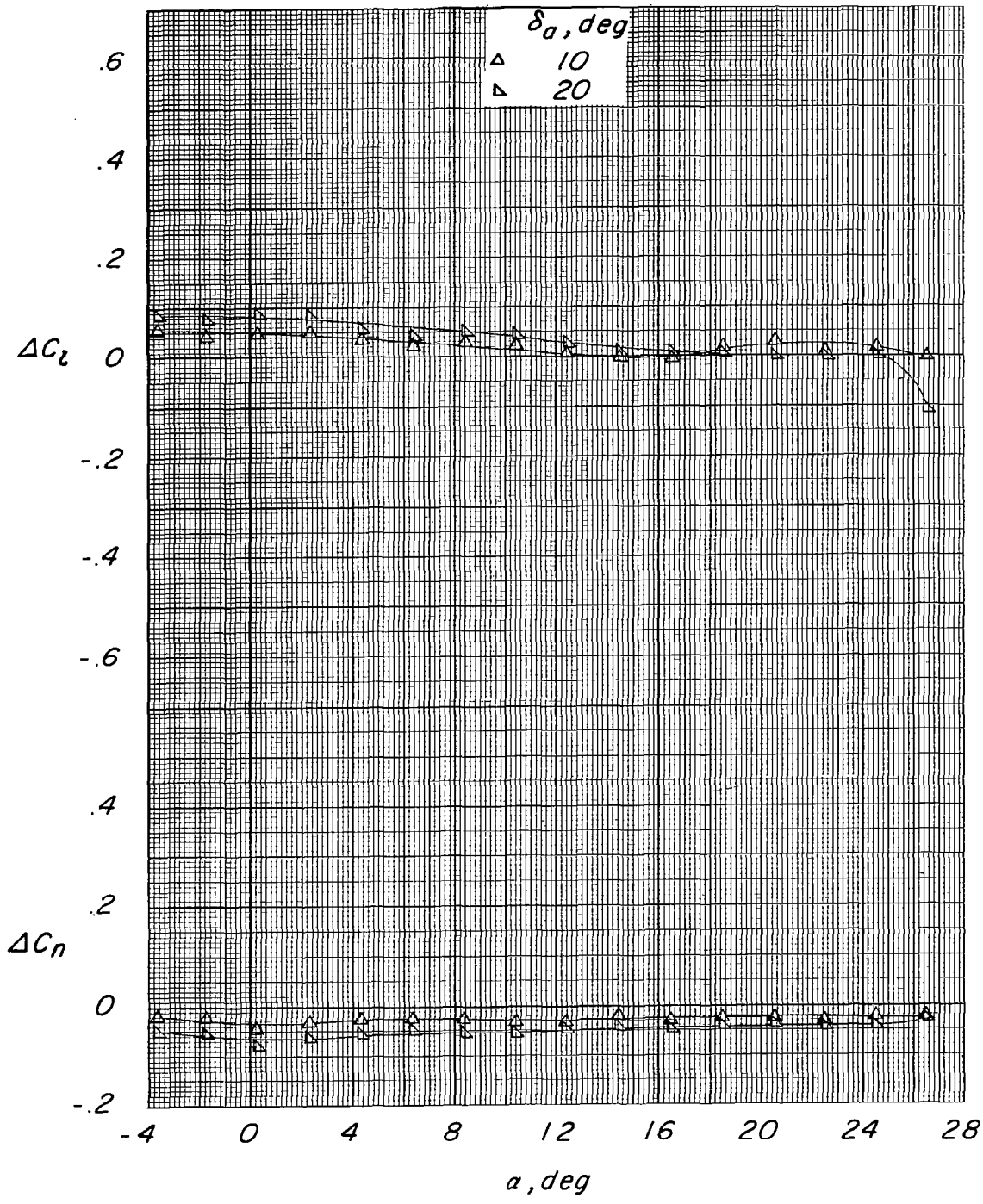

(b) Concluded.

Figure 7.- Continued.

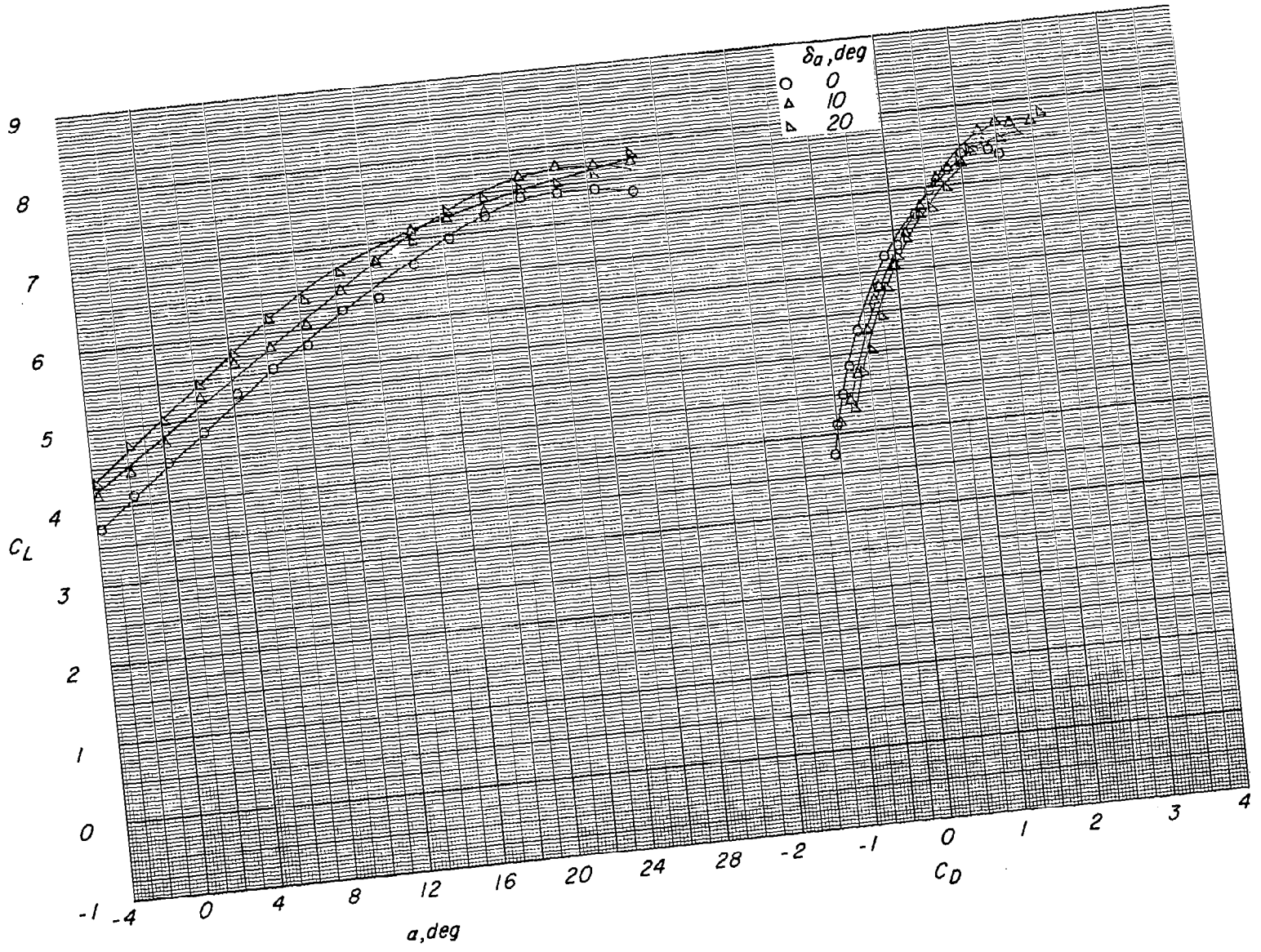

(c) $C_T \approx 2.7$.

Figure 7.- Continued.

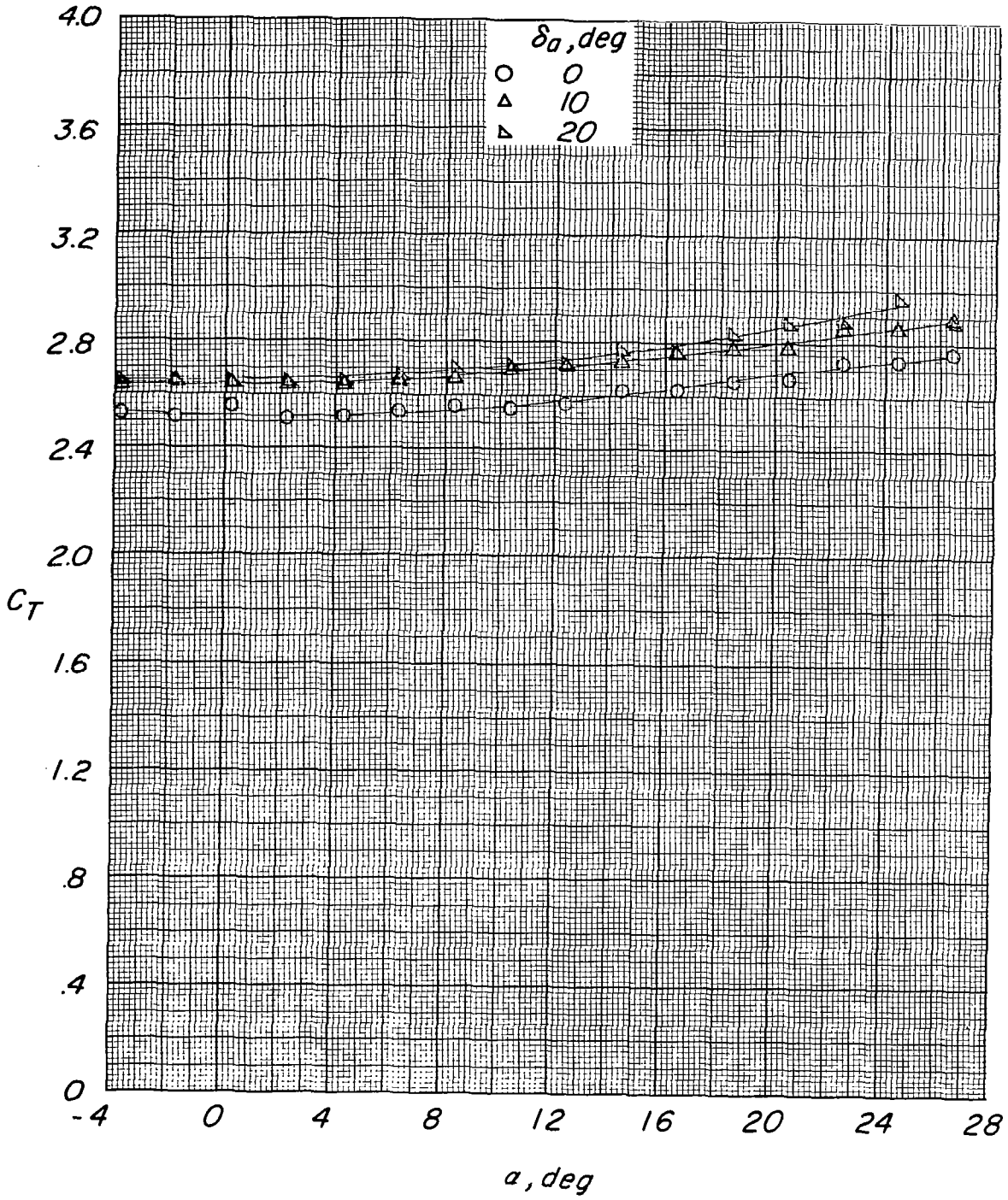

(c) Continued.

Figure 7.- Continued.

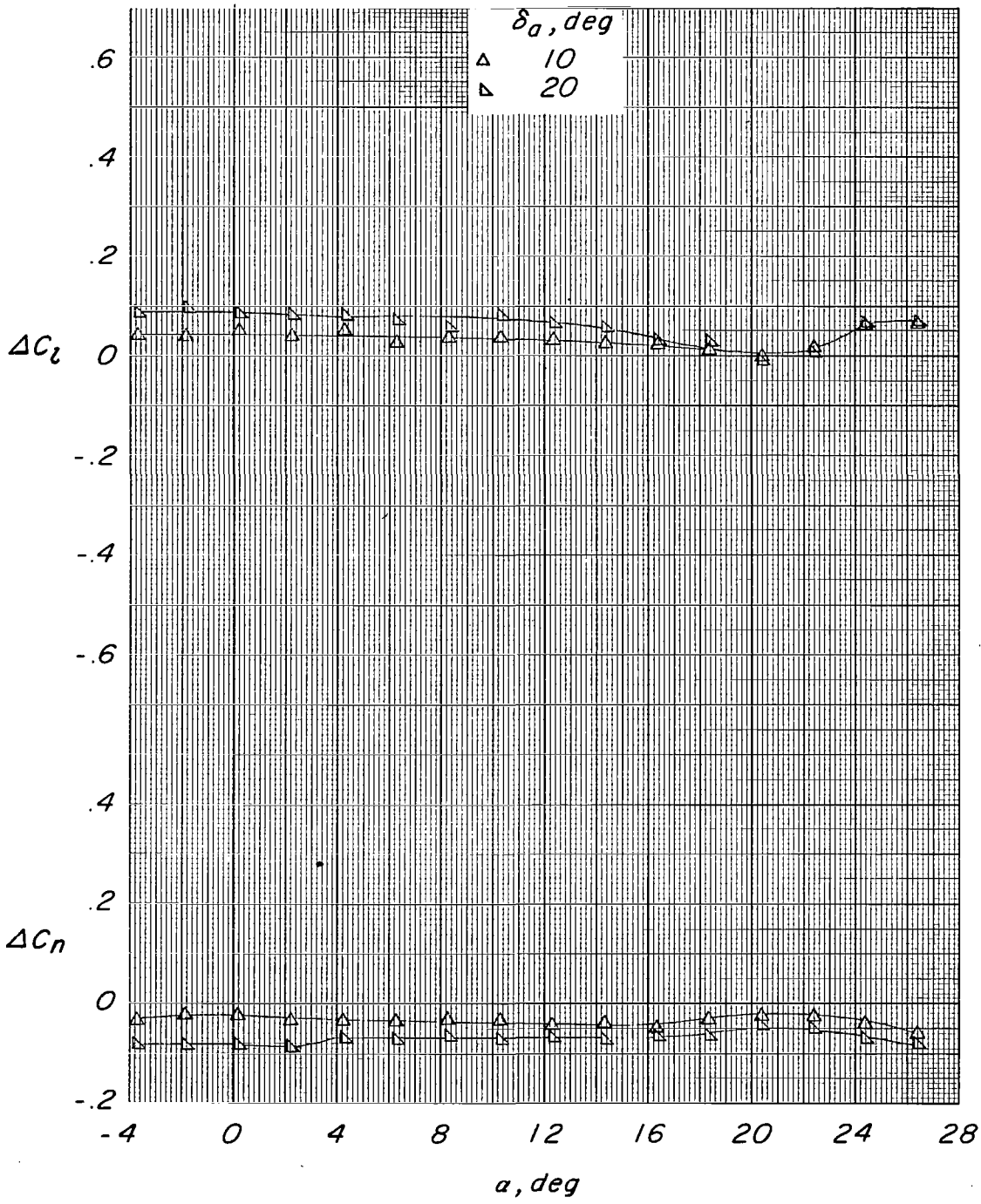

(c) Concluded.

Figure 7.- Concluded.

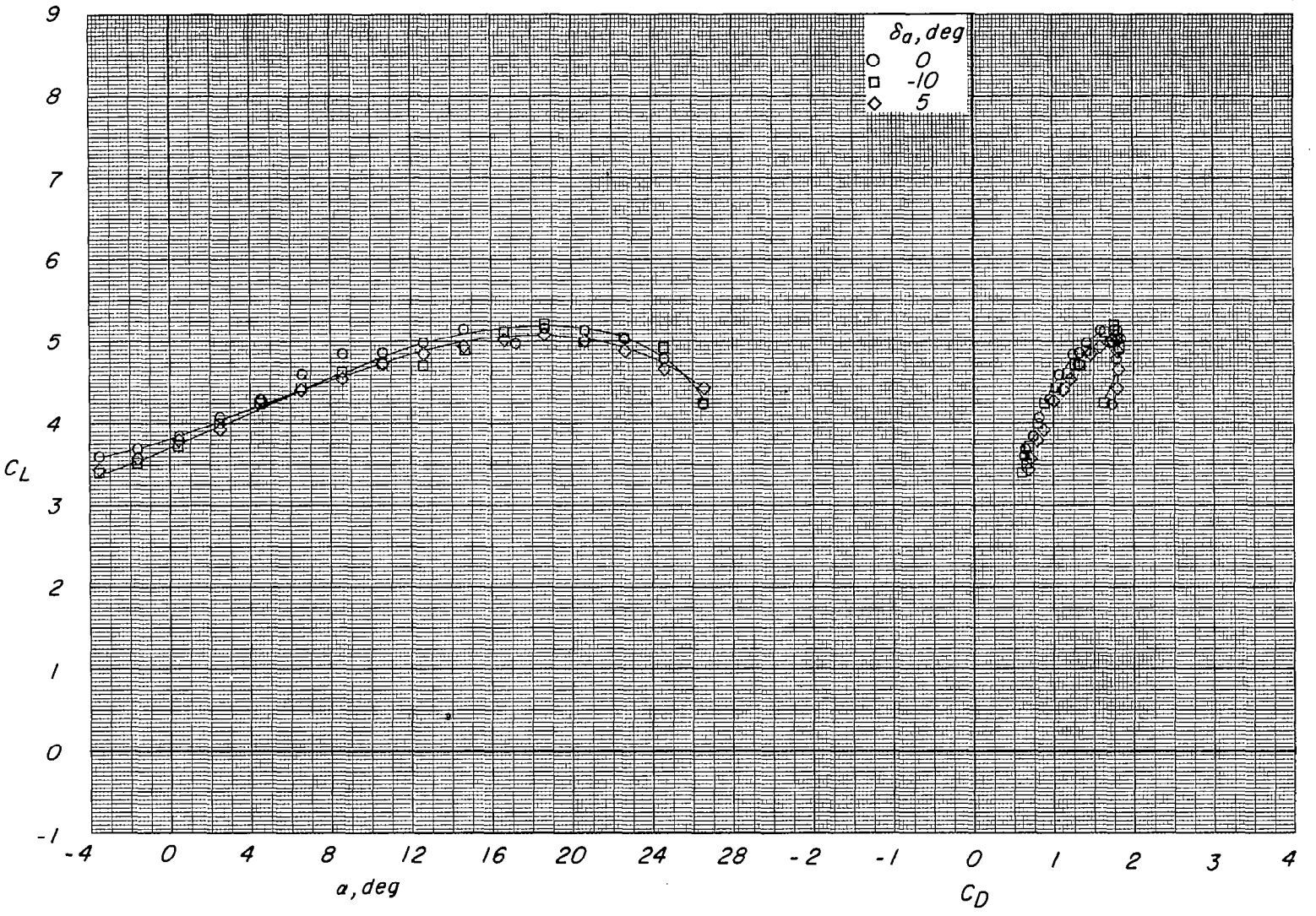

(a) $C_T \approx 0.9$.

Figure 8.- Effect of aileron deflection on configuration D (long span, $\delta_f = 75^\circ$) at several thrust coefficients.

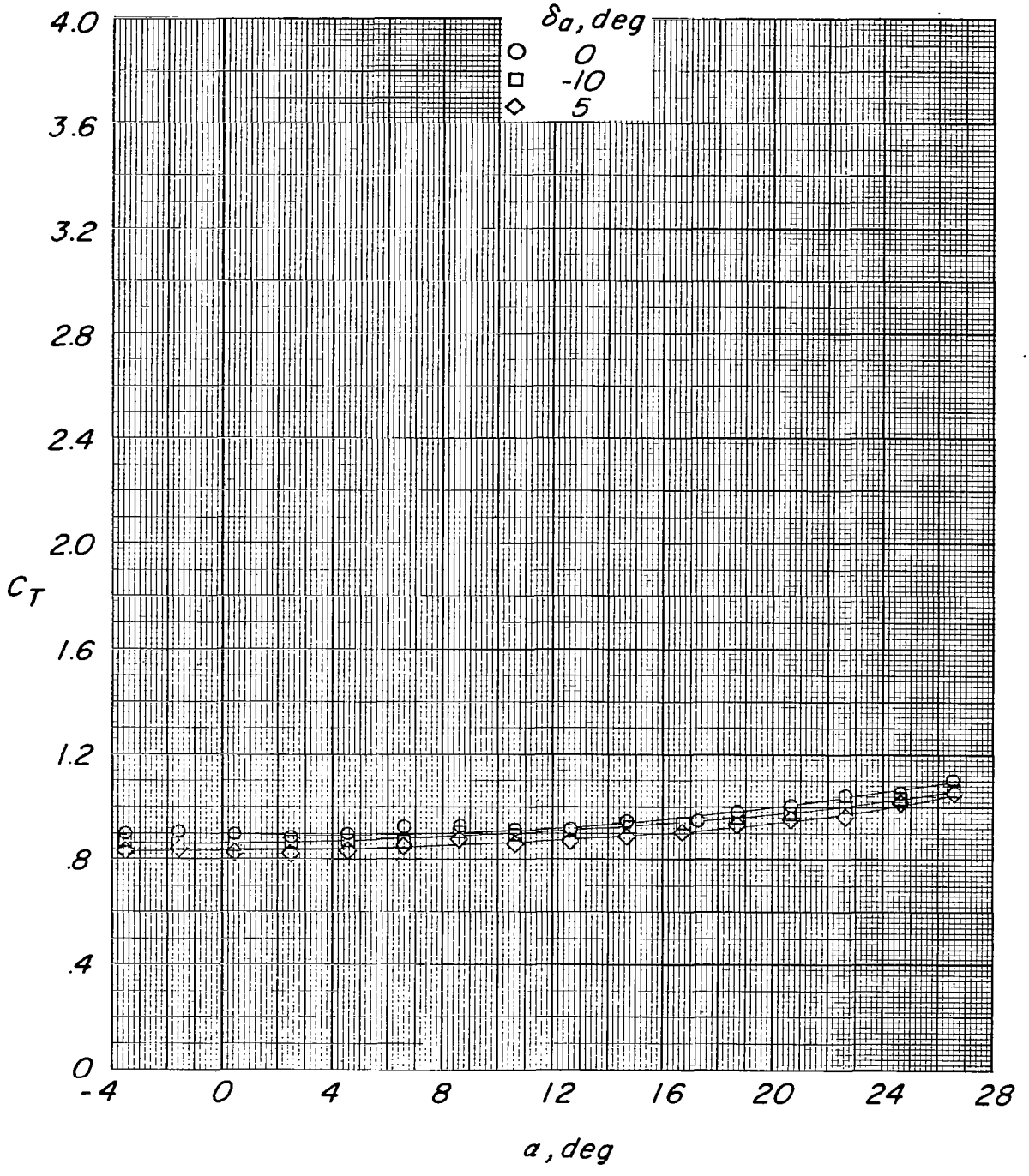

(a) Continued.

Figure 8.- Continued.

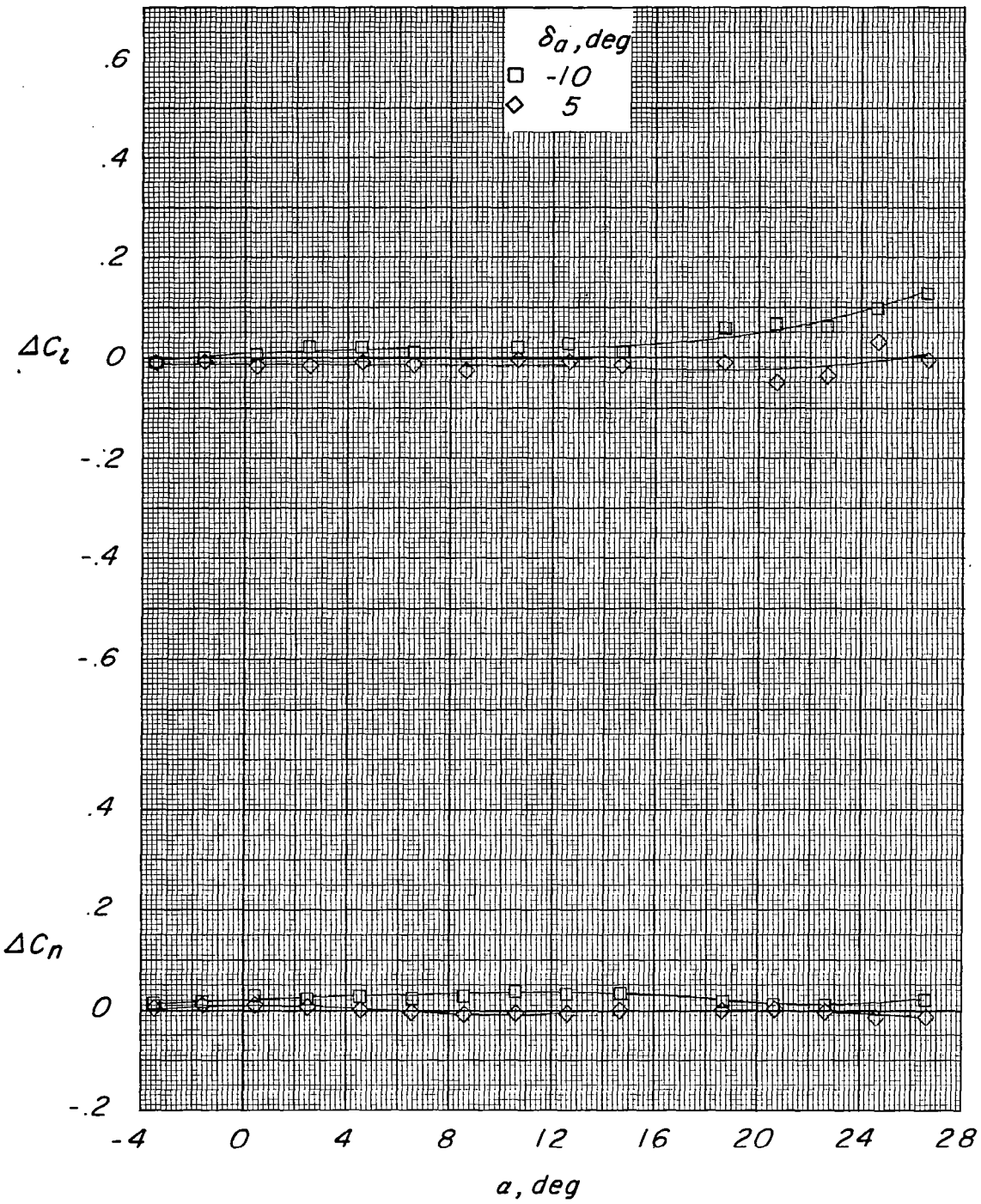

(a) Concluded.

Figure 8.- Continued.

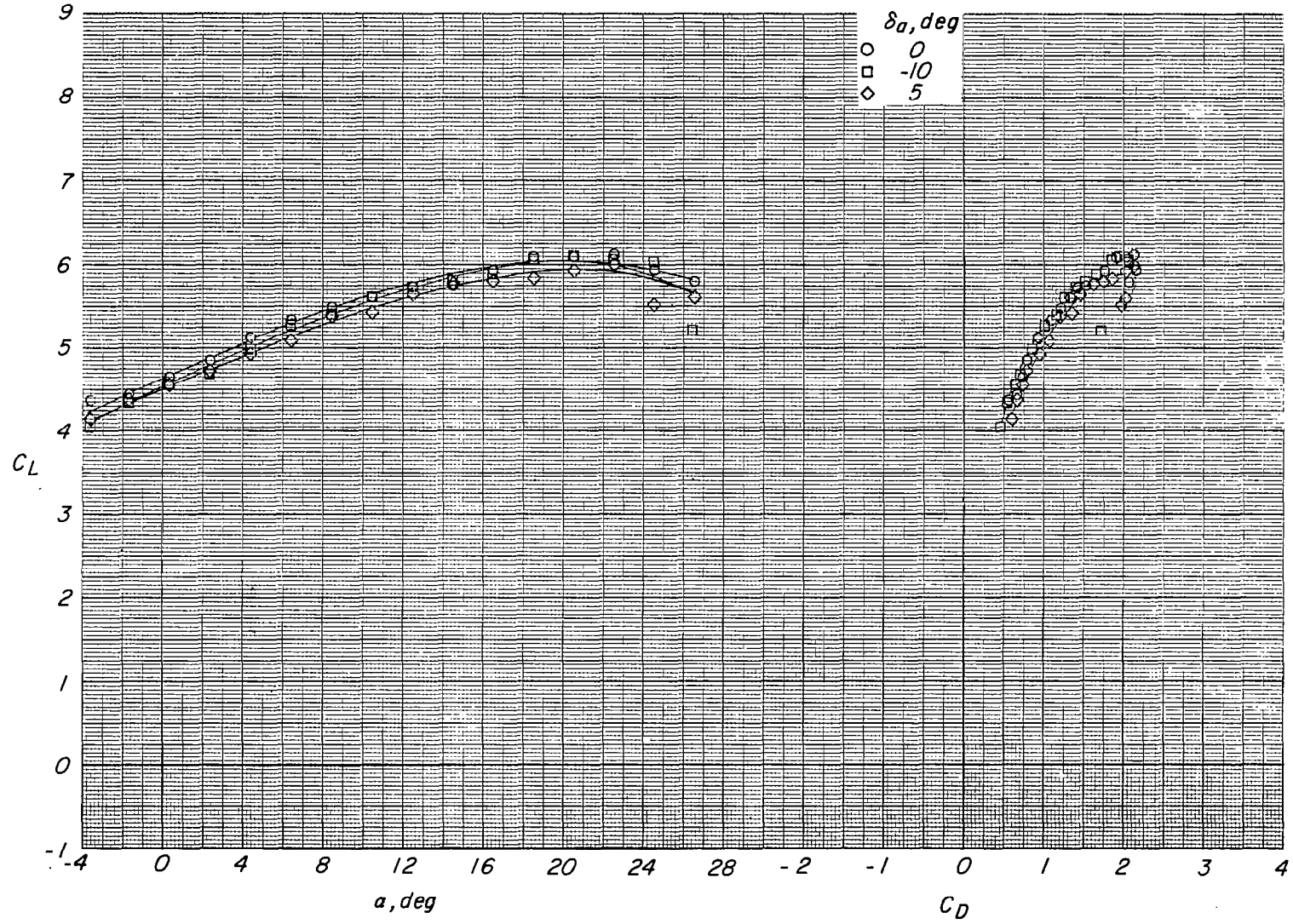

(b) $C_T \approx 1.6$.

Figure 8.- Continued.

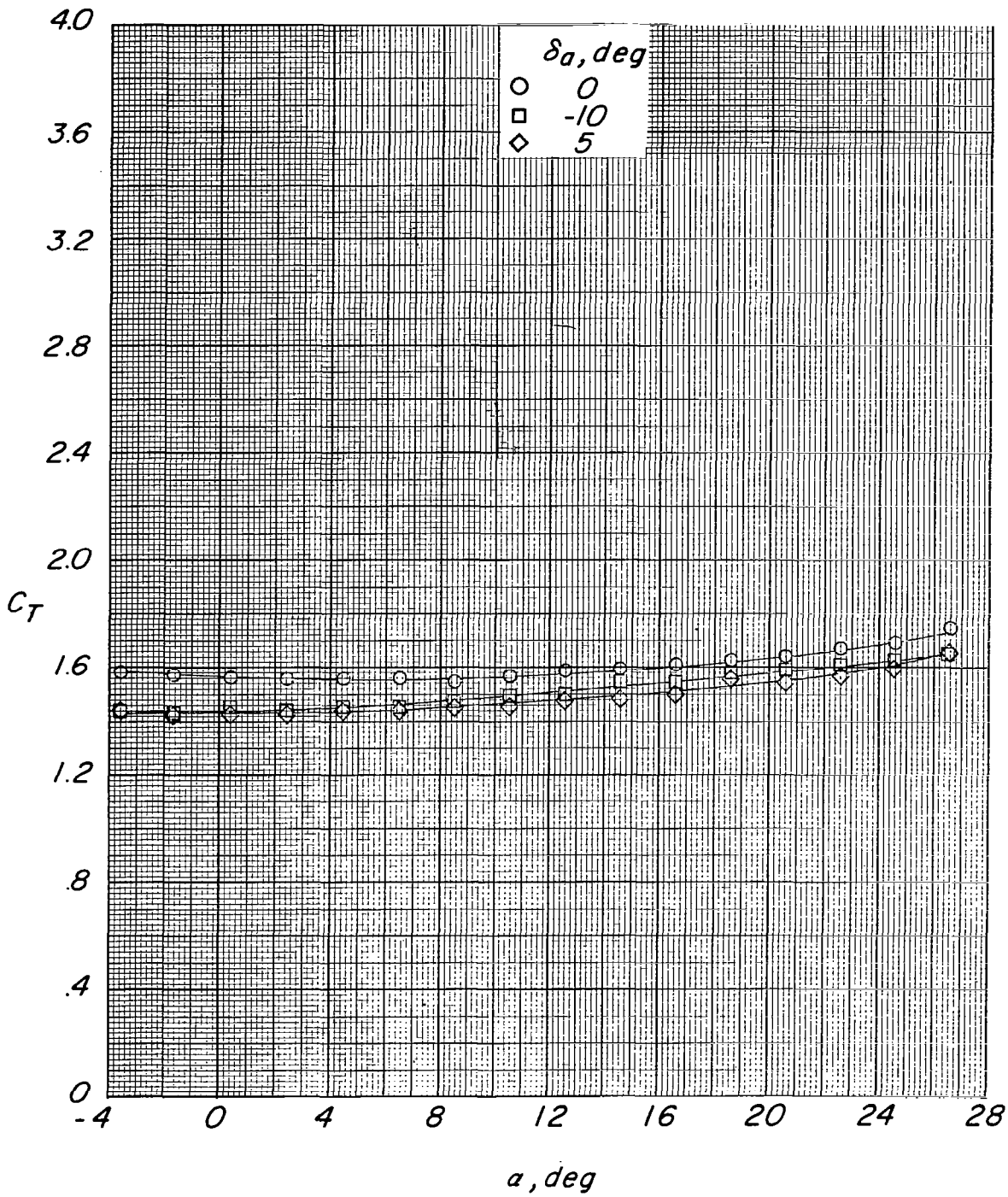

(b) Continued.

Figure 8.- Continued.

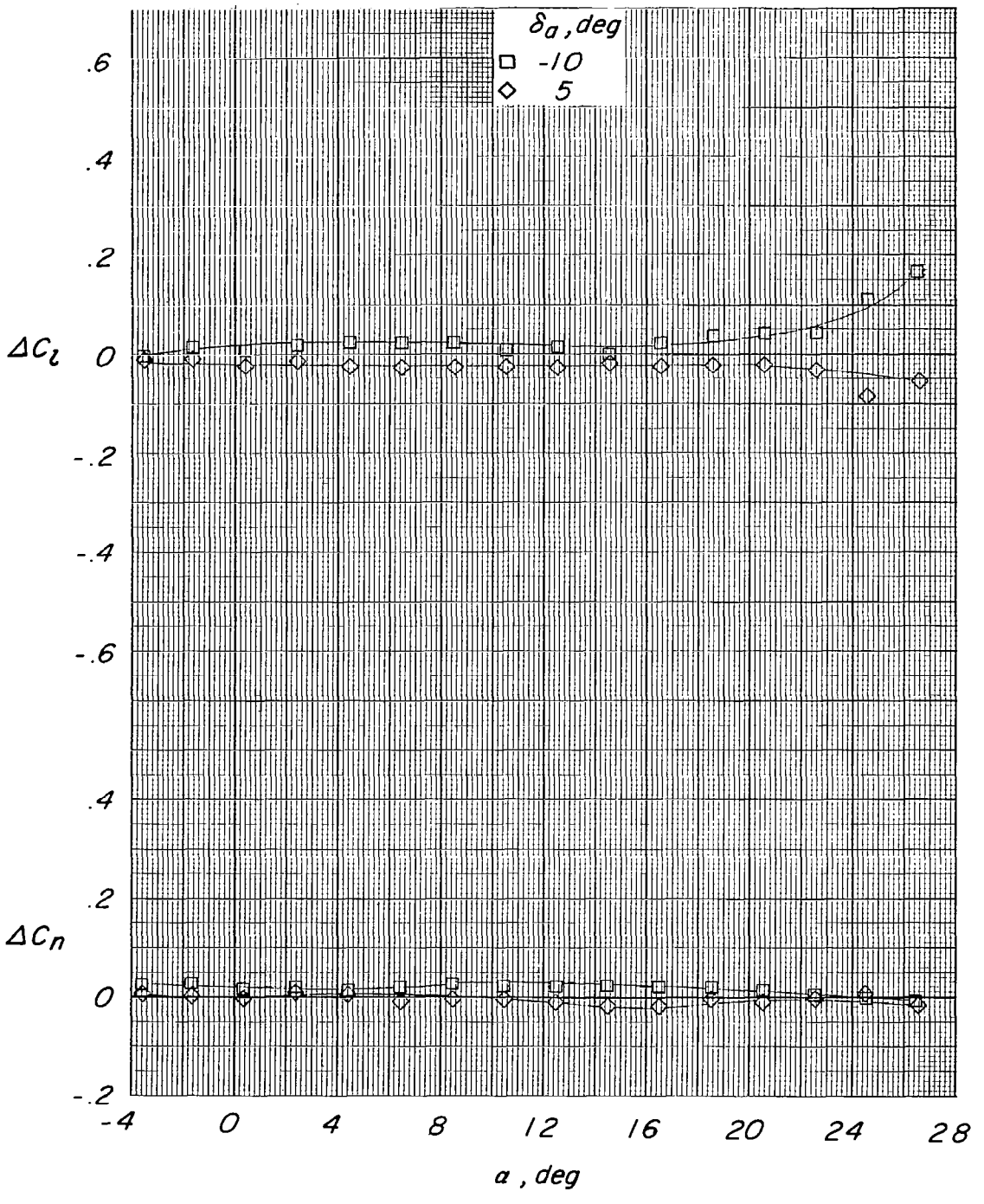

(b) Concluded.

Figure 8.- Continued.

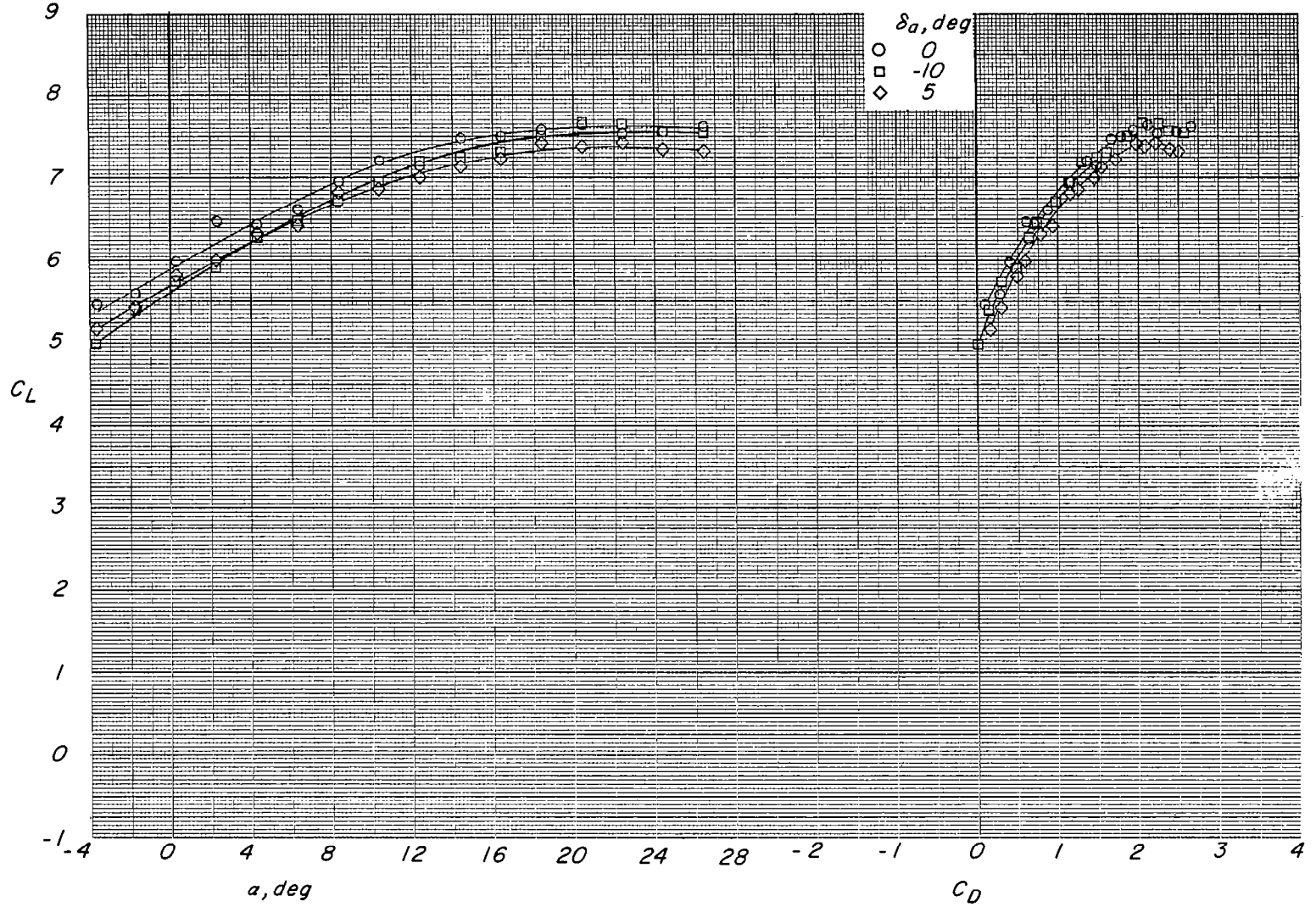

(c) $C_T \approx 2.7$.

Figure 8.- Continued.

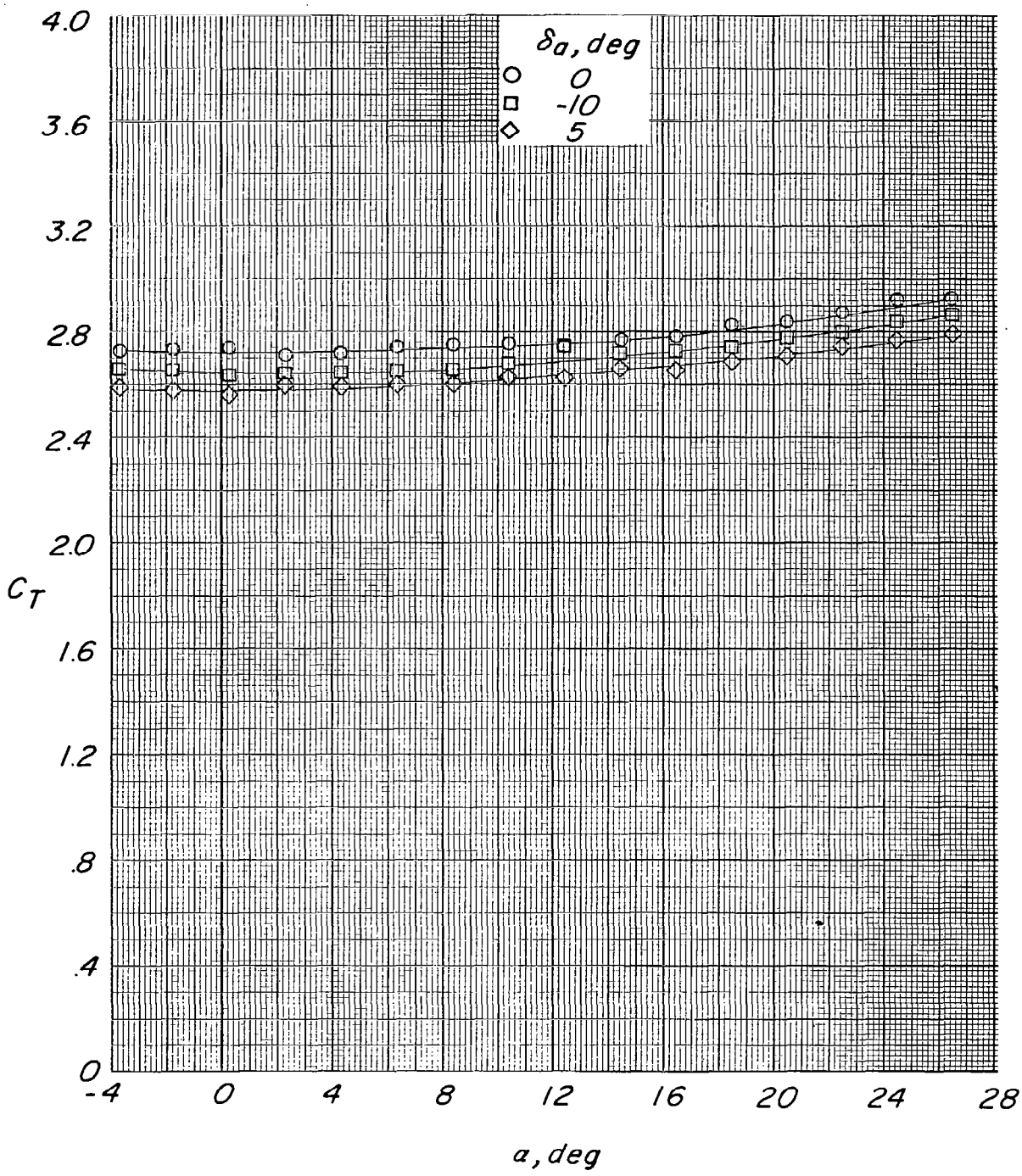

(c) Continued.

Figure 8.- Continued.

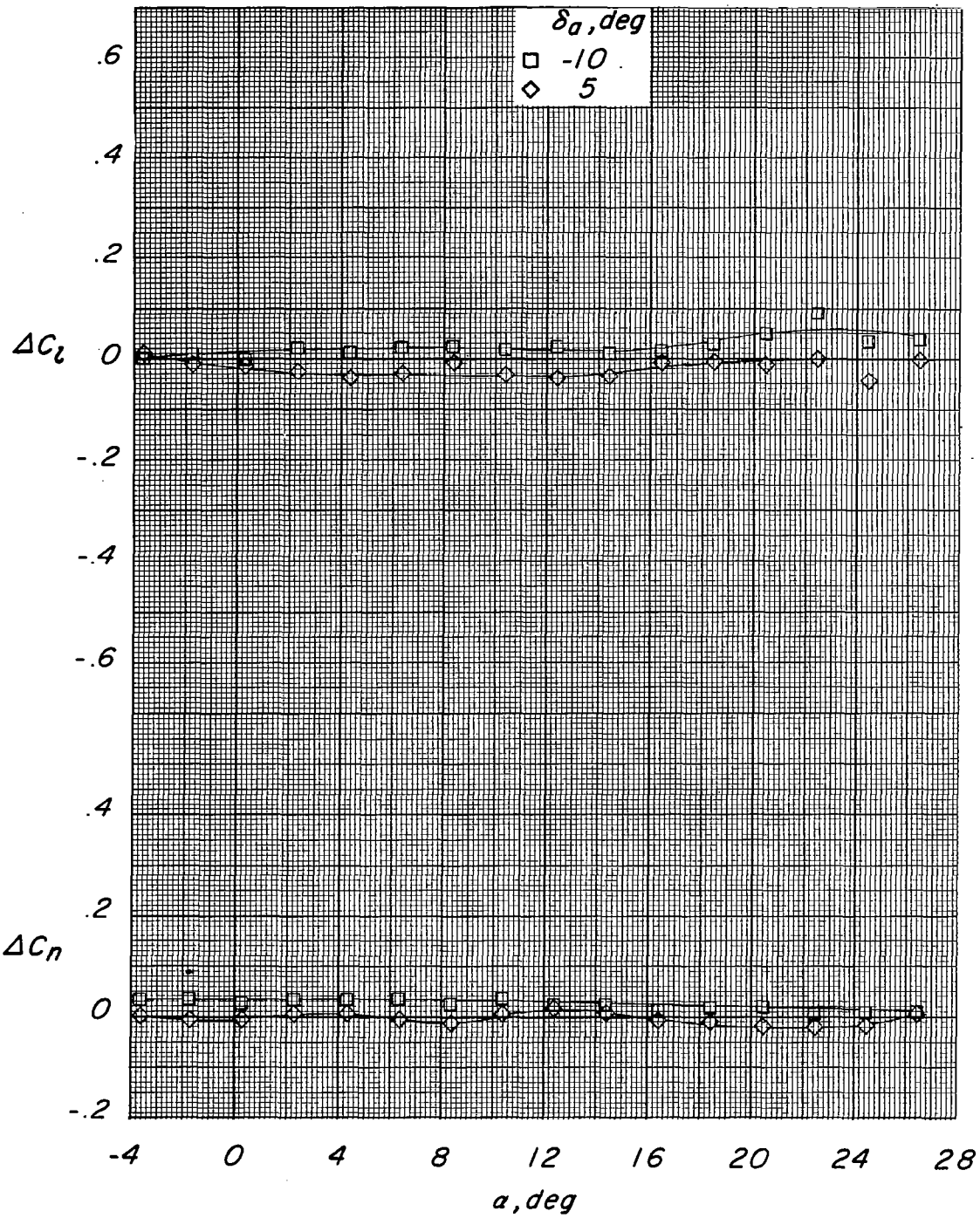

(c) Concluded.

Figure 8.- Concluded.

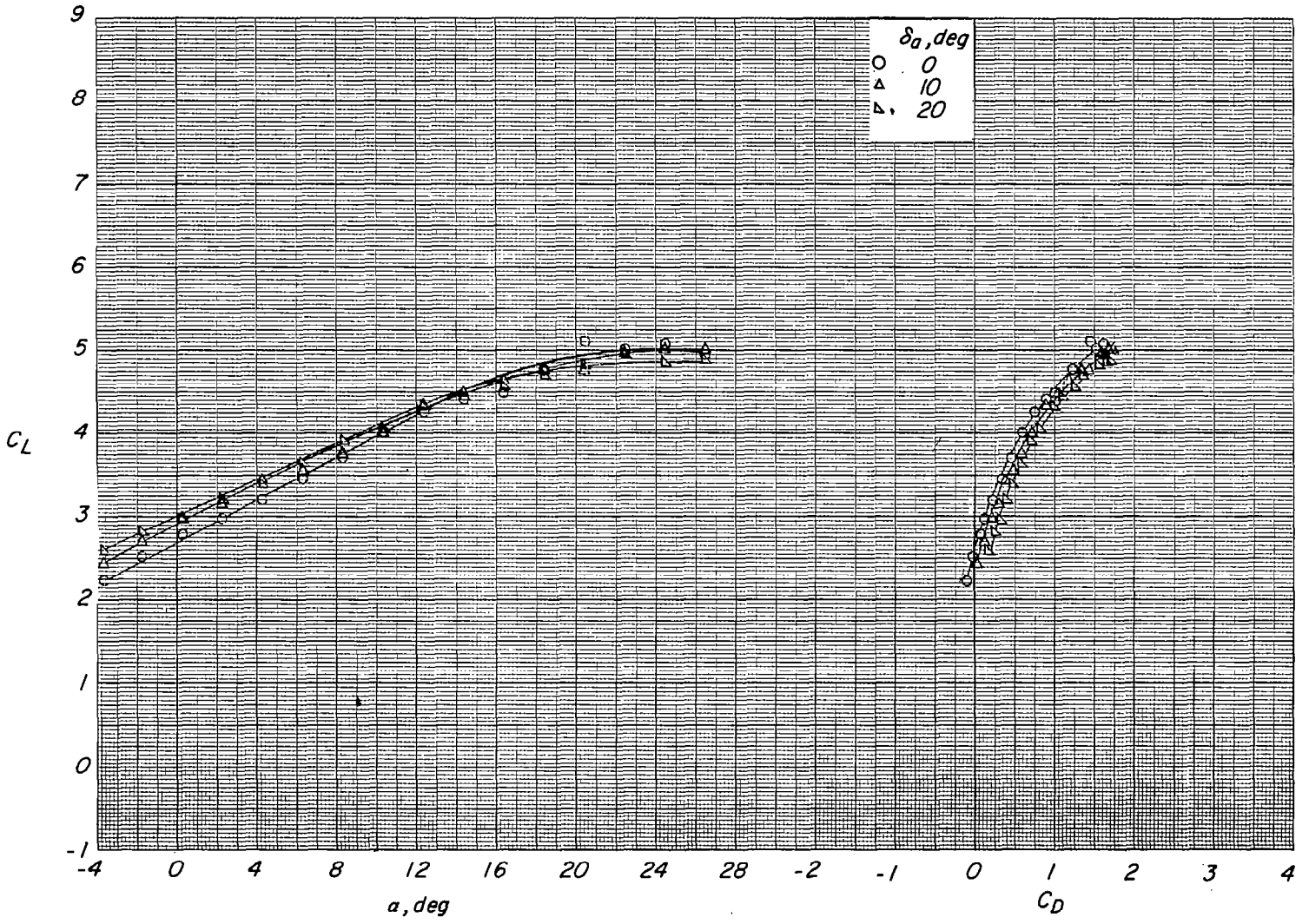

(a) $C_T \approx 1.3$.

Figure 9.- Effect of aileron deflection on configuration F (short span, $\delta_f = 45^\circ$) at several thrust coefficients.

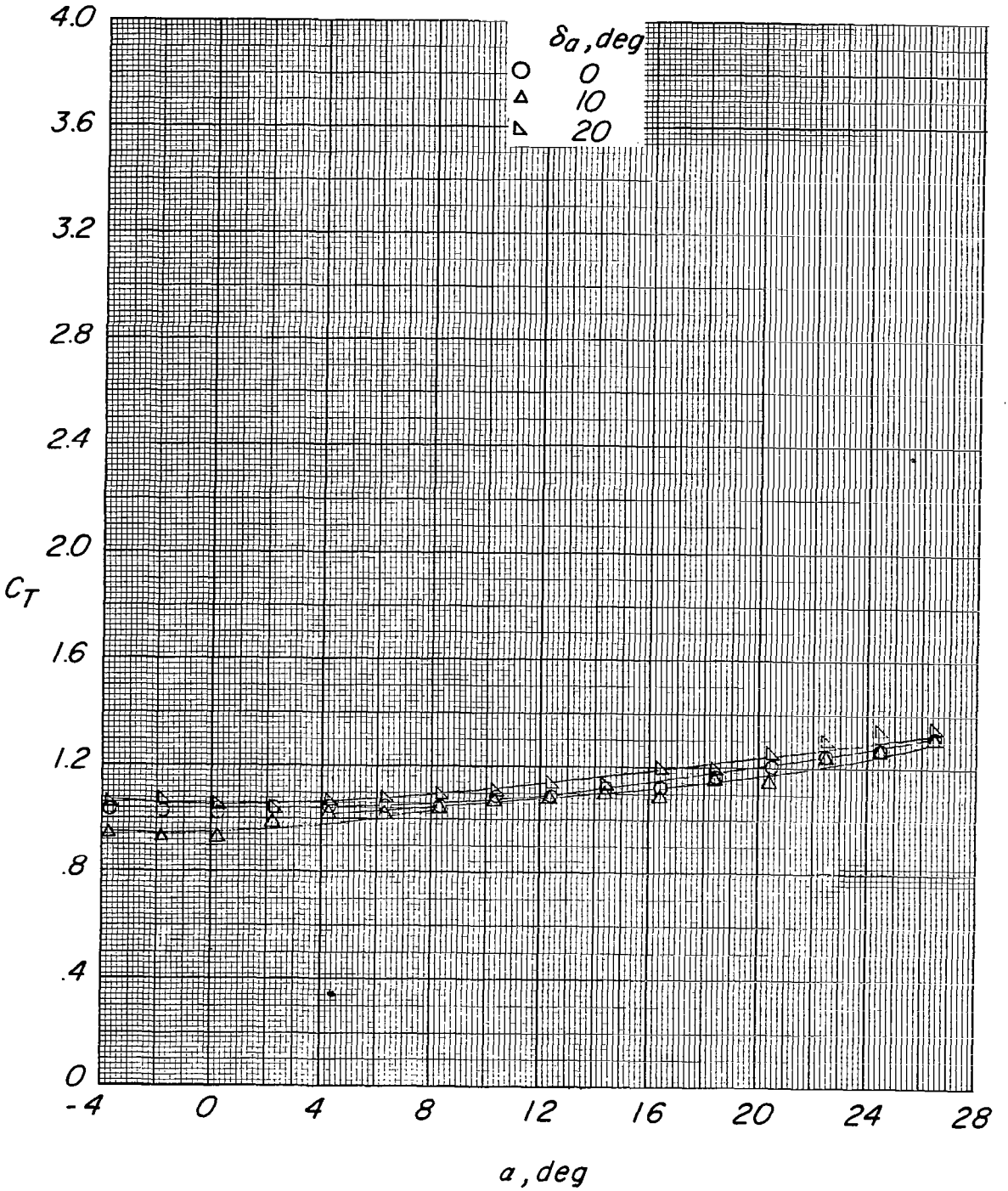

(a) Continued.

Figure 9.- Continued.

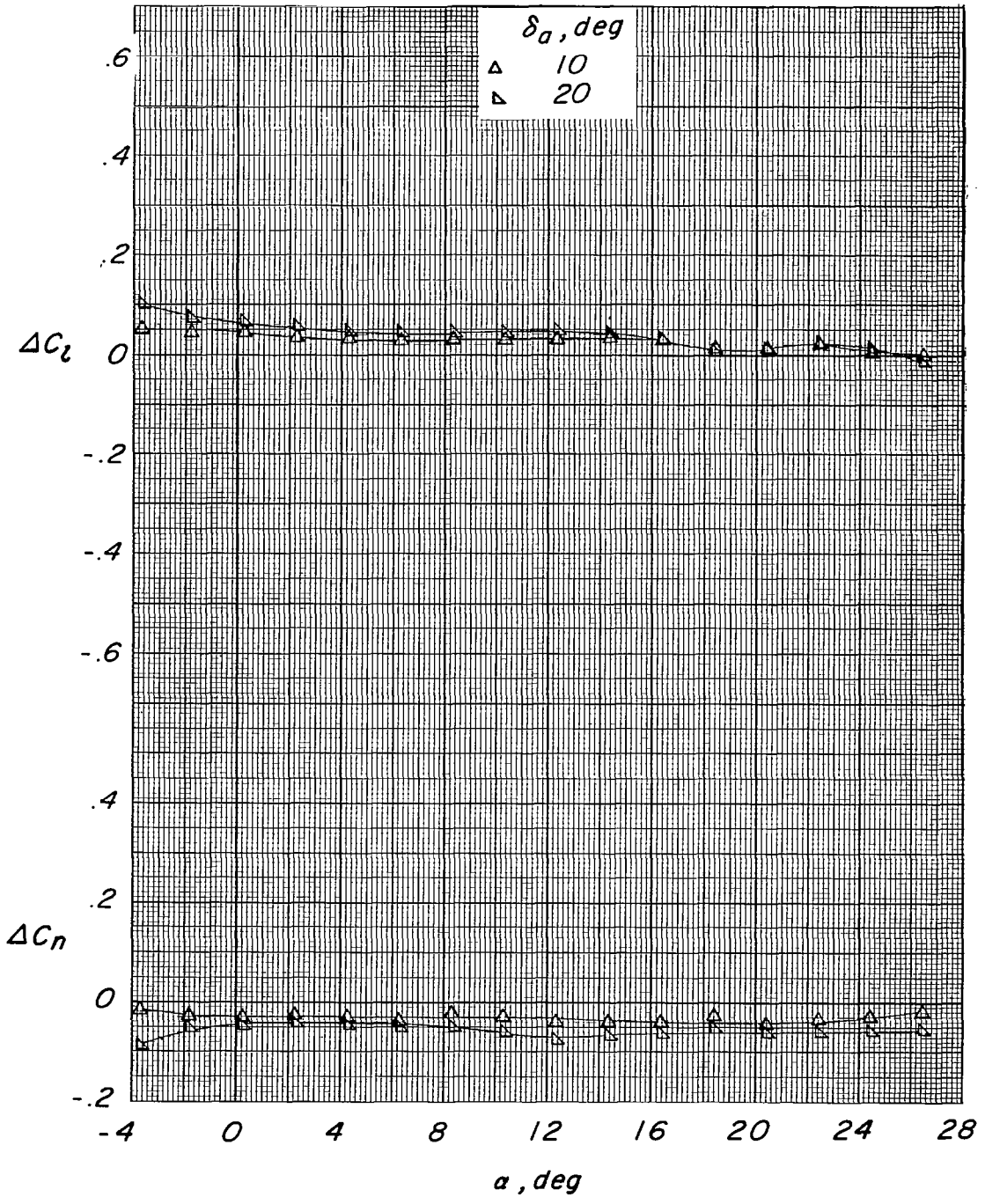

(a) Concluded.

Figure 9.- Continued.

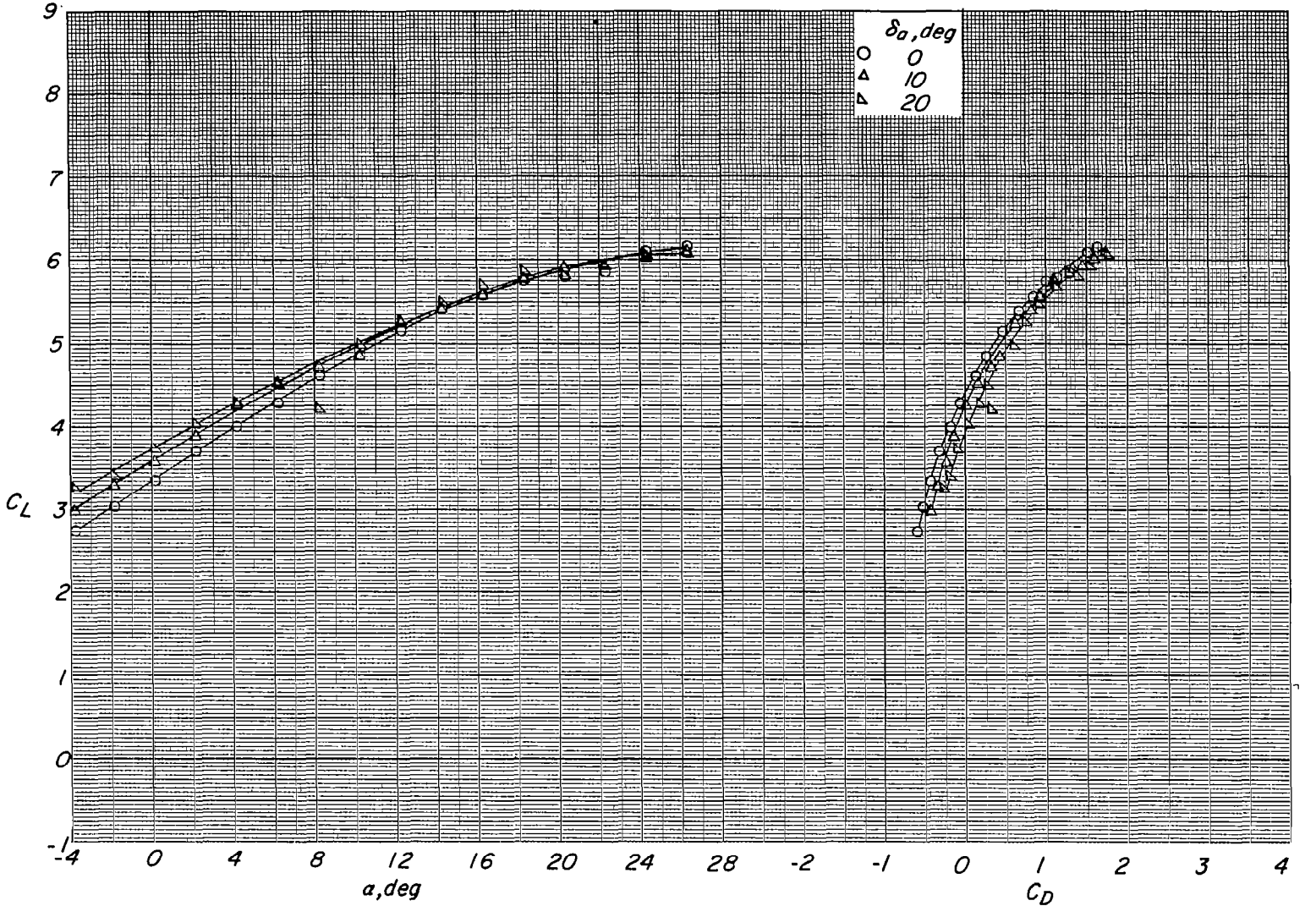

(b) $C_T \approx 2.2$.

Figure 9.- Continued.

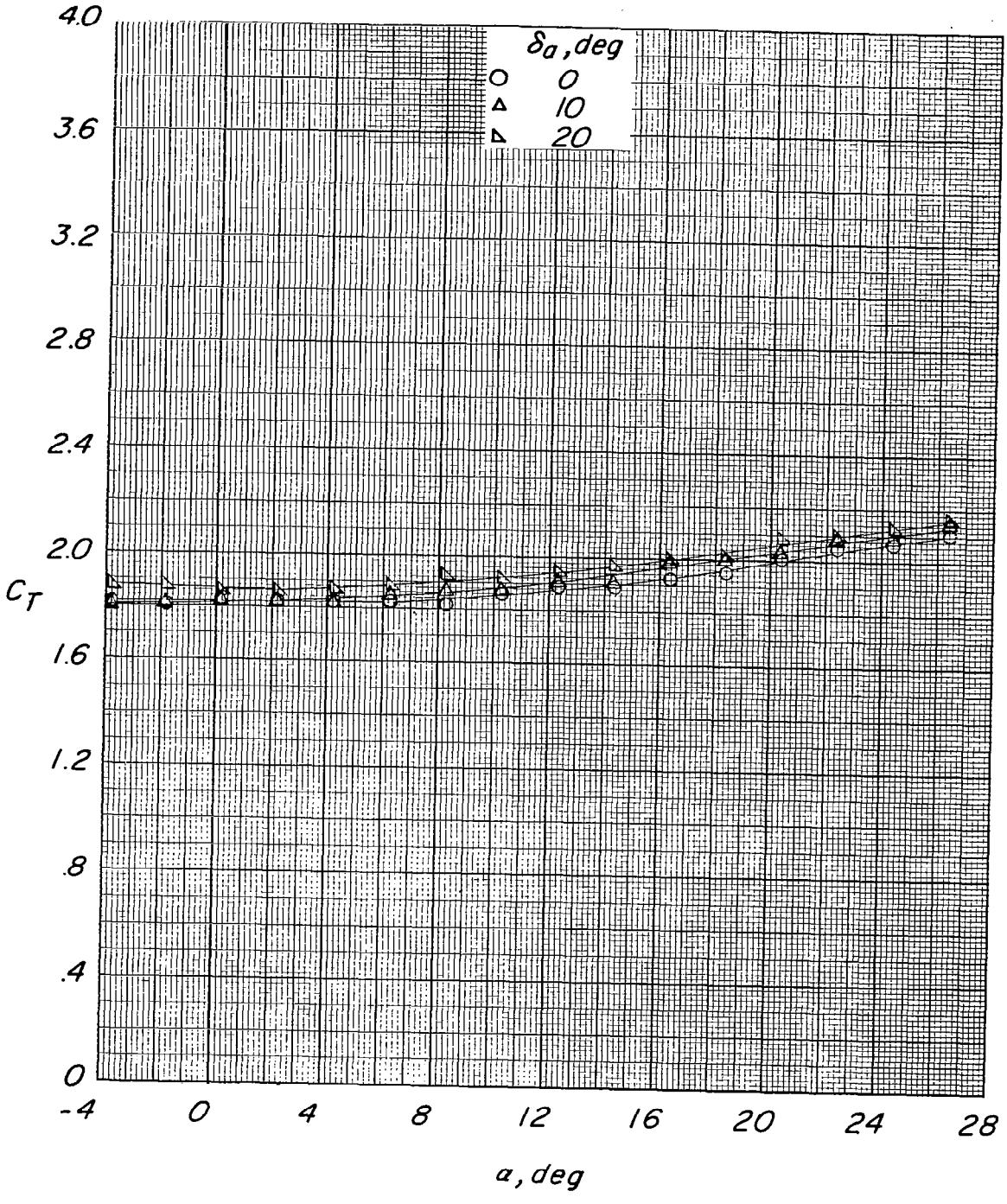

(b) Continued.

Figure 9.- Continued.

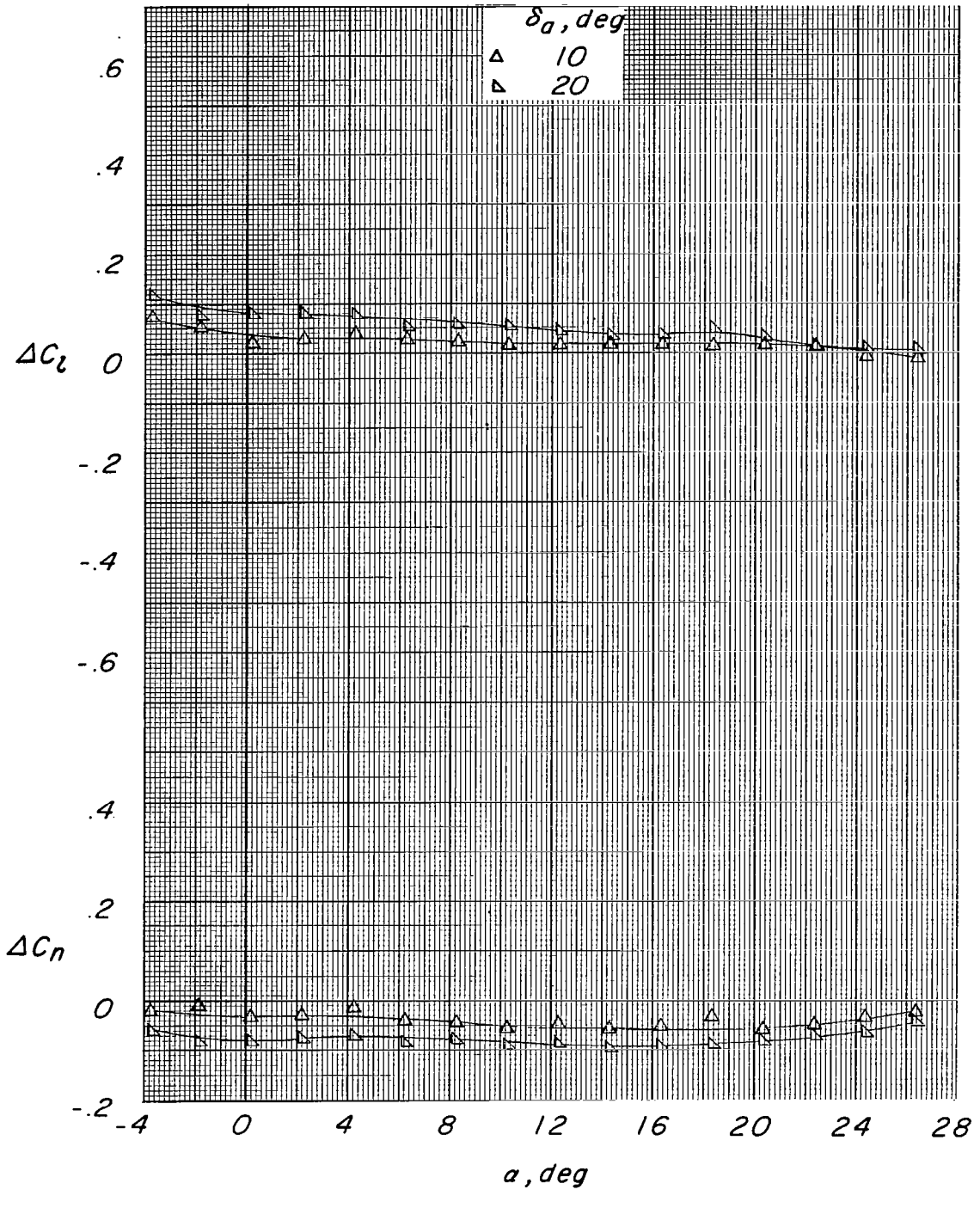

(b) Concluded.

Figure 9.- Continued.

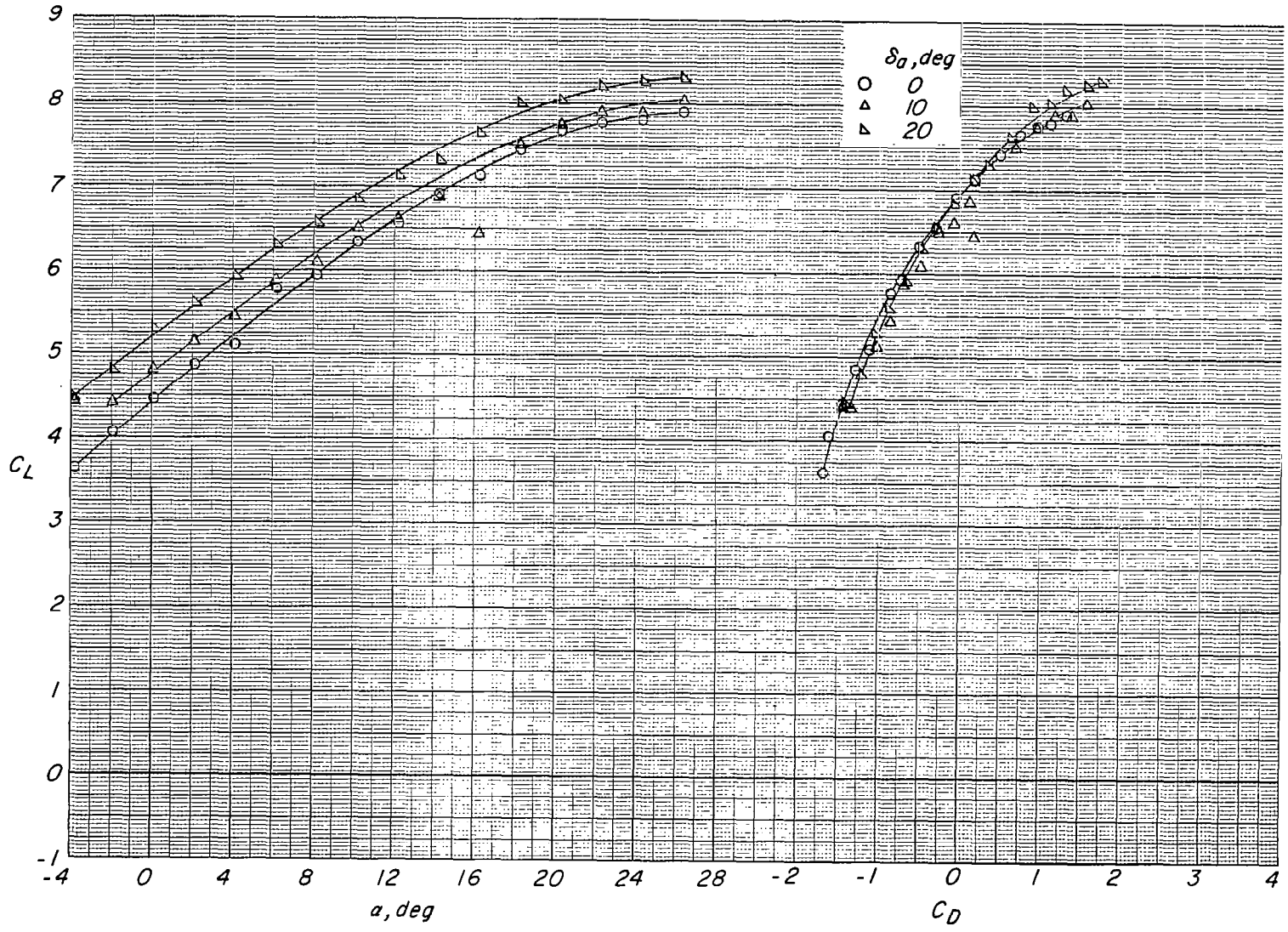

(c) $C_T \approx 3.8$.

Figure 9.- Continued.

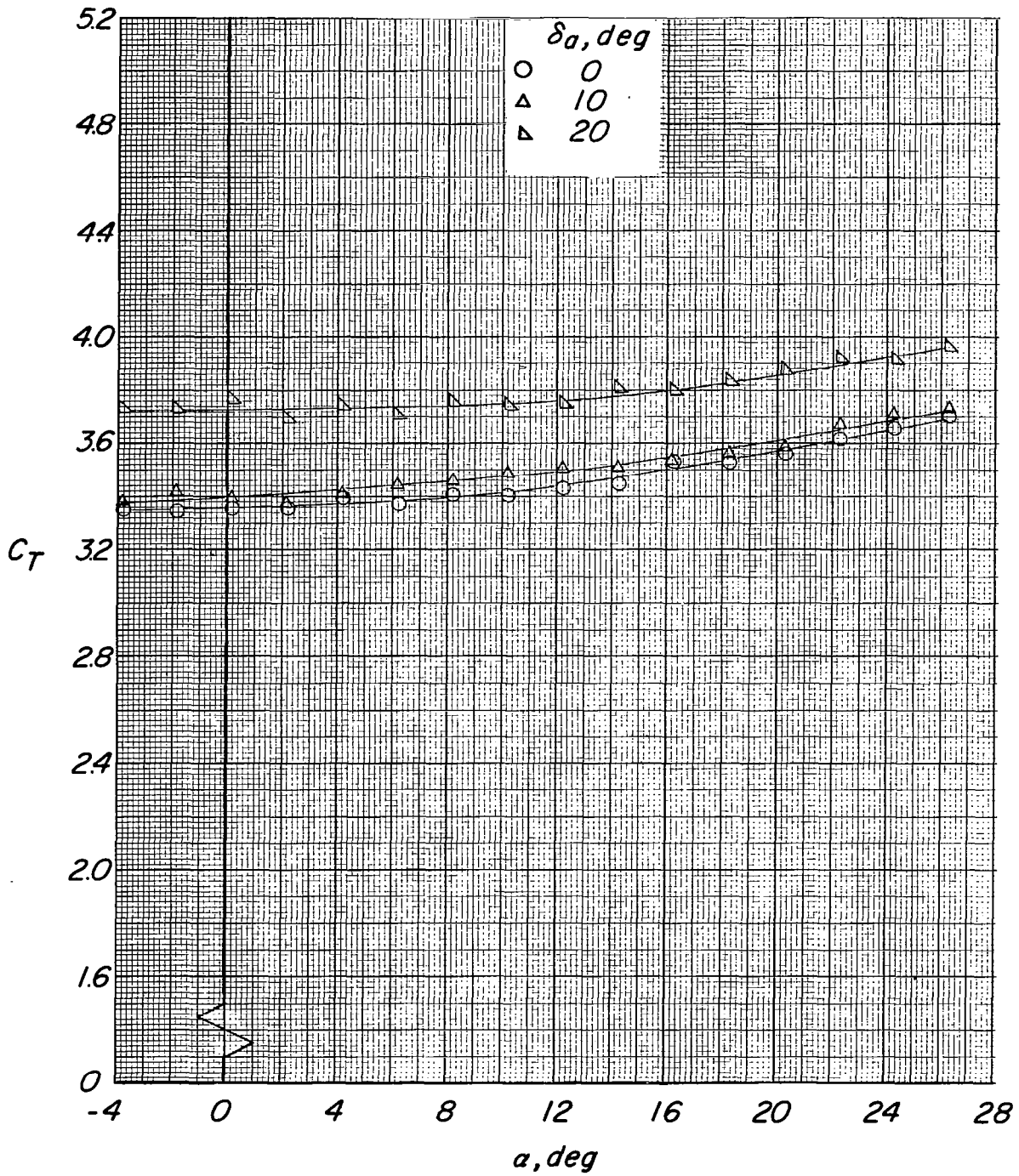

(c) Continued.

Figure 9.- Continued.

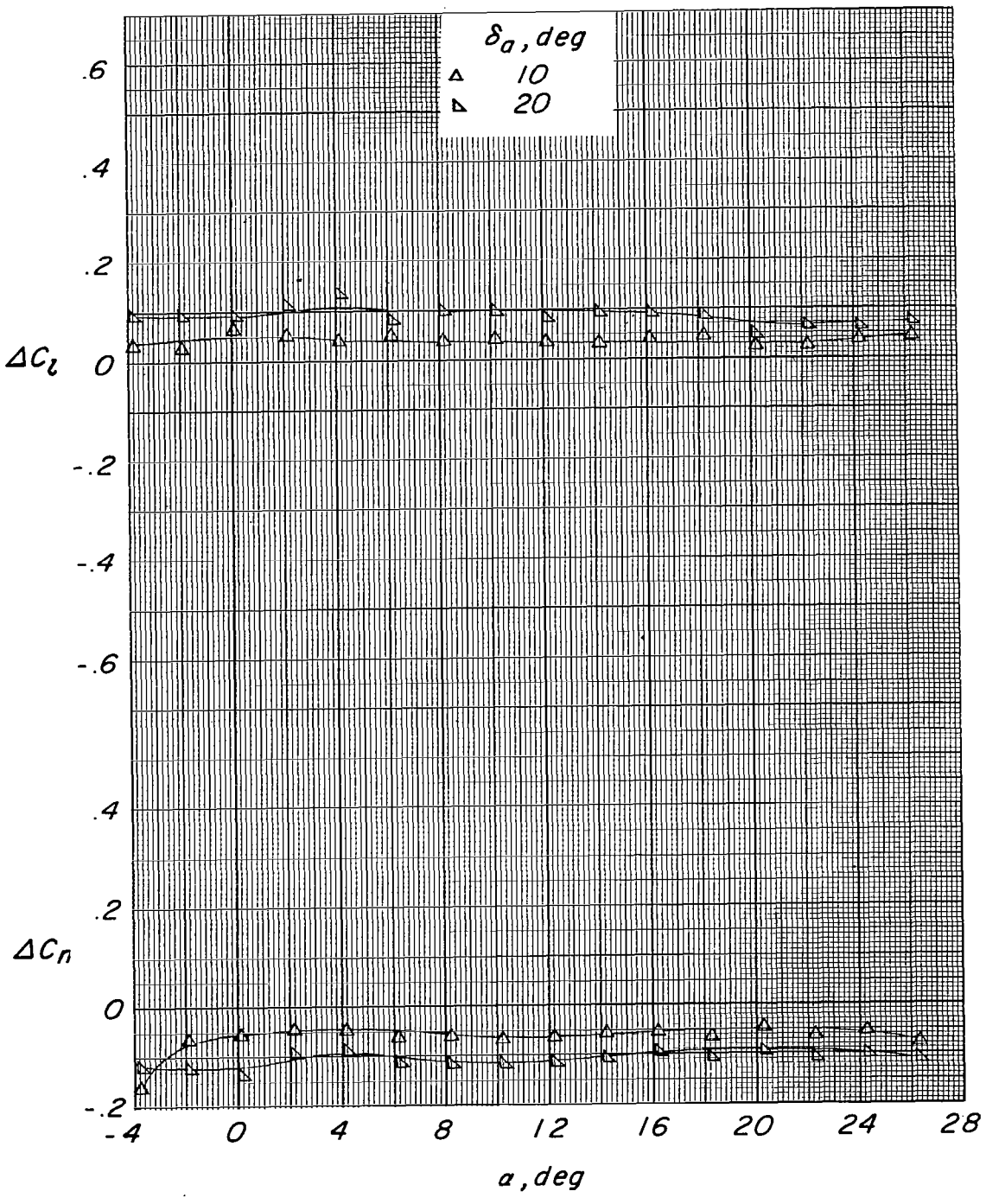

(c) Concluded.

Figure 9.- Concluded.

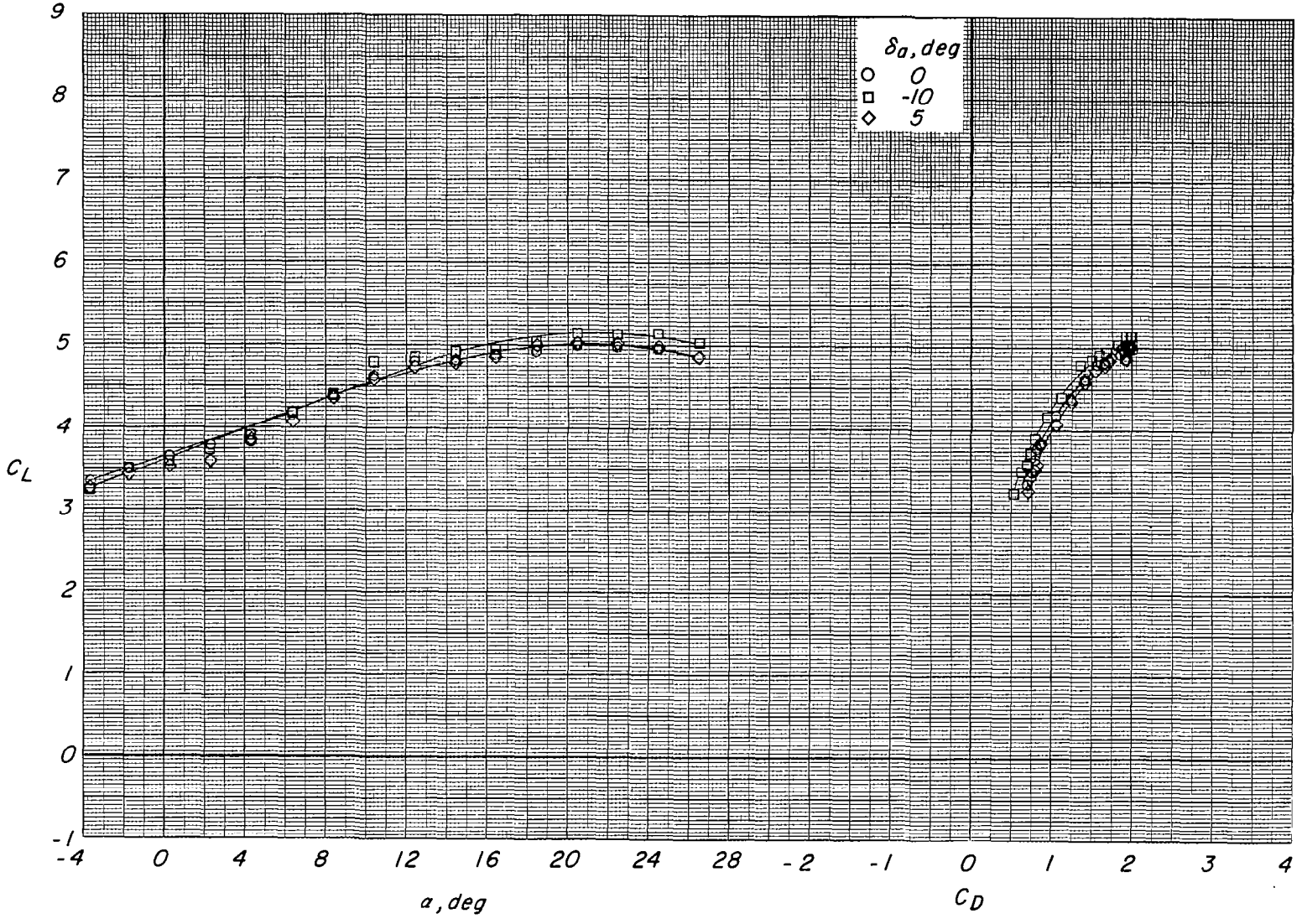

(a) $C_T \approx 1.3$.

Figure 10.- Effect of aileron deflection on configuration G (short span, $\delta_f = 75^\circ$) at several thrust coefficients.

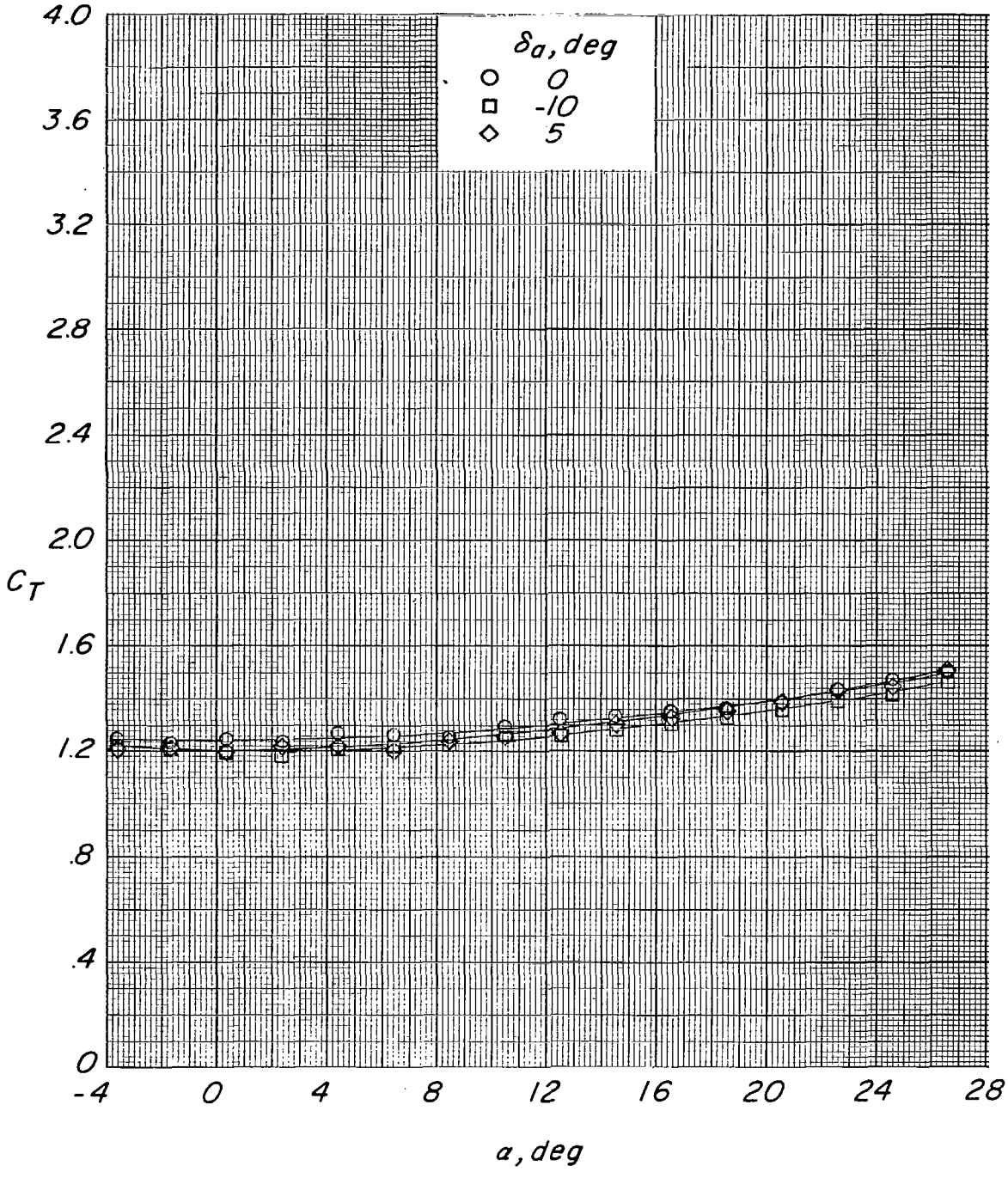

(a) Continued.

Figure 10.- Continued.

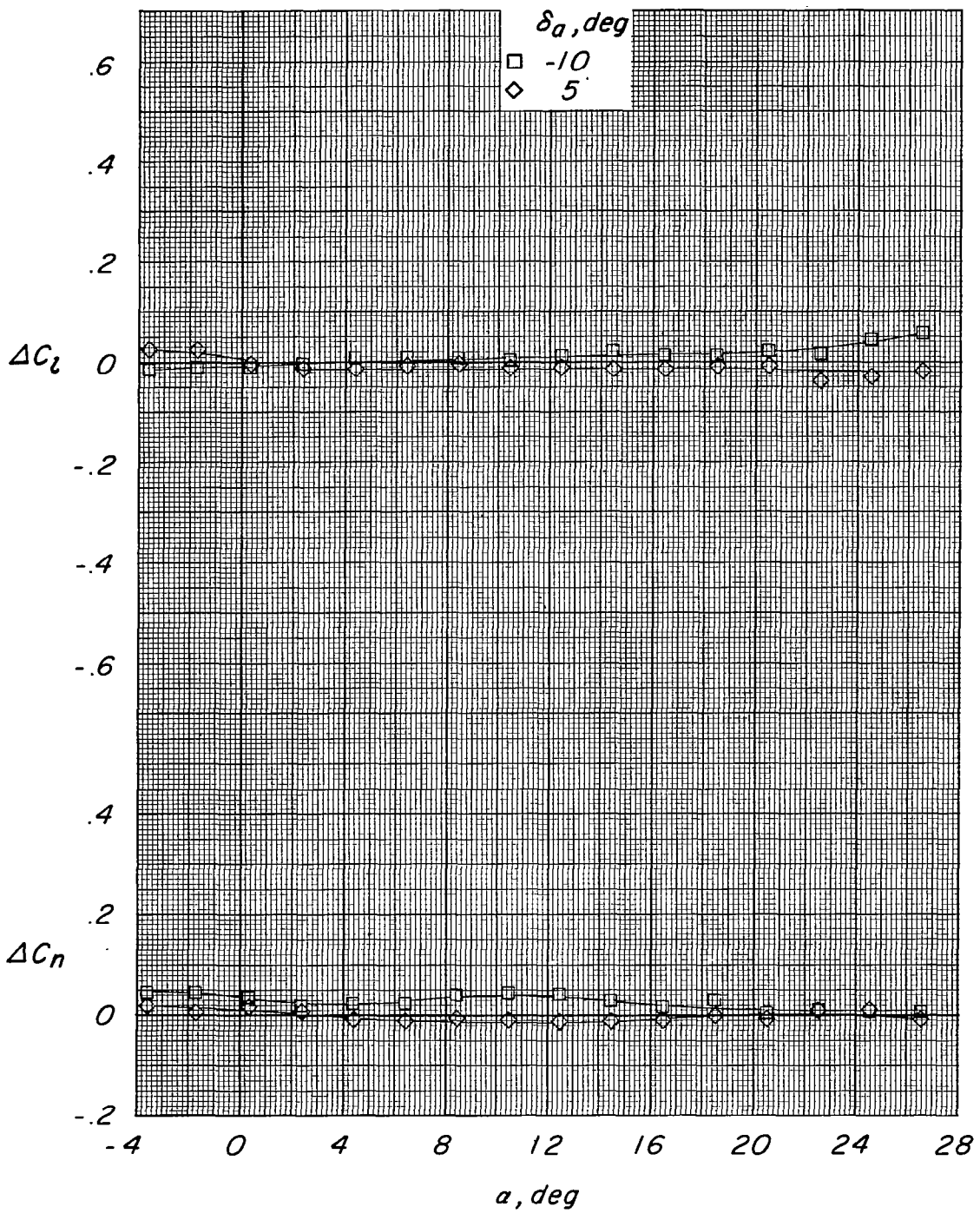

(a) Concluded.

Figure 10.- Continued.

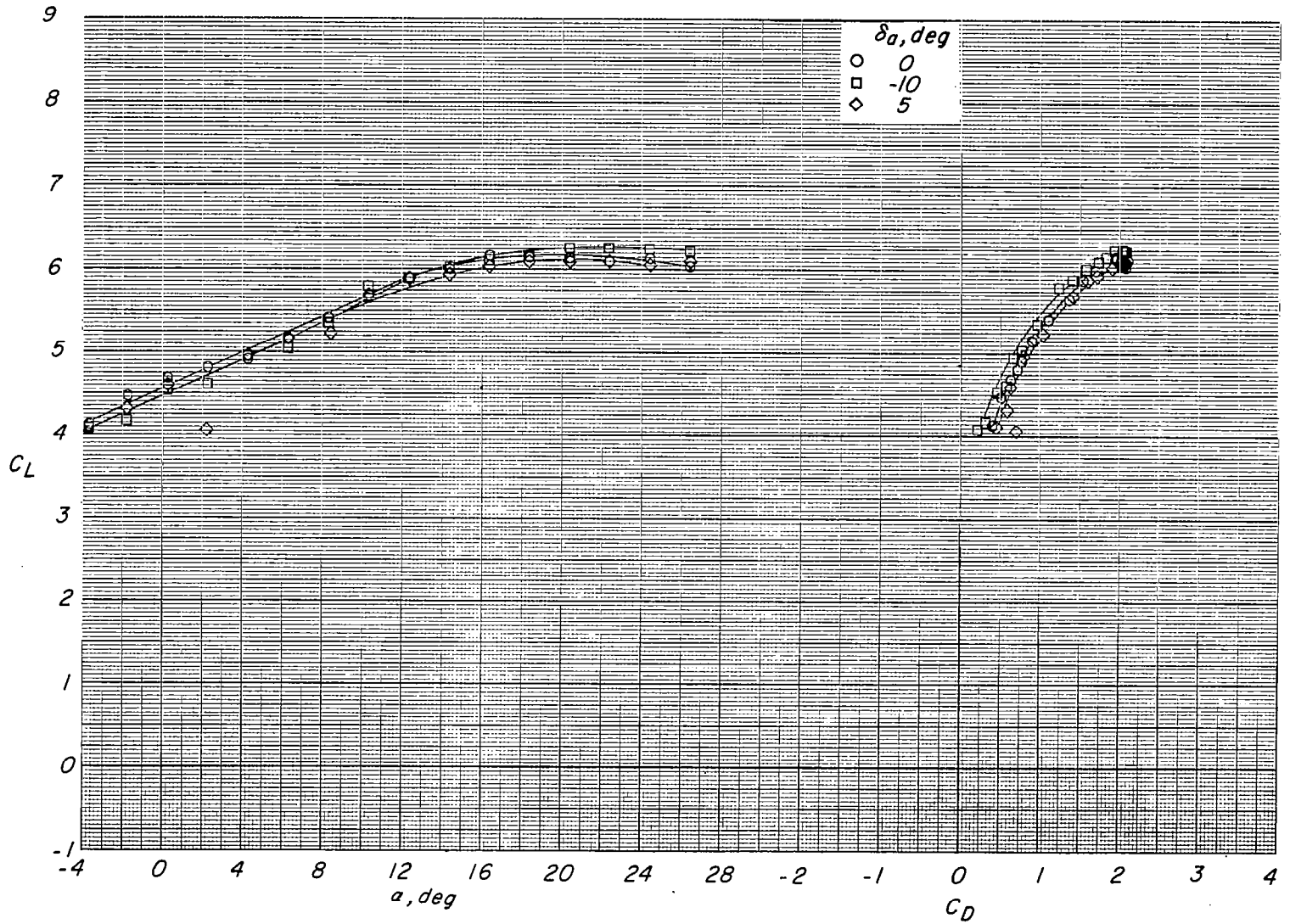

(b) $C_T \approx 2.2$.

Figure 10.- Continued.

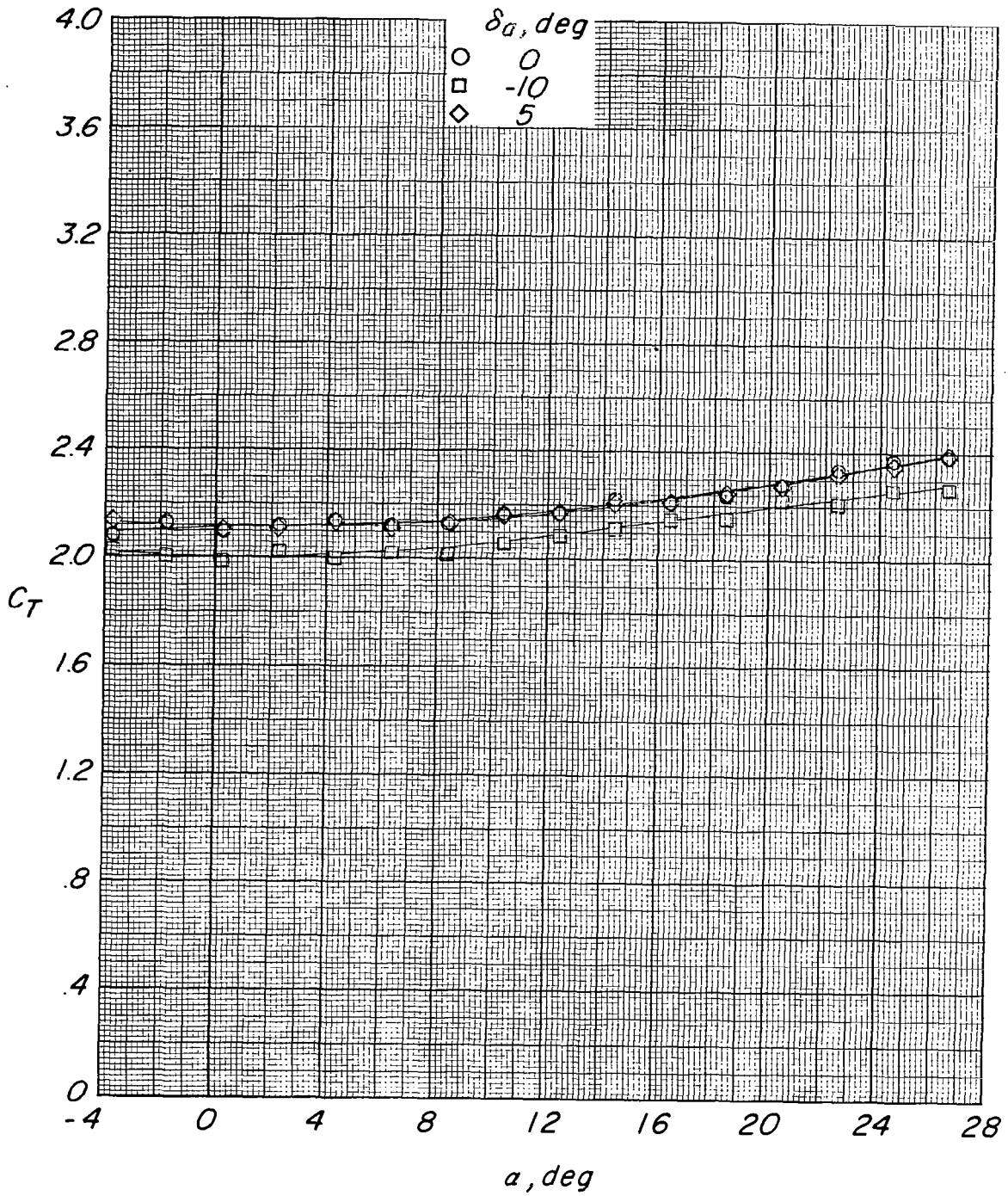

(b) Continued.

Figure 10.- Continued.

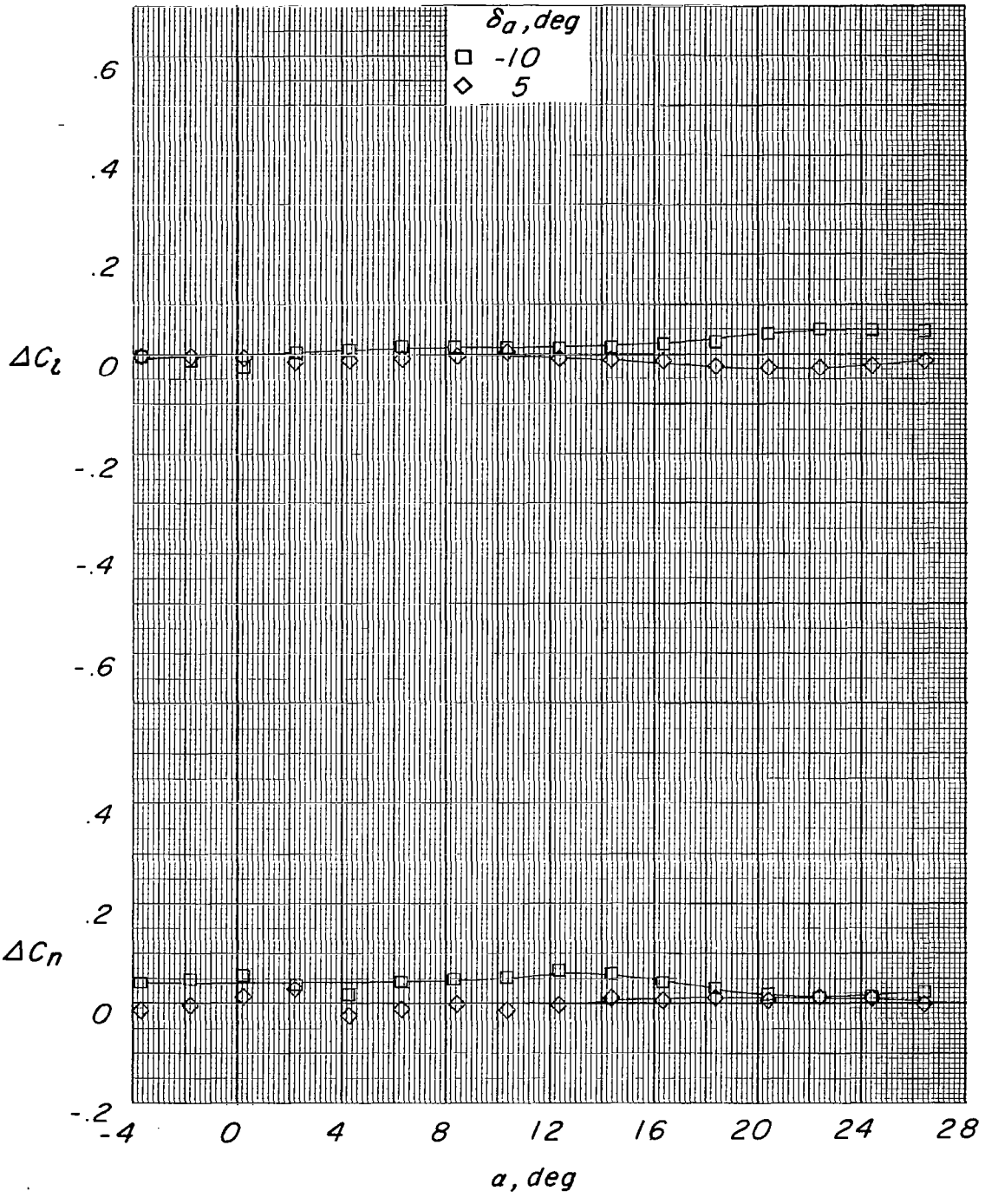

(b) Concluded.

Figure 10.- Continued.

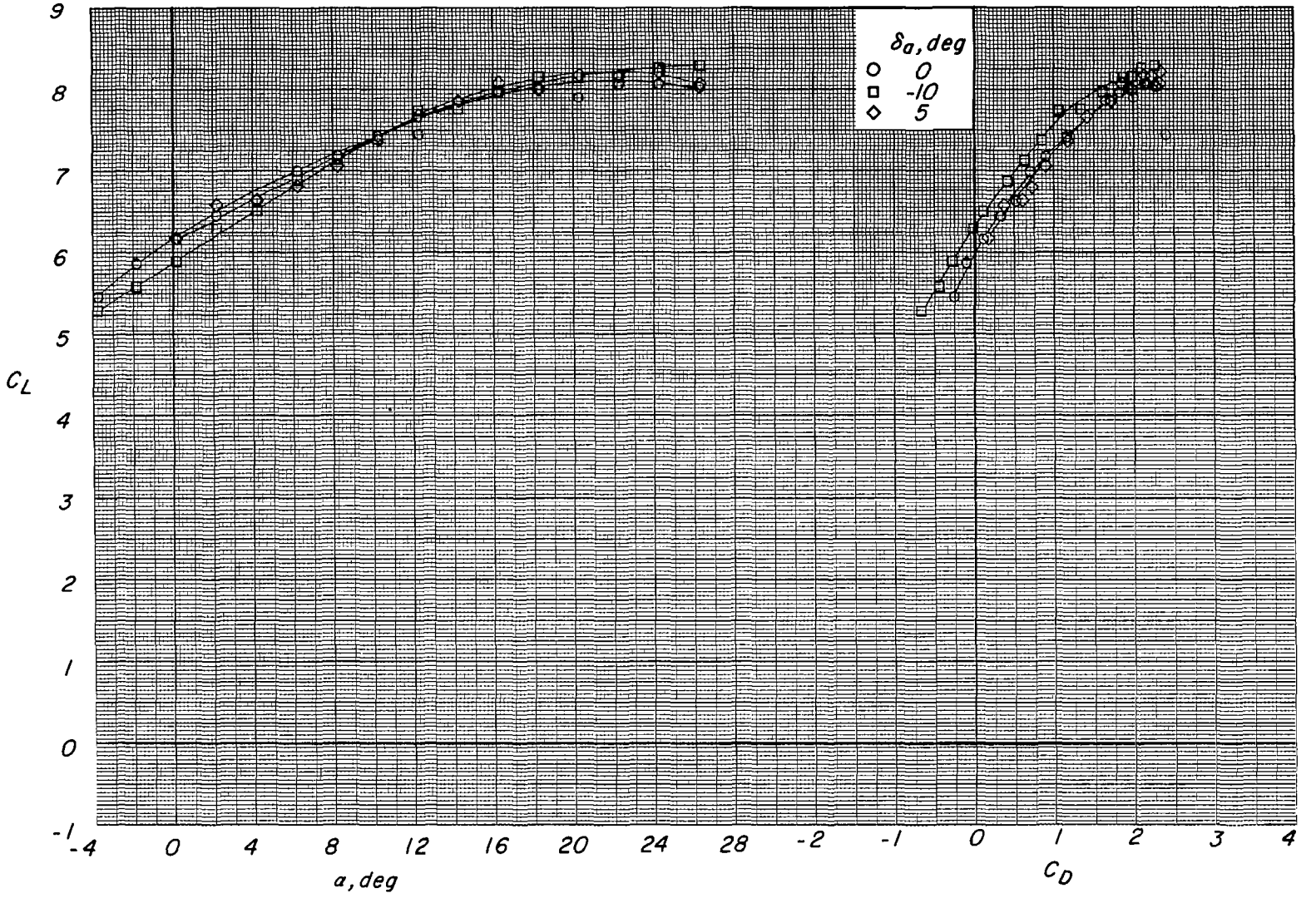

(c) $C_T \approx 3.8$.

Figure 10.- Continued.

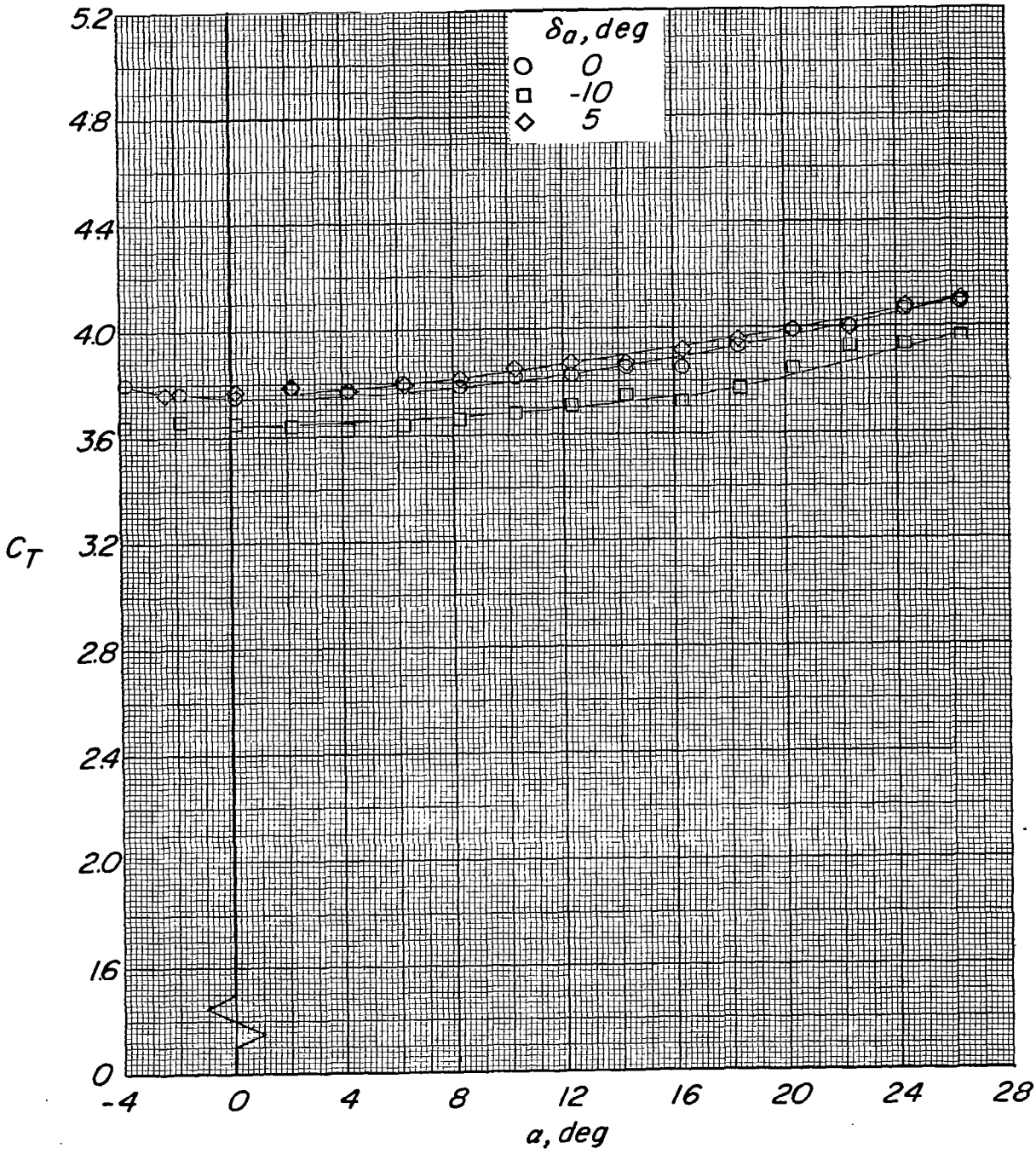

(c) Continued.

Figure 10.- Continued.

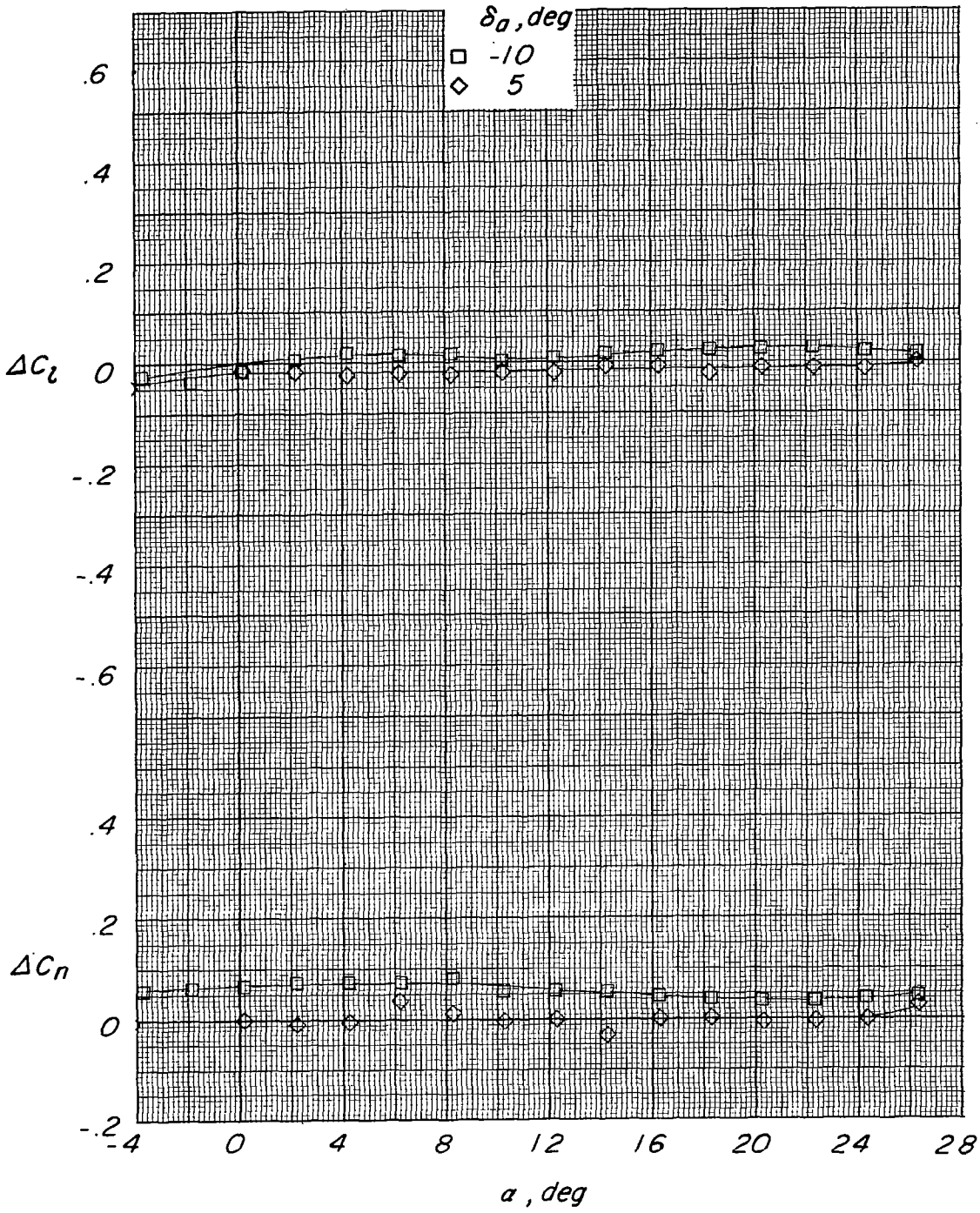

(c) Concluded.

Figure 10.- Concluded.

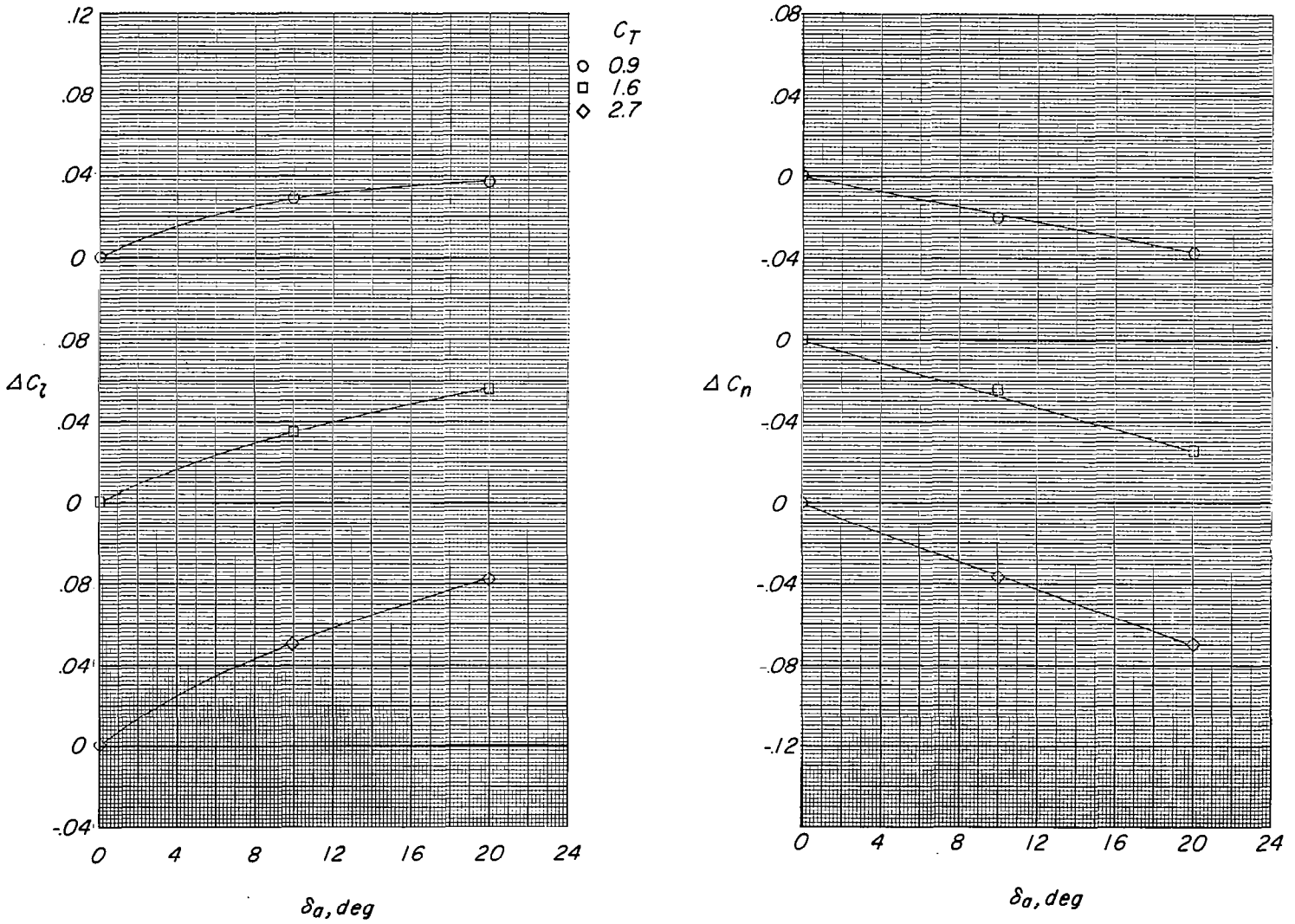

(a) Configuration C (long span, $\delta_f = 45^\circ$).

Figure 11.- Summary of the rolling-moment coefficient and yawing-moment coefficient produced at $\alpha = 4^\circ$ by aileron deflection at several thrust coefficients.

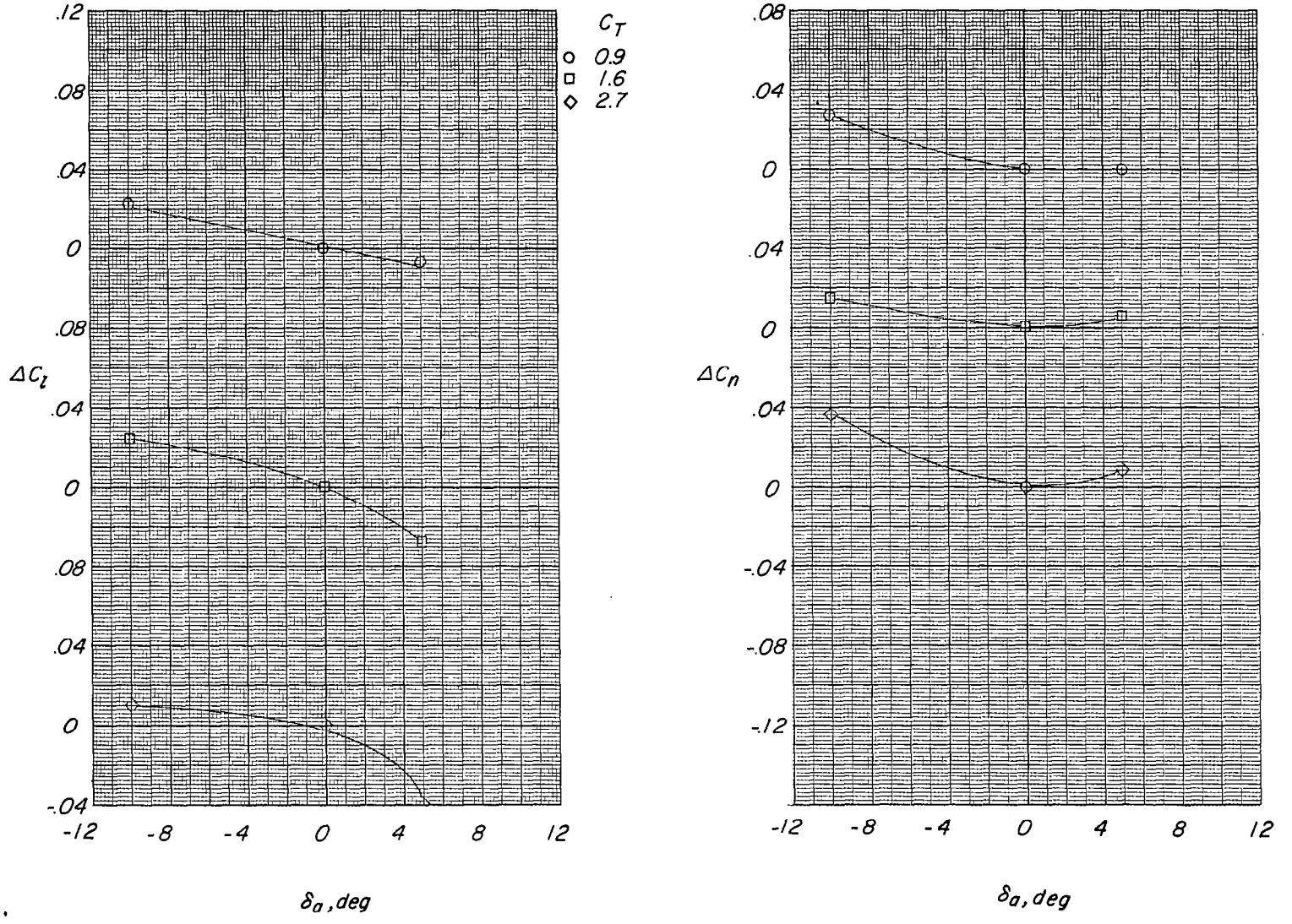

(b) Configuration D (long span, $\delta_f = 75°$).

Figure 11.- Continued.

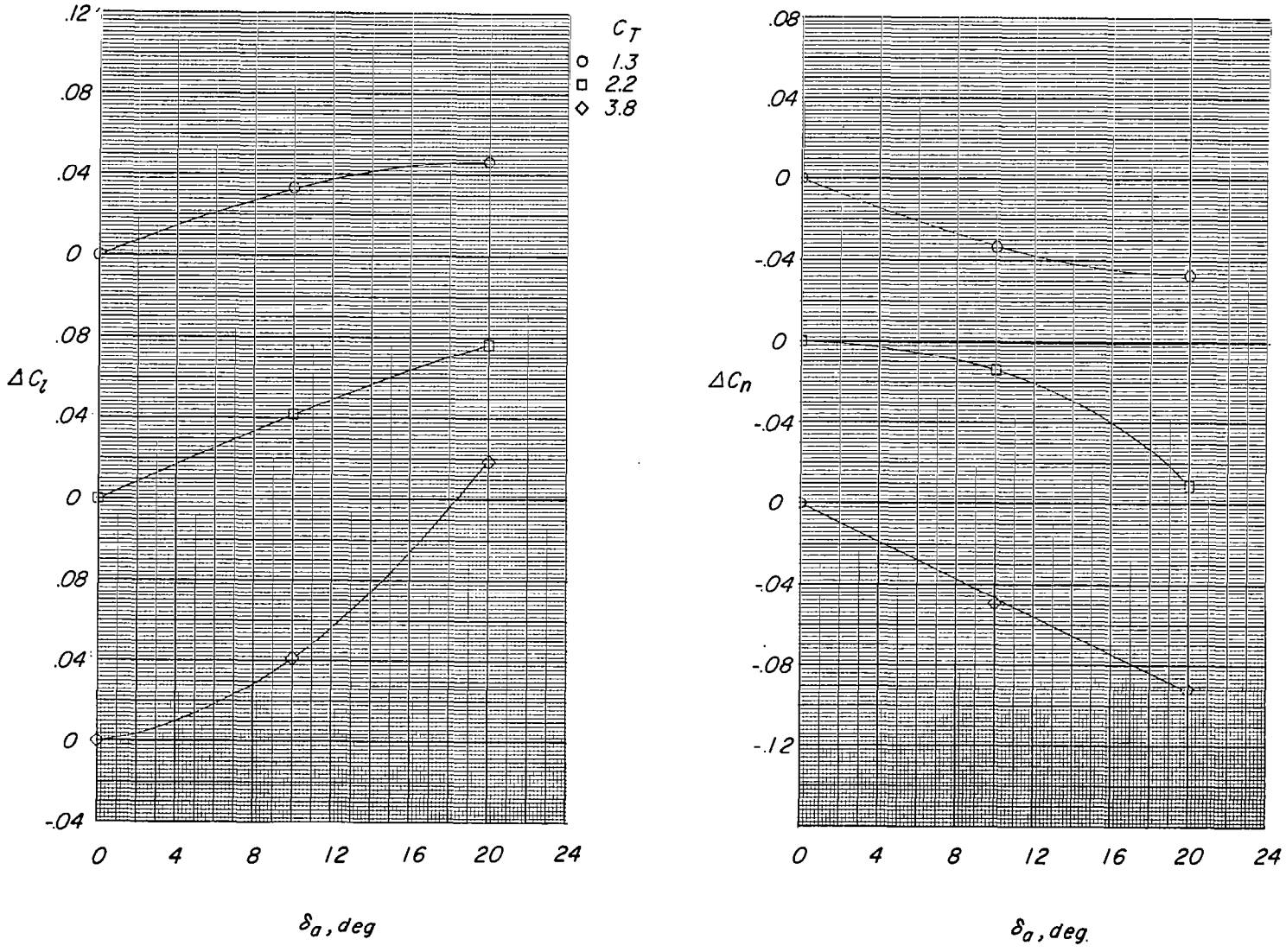

(c) Configuration F (short span, $\delta_f = 45^\circ$).

Figure 11.- Continued.

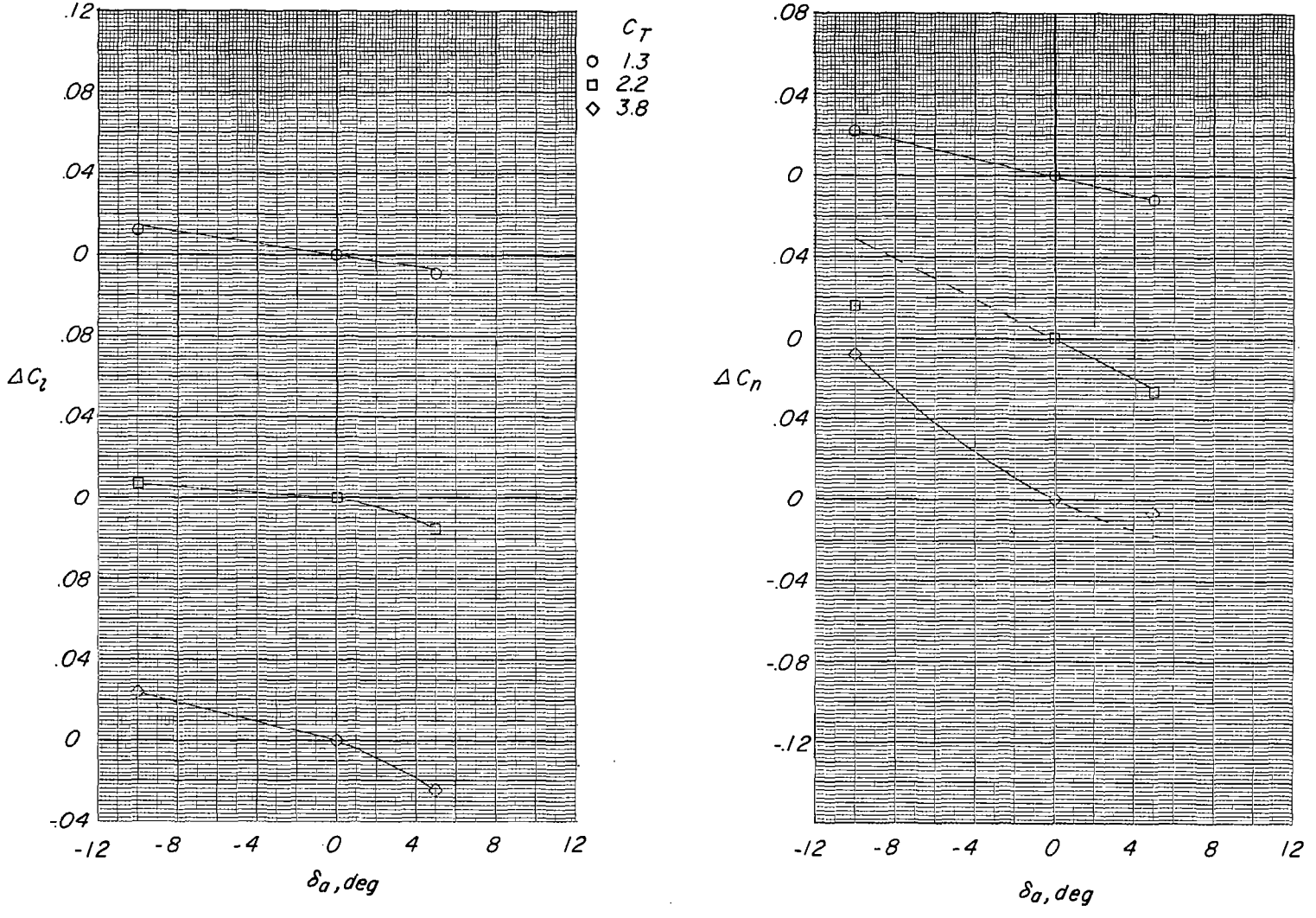

(d) Configuration G (short span, $\delta_f = 75^\circ$).

Figure 11.- Concluded.

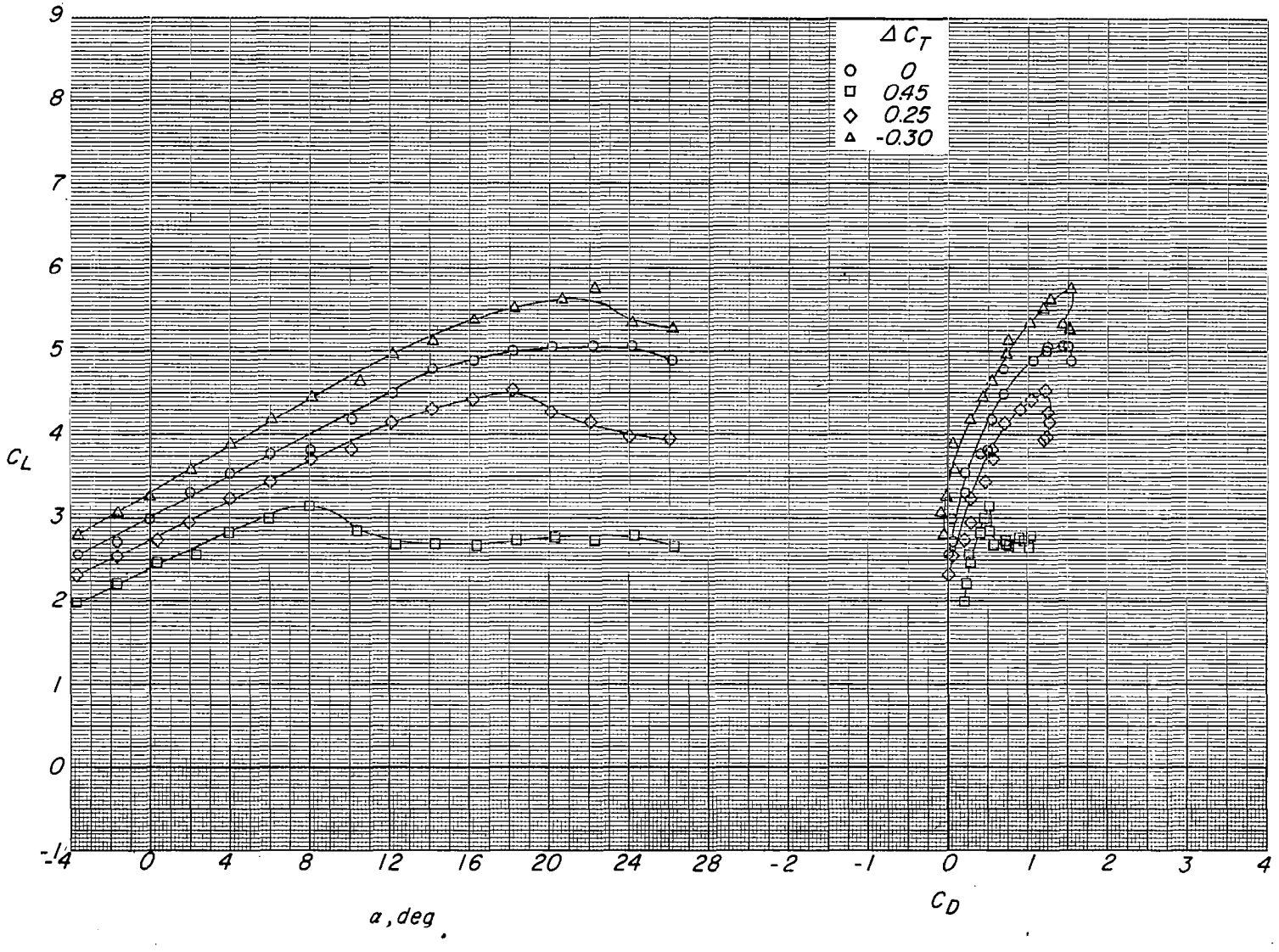

(a) Lift coefficient as a function of angle of attack and of drag coefficient at basic $C_T \approx 0.9$.

Figure 12.- Effect of differential propeller thrust on configuration C (long span, $\delta_f = 45°$) at several thrust coefficients.

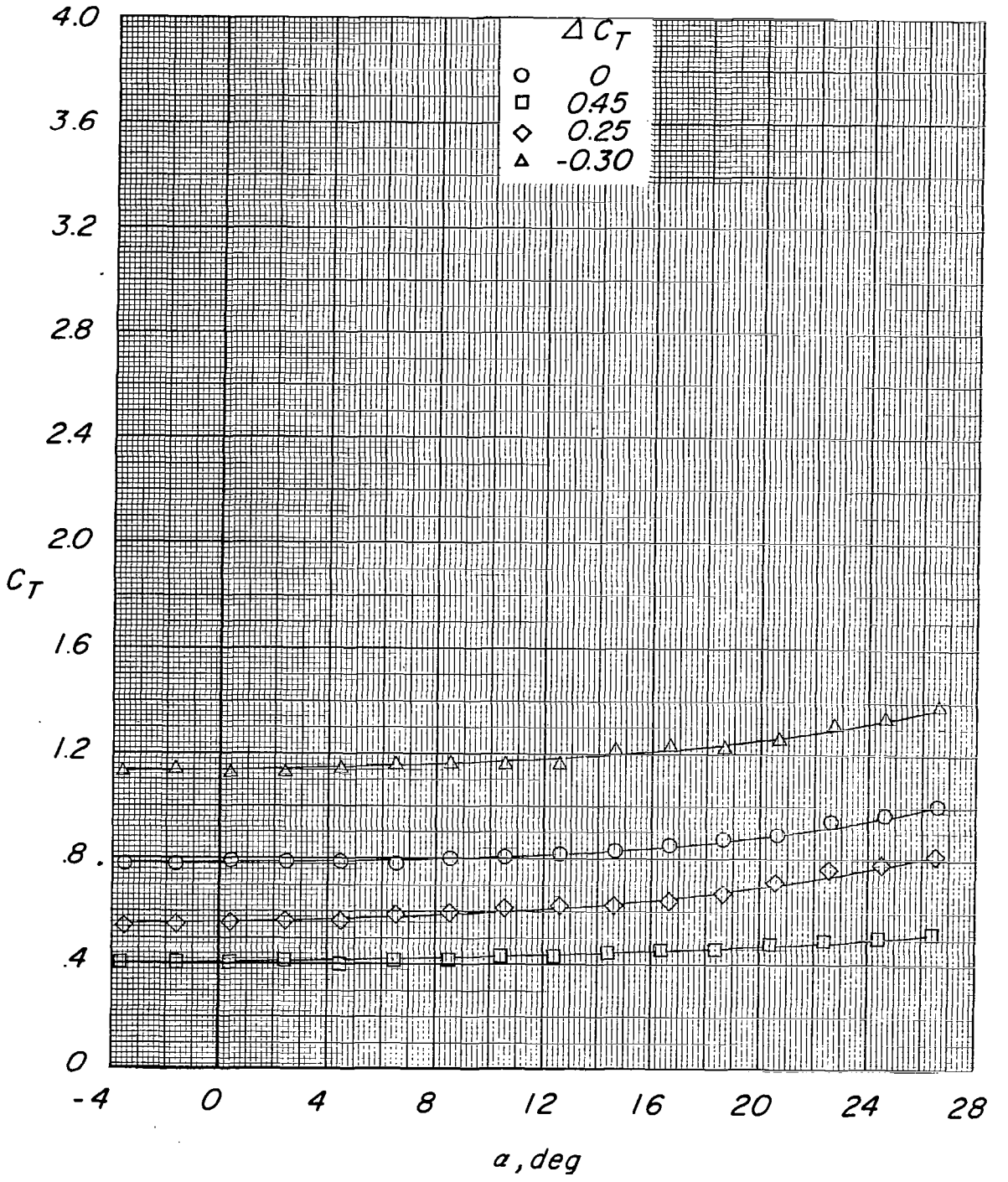

(a) Continued. Total thrust coefficient at basic $C_T \approx 0.9$.

Figure 12.- Continued.

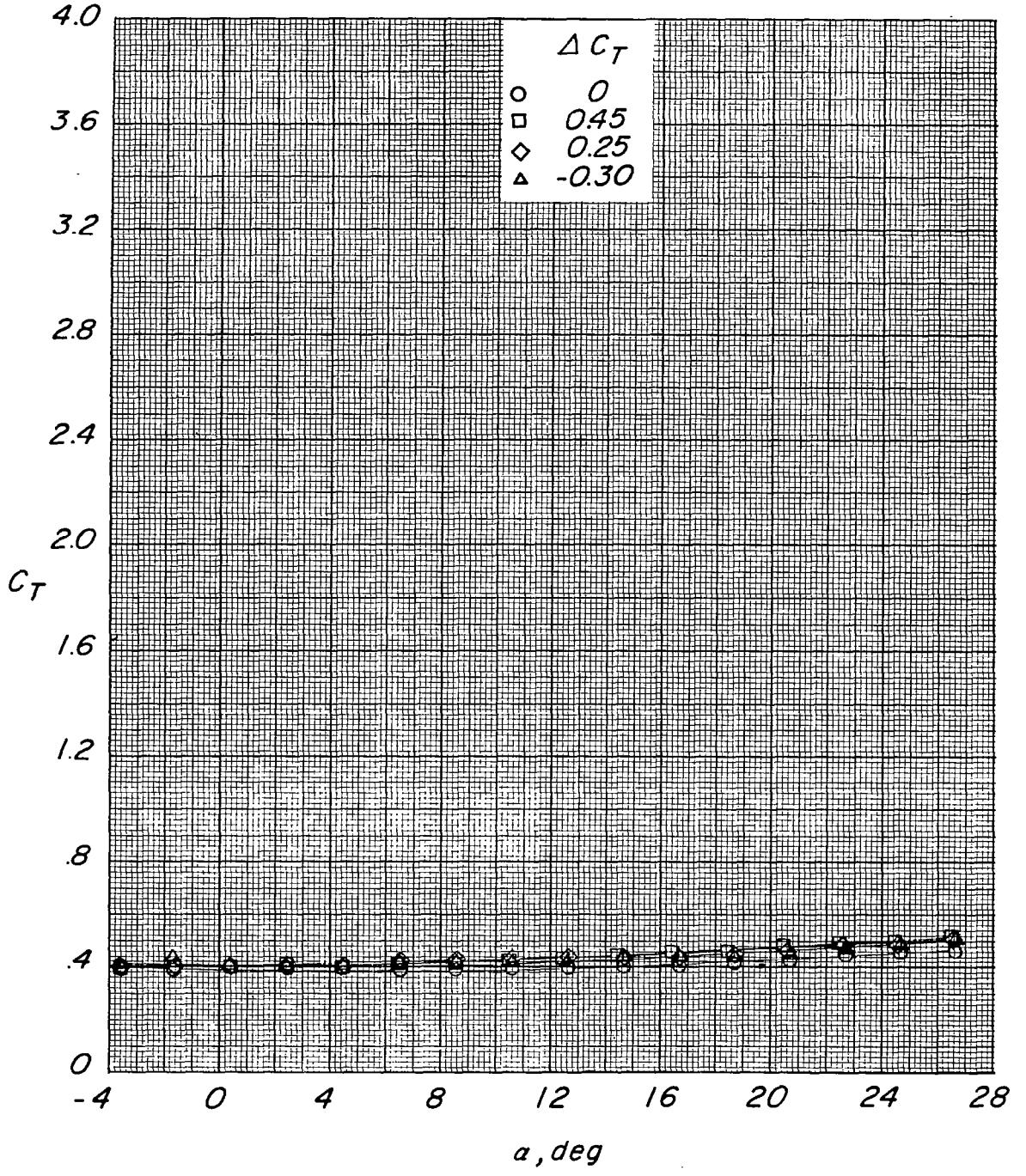

(a) Continued. Thrust coefficient for left motor at basic $C_T \approx 0.9$.

Figure 12.- Continued.

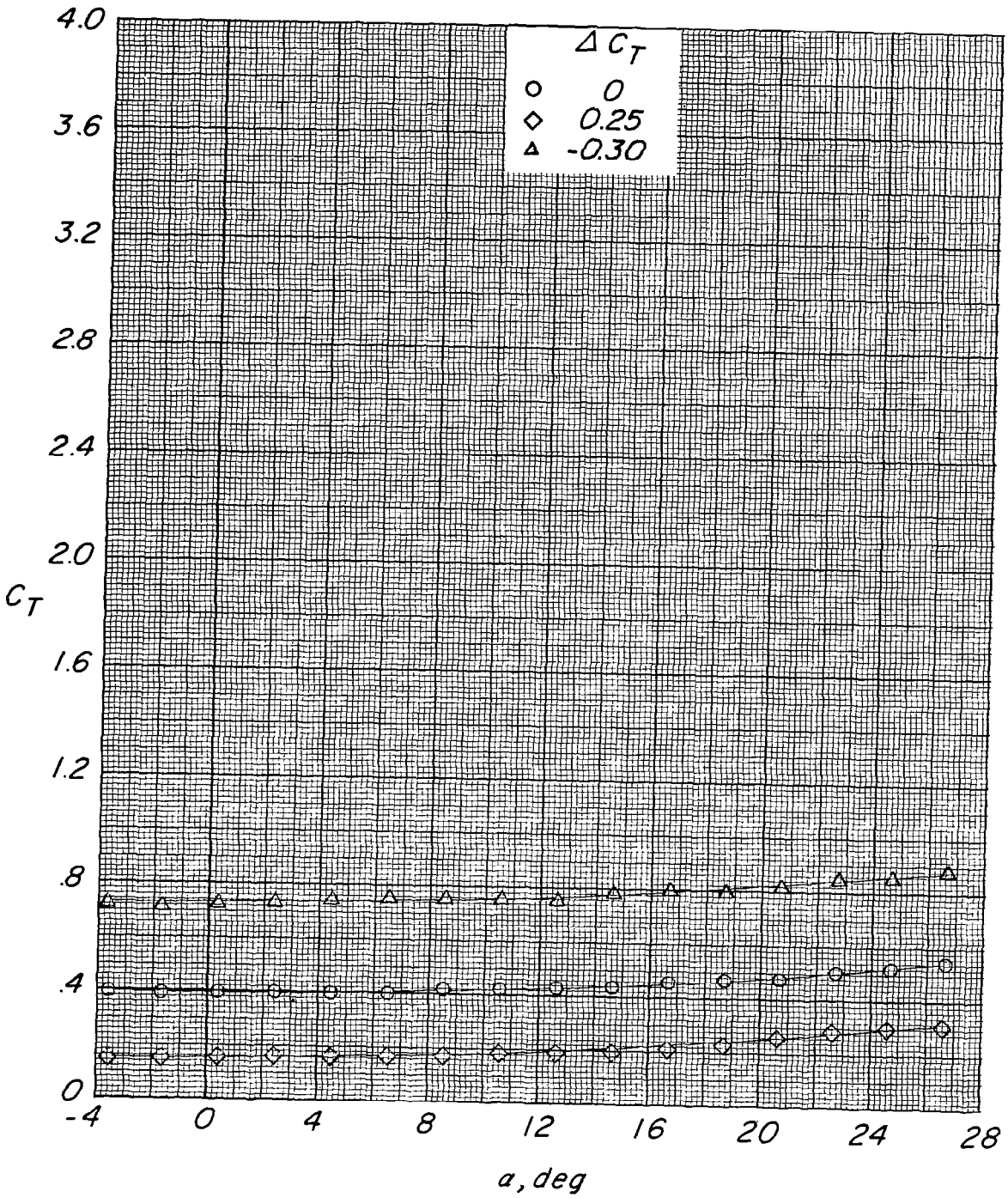

(a) Continued. Thrust coefficient for right motor at basic $C_T \approx 0.9$.

Figure 12.- Continued.

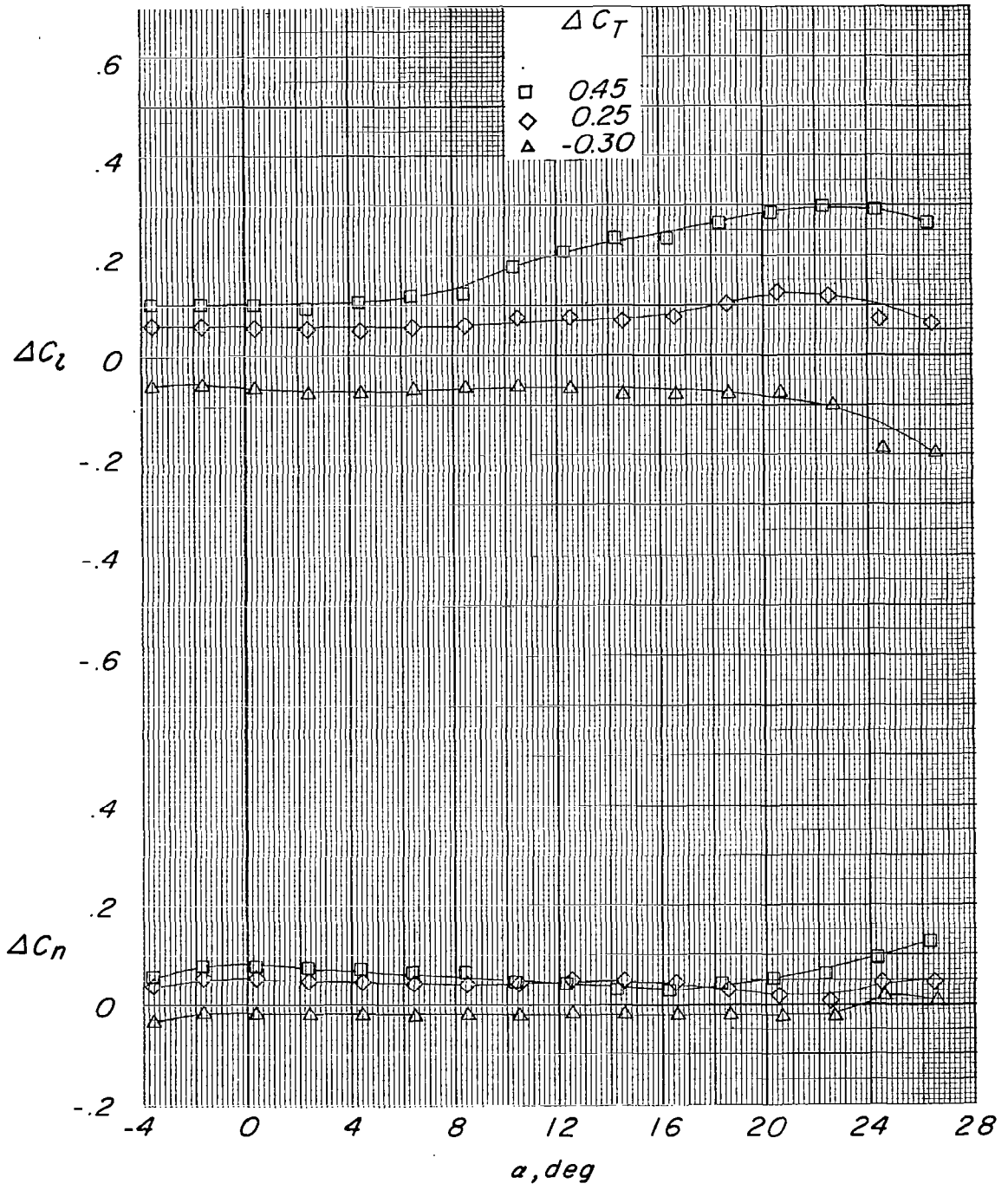

(a) Concluded. Rolling-moment coefficient and yawing-moment coefficient at basic $C_T \approx 0.9$.

Figure 12.- Continued.

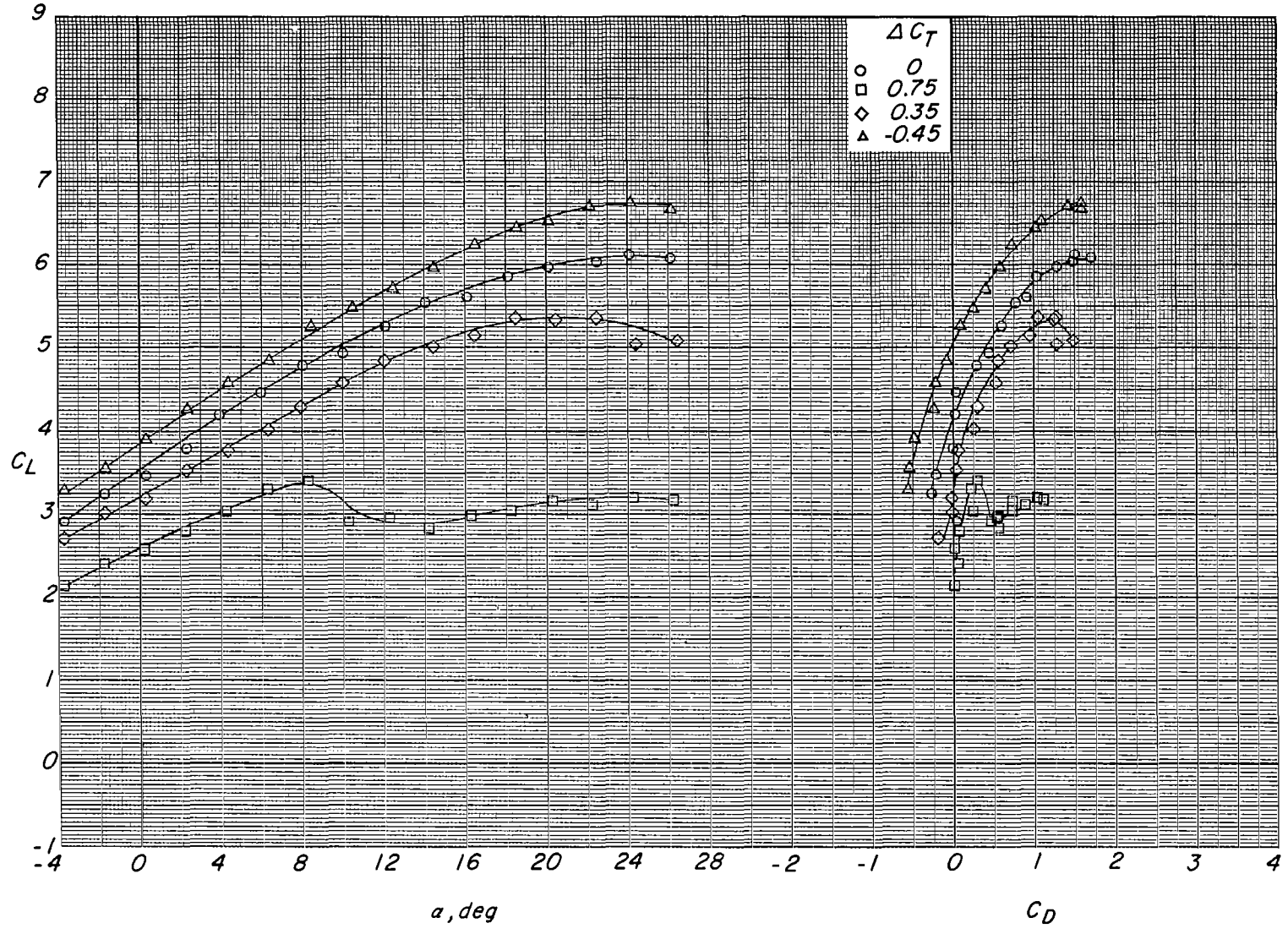

(b) Lift coefficient as a function of angle of attack and of drag coefficient at basic $C_T \approx 1.6$.

Figure 12.- Continued.

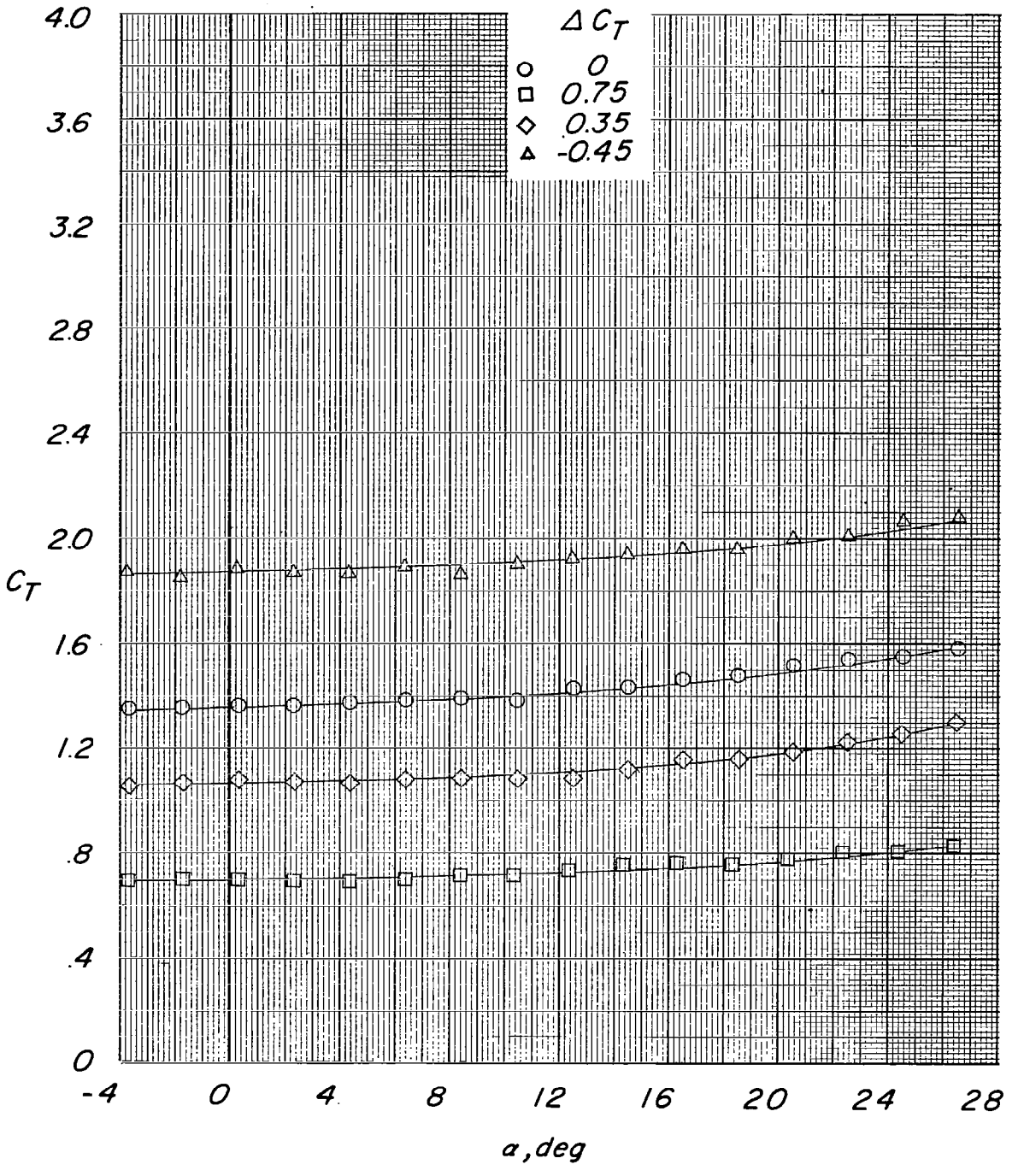

(b) Continued. Total thrust coefficient at basic $C_T \approx 1.6$.

Figure 12.- Continued.

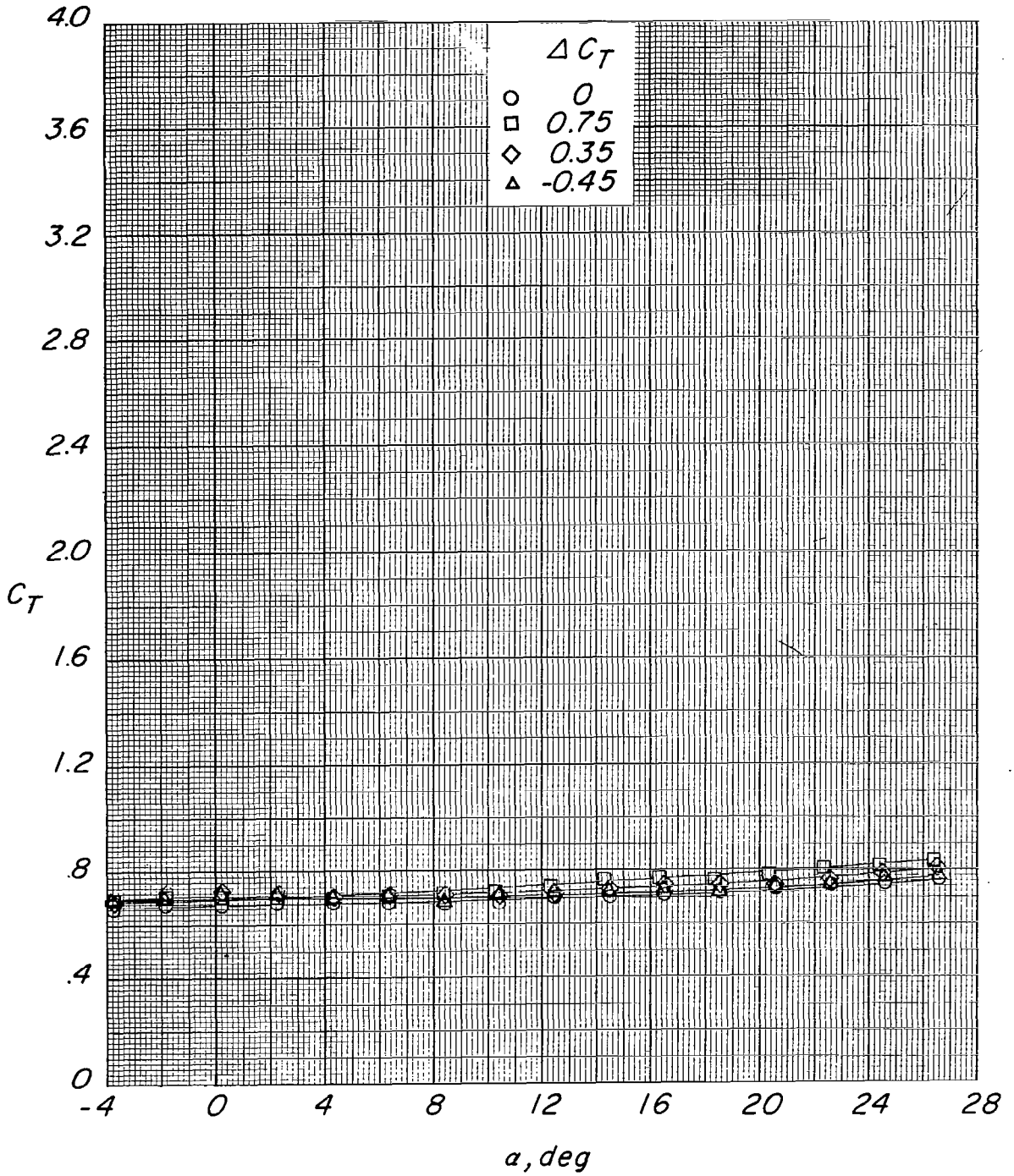

(b) Continued. Thrust coefficient for left motor at basic $C_T \approx 1.6$.

Figure 12.- Continued.

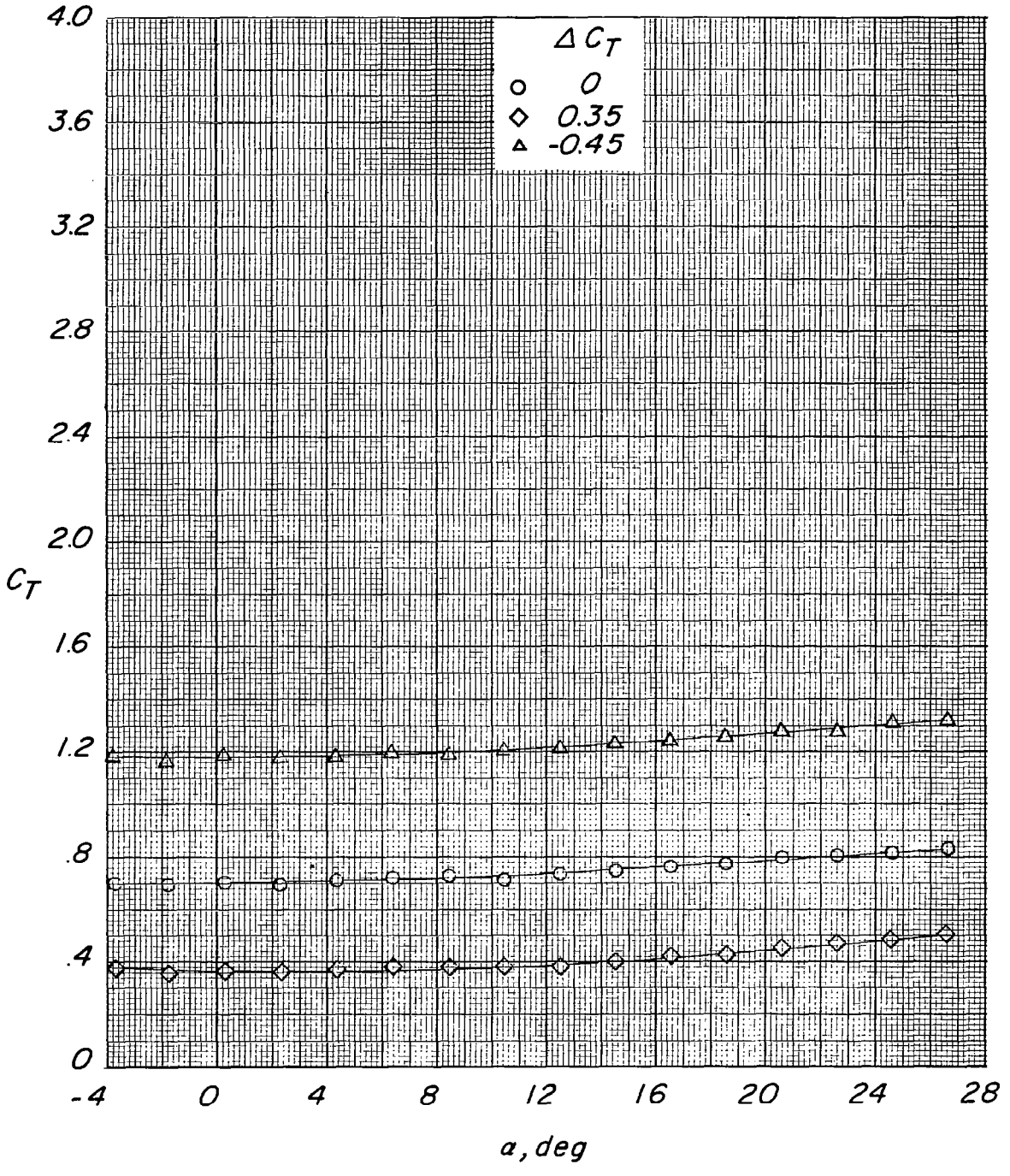

(b) Continued. Thrust coefficient for right motor at basic $C_T \approx 1.6$.

Figure 12.- Continued.

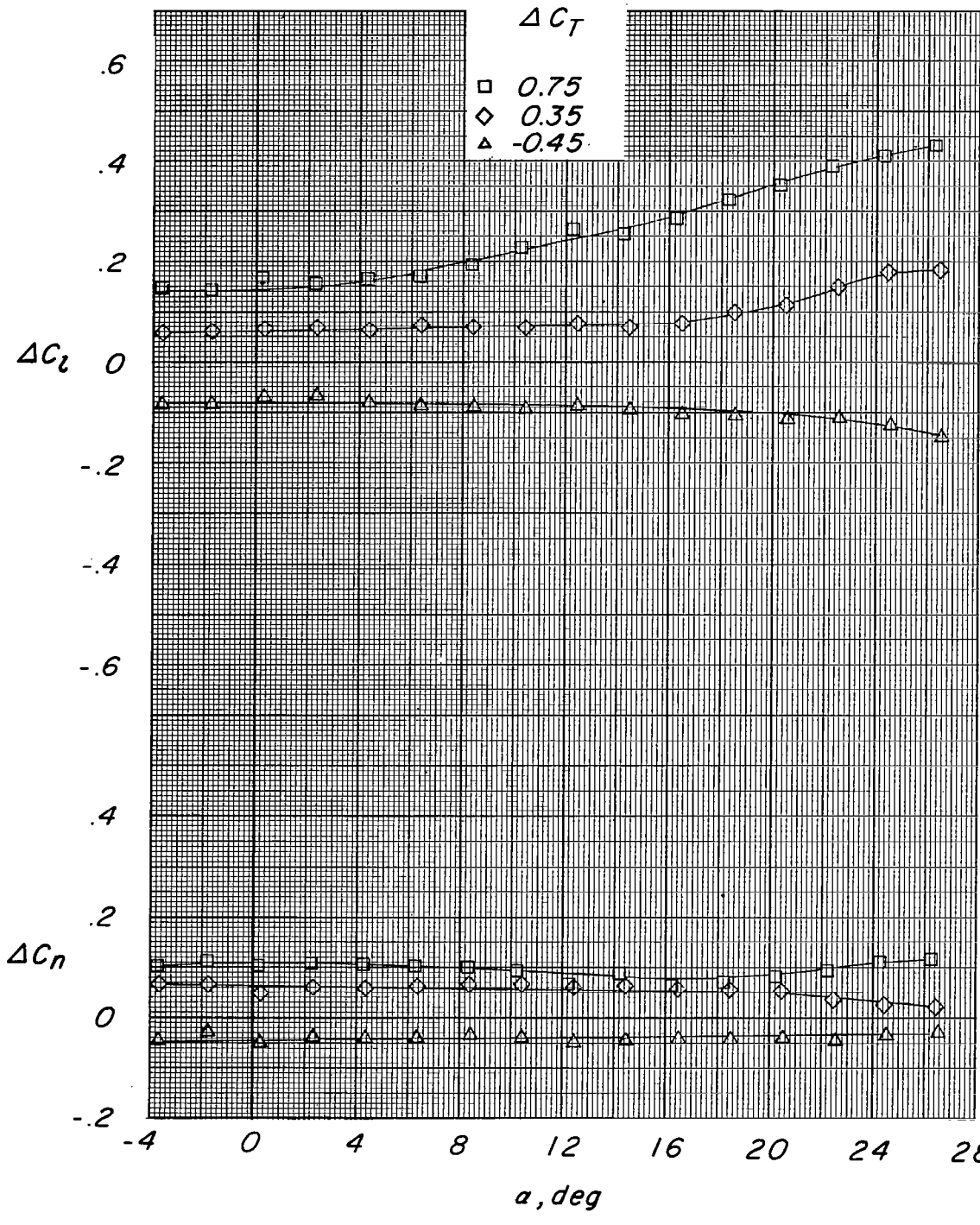

(b) Concluded. Rolling-moment coefficient and yawing-moment coefficient at basic $C_T \approx 1.6$.

Figure 12.- Continued.

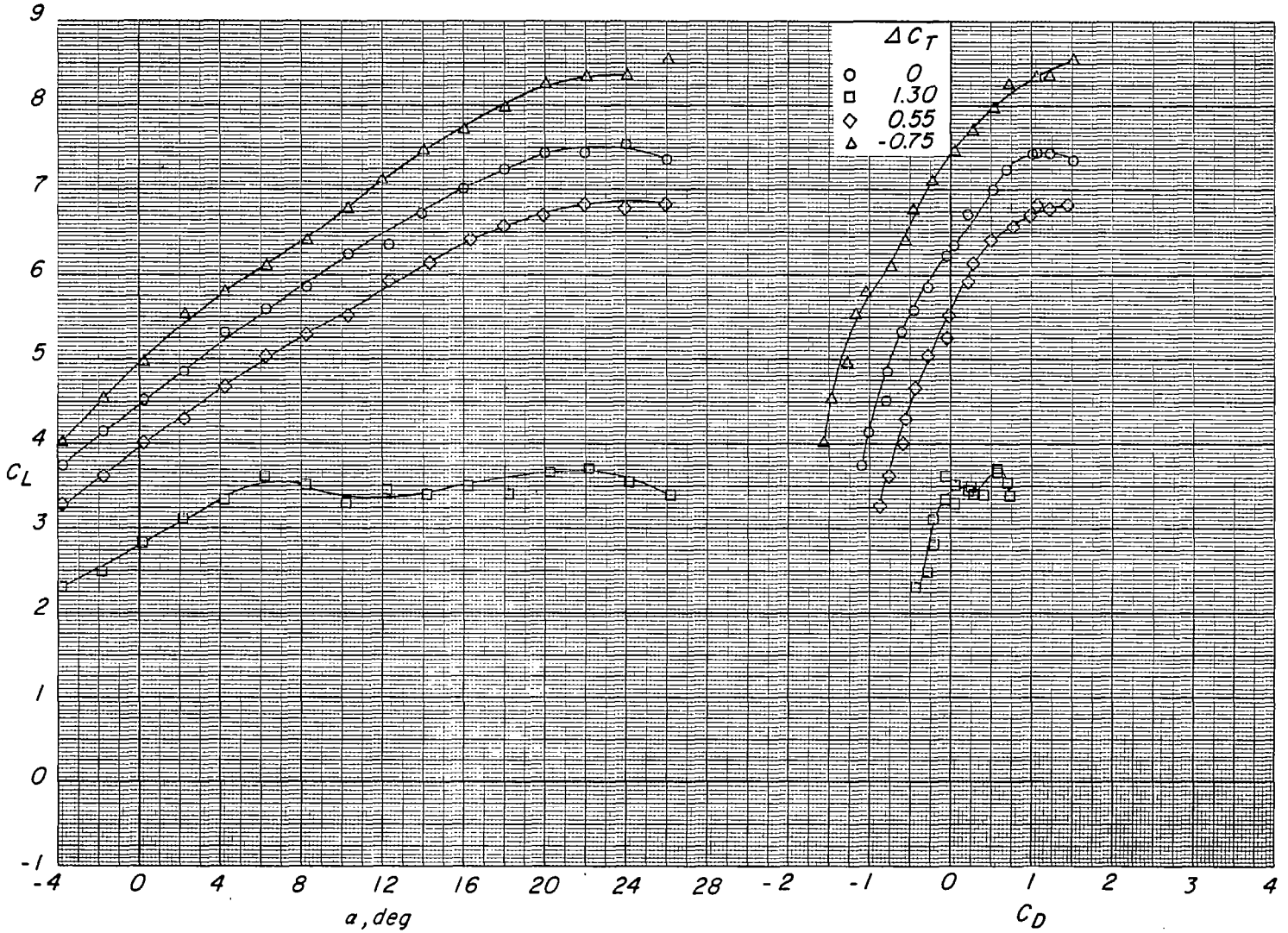

(c) Lift coefficient as a function of angle of attack and of drag coefficient at basic $C_T \approx 2.7$.

Figure 12.- Continued.

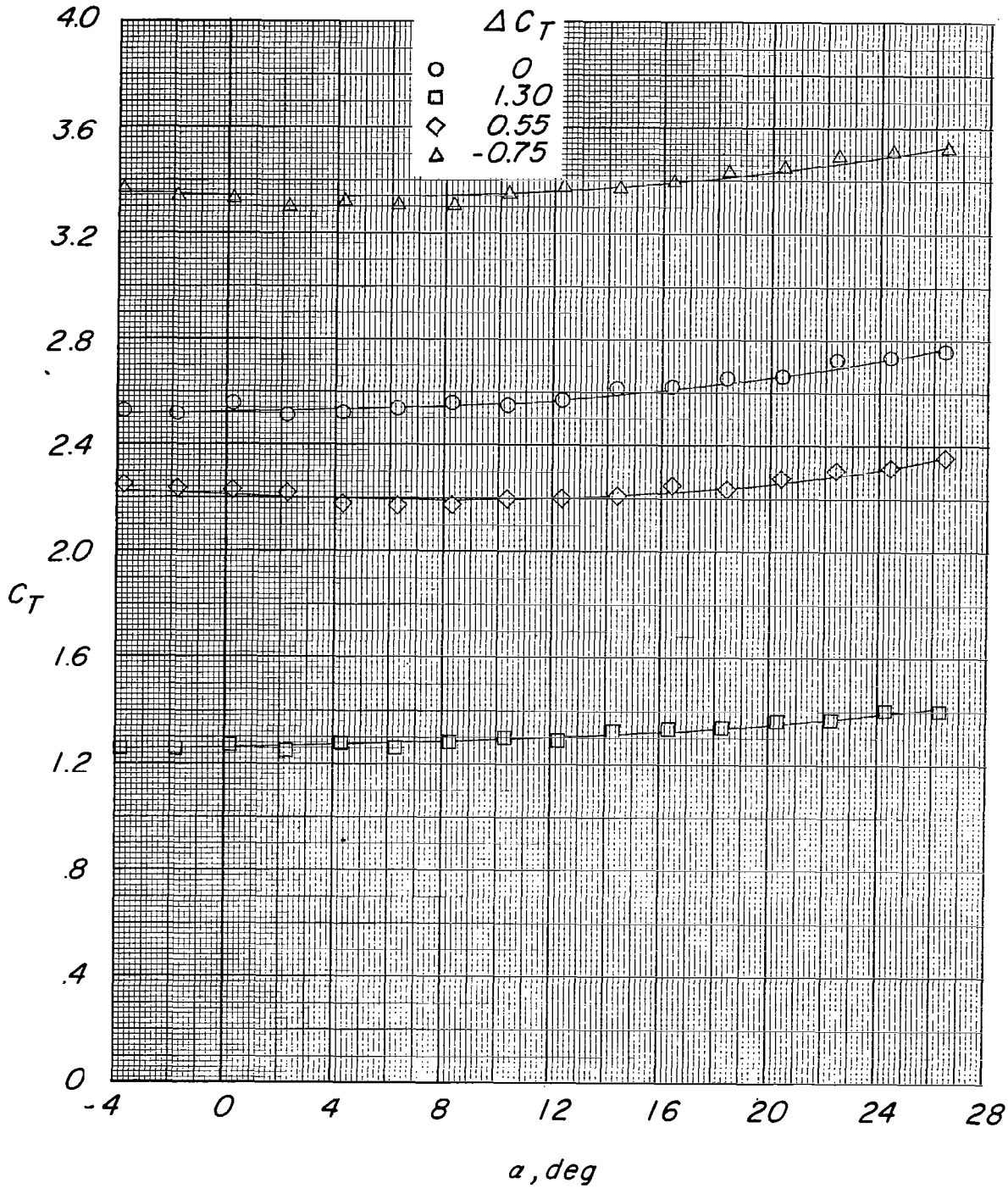

(c) Continued. Total thrust coefficient at basic $C_T \approx 2.7$.

Figure 12.- Continued.

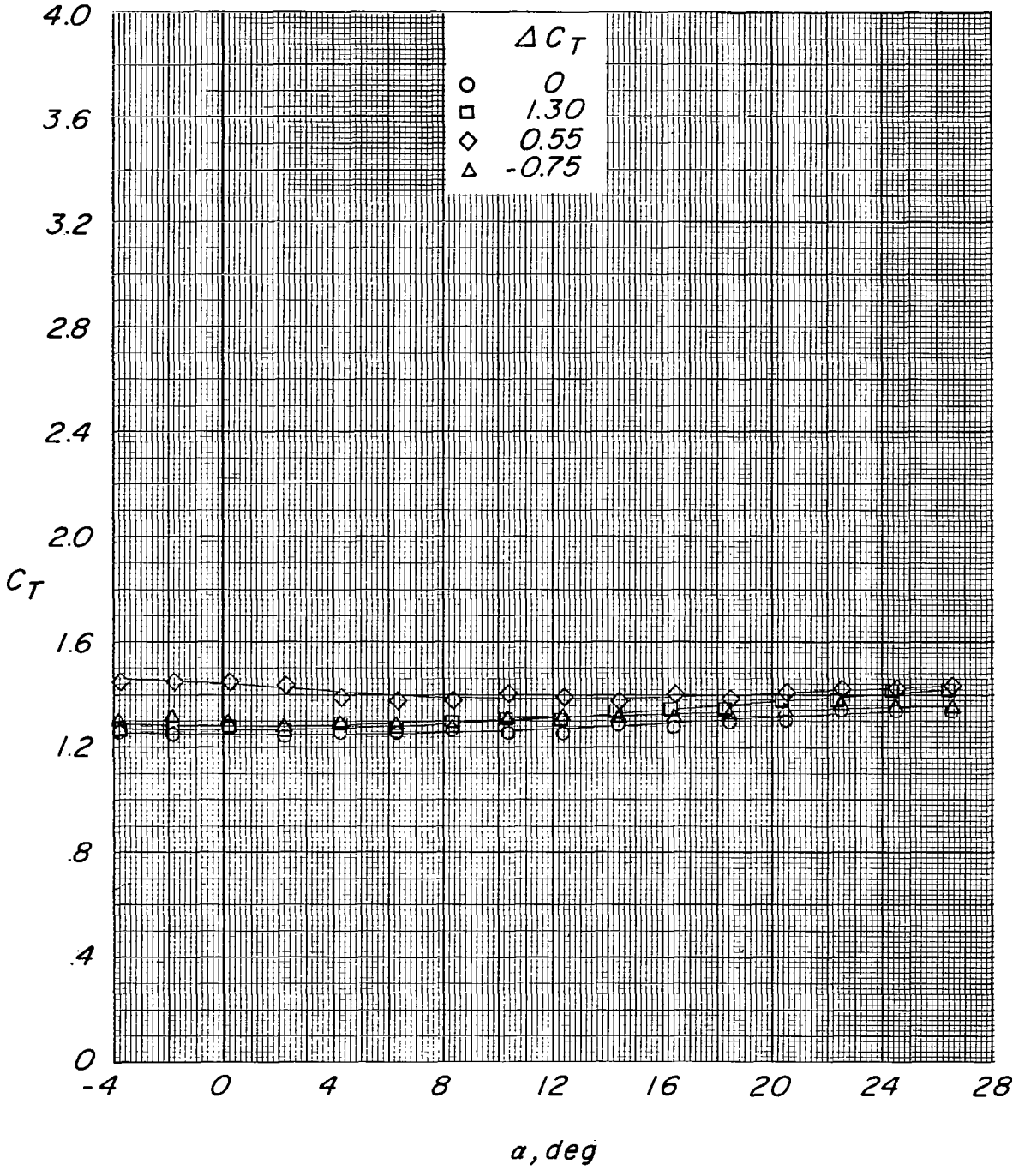

(c) Continued. Thrust coefficient for left motor at basic $C_T \approx 2.7$.

Figure 12.- Continued.

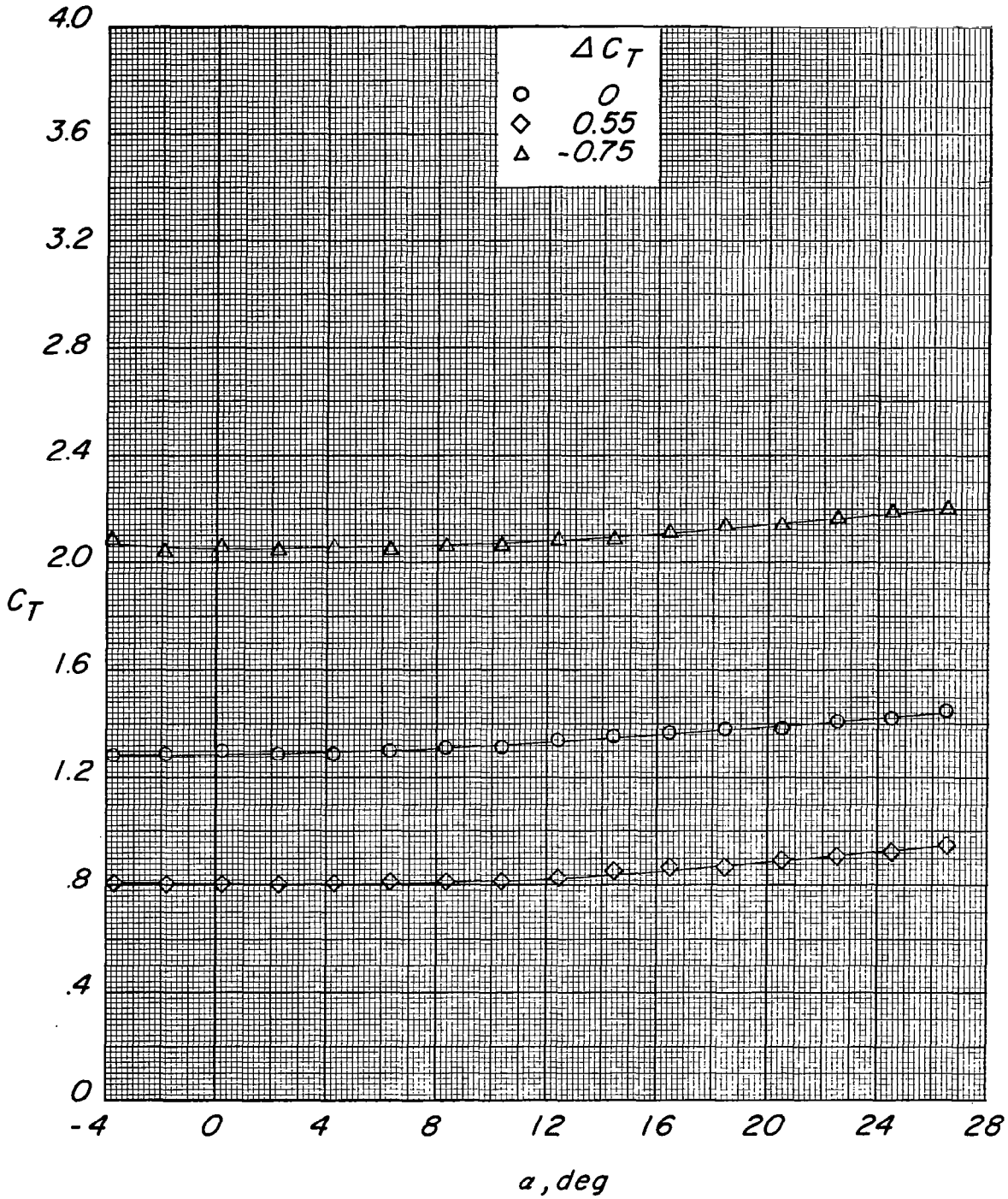

(c) Continued. Thrust coefficient for right motor at basic $C_T \approx 2.7$.

Figure 12.- Continued.

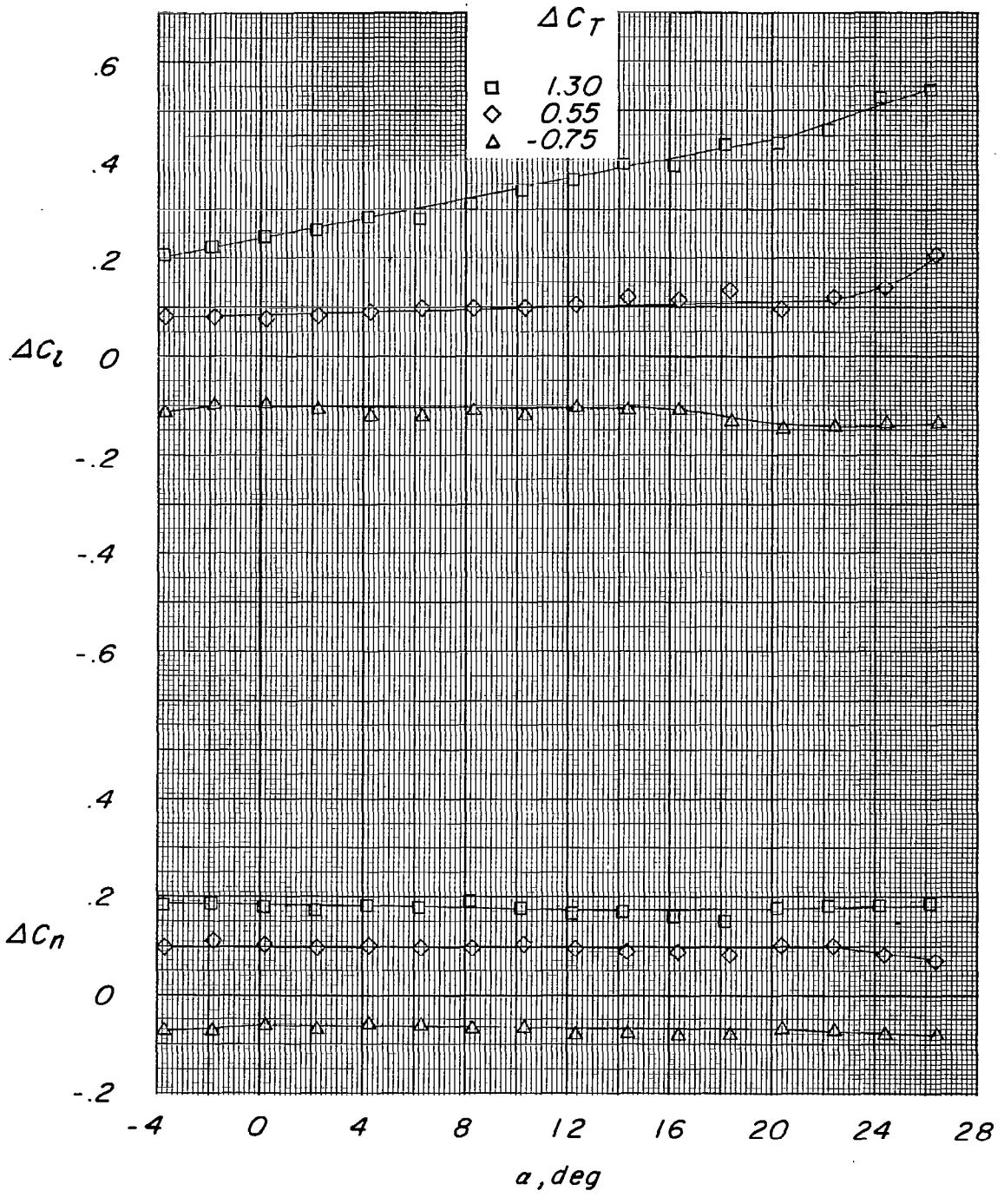

(c) Concluded. Rolling-moment coefficient and yawing-moment coefficient at basic $C_T \approx 2.7$.

Figure 12.- Concluded.

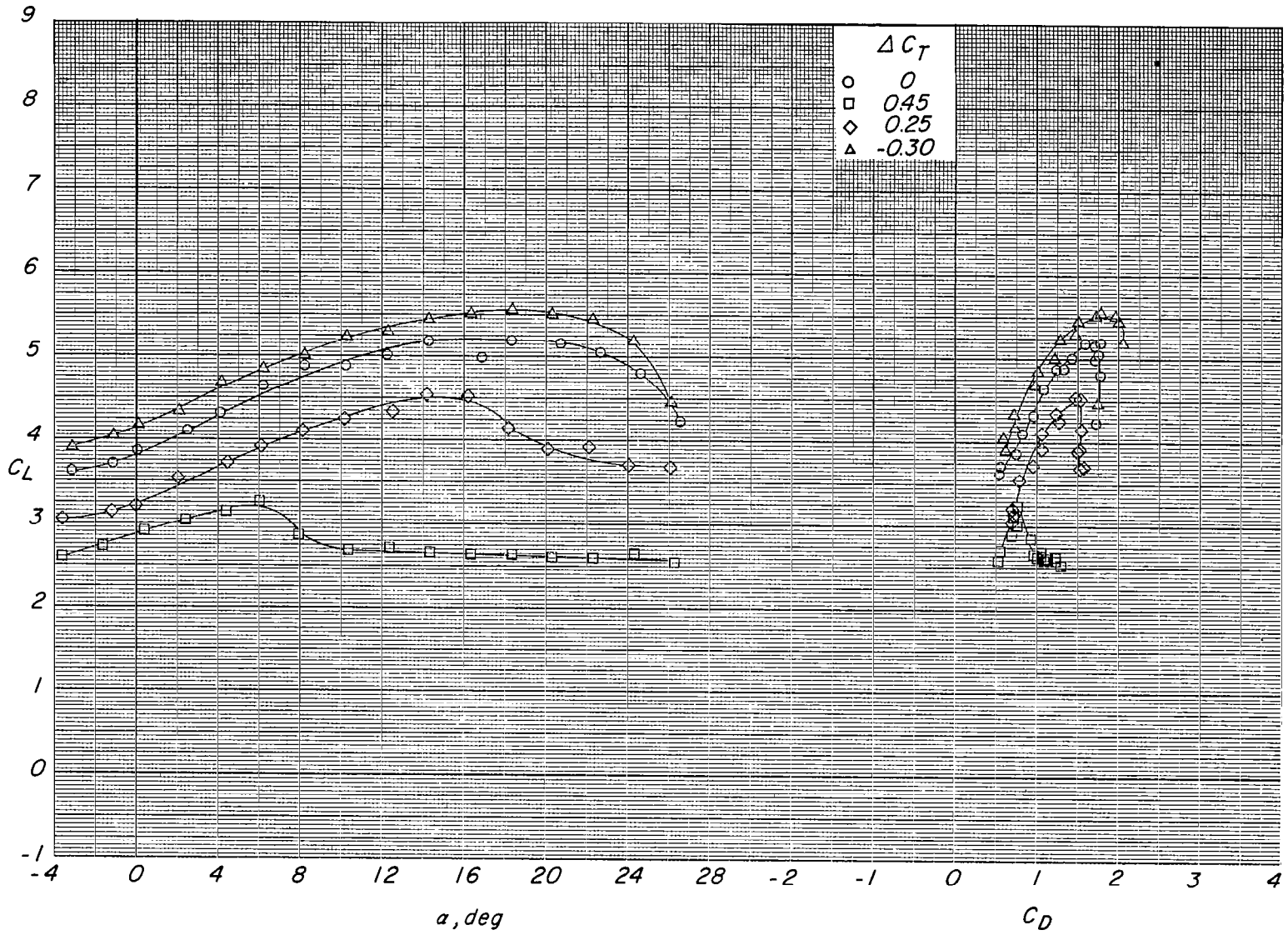

(a) Lift coefficient as a function of angle of attack and of drag coefficient at basic $C_T \approx 0.9$.

Figure 13.- Effect of differential propeller thrust on configuration D (long span; $\delta_f = 75^\circ$) at several thrust coefficients.

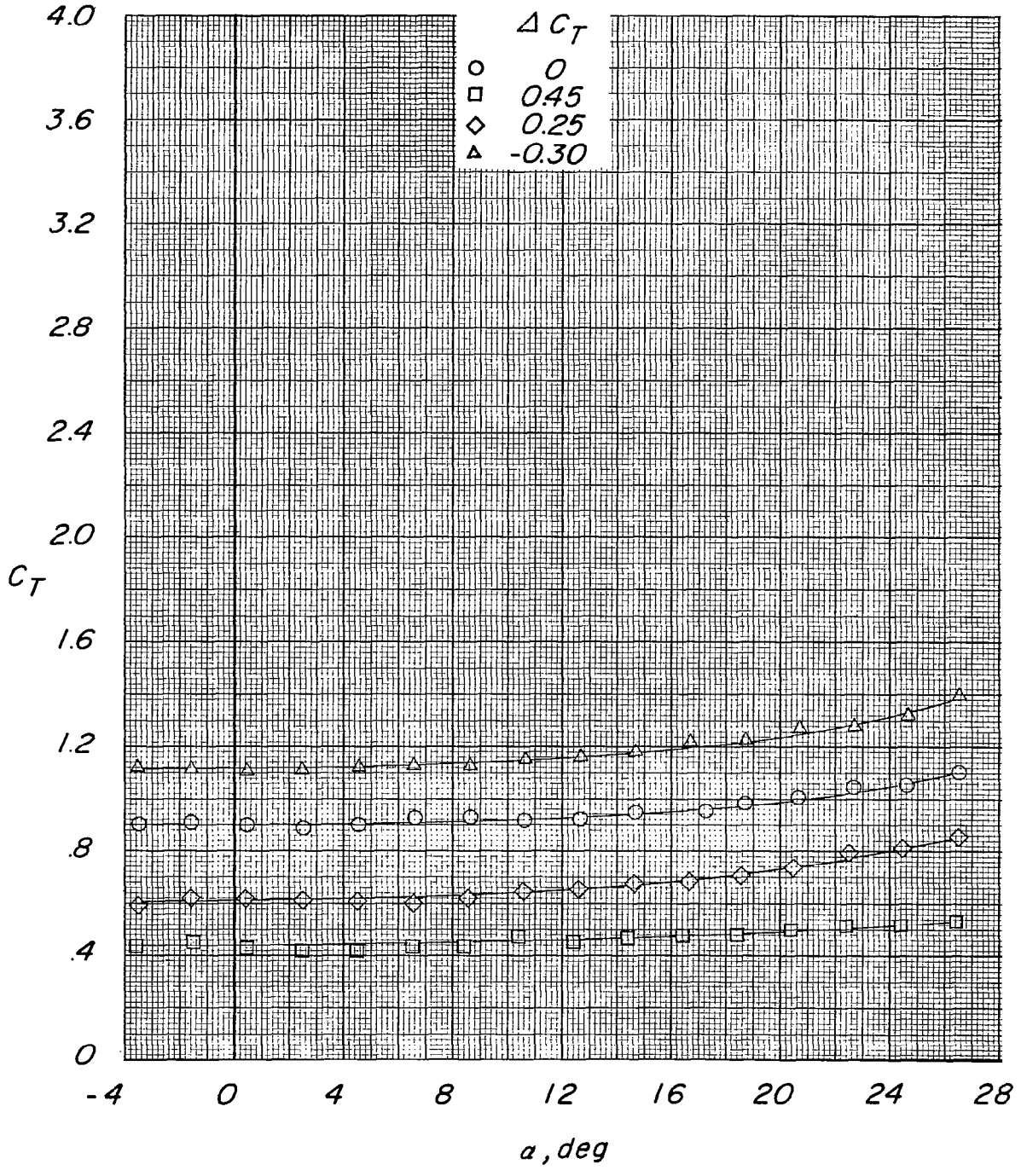

(a) Continued. Total thrust coefficient at basic $C_T \approx 0.9$.

Figure 13.- Continued.

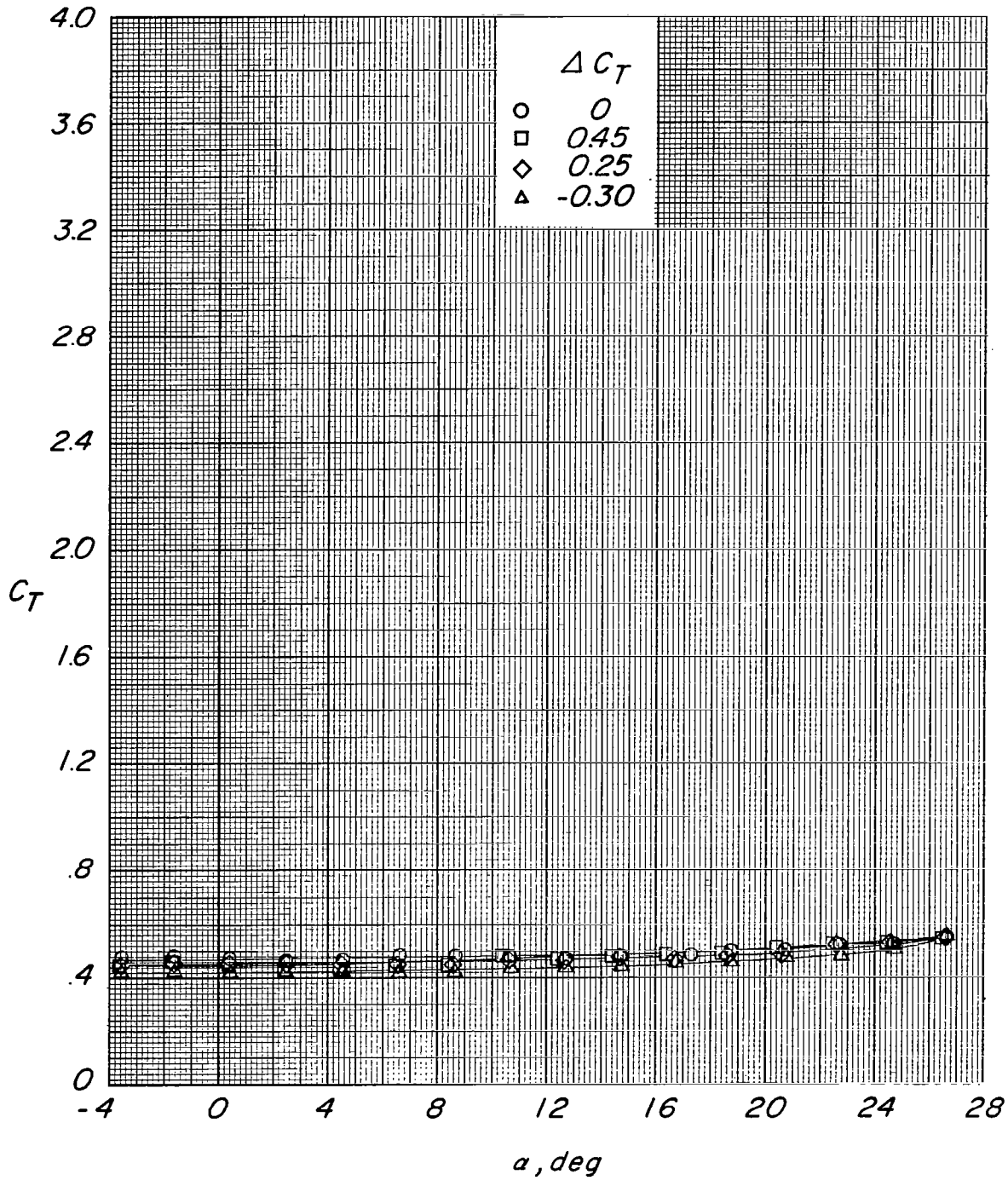

(a) Continued. Thrust coefficient for left motor at basic $C_T \approx 0.9$.

Figure 13.- Continued.

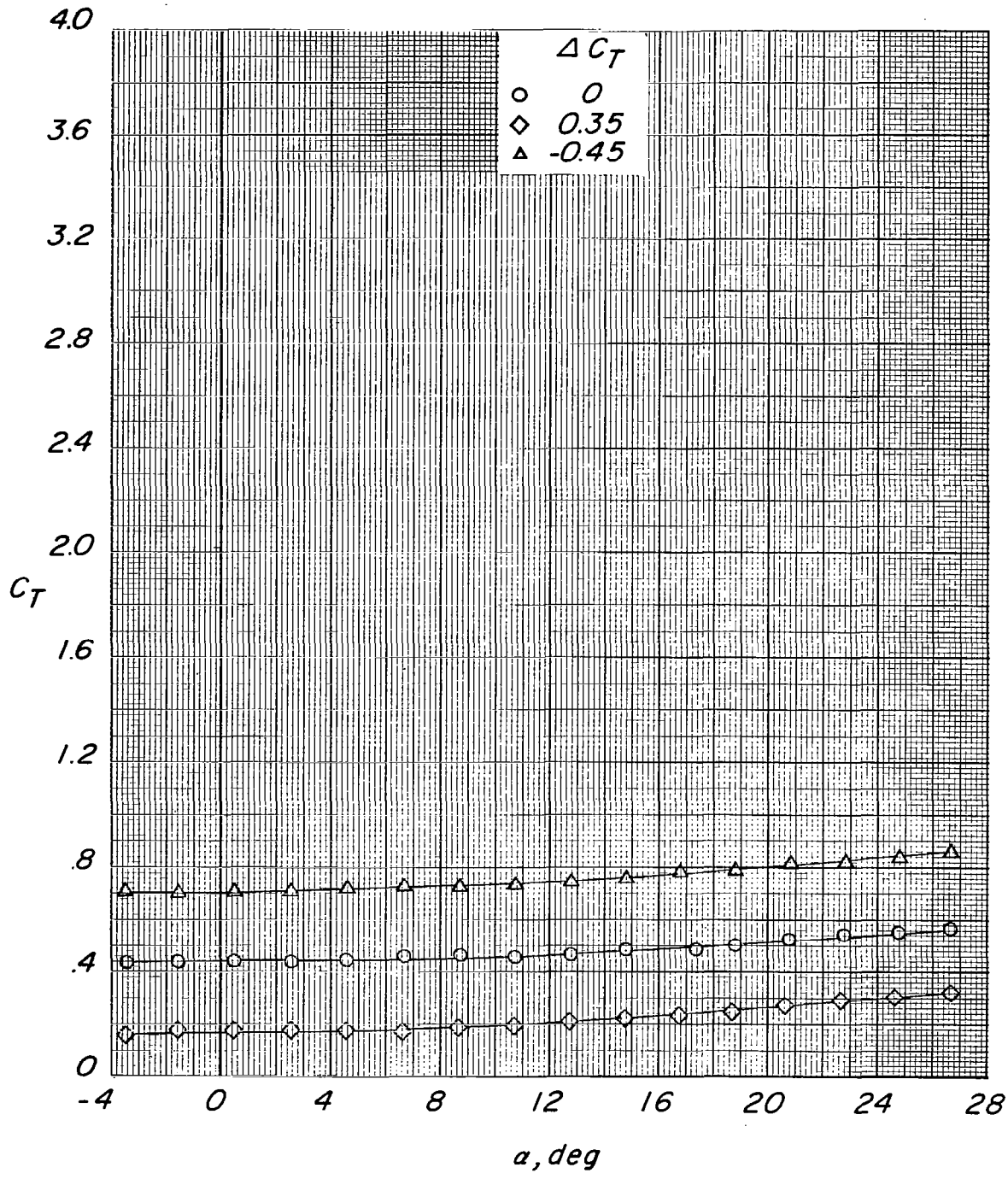

(a) Continued. Thrust coefficient for right motor at basic $C_T \approx 0.9$.

Figure 13.- Continued.

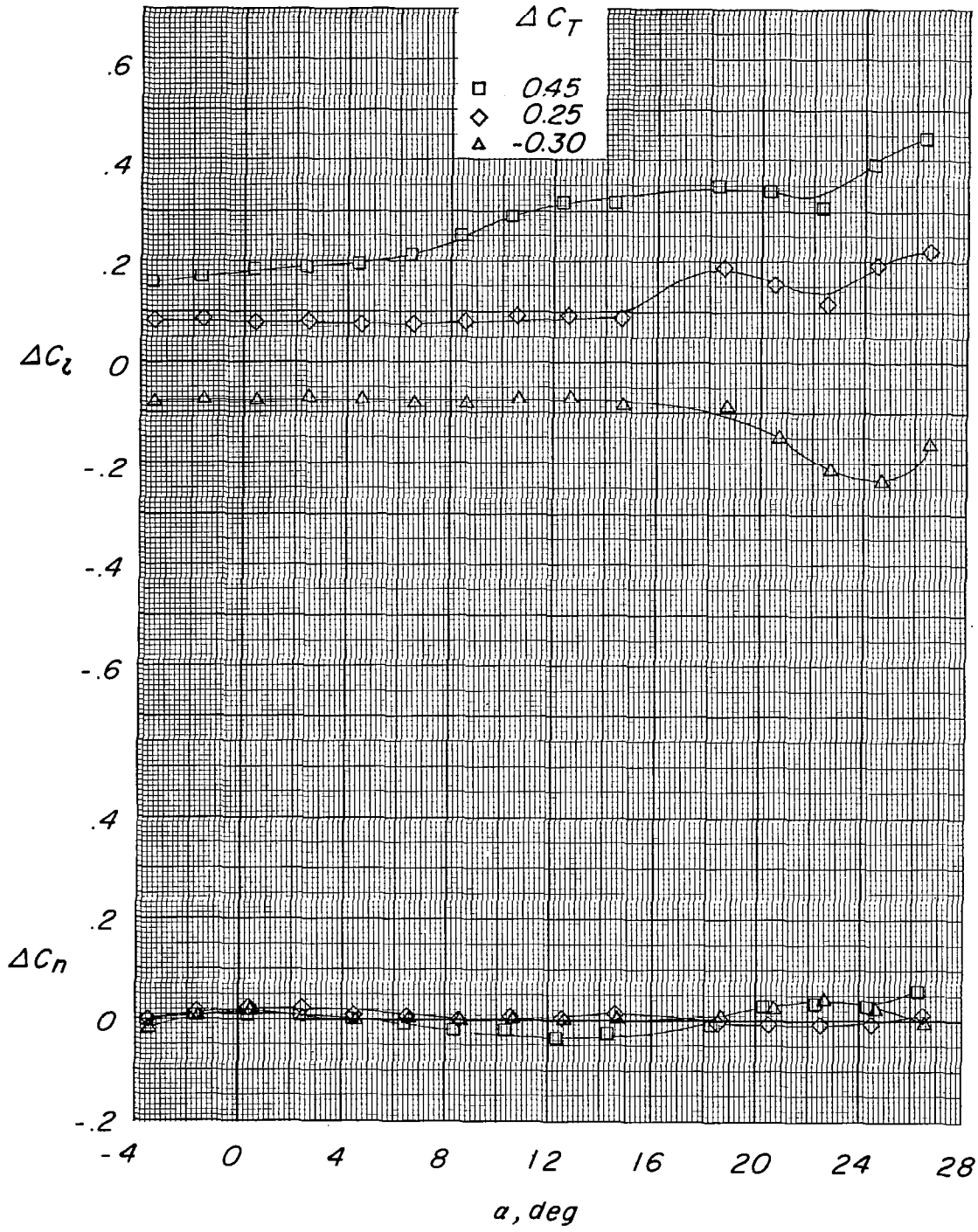

(a) Concluded. Rolling-moment coefficient and yawing-moment coefficient at basic $C_T \approx 0.9$.

Figure 13.- Continued.

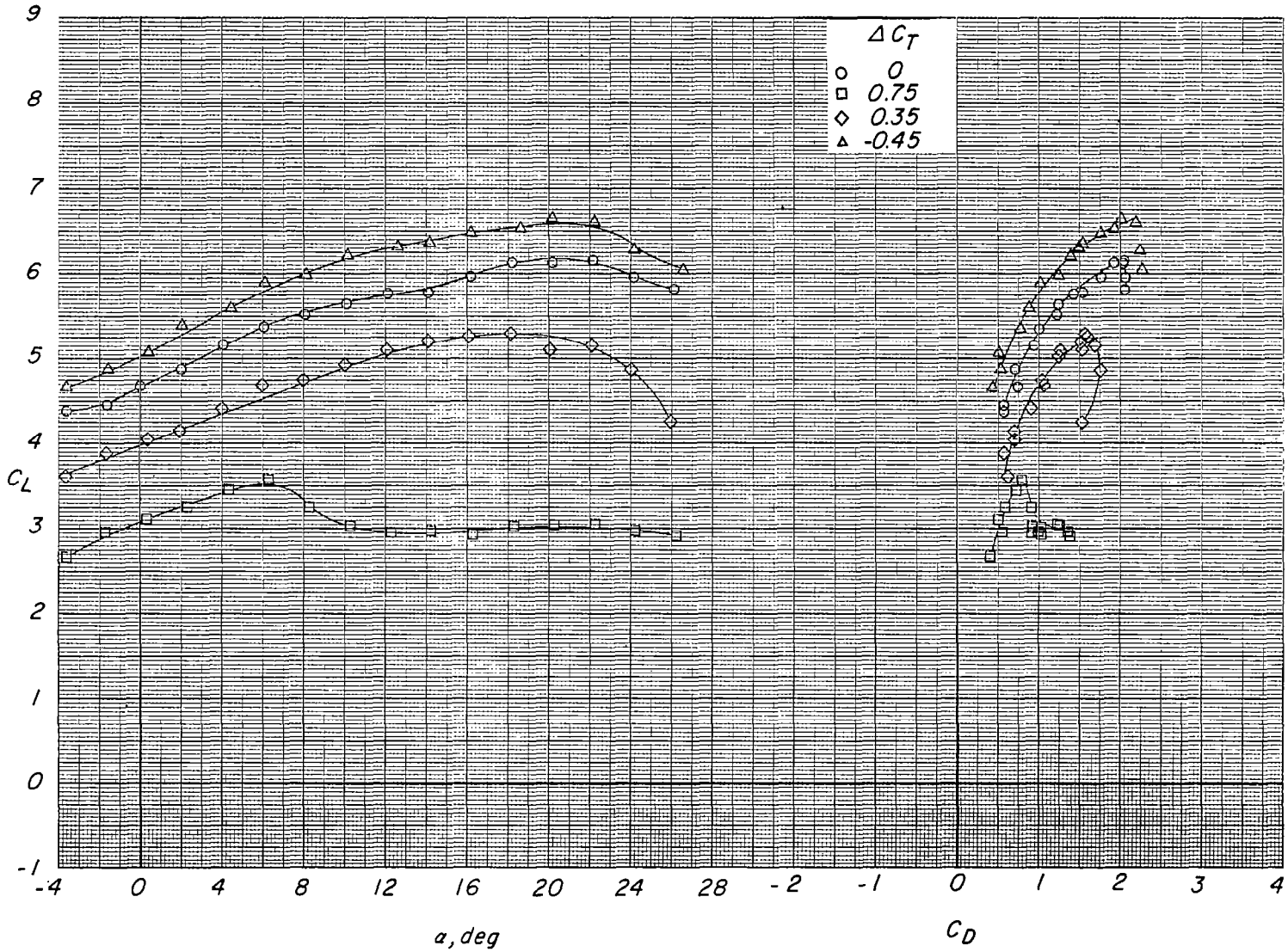

(b) Lift coefficient as a function of angle of attack and of drag coefficient at basic $C_T \approx 1.6$.

Figure 13.- Continued.

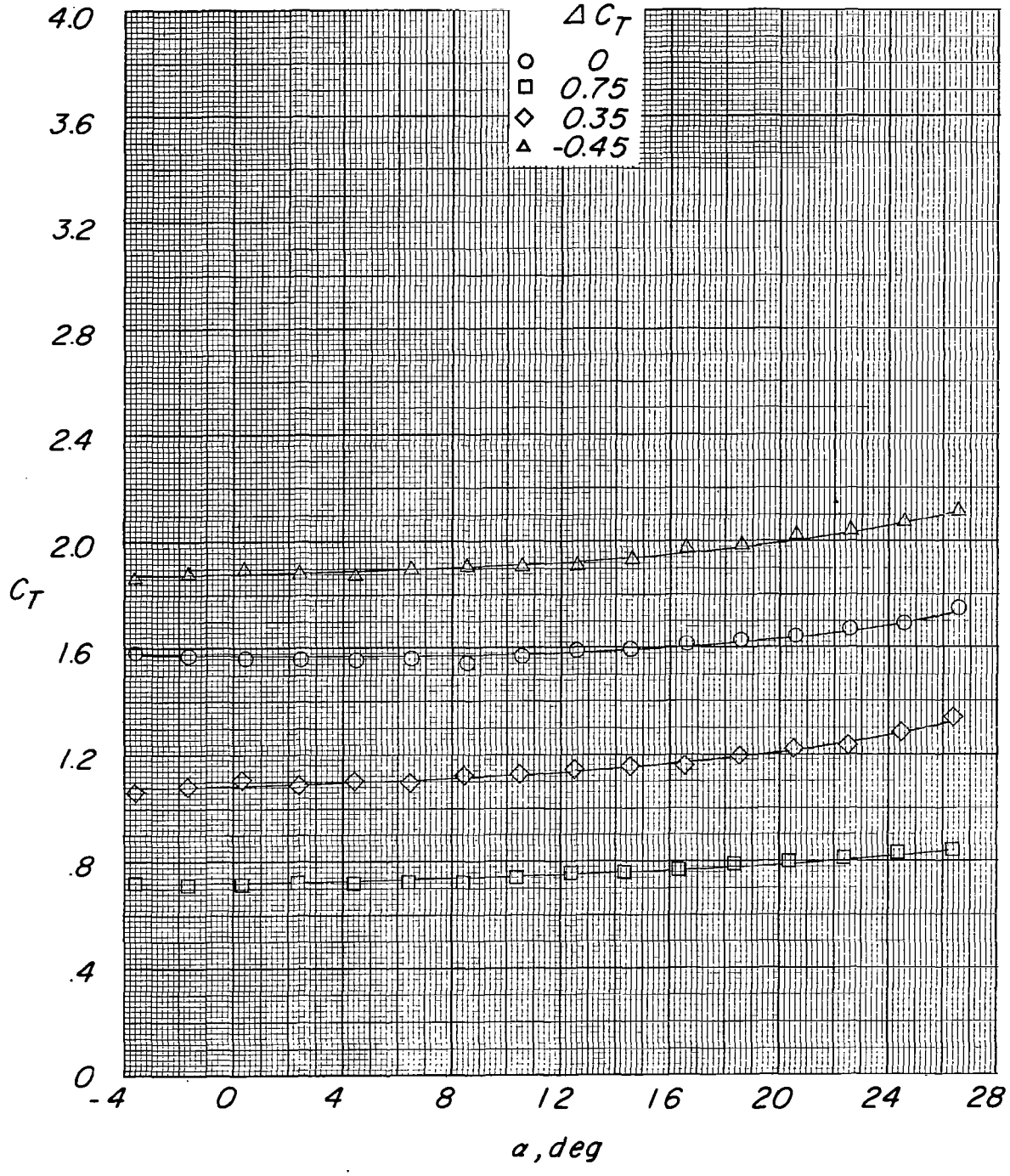

(b) Continued. Total thrust coefficient at basic $C_T \approx 1.6$.

Figure 13.- Continued.

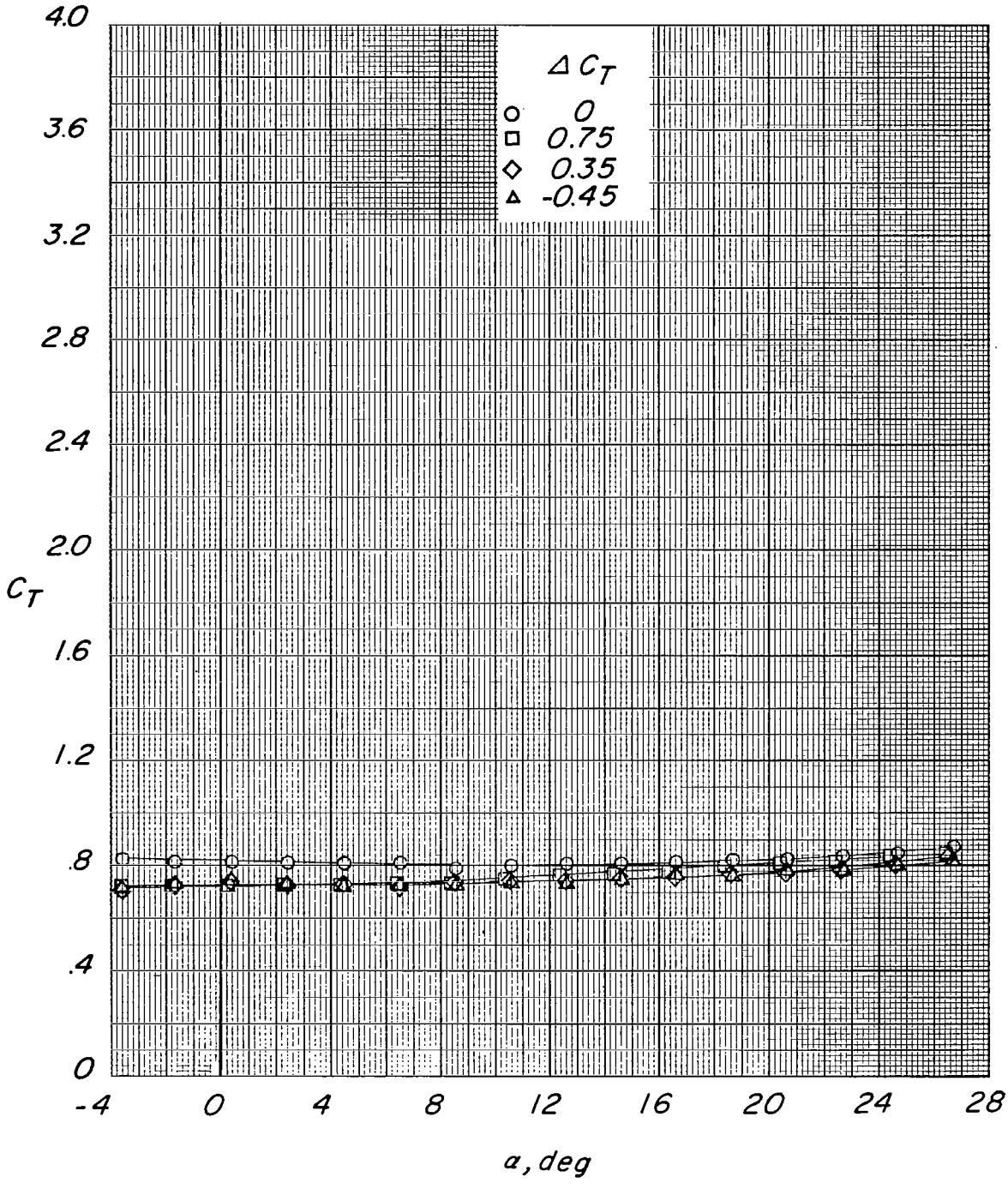

(b) Continued. Thrust coefficient for left motor at basic $C_T \approx 1.6$.

Figure 13.- Continued.

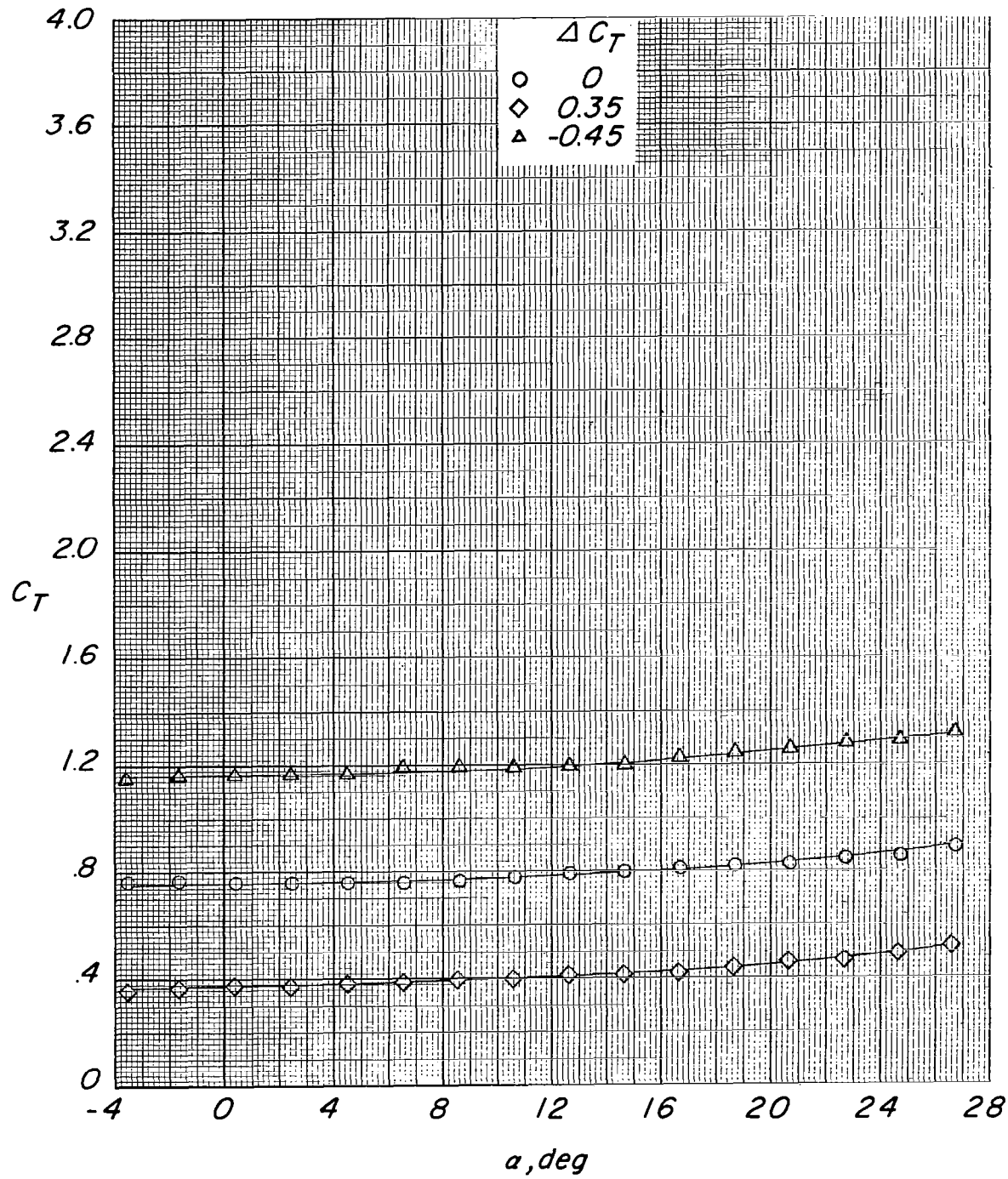

(b) Continued. Thrust coefficient for right motor at basic $C_T \approx 1.6$.

Figure 13.- Continued.

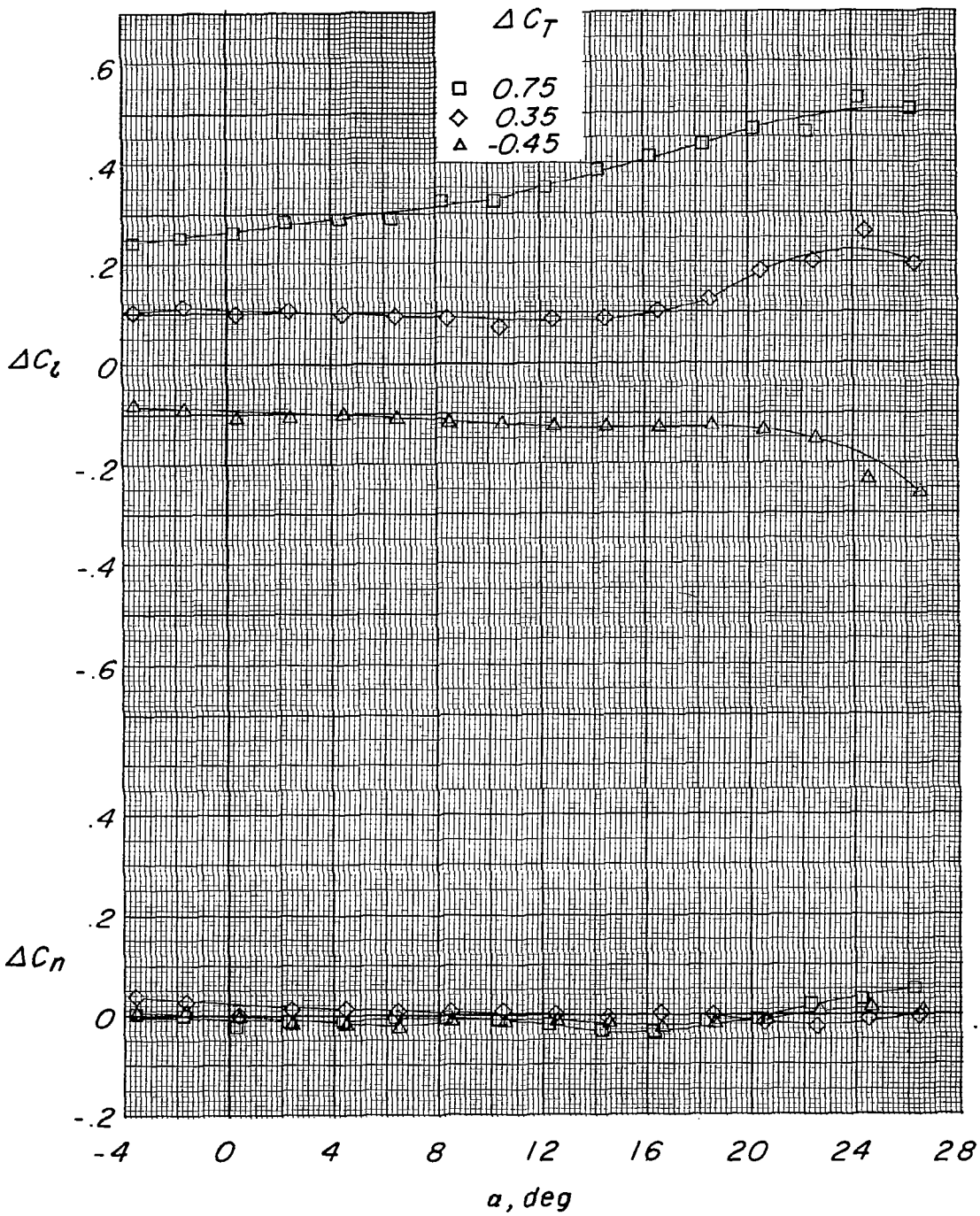

(b) Concluded. Rolling-moment coefficient and yawing-moment coefficient at basic $C_T \approx 1.6$.

Figure 13.- Continued.

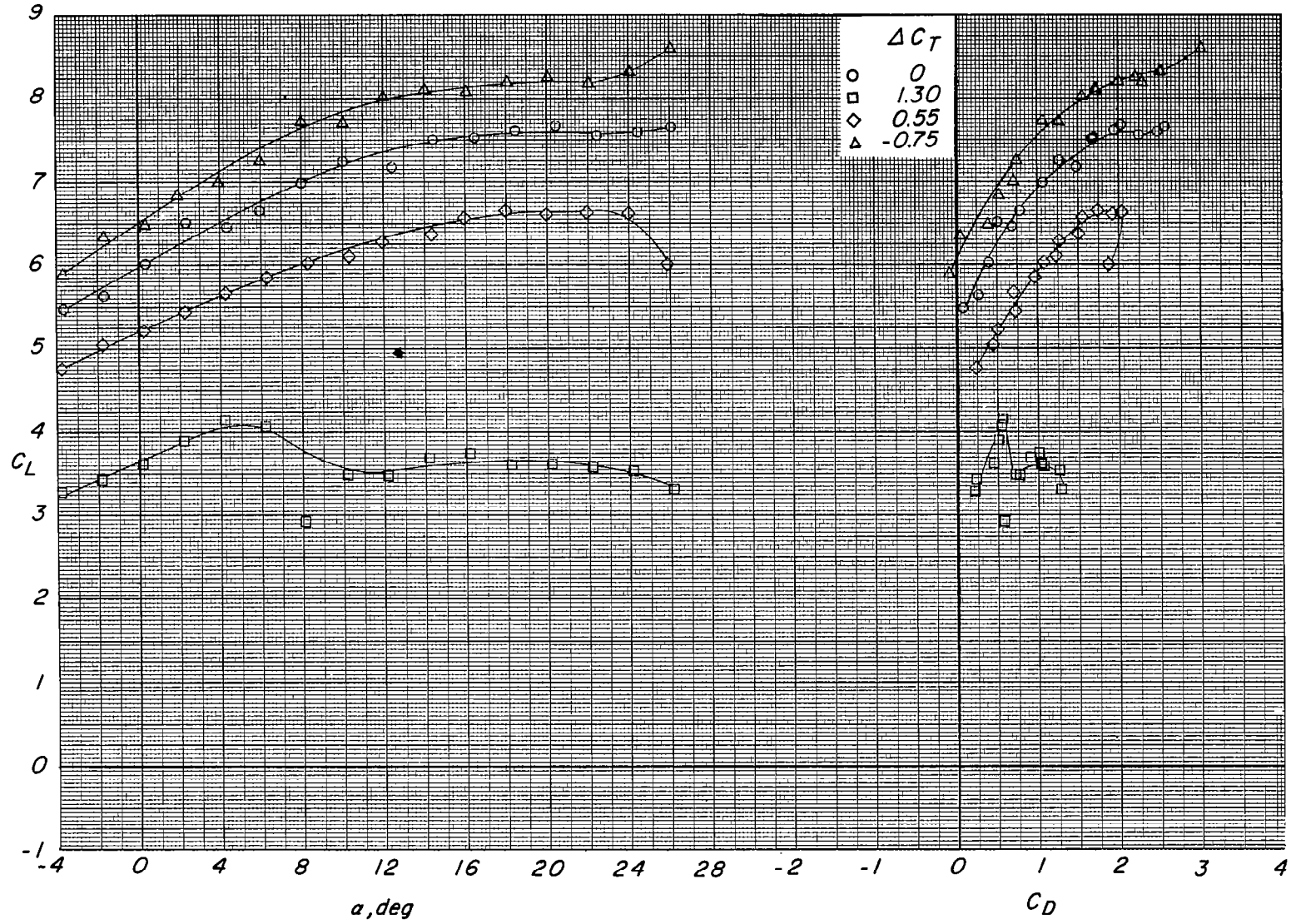

(c) Lift coefficient as a function of angle of attack and of drag coefficient at basic $C_T \approx 2.7$.

Figure 13.- Continued.

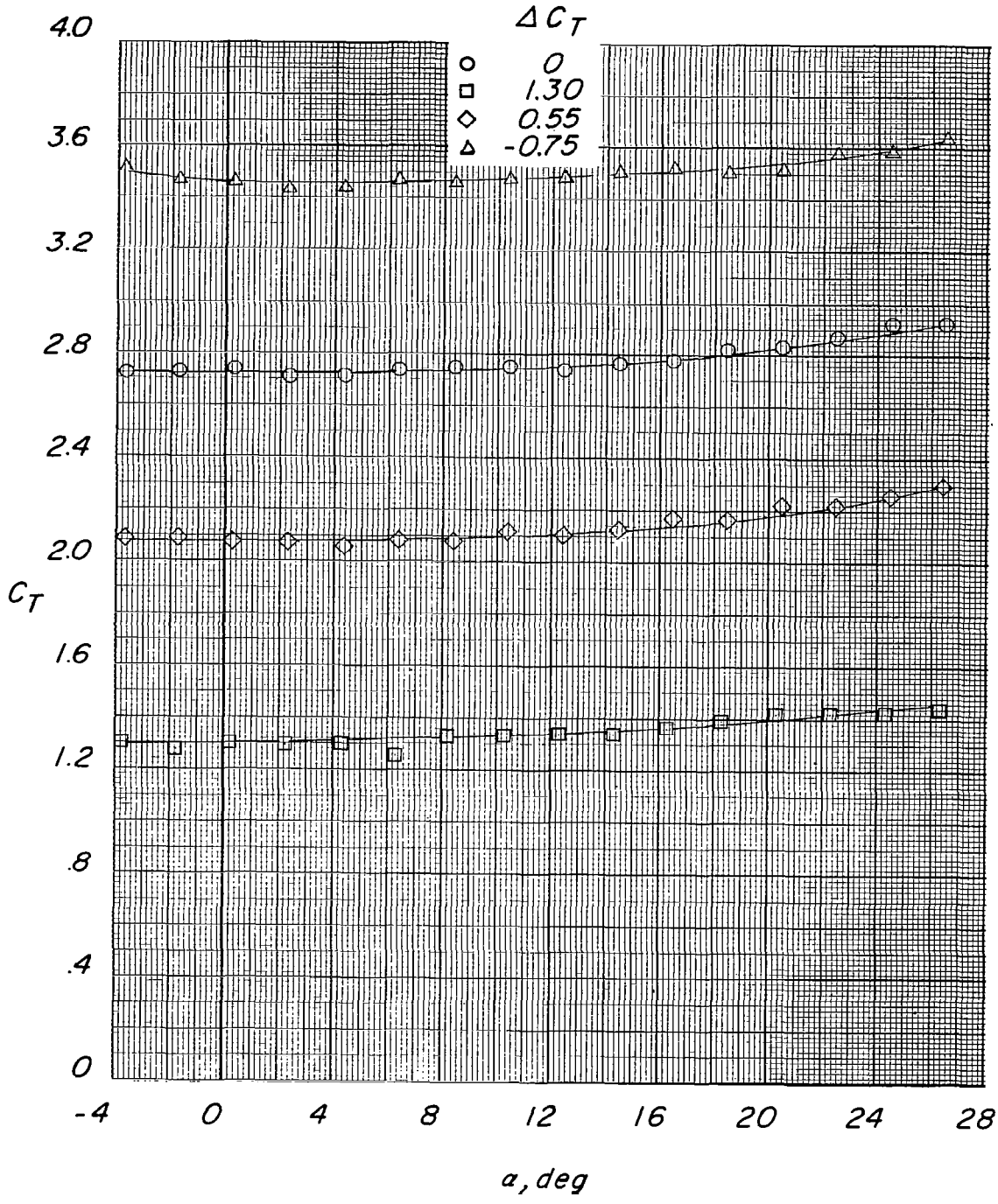

(c) Continued. Total thrust coefficient at basic $C_T \approx 2.7$.

Figure 13.- Continued.

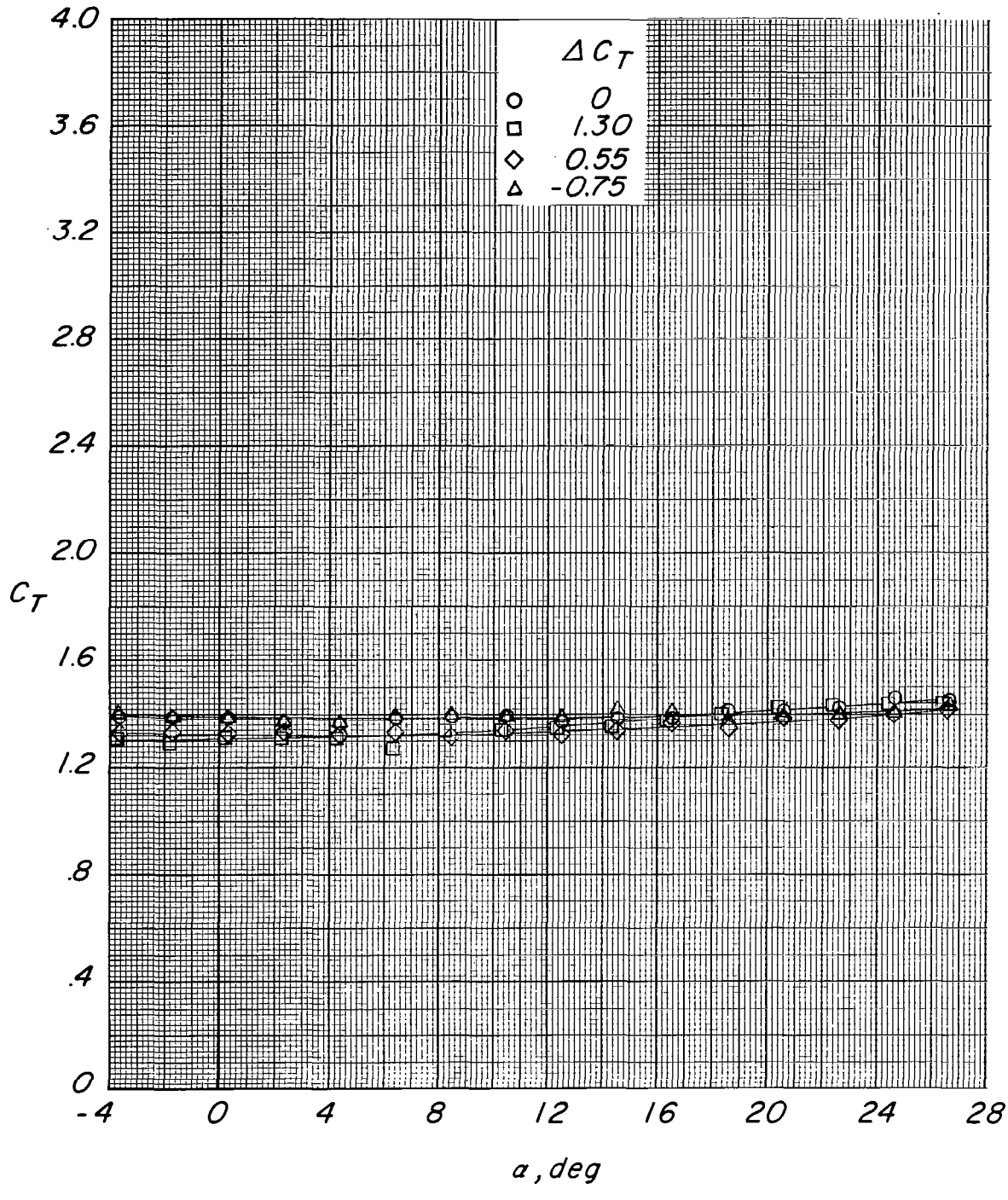

(c) Continued. Thrust coefficient for left motor at basic $C_T \approx 2.7$.

Figure 13.- Continued.

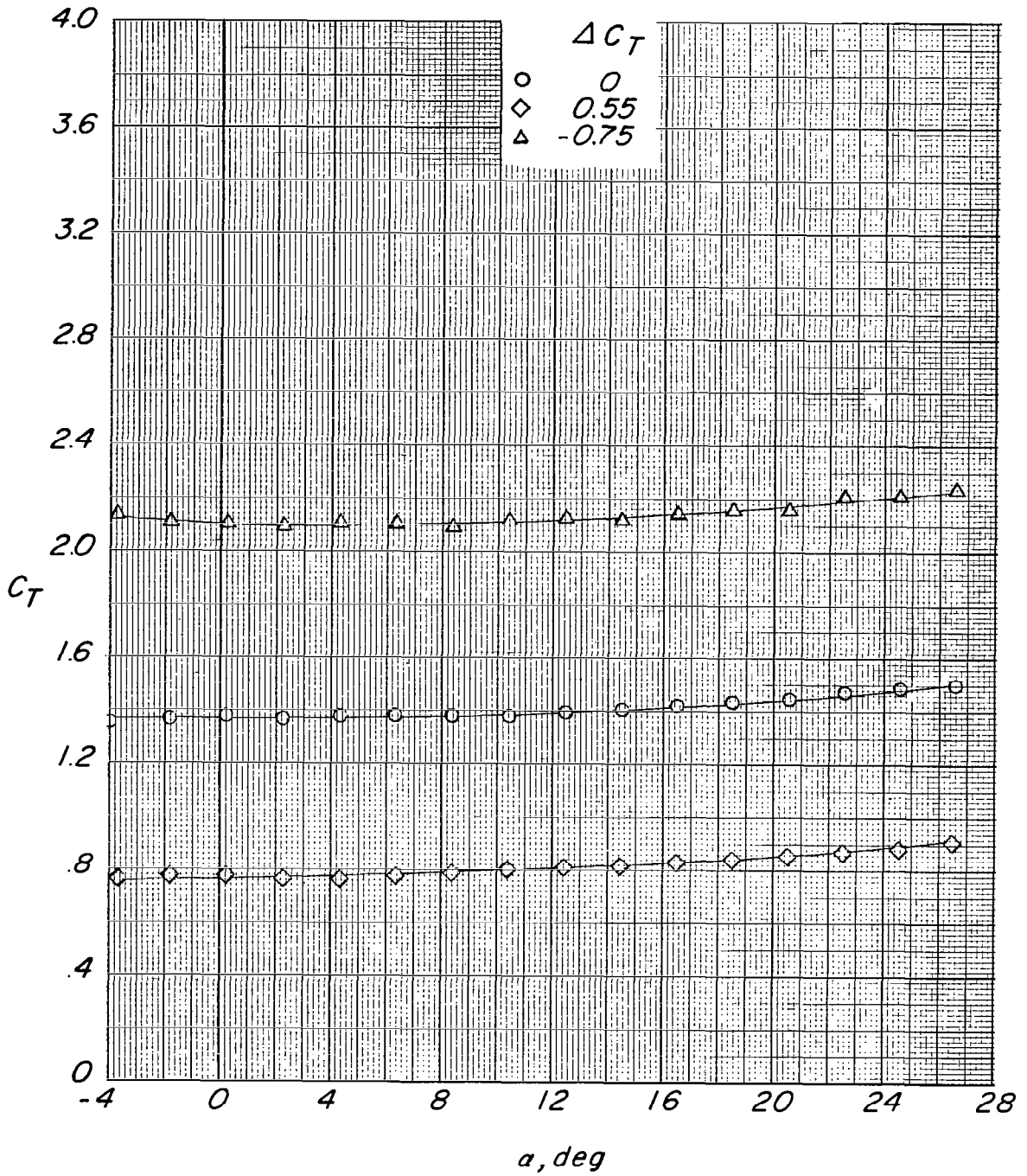

(c) Continued. Thrust coefficient for right motor at basic $C_T \approx 2.7$.

Figure 13.- Continued.

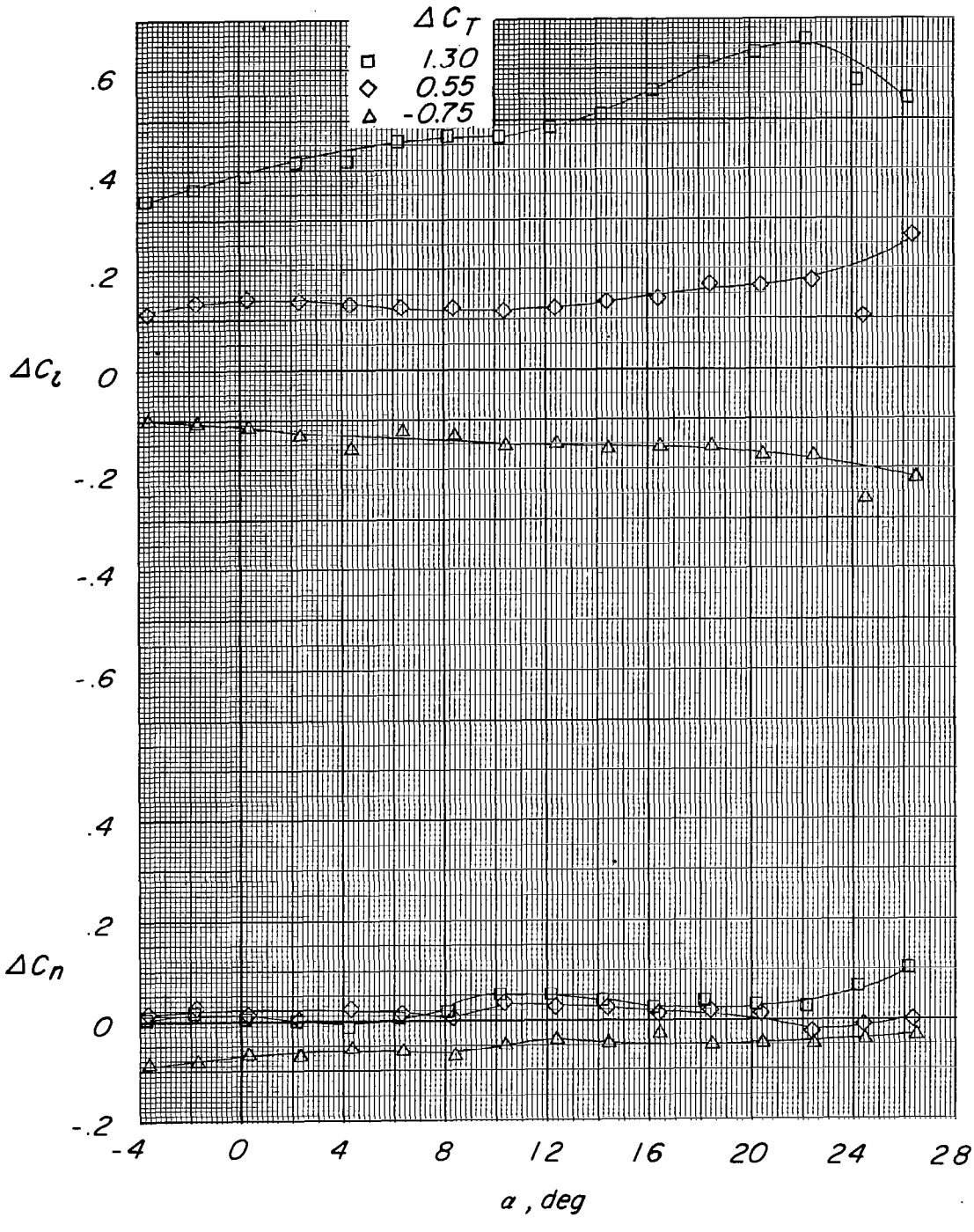

(c) Concluded. Rolling-moment coefficient and yawing-moment coefficient at basic $C_T \approx 2.7$.

Figure 13.- Concluded.

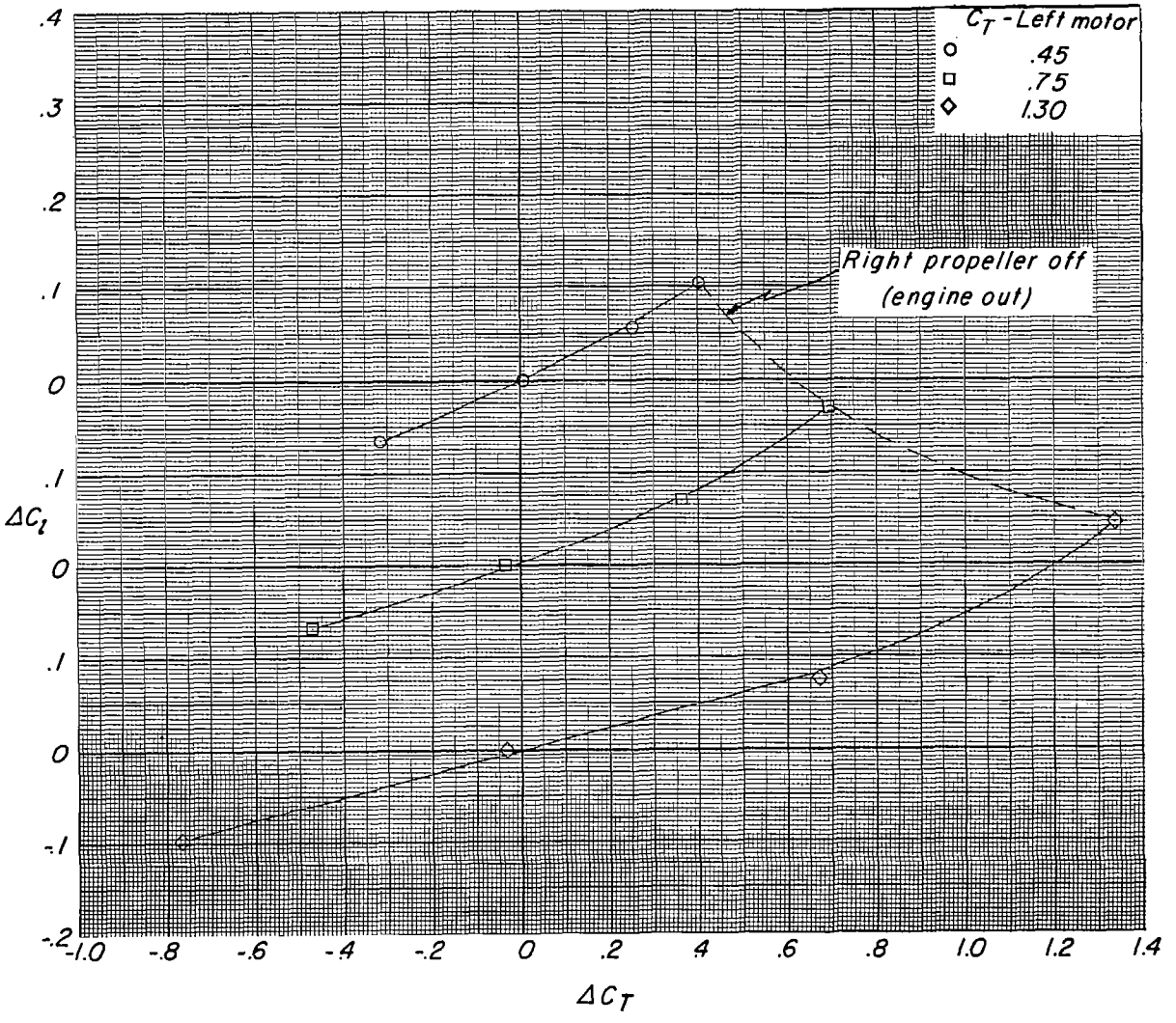

(a) $\alpha = 0^\circ$.

Figure 14.- Summary of the effect of differential propeller thrust on rolling-moment coefficient and on yawing-moment coefficient at several thrust coefficients for configuration C (long span, $\delta_f = 45^\circ$).

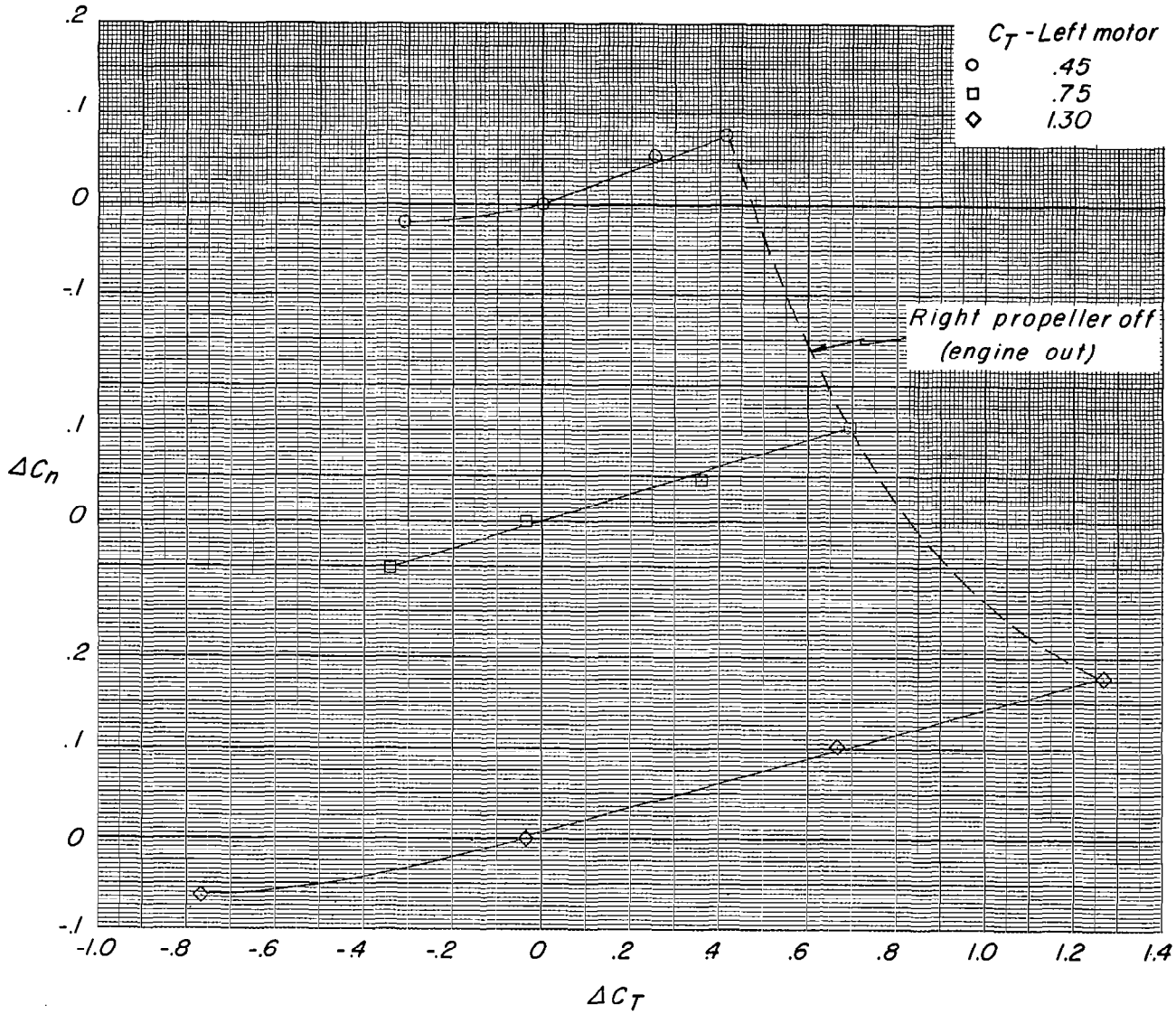

(a) Concluded.

Figure 14.- Continued.

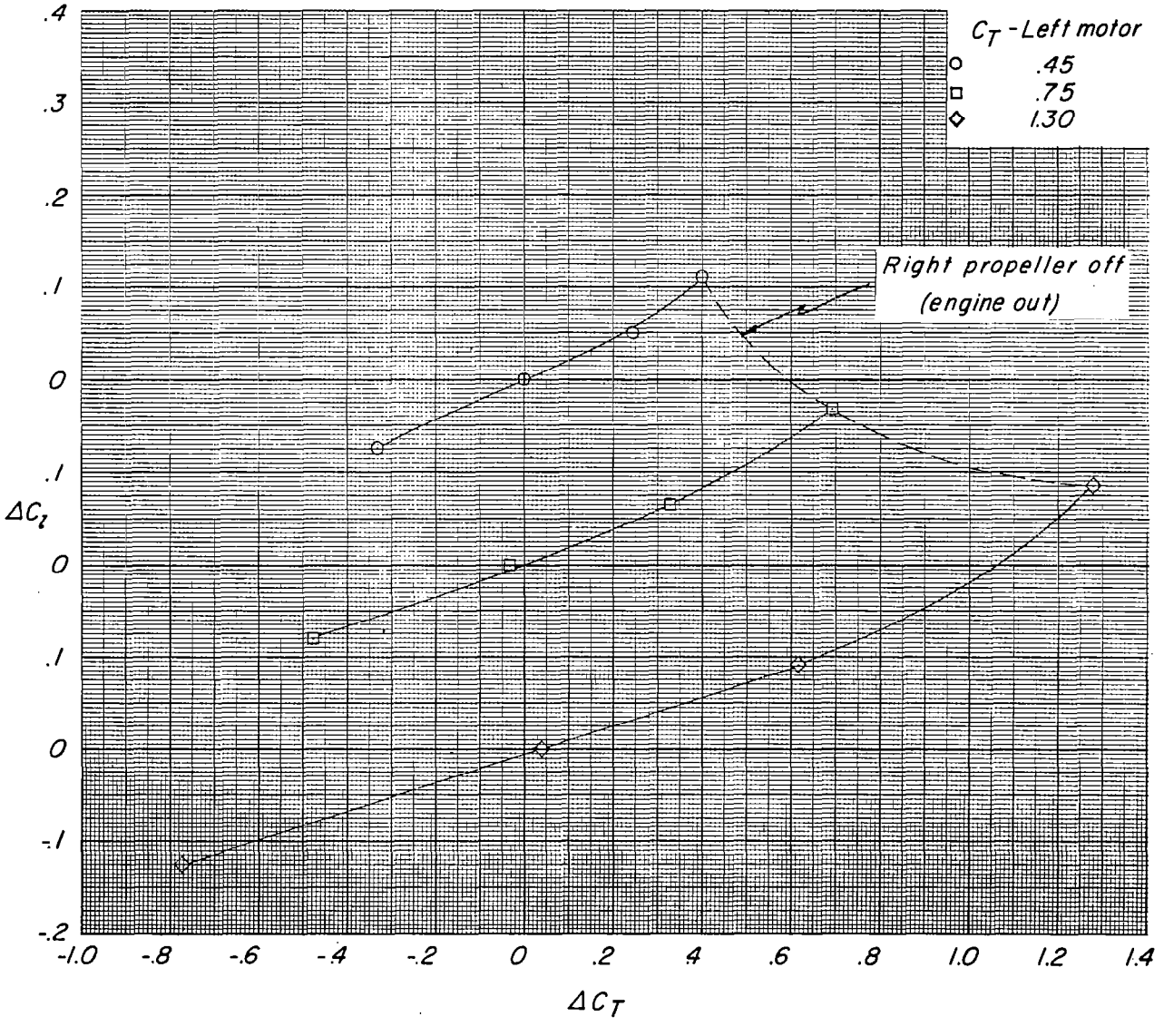

(b) $\alpha = 4^\circ$.

Figure 14.- Continued.

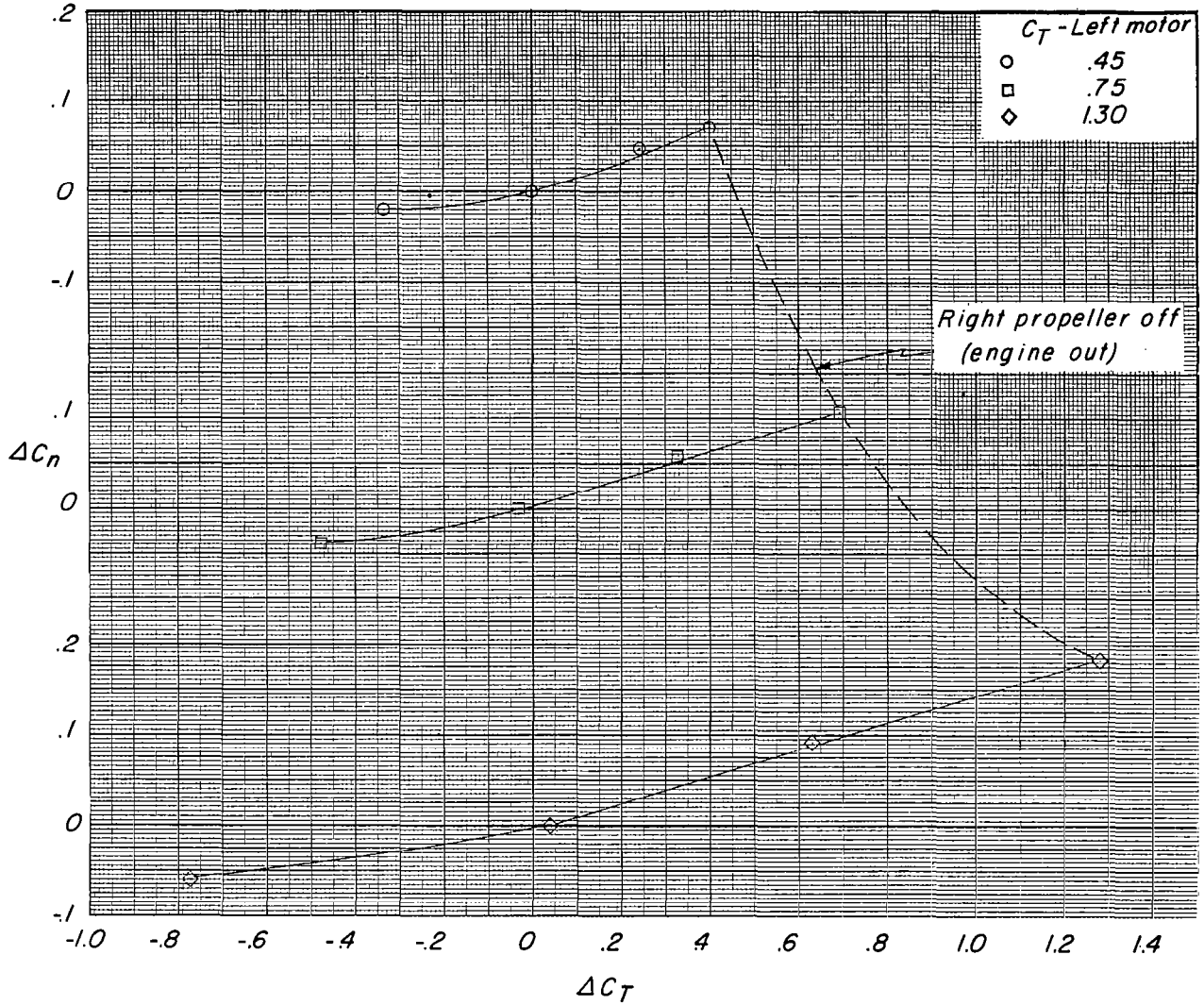

(b) Concluded.

Figure 14.- Continued.

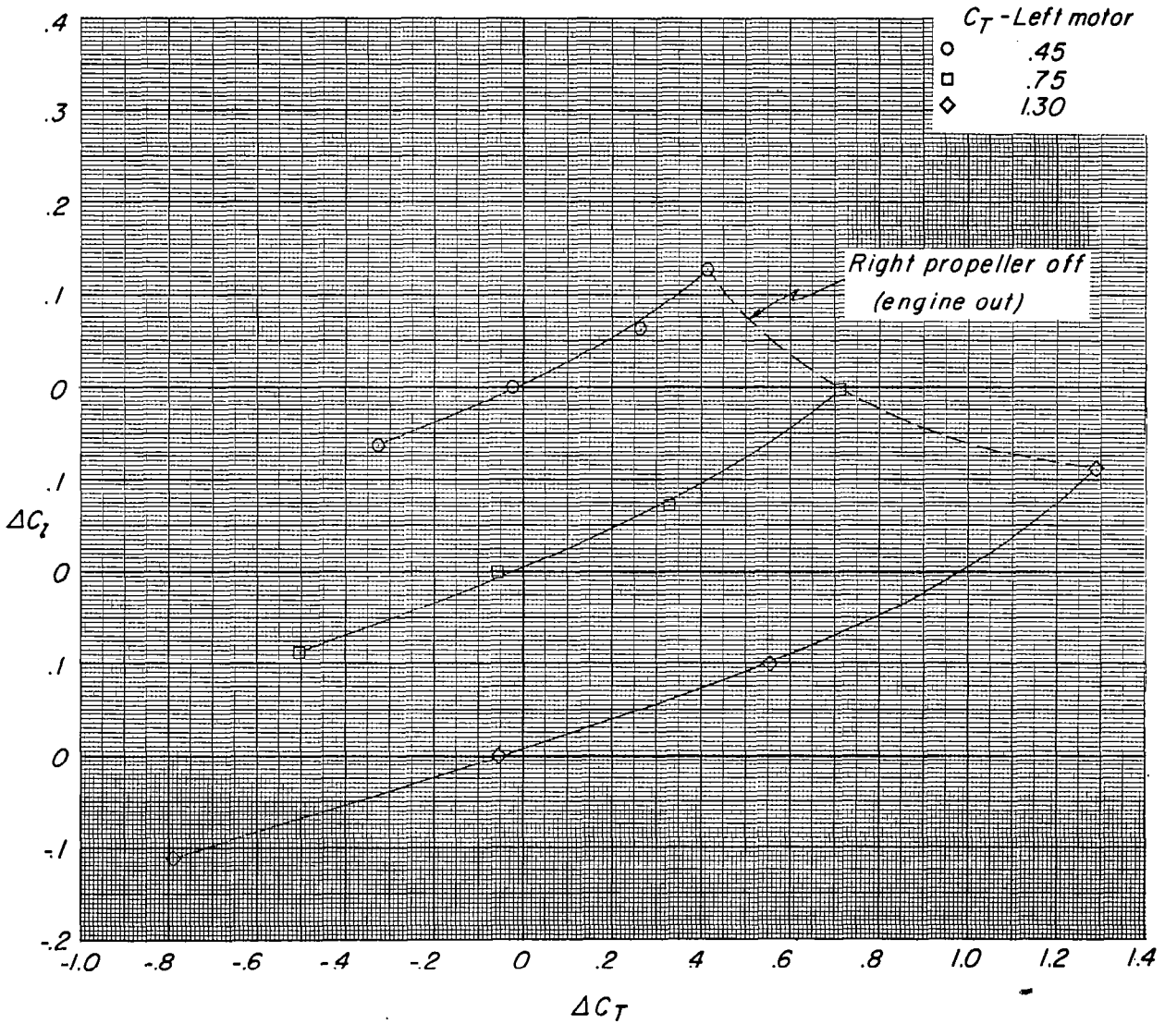

(c) $\alpha = 8^{\circ}$.

Figure 14.- Continued.

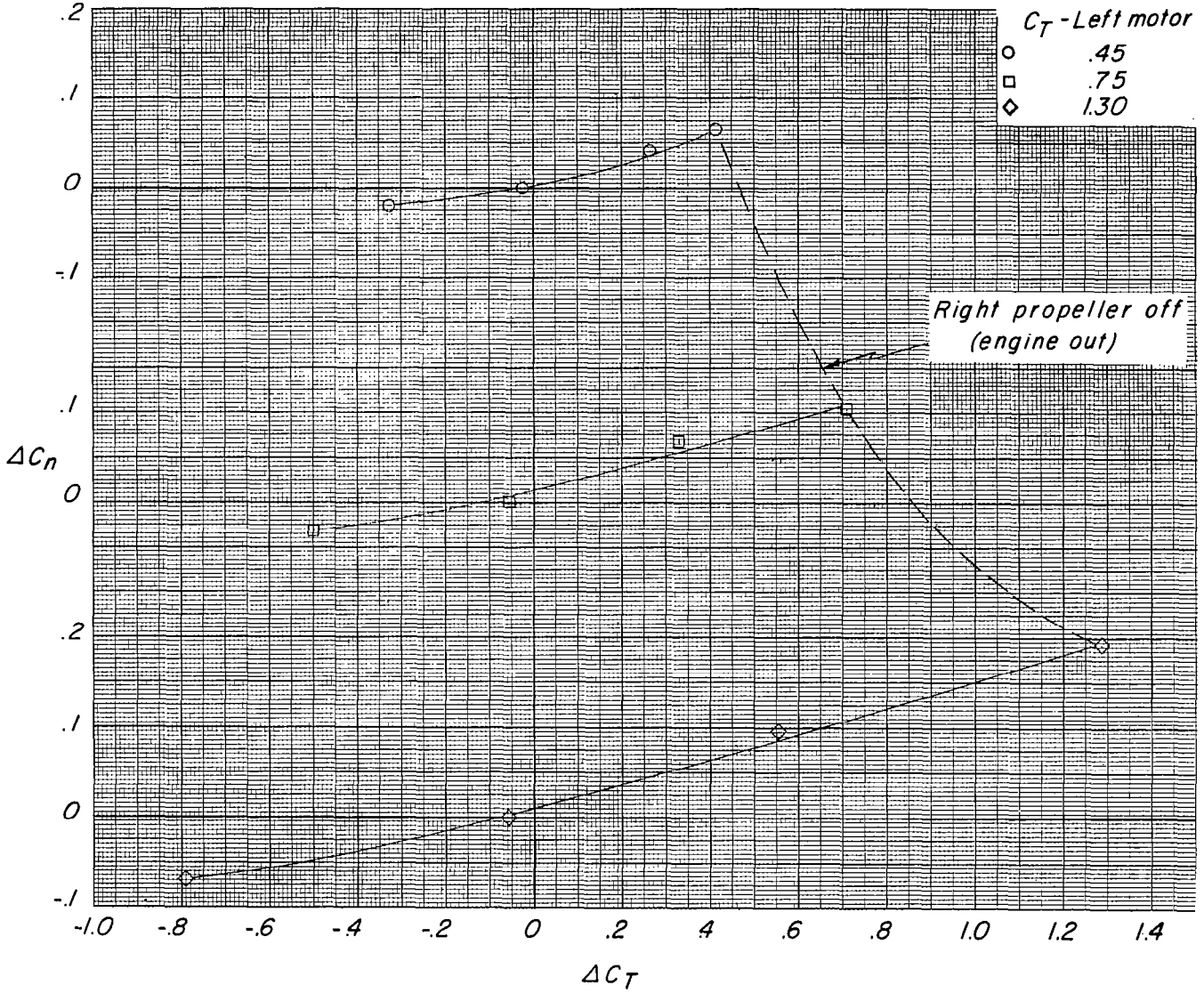

(c) Concluded.

Figure 14.- Concluded.

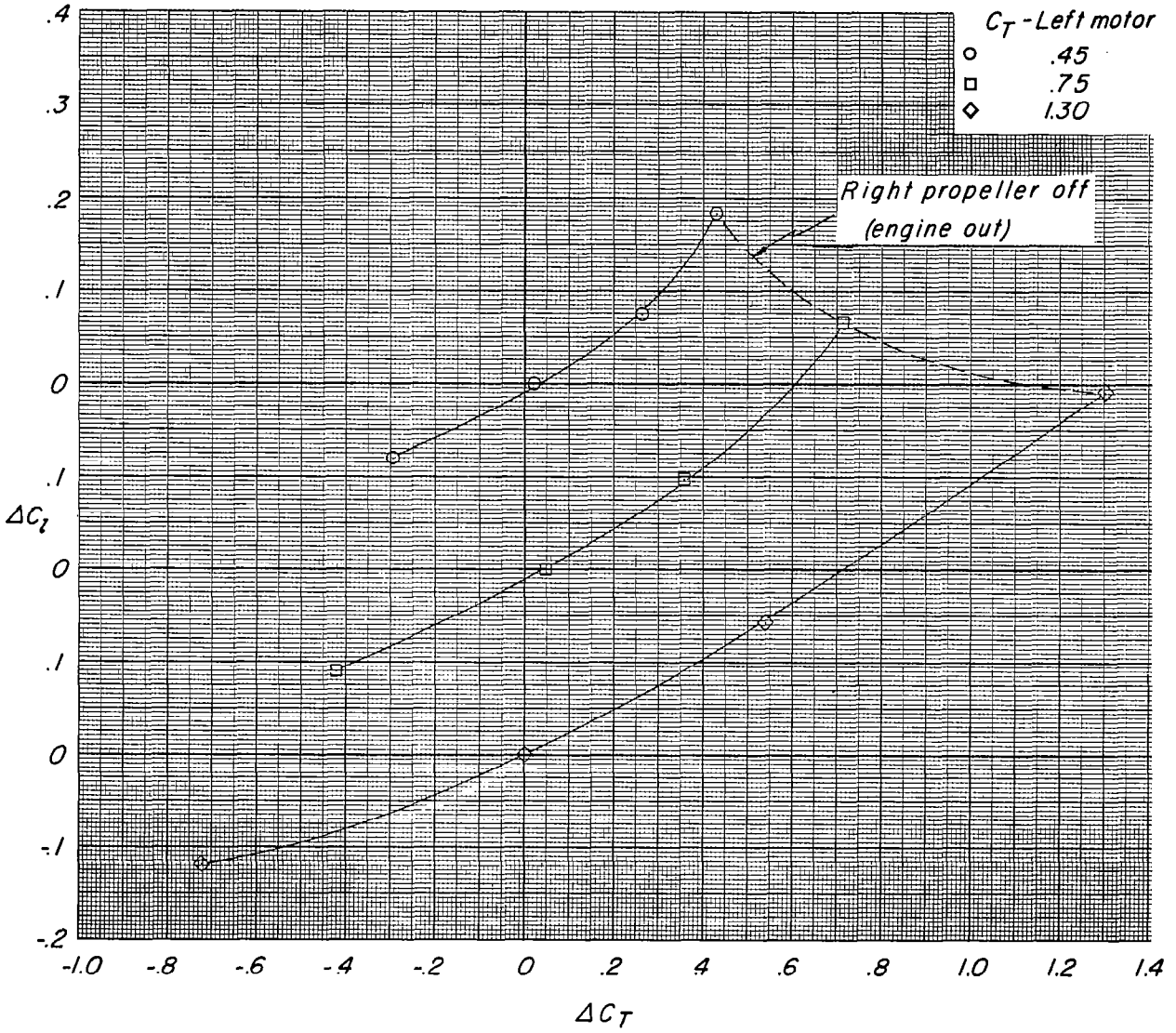

(a) $\alpha = 0^{\circ}$.

Figure 15.- Summary of the effect of differential propeller thrust on rolling-moment coefficient and on yawing-moment coefficient at several thrust coefficients for configuration D (long span, $\delta_f = 75^{\circ}$).

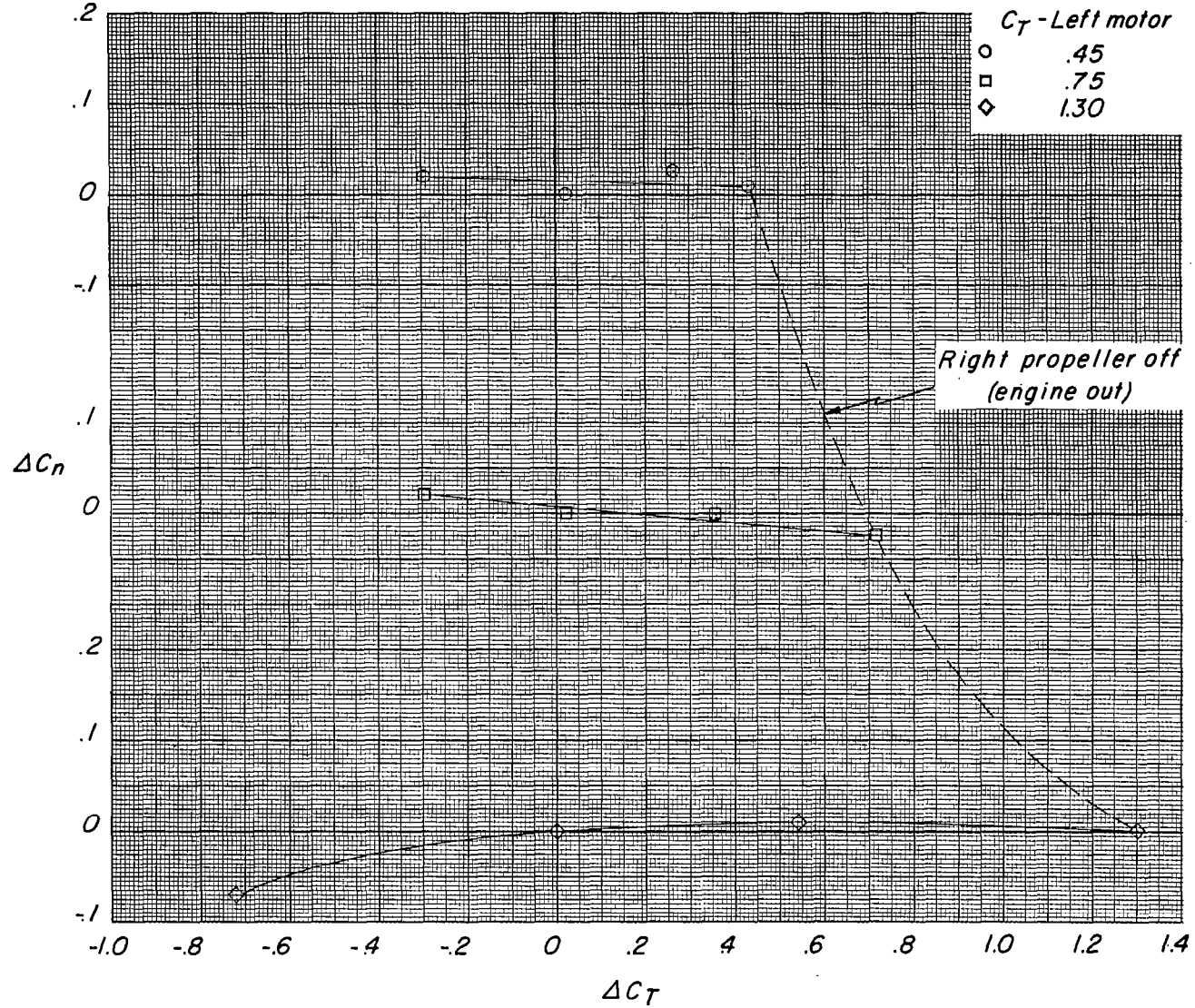

(a) Concluded.

Figure 15.- Continued.

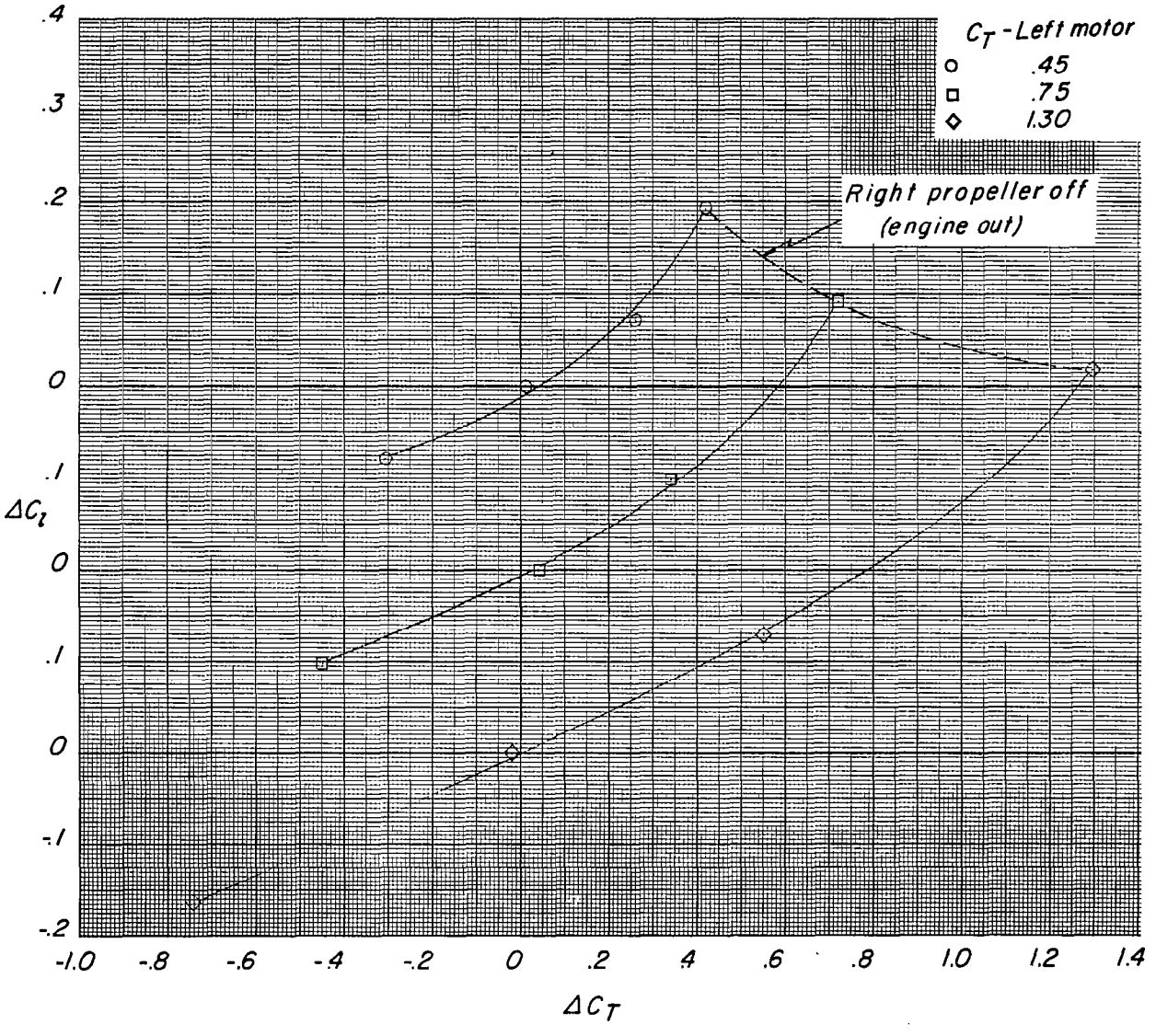

(b) $\alpha = 4^{\circ}$.

Figure 15.- Continued.

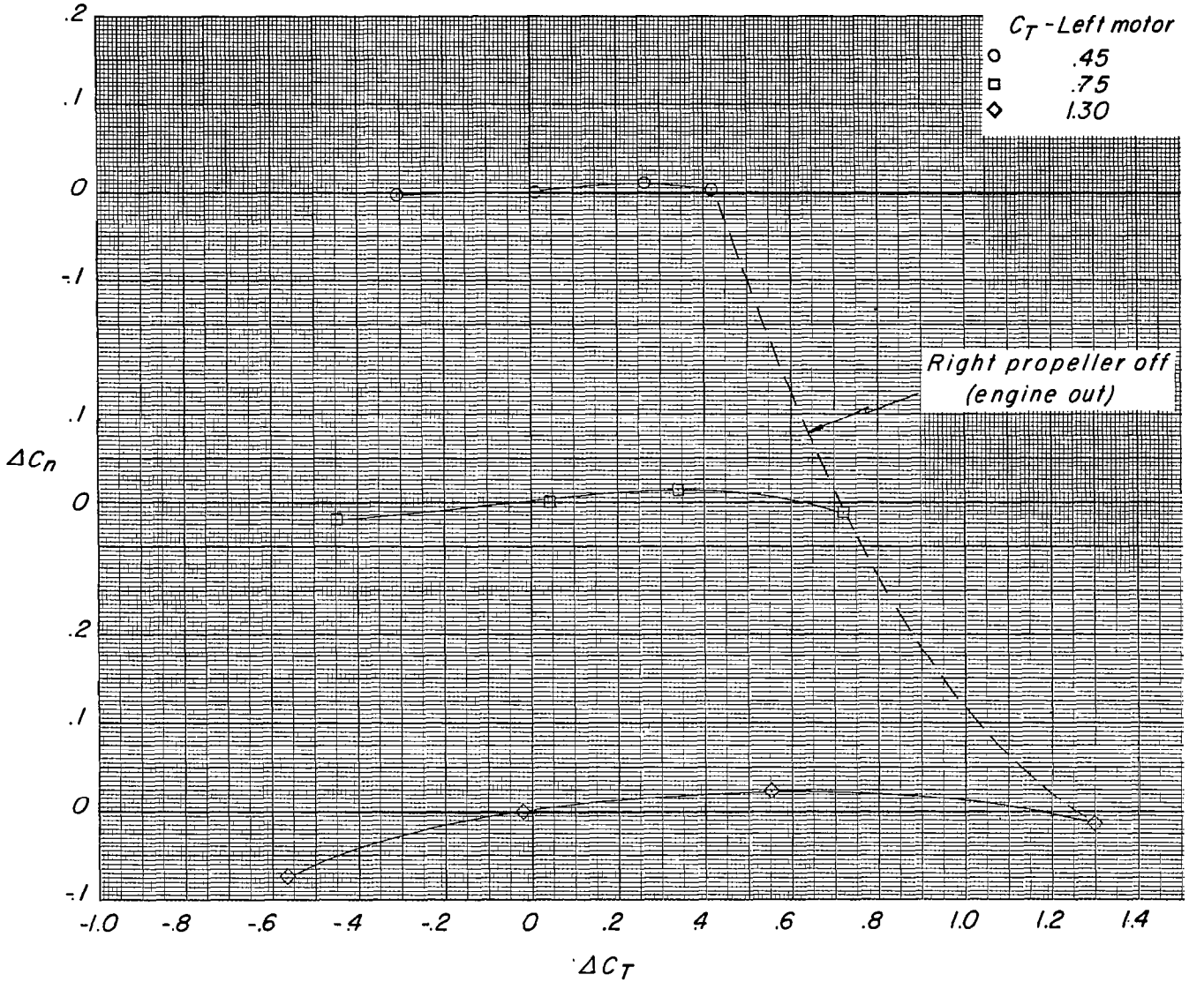

(b) Concluded.

Figure 15.- Continued.

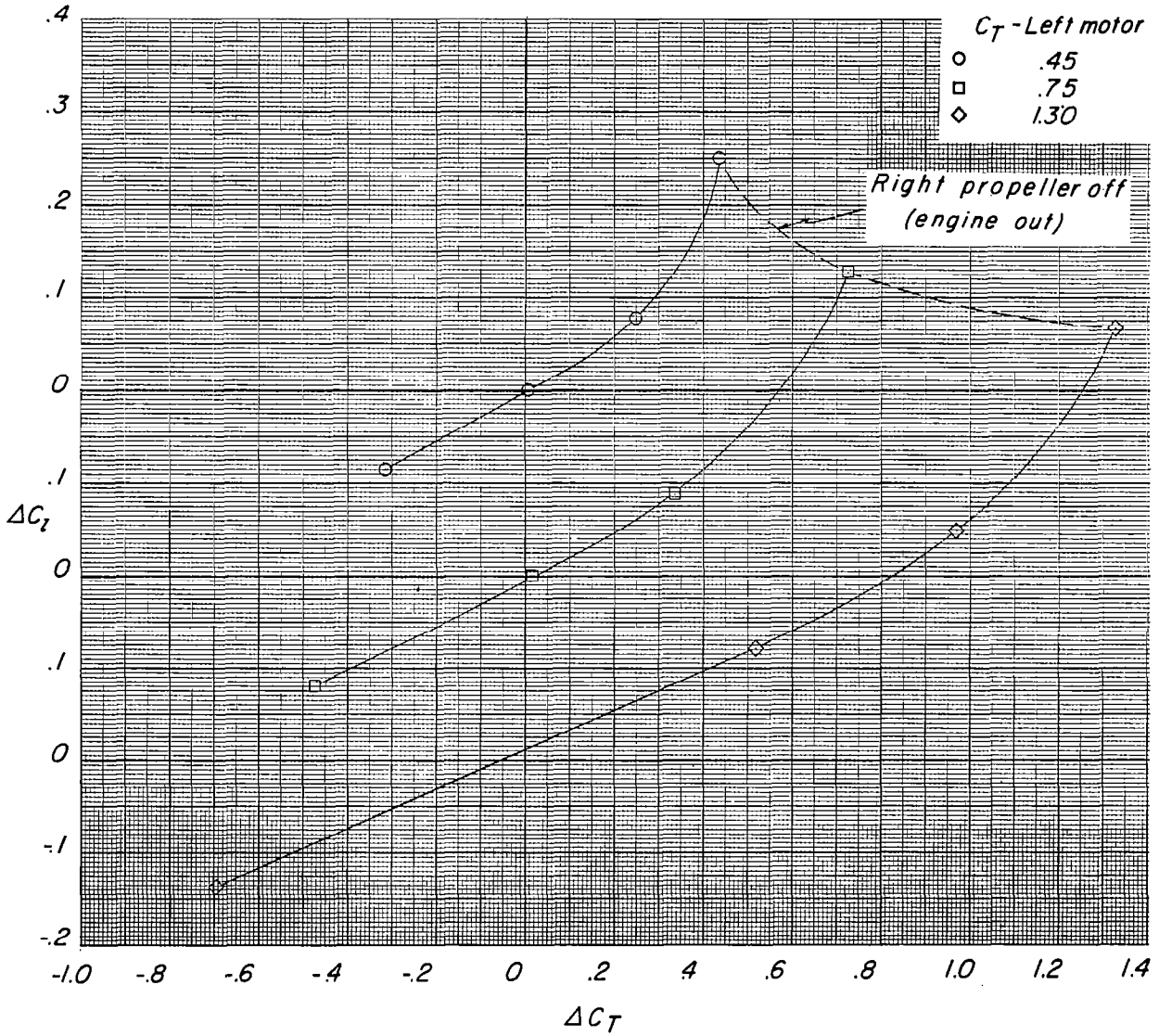

(c) $\alpha = 8^{\circ}$.

Figure 15.- Continued.

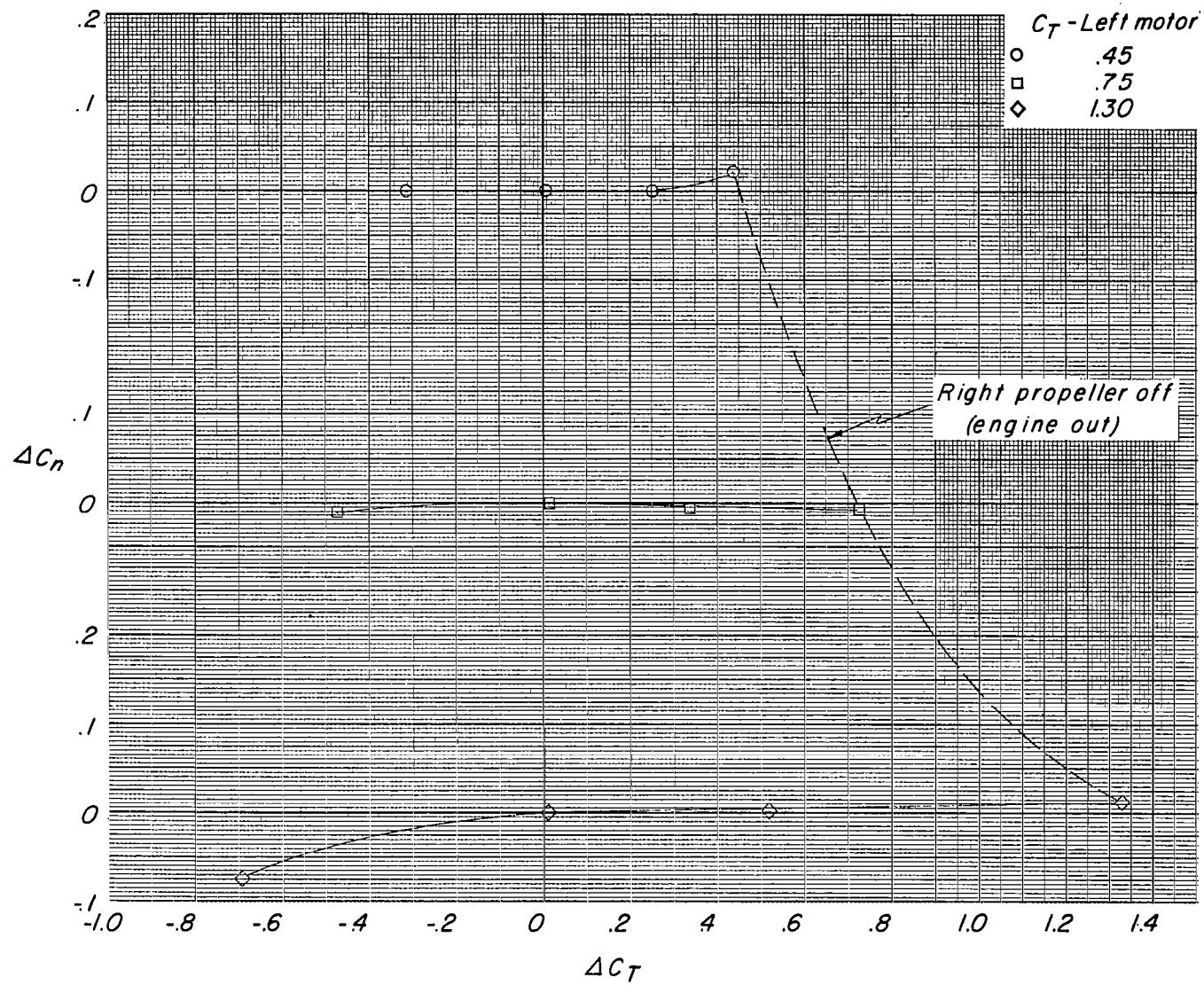

(c) Concluded.

Figure 15.- Concluded.

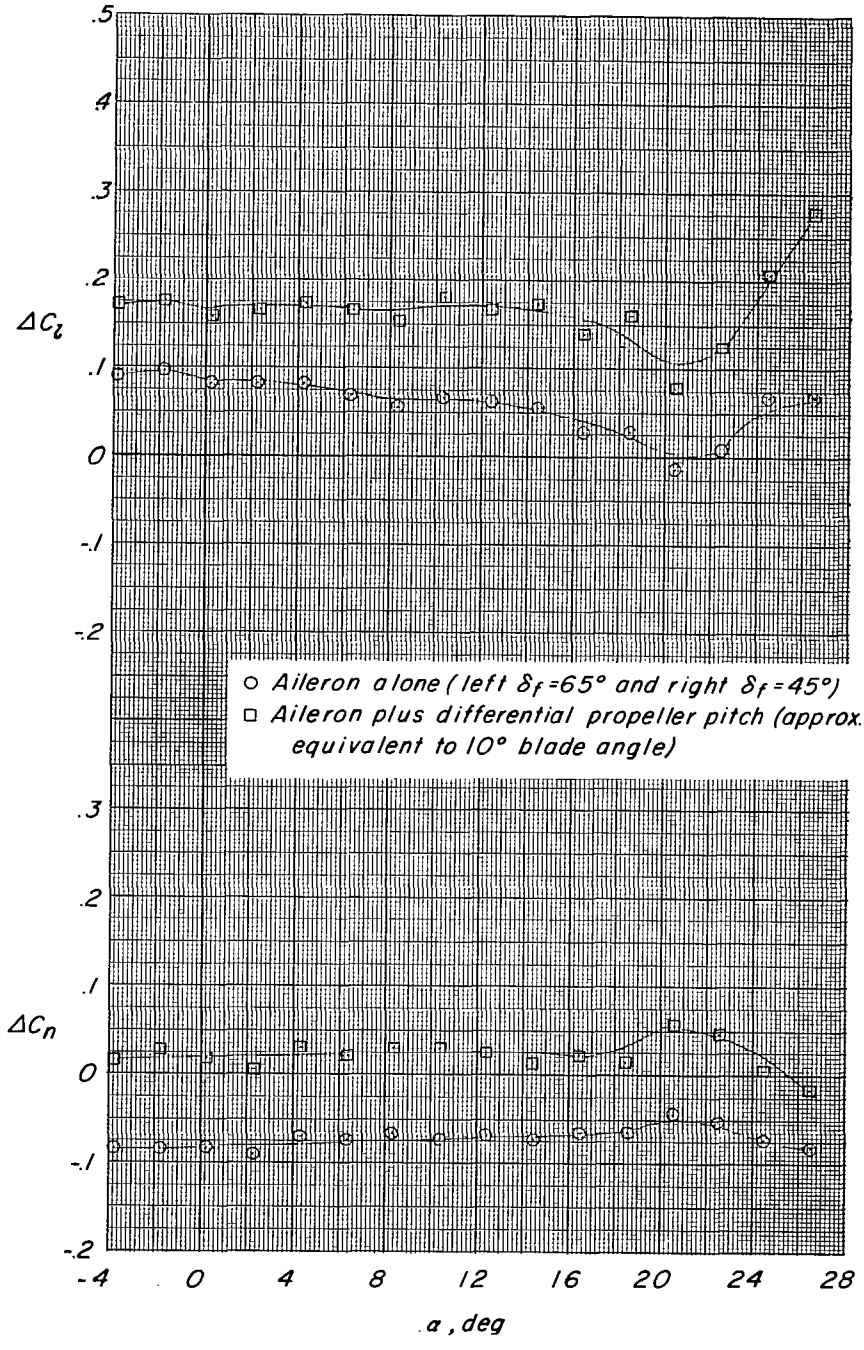

(a) Combination for rolling-moment control.

Figure 16.- Combination of aileron and differential propeller thrust on configuration C (long span, $\delta_f = 45°$, $C_T \approx 2.7$) for rolling-moment and for yawing-moment control.

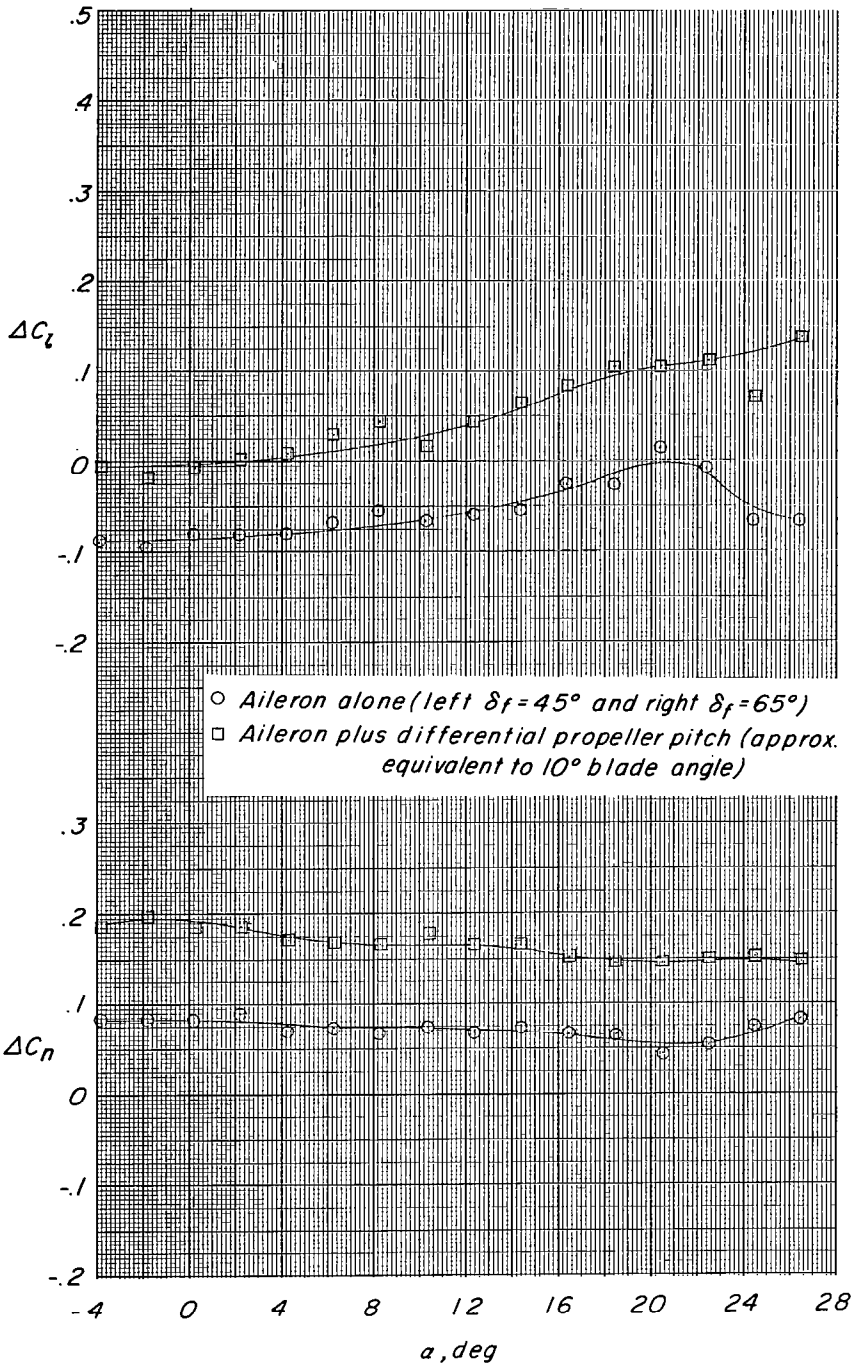

(b) Combination for yawing-moment control.

Figure 16.- Concluded.

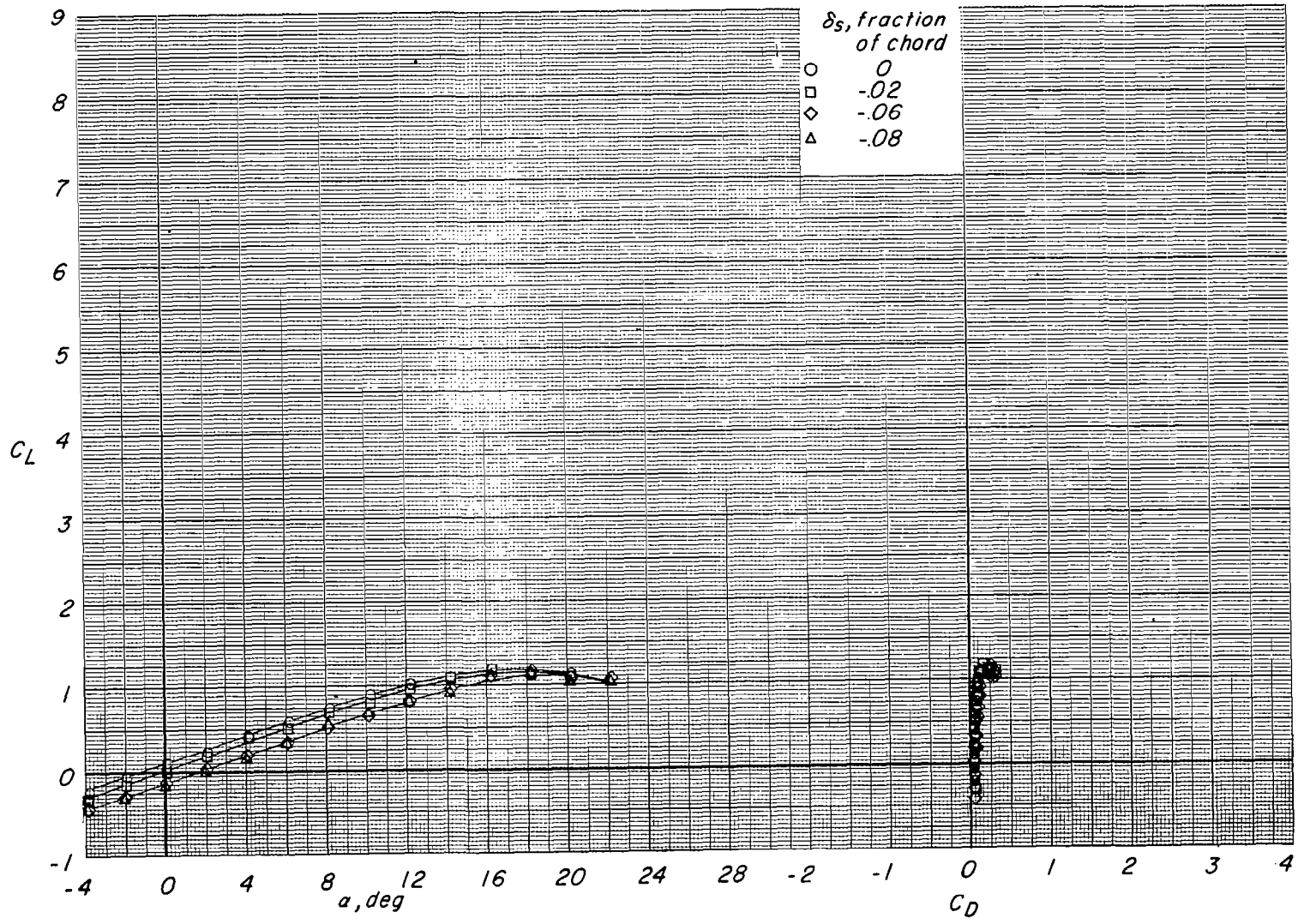

(a) $C_T = 0$ (propeller off).

Figure 17.- Effect of spoiler projection for configuration A (long span, $\delta_f = 0^o$).

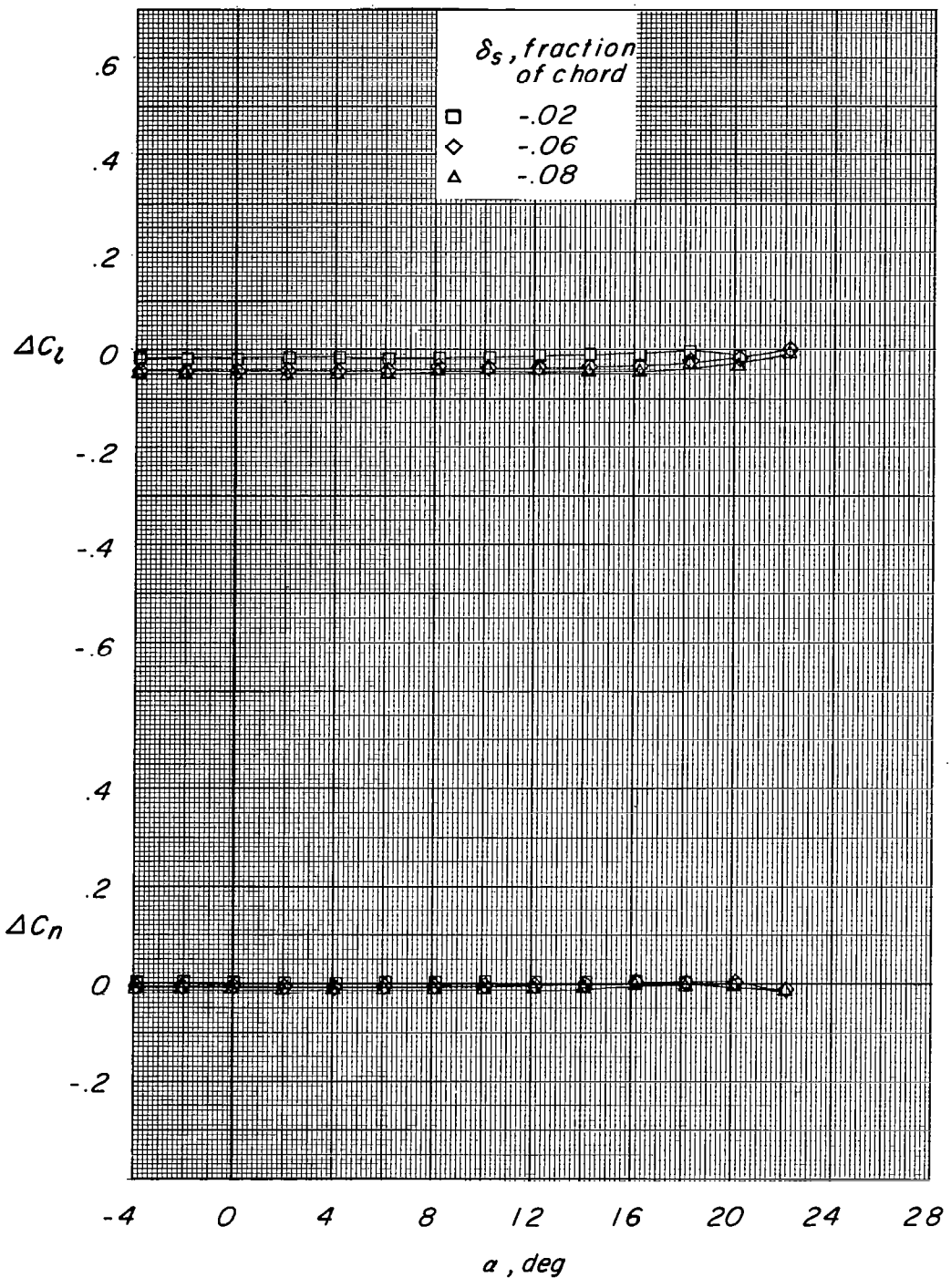

(a) Concluded.

Figure 17.- Continued.

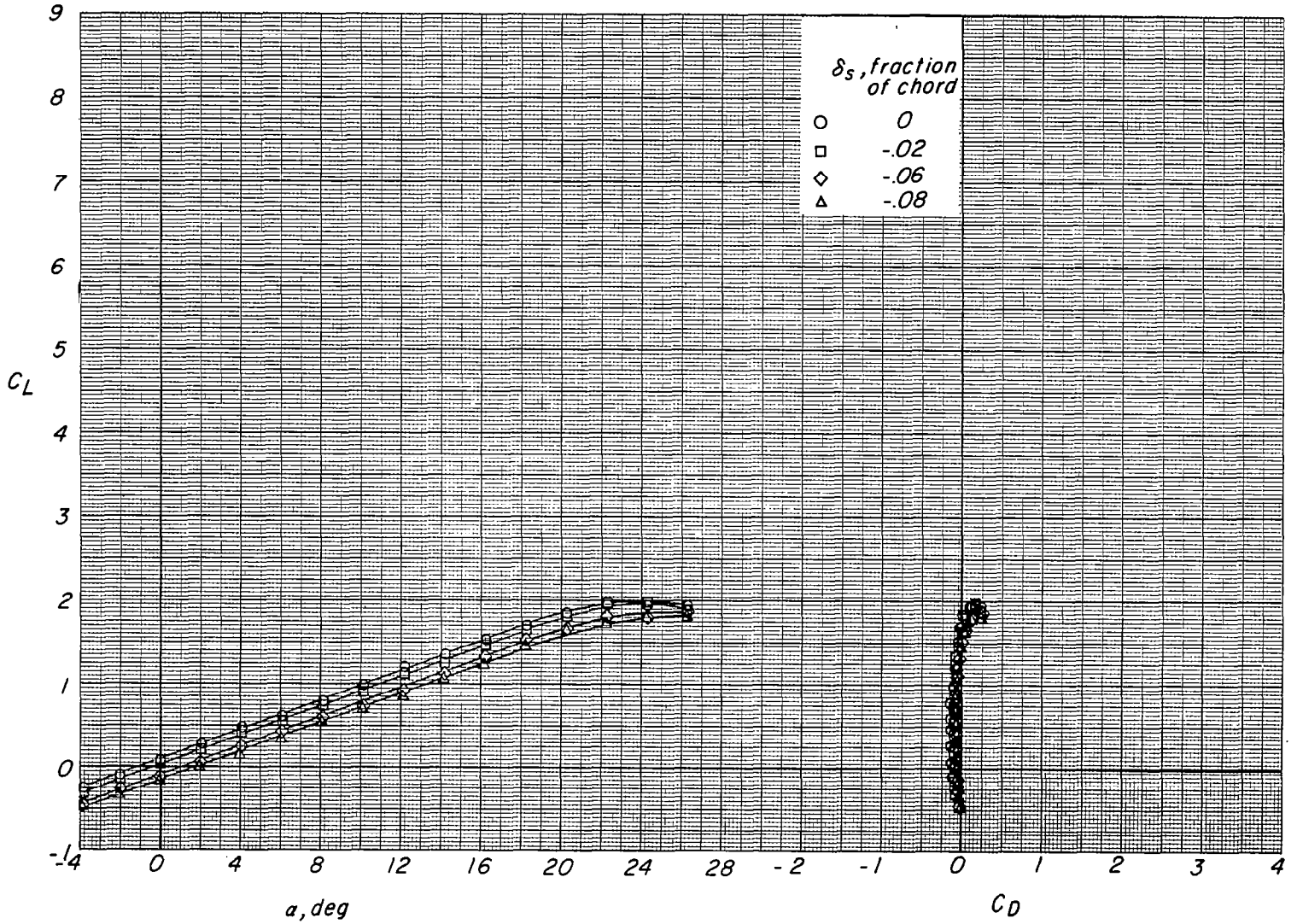

(b) $C_T \approx 0.2$.

Figure 17.- Continued.

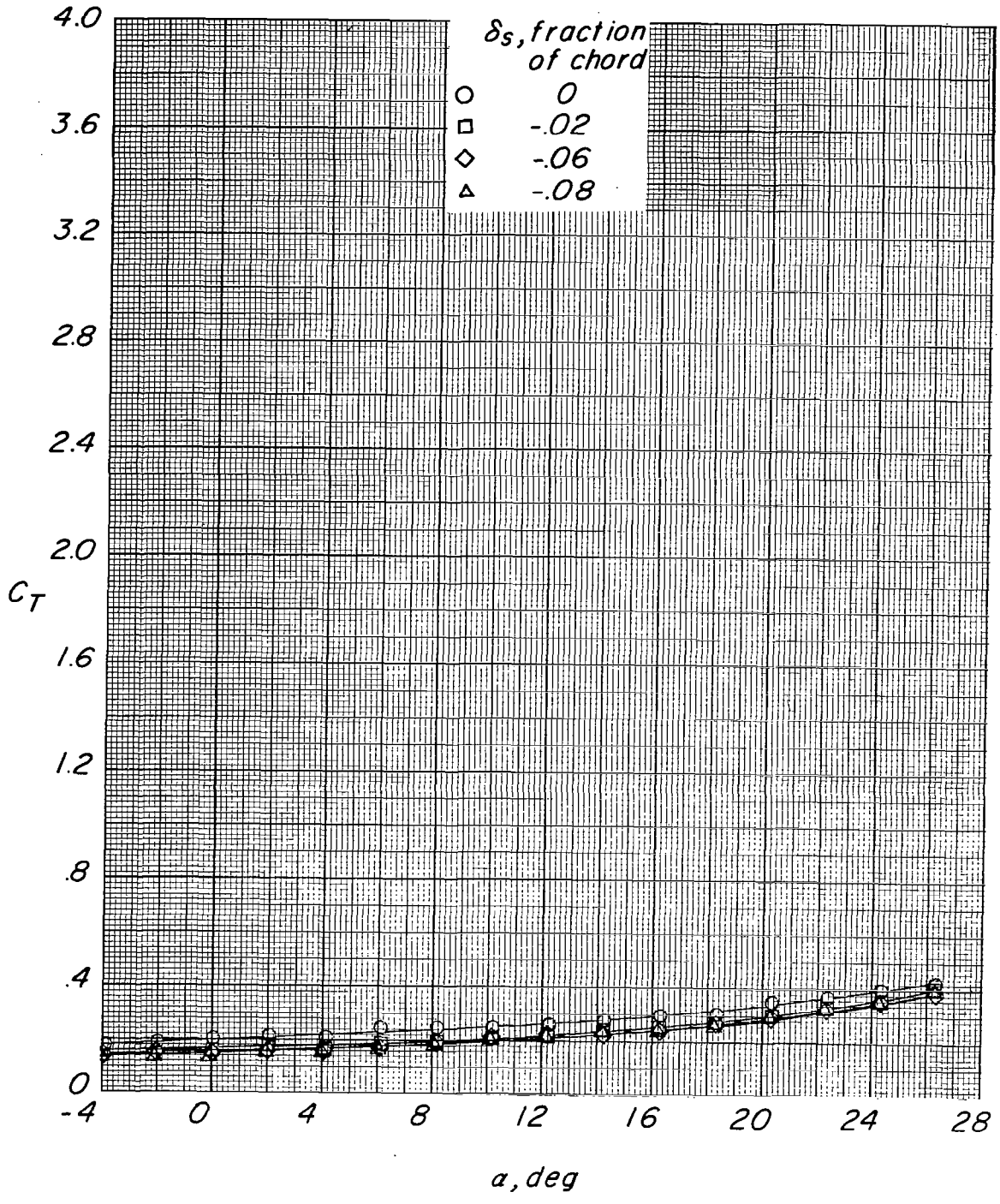

(b) Continued.

Figure 17.- Continued.

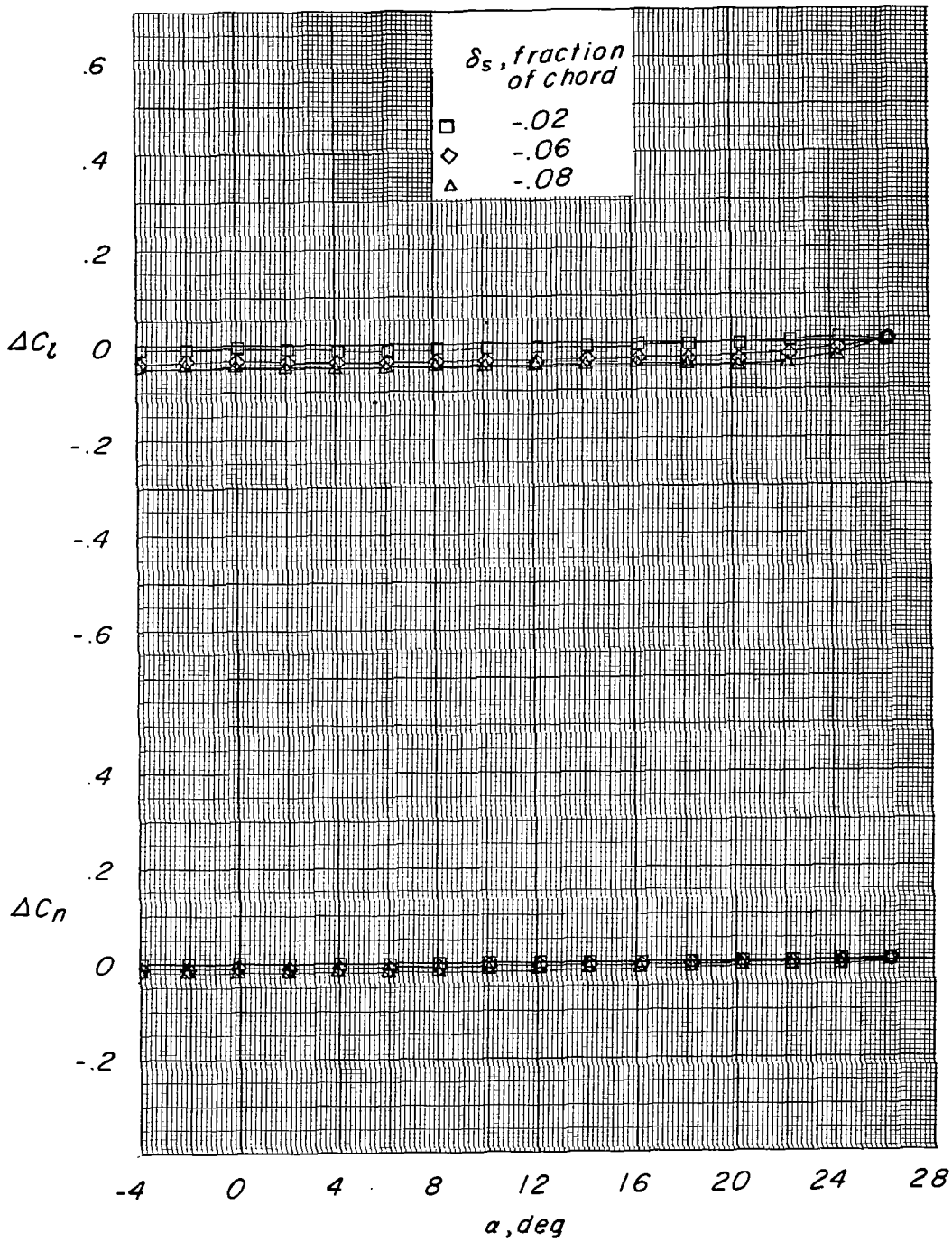

(b) Concluded.

Figure 17.- Continued.

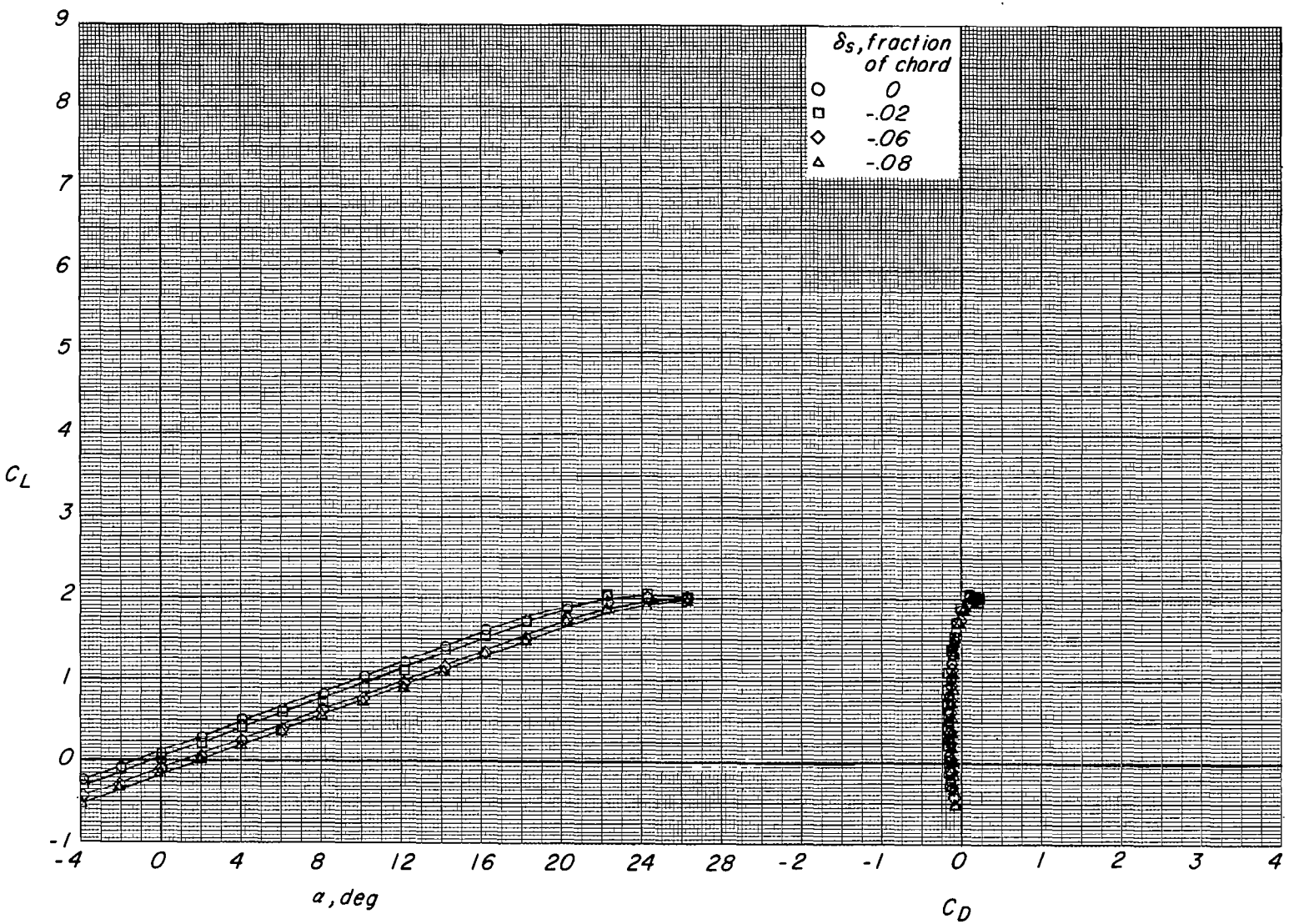

(c) $C_T \approx 0.3$.

Figure 17.- Continued.

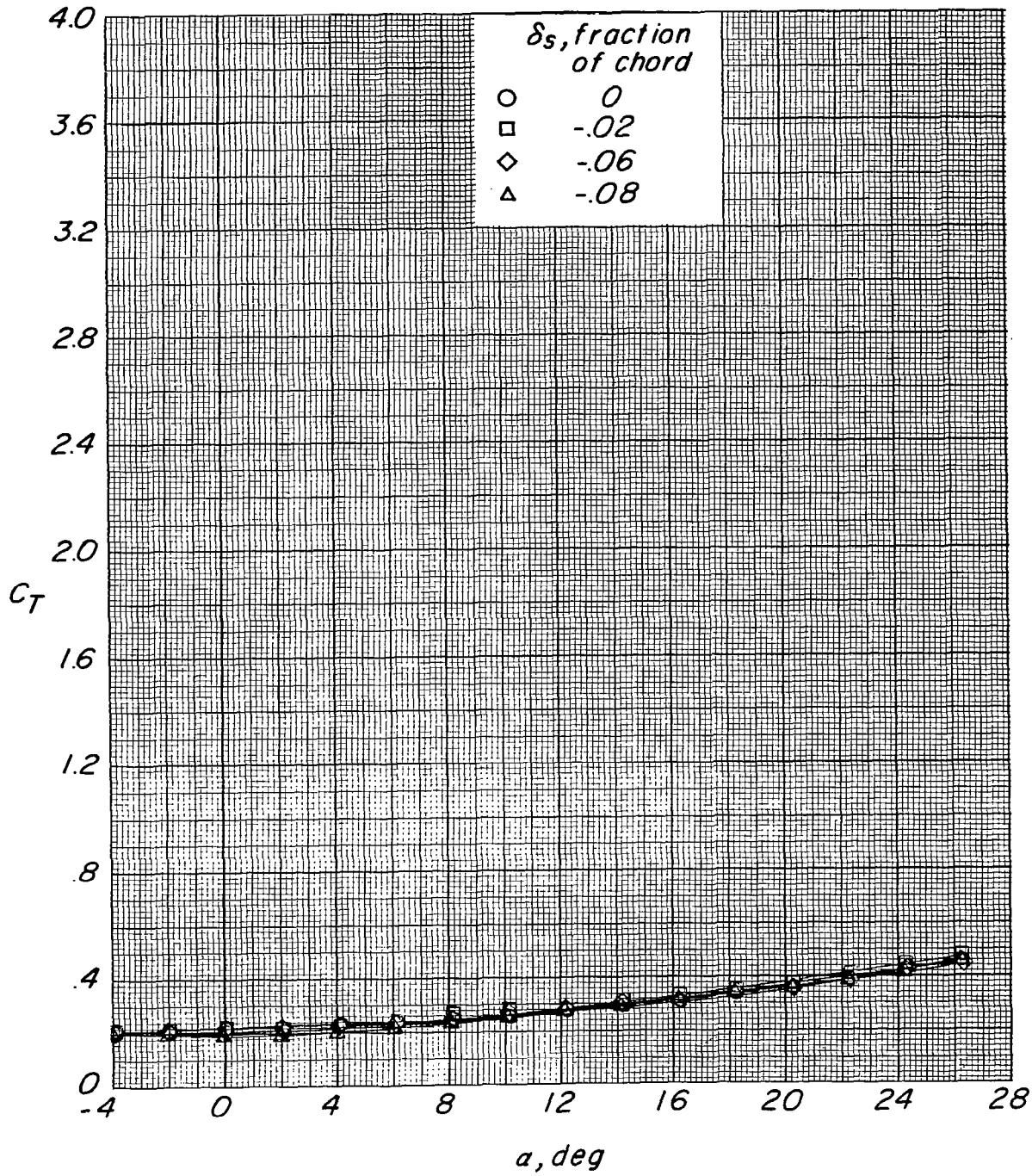

(c) Continued.

Figure 17.- Continued.

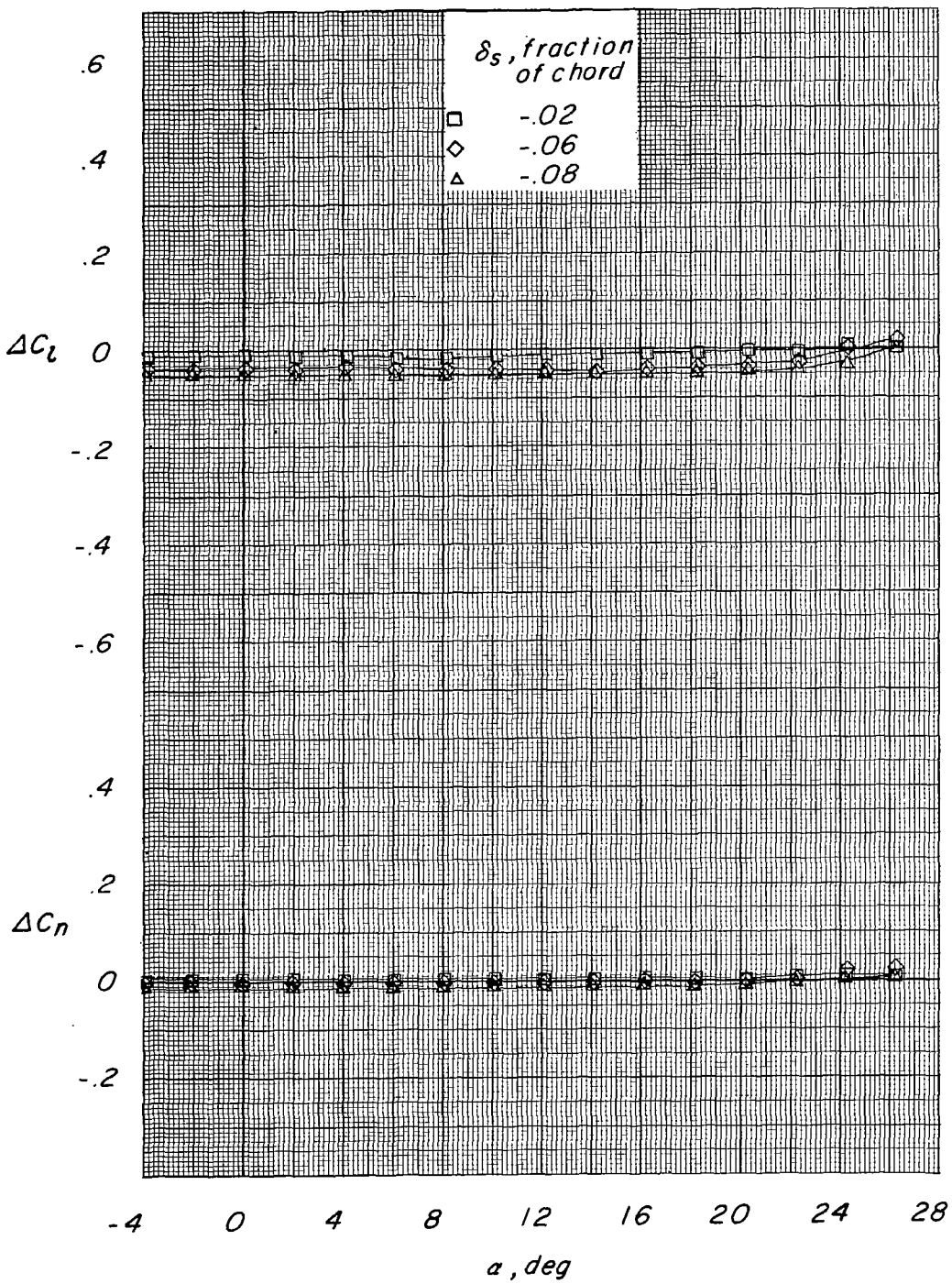

(c) Concluded.

Figure 17.- Concluded.

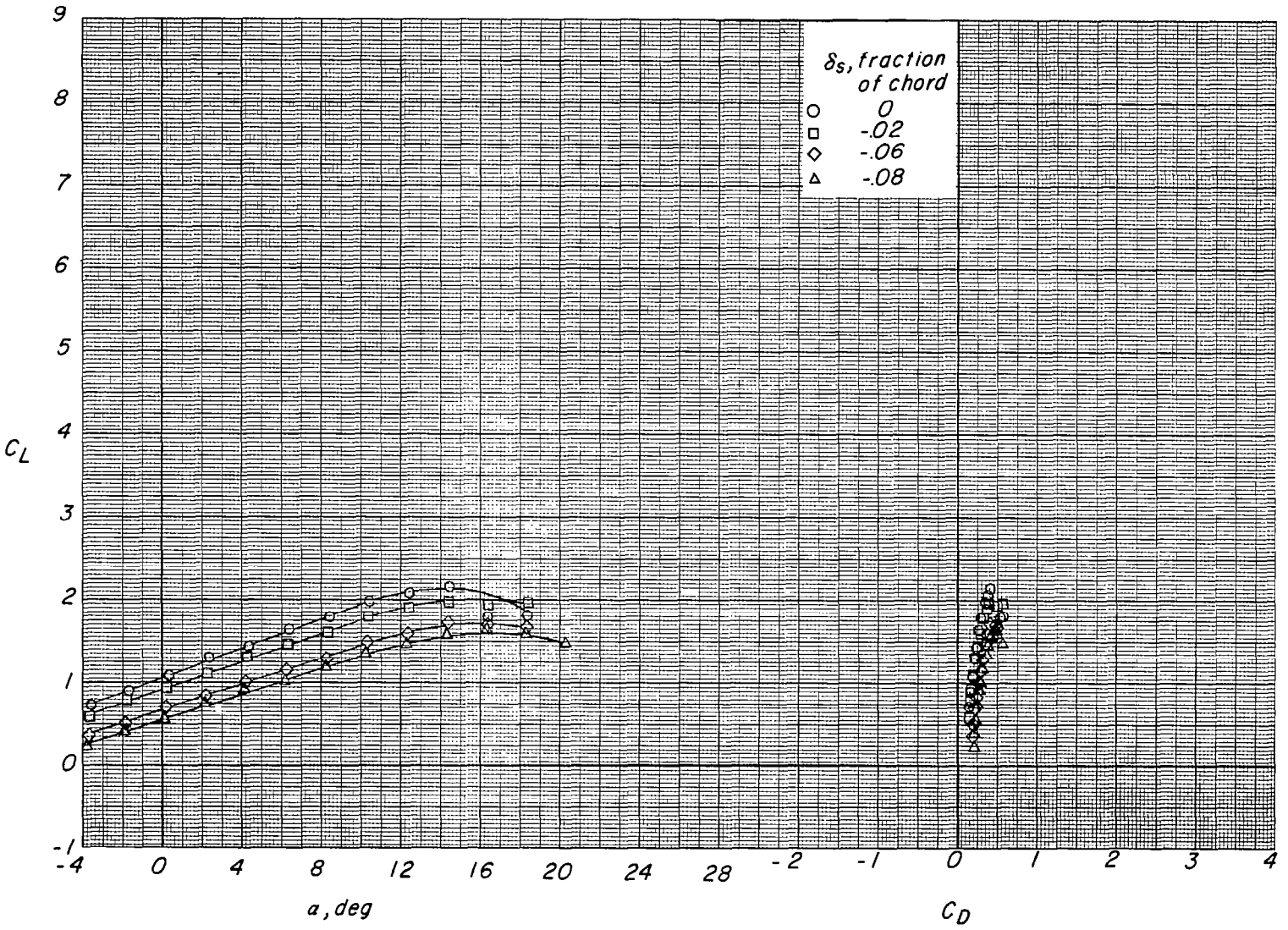

(a) $C_T = 0$ (propeller off).

Figure 18.- Effect of spoiler projection for configuration B (long span, $\delta_f = 32.5^\circ$).

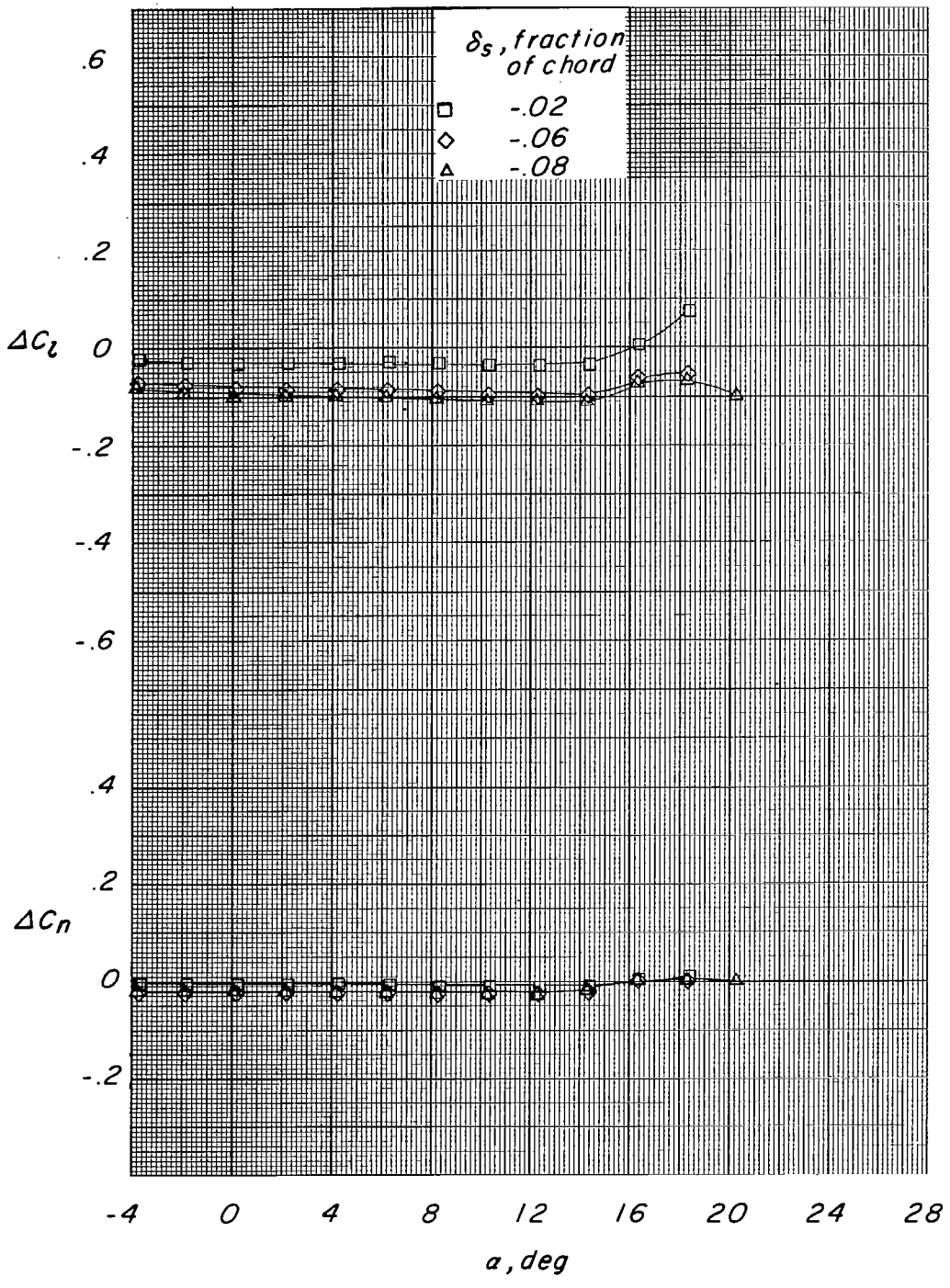

(a) Concluded.

Figure 18.- Continued.

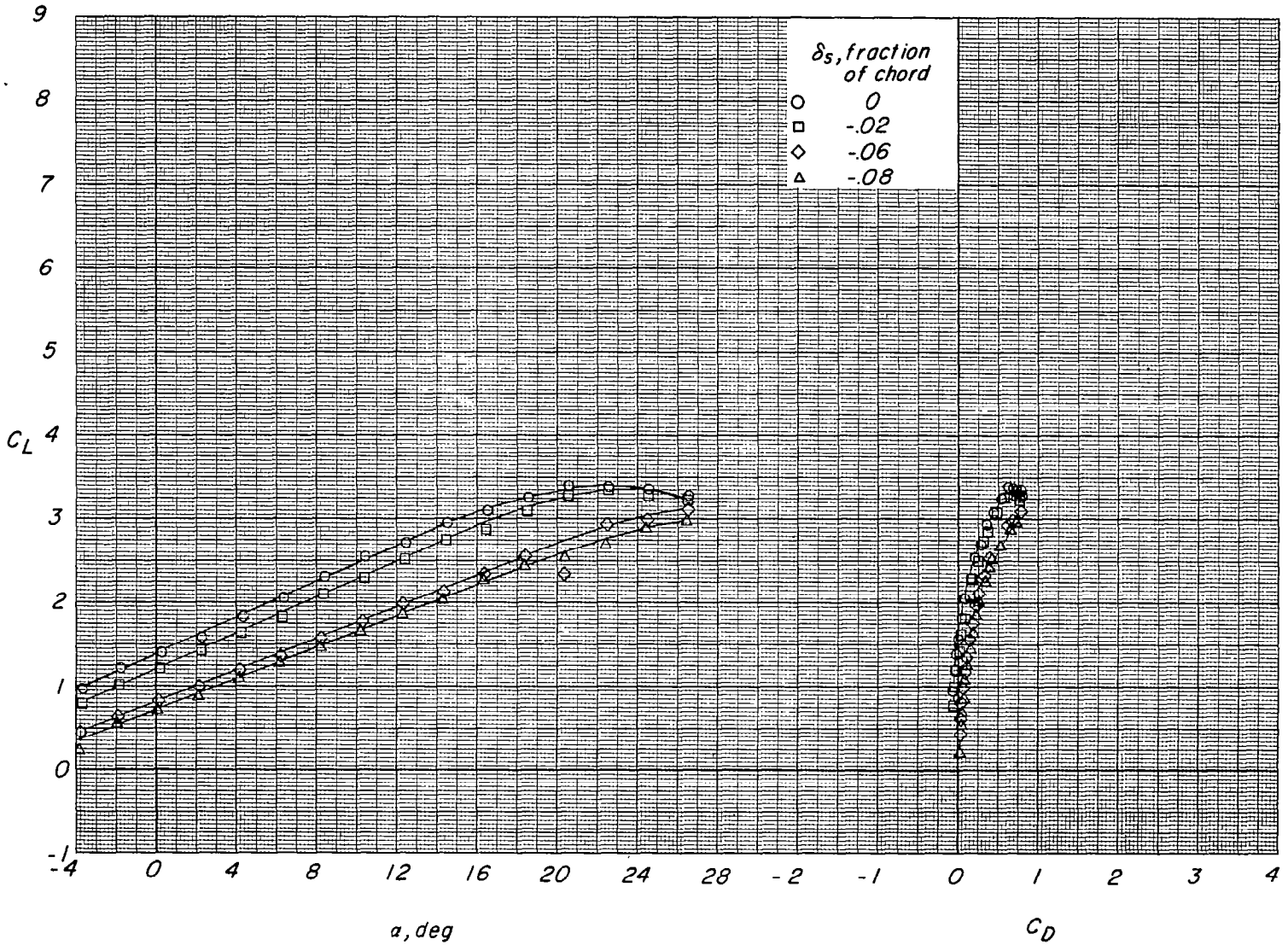

(b) $C_T \approx 0.3$.

Figure 18.- Continued.

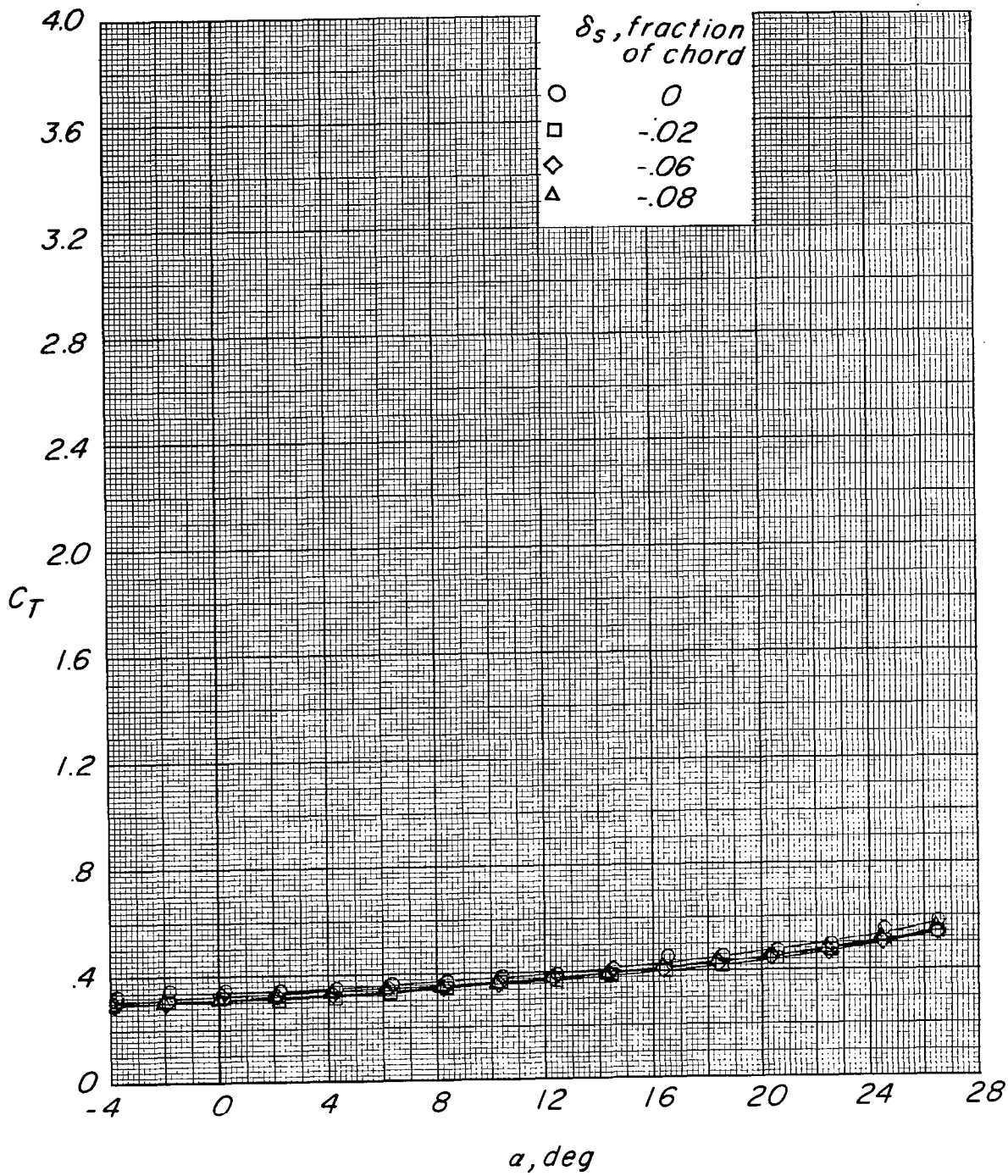

(b) Continued.

Figure 18.- Continued.

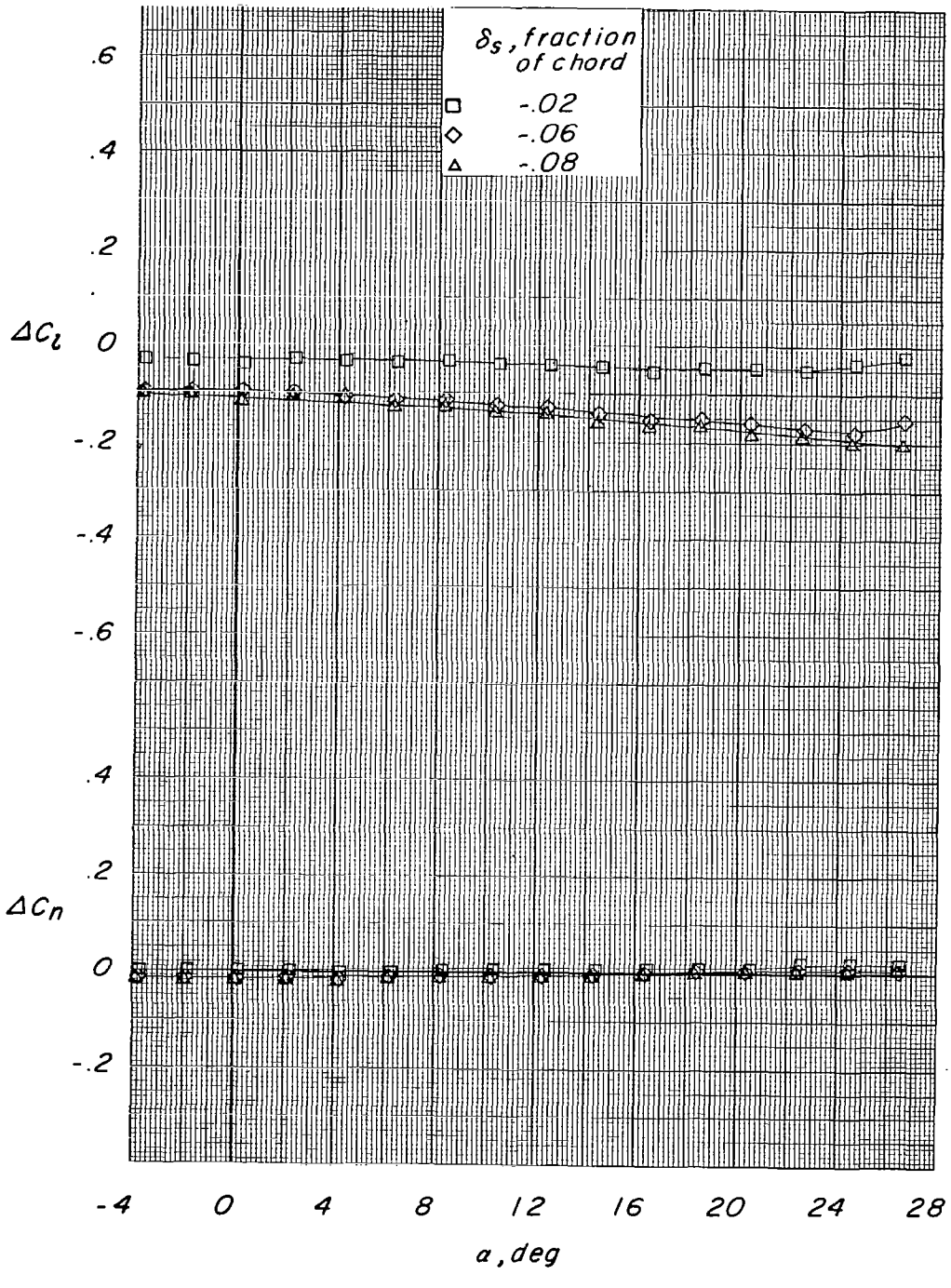

(b) Concluded.

Figure 18.- Continued.

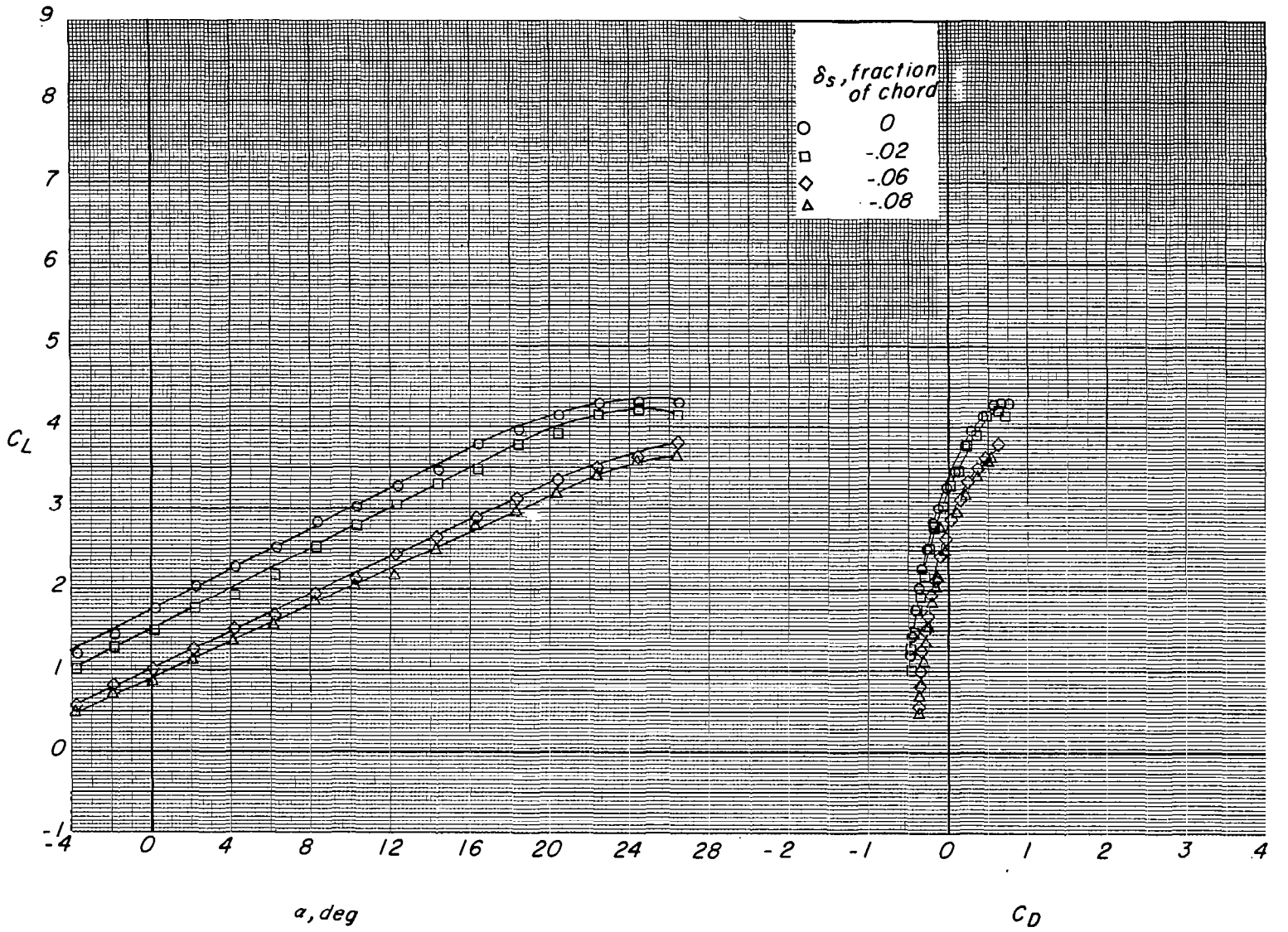

(c) $C_T \approx 0.9$.

Figure 18.- Continued.

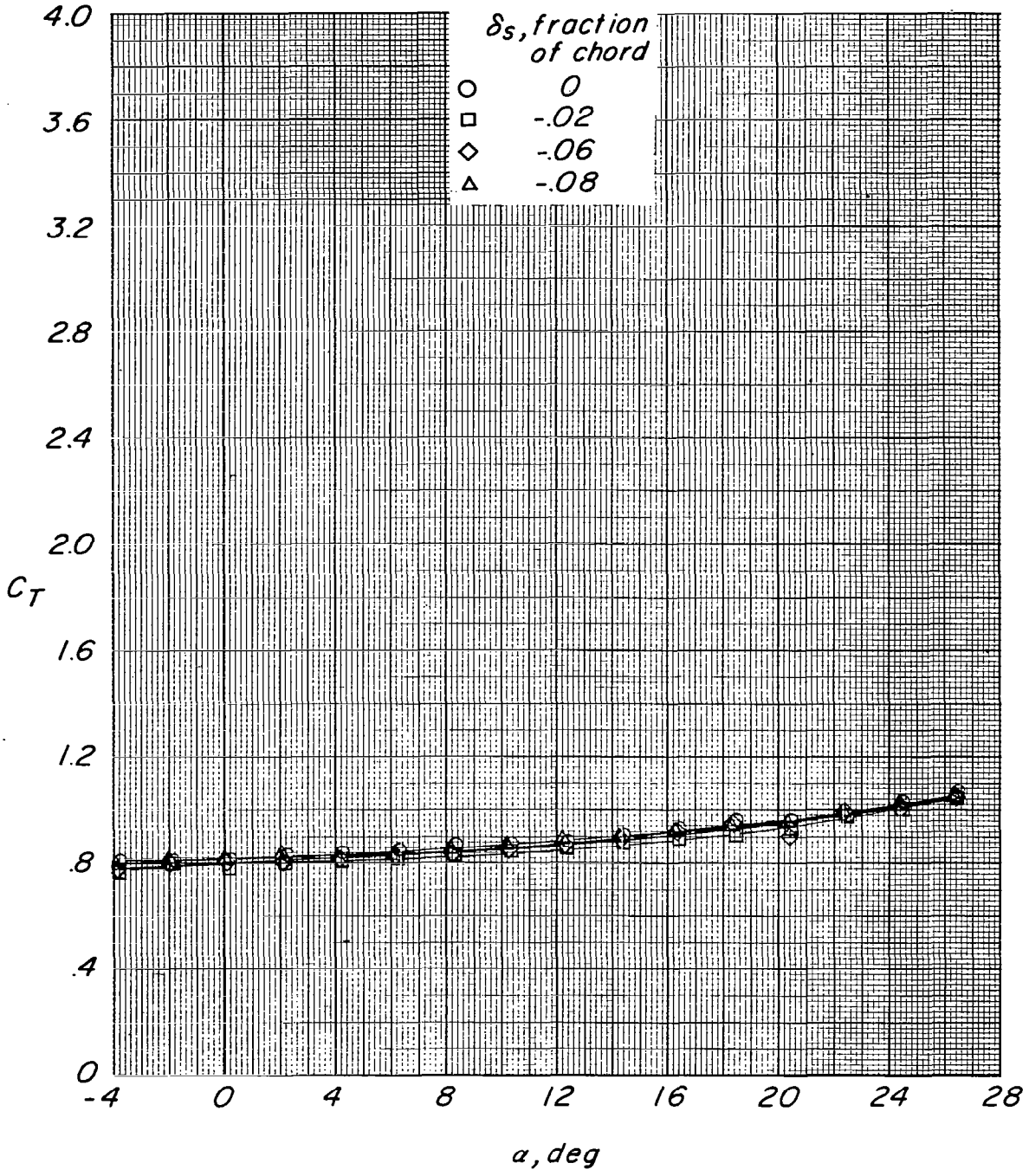

(c) Continued.

Figure 18.- Continued.

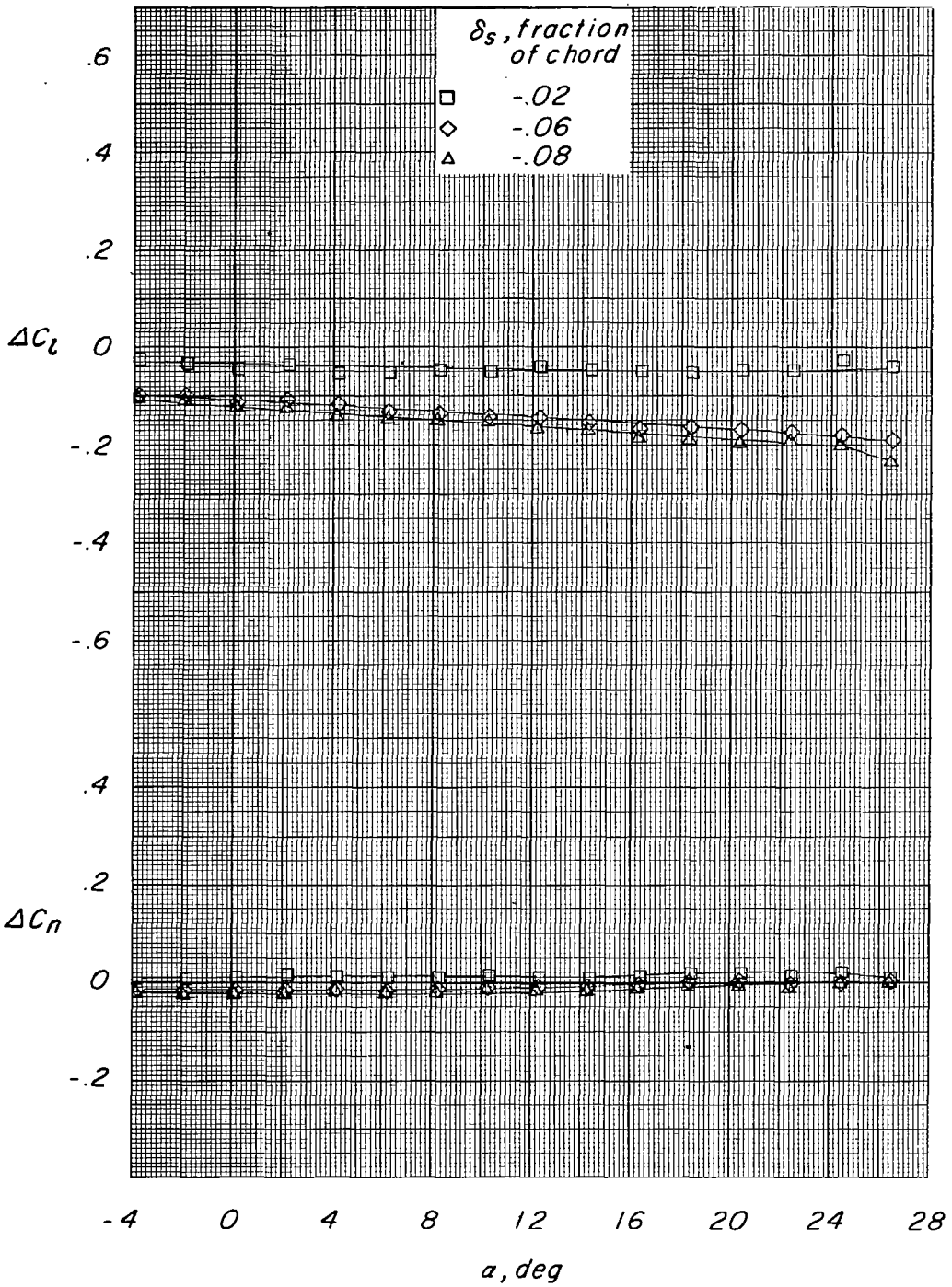

(c) Concluded.

Figure 18.- Continued.

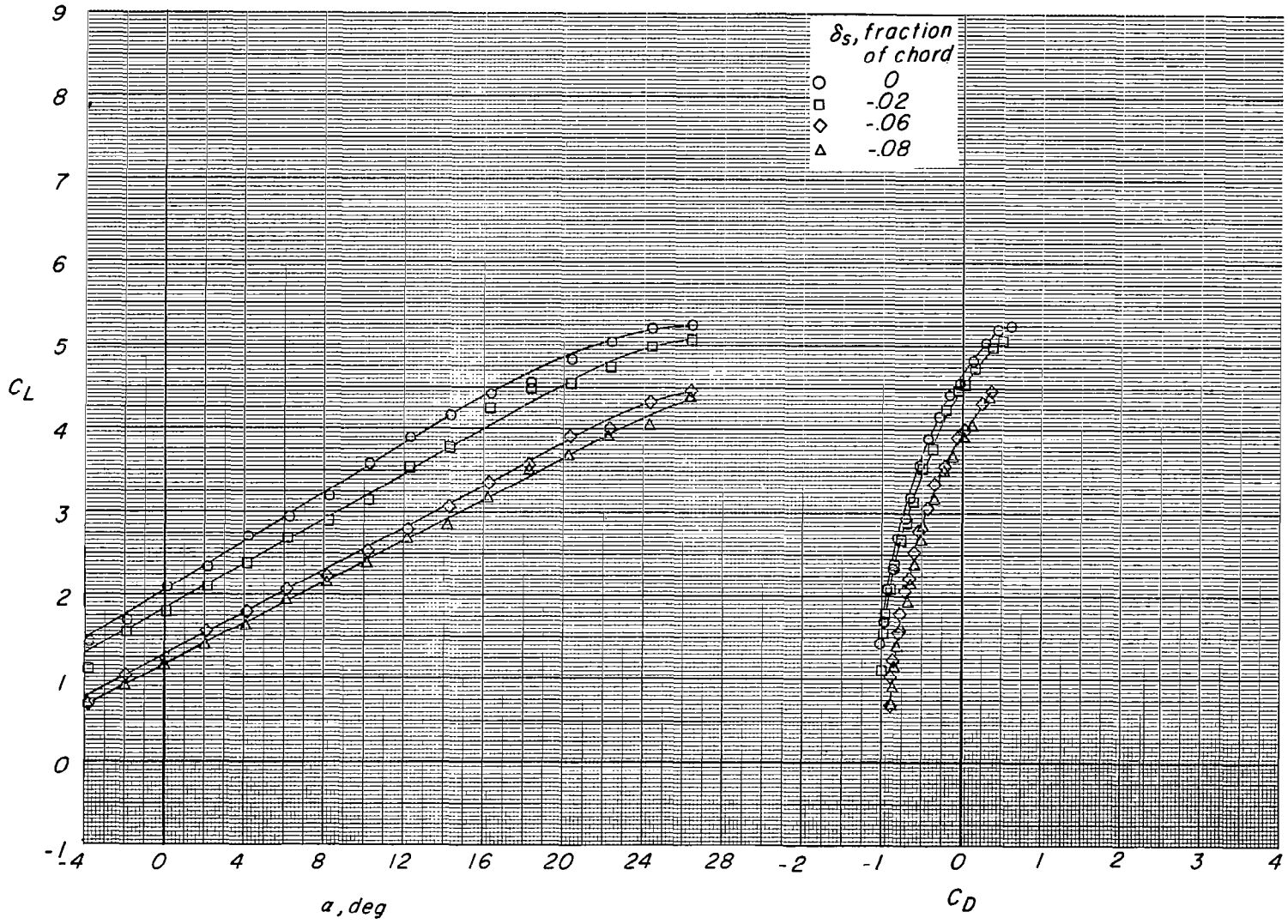

(d) $C_T \approx 1.6$.

Figure 18.- Continued.

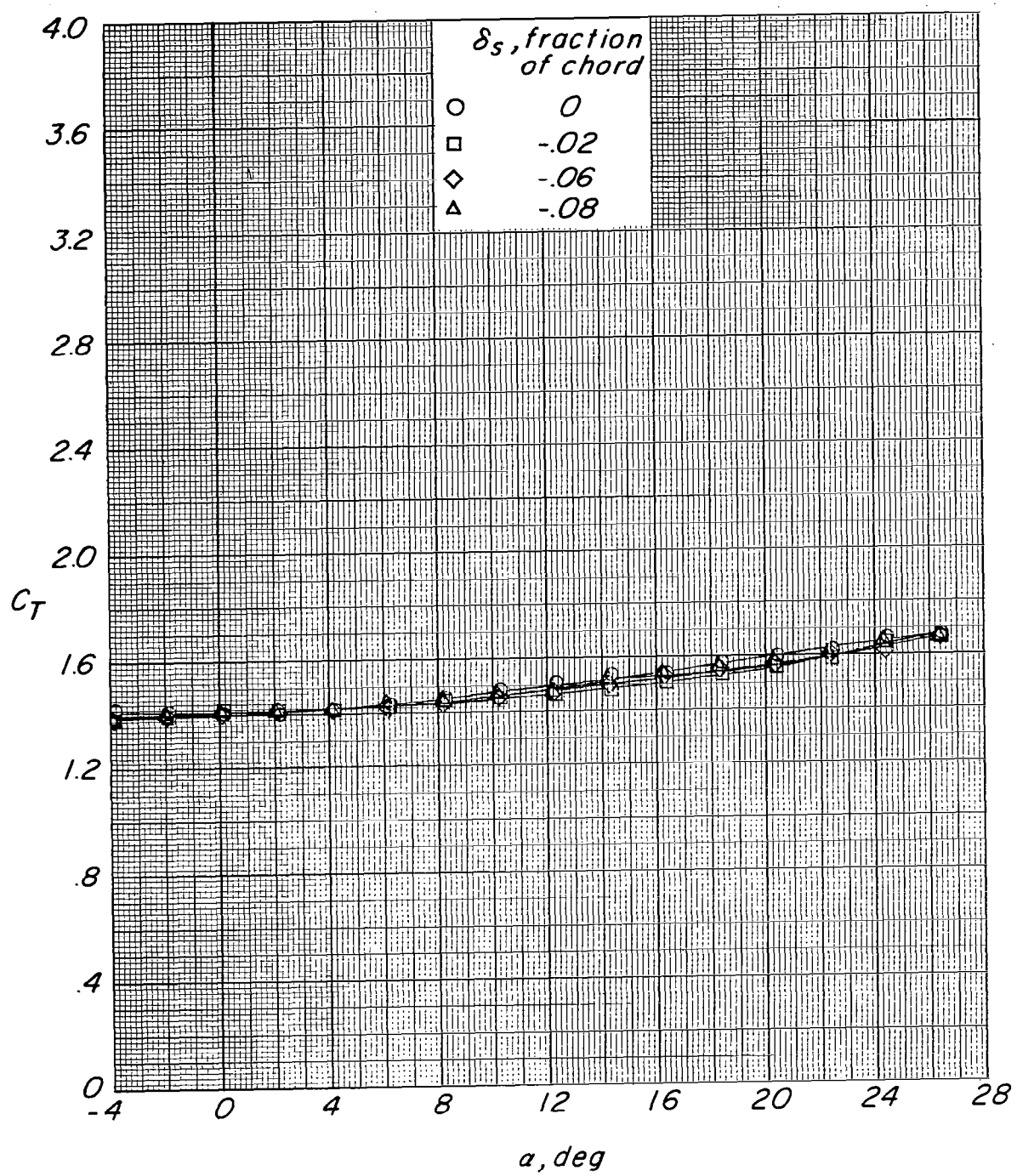

(d) Continued.

Figure 18.- Continued.

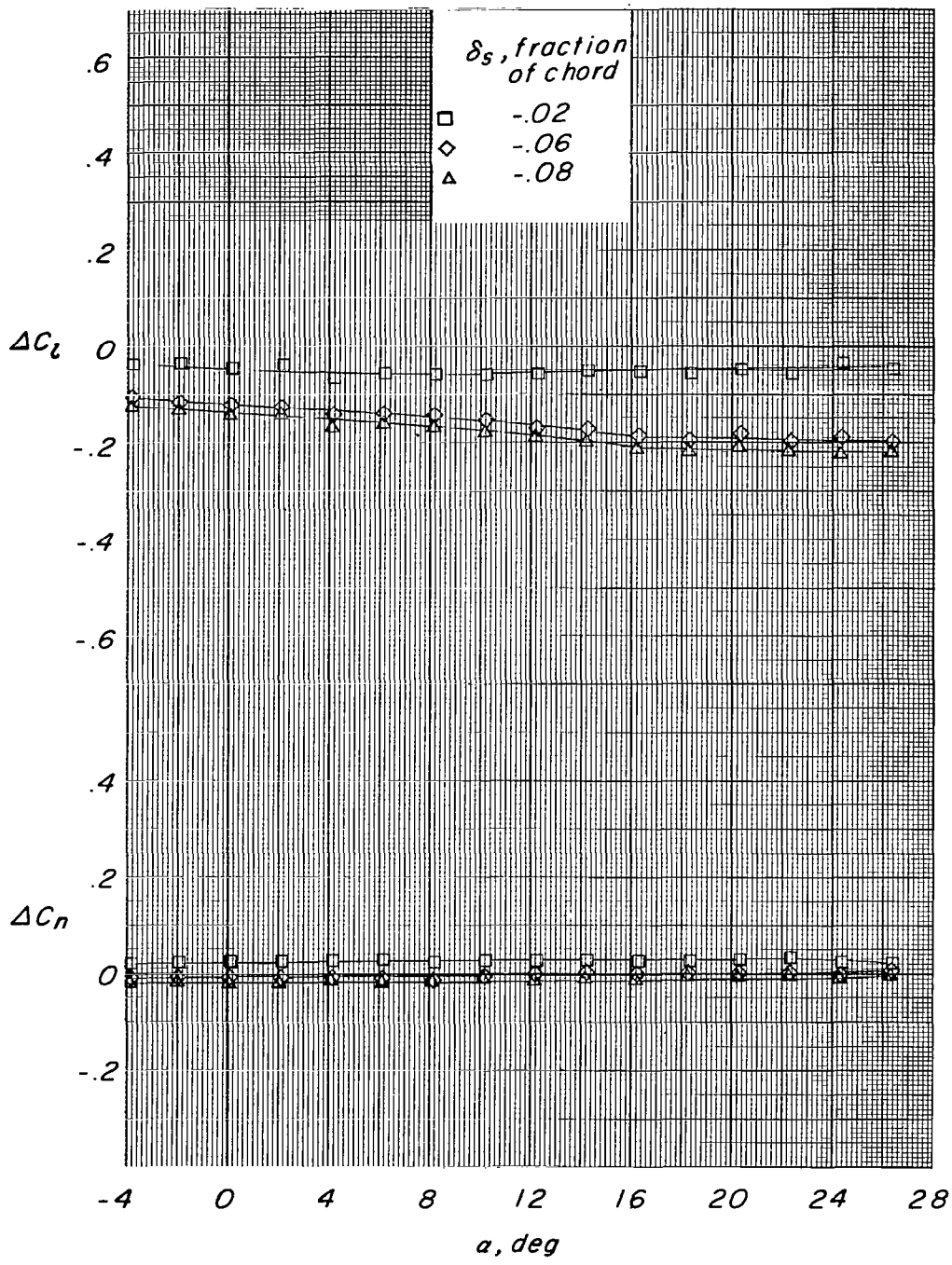

(d) Concluded.

Figure 18.- Concluded.

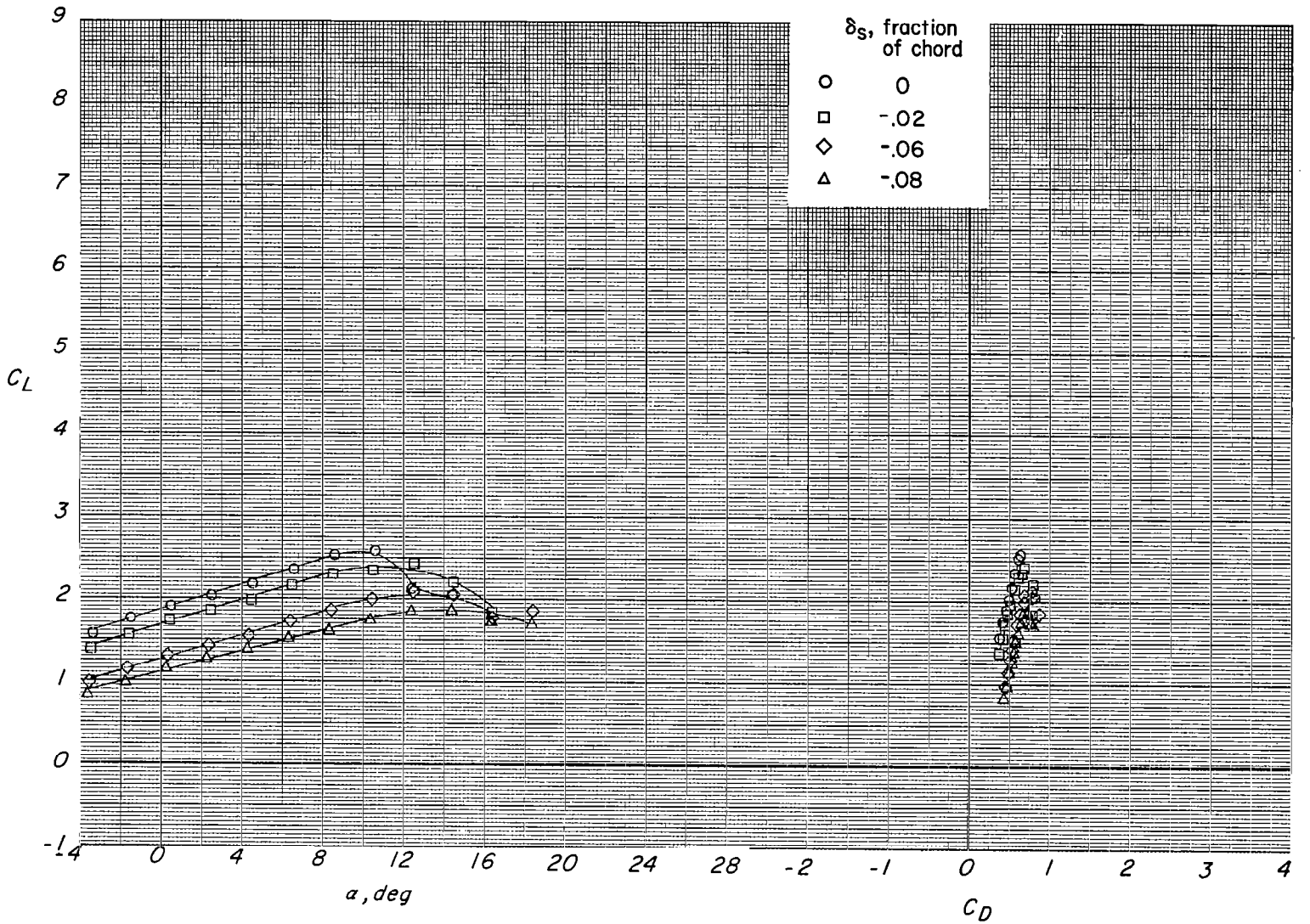

(a) $C_T = 0$ (propeller off).

Figure 19.- Effect of spoiler projection for configuration C (long span, $\delta_f = 45°$).

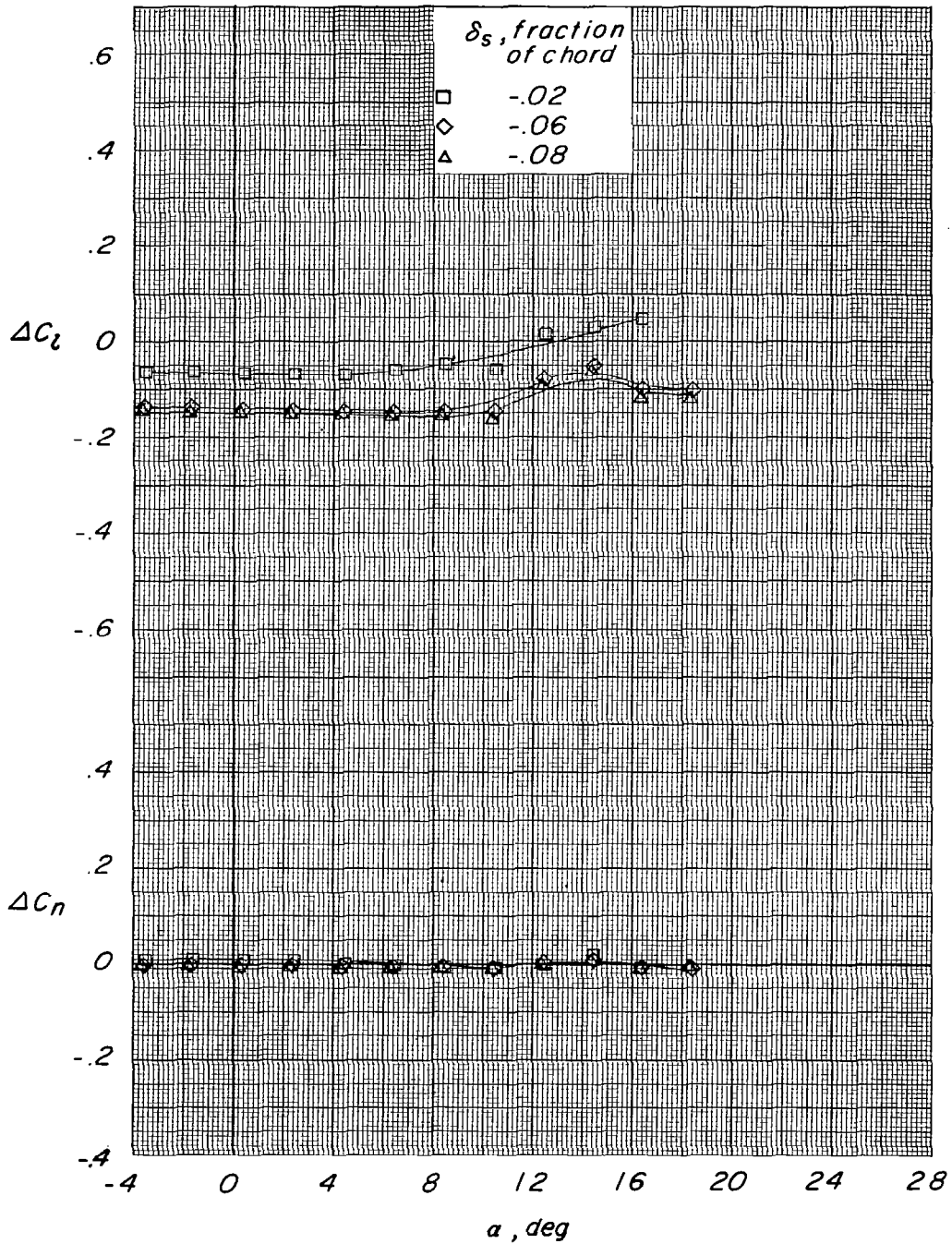

(a) Concluded.

Figure 19.- Continued.

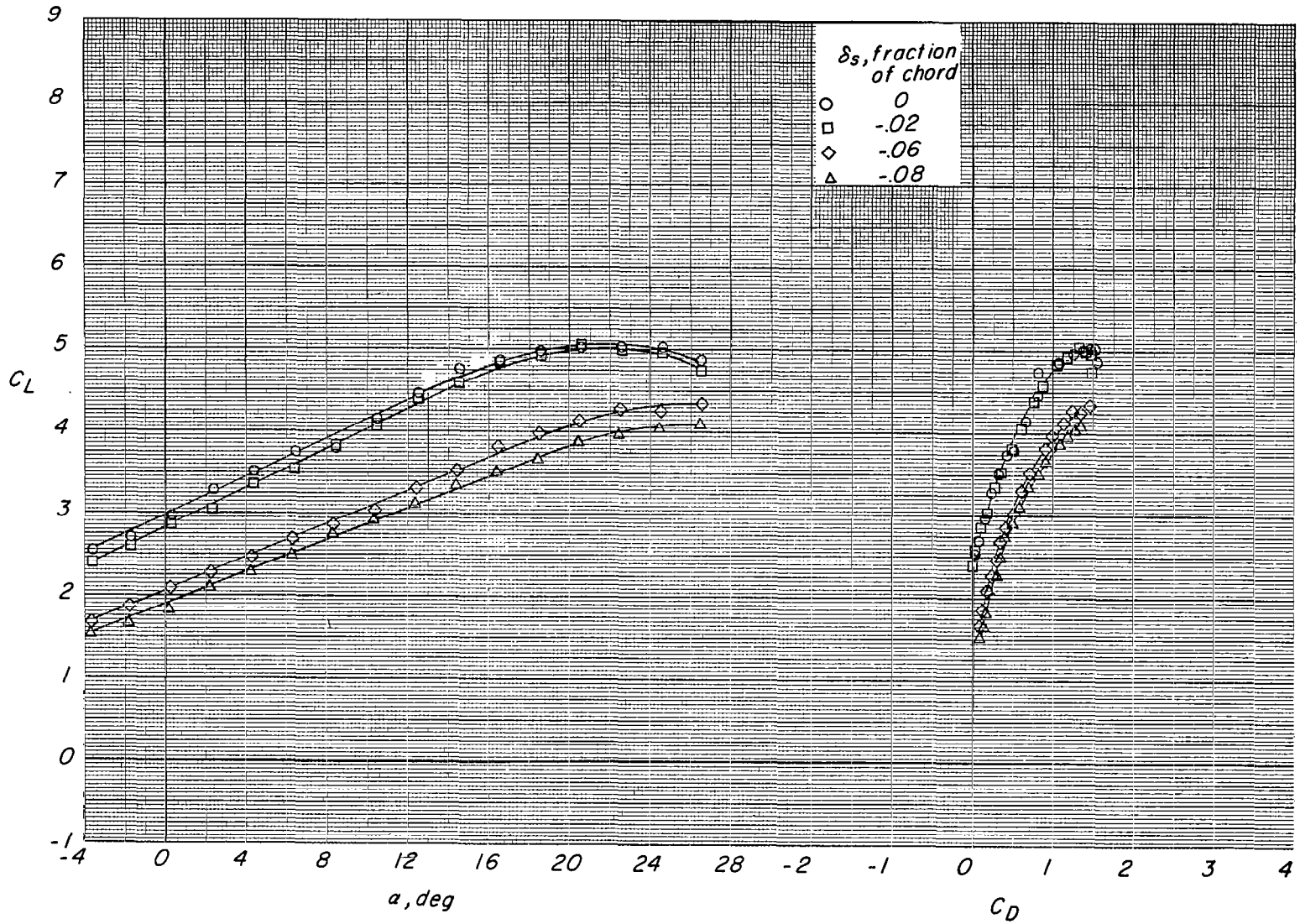

(b) $C_T \approx 0.9$.

Figure 19.- Continued.

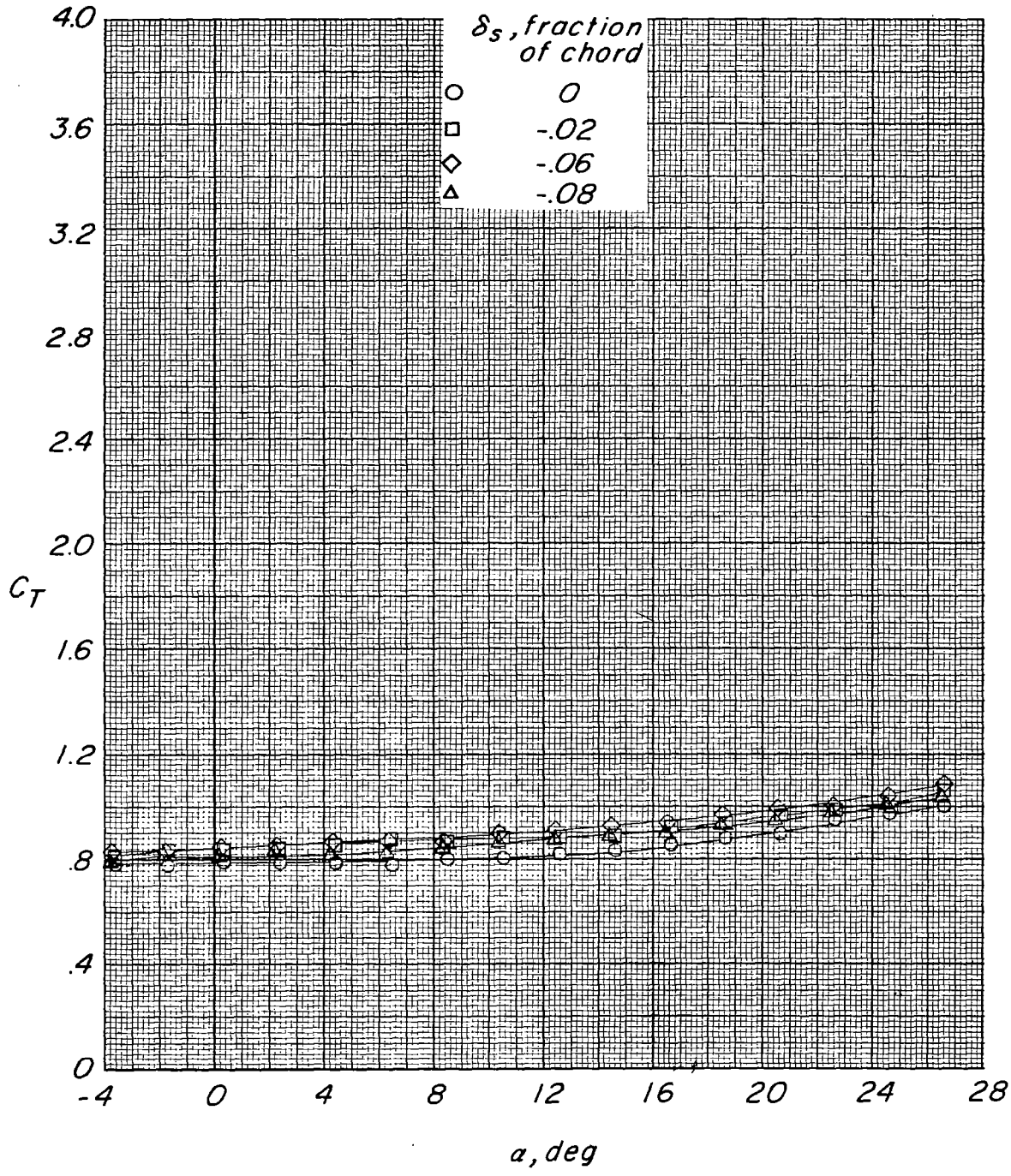

(b) Continued.

Figure 19.- Continued.

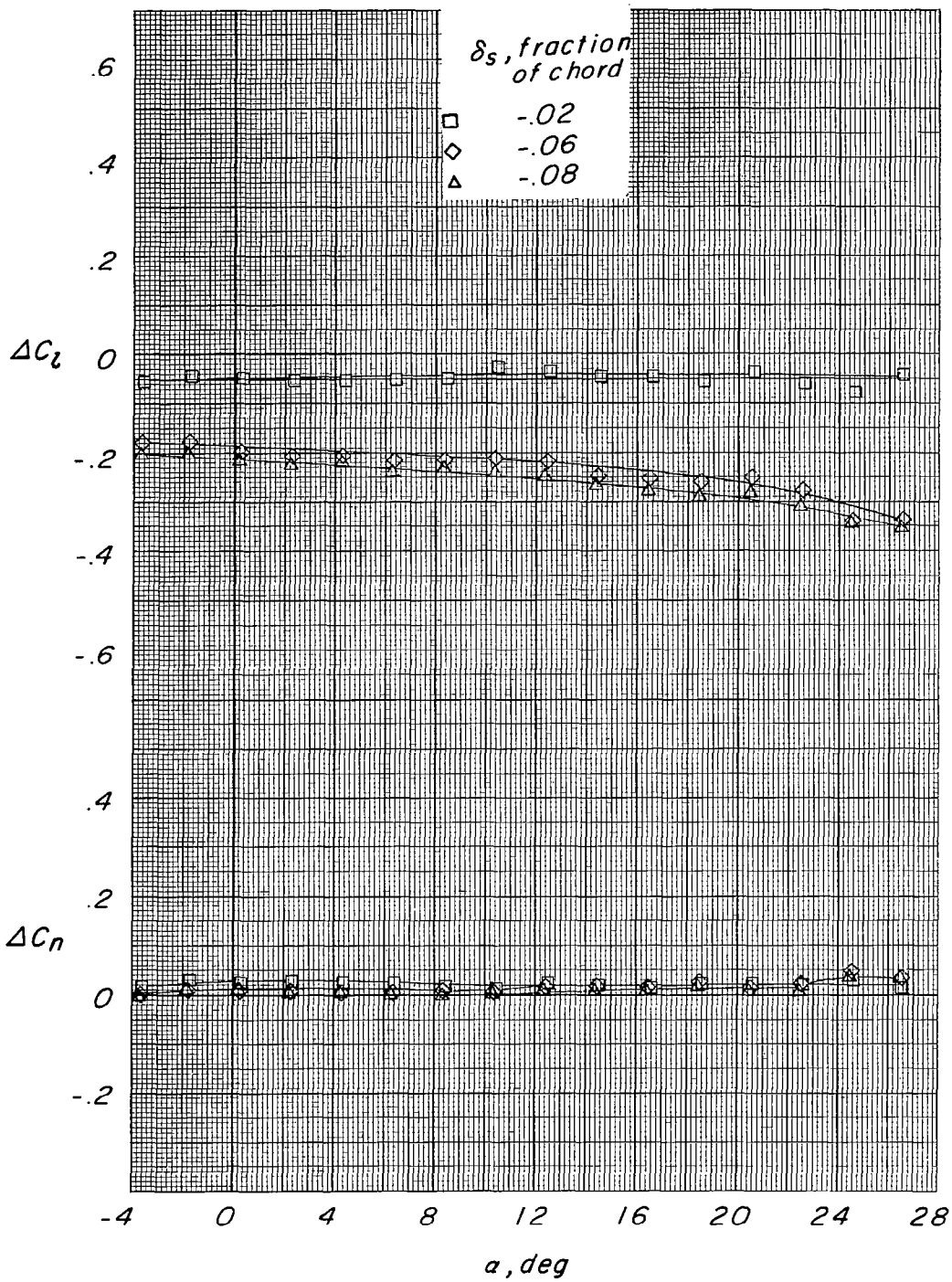

(b) Concluded.

Figure 19.- Continued.

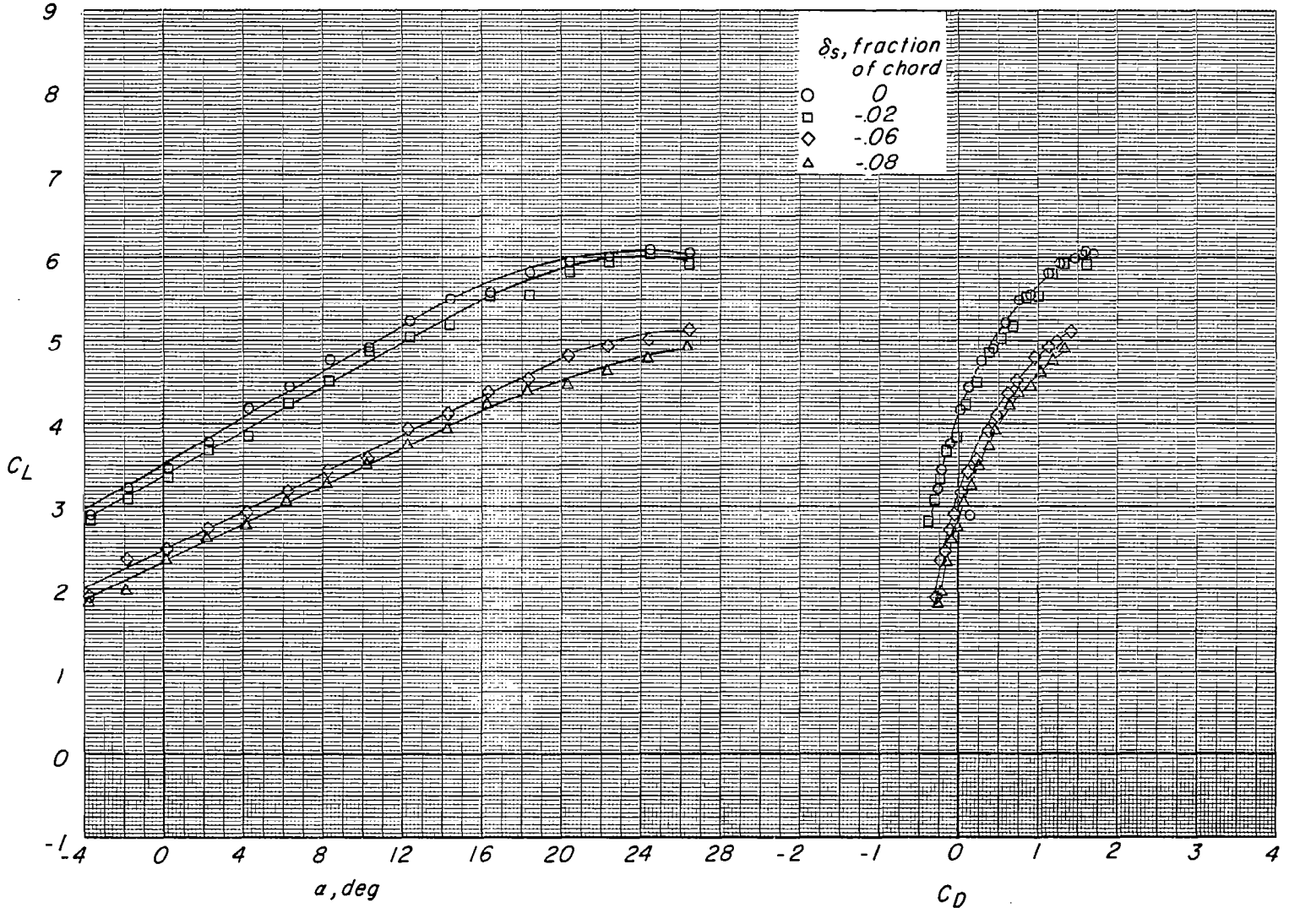

(c) $C_T \approx 1.6$.

Figure 19.- Continued.

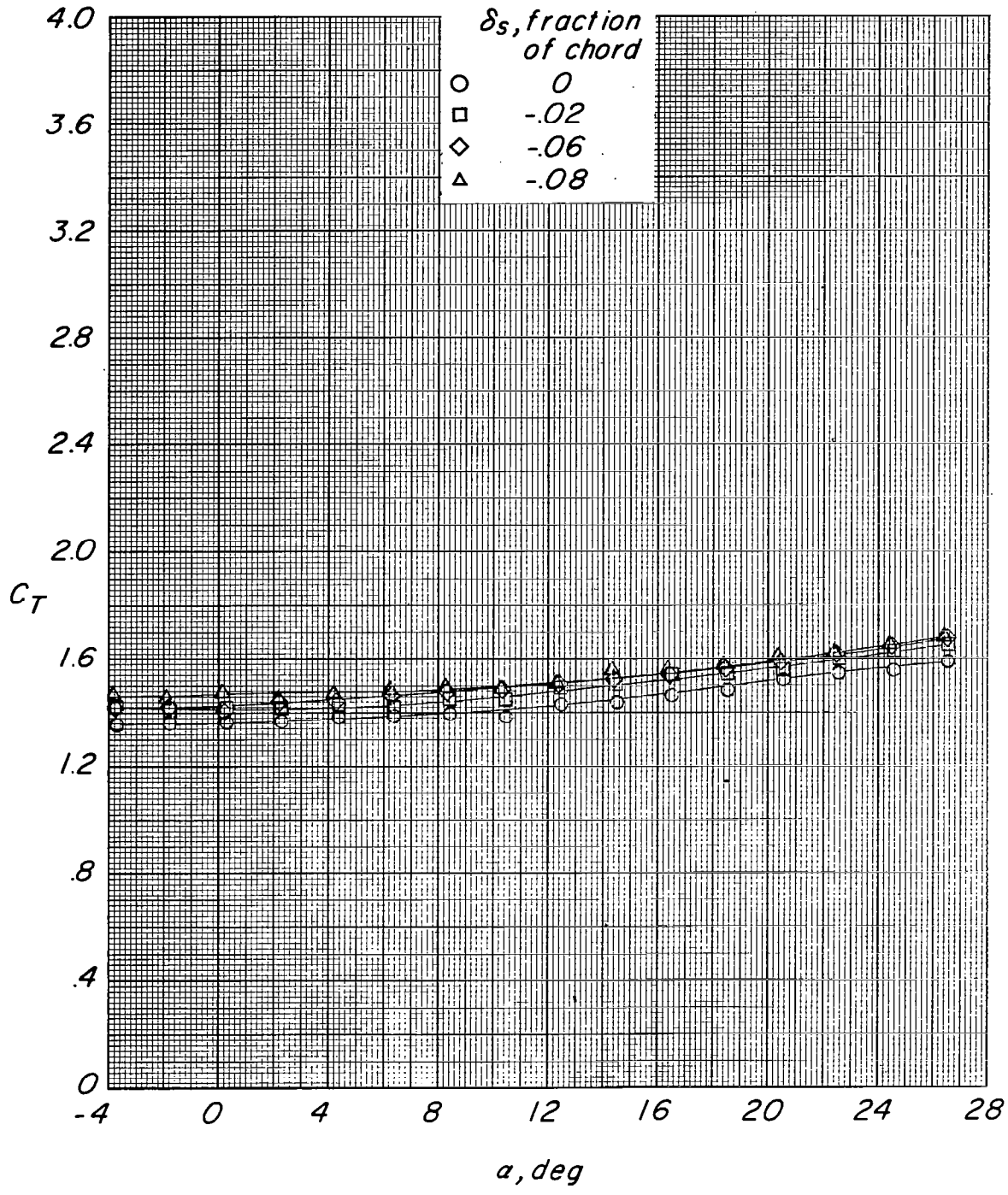

(c) Continued.

Figure 19.- Continued.

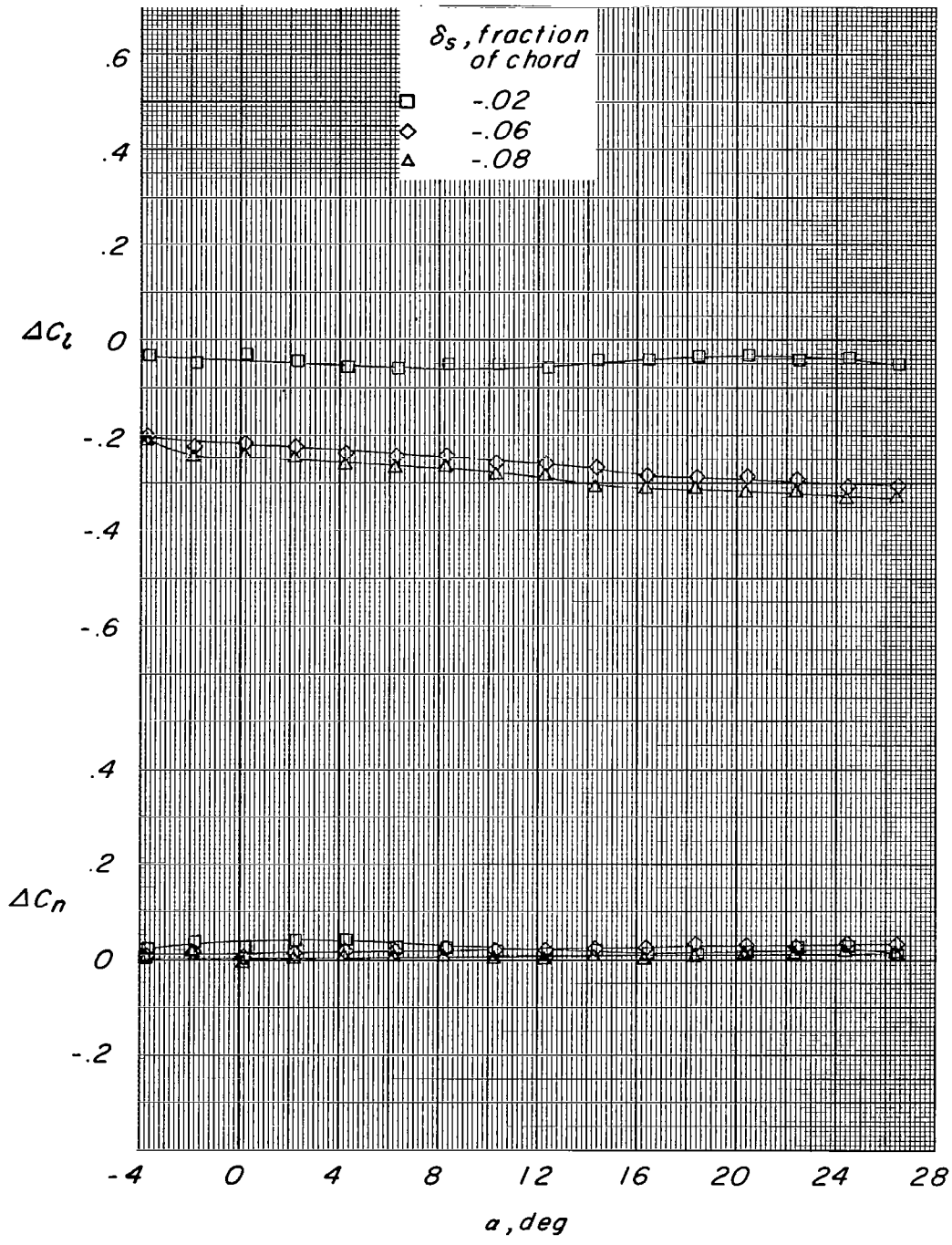

(c) Concluded.

Figure 19.- Continued.

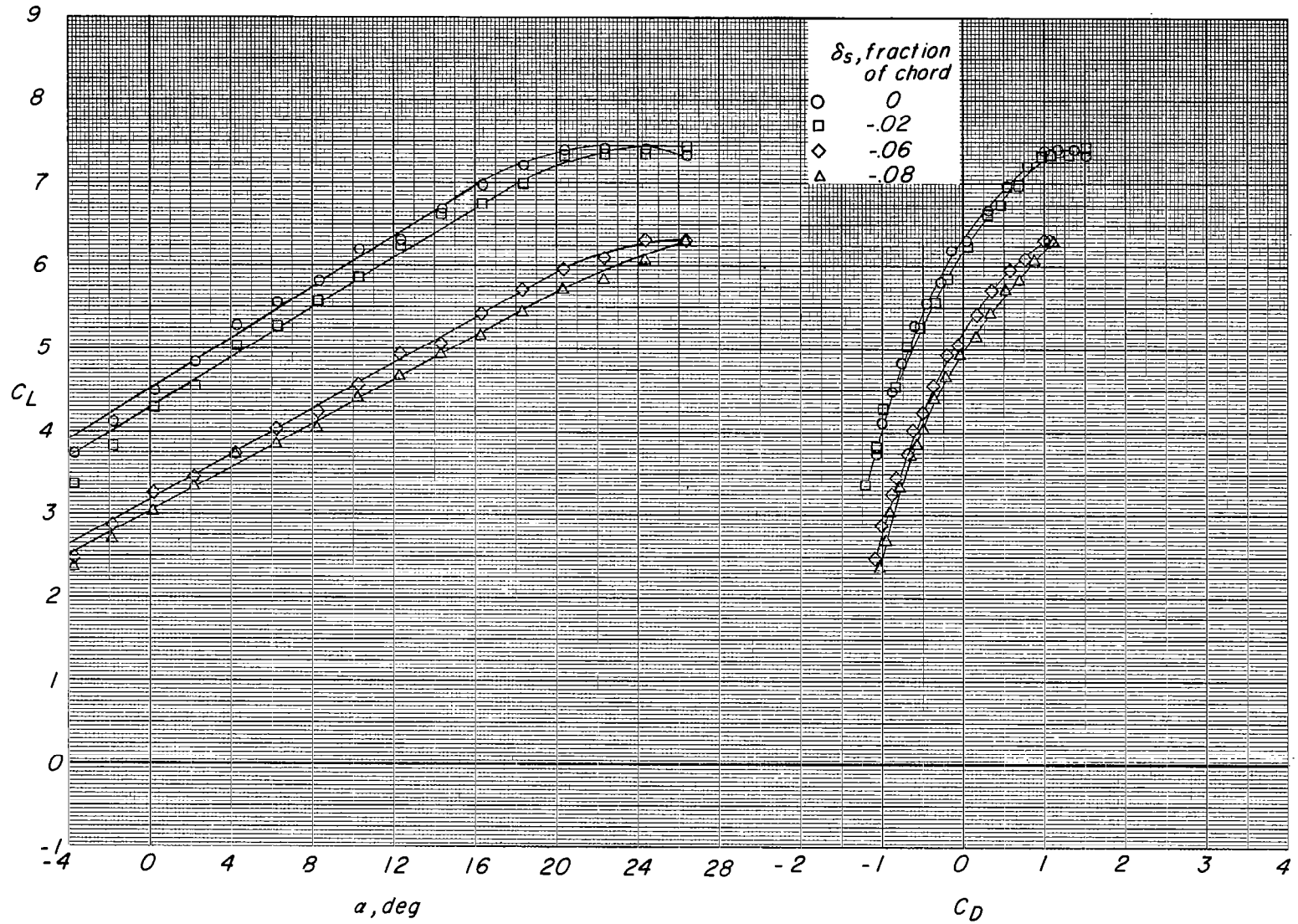

(d) $C_T \approx 2.7$.

Figure 19.- Continued.

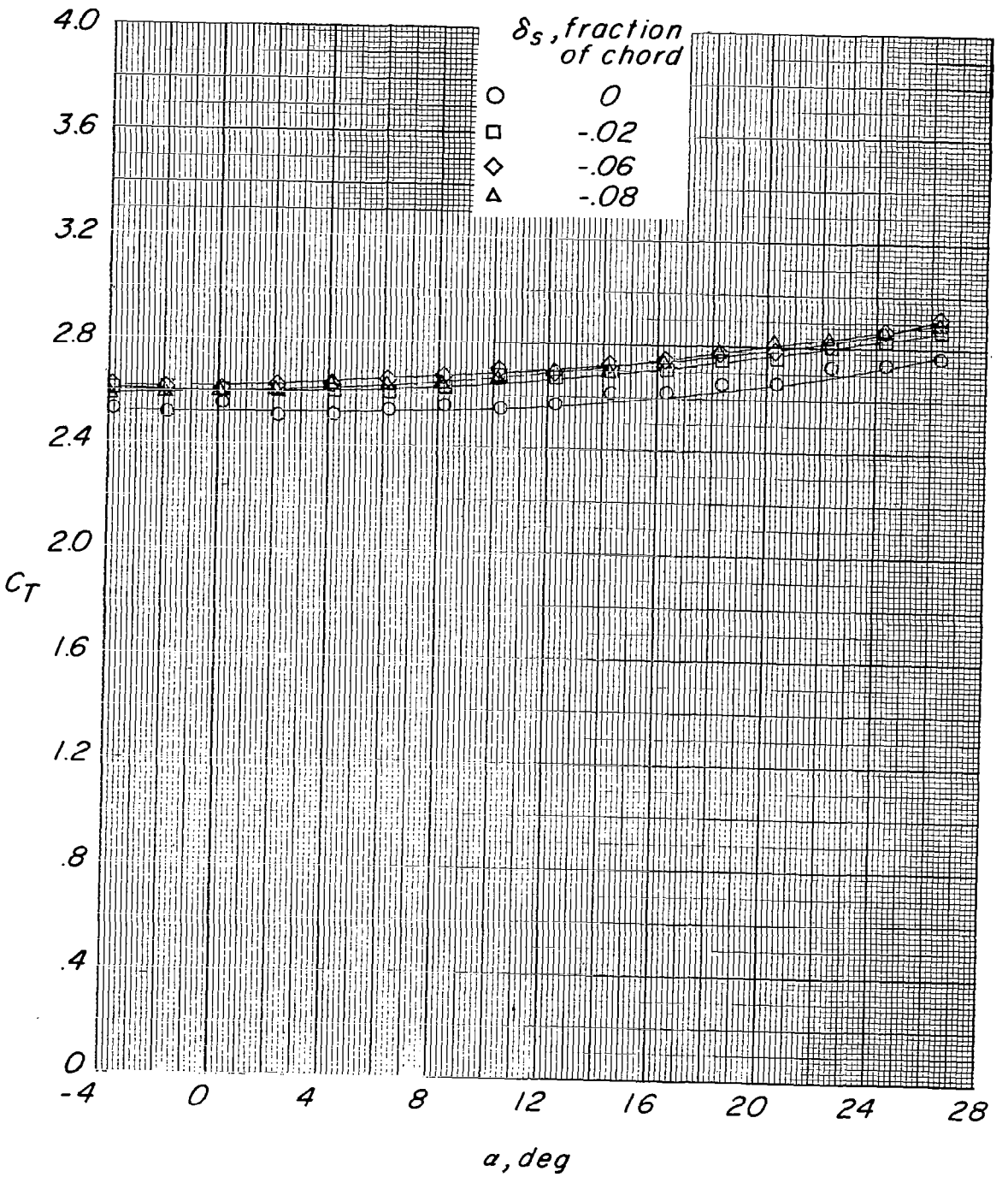

(d) Continued.

Figure 19.- Continued.

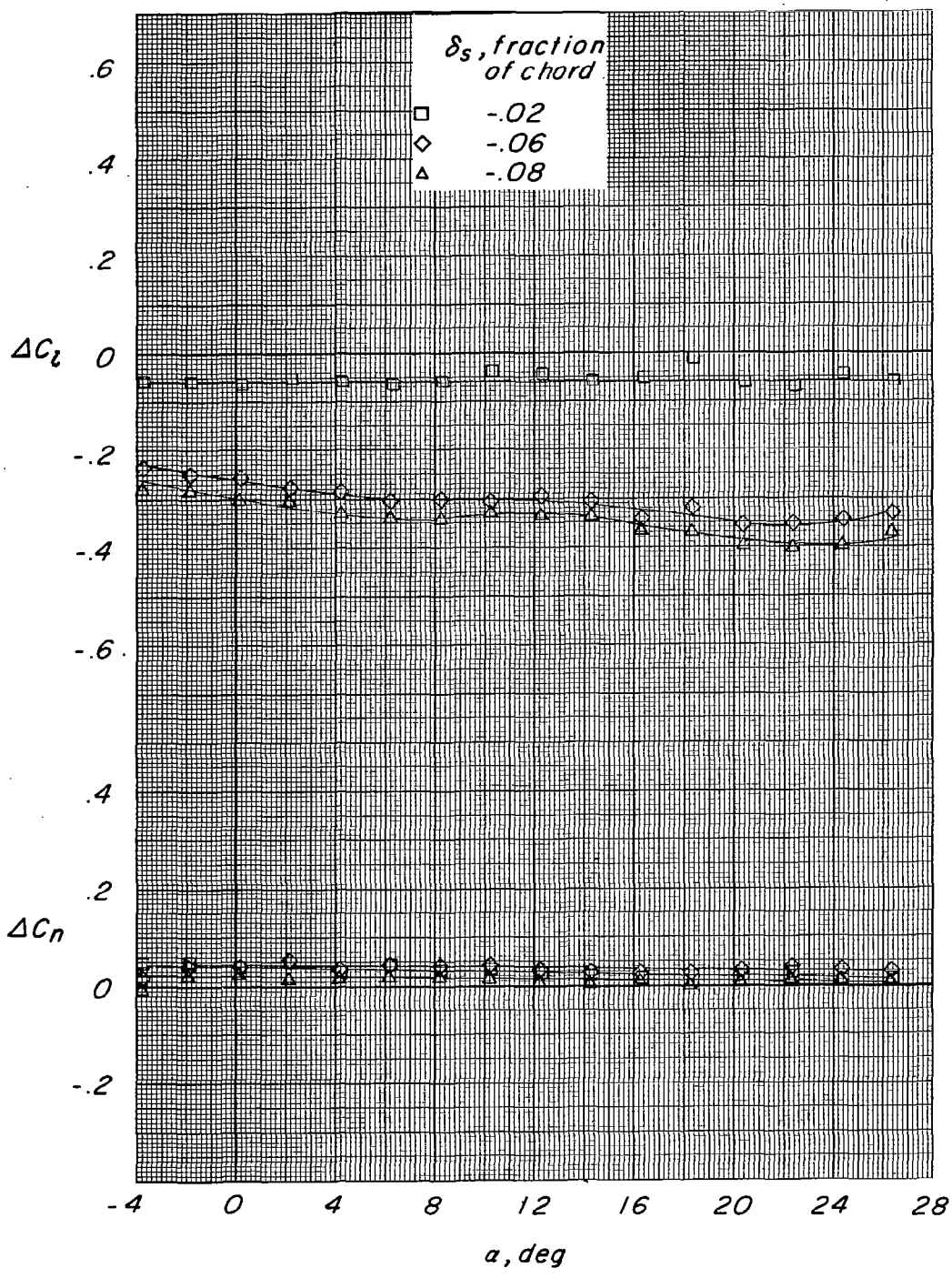

(d) Concluded.

Figure 19.- Concluded.

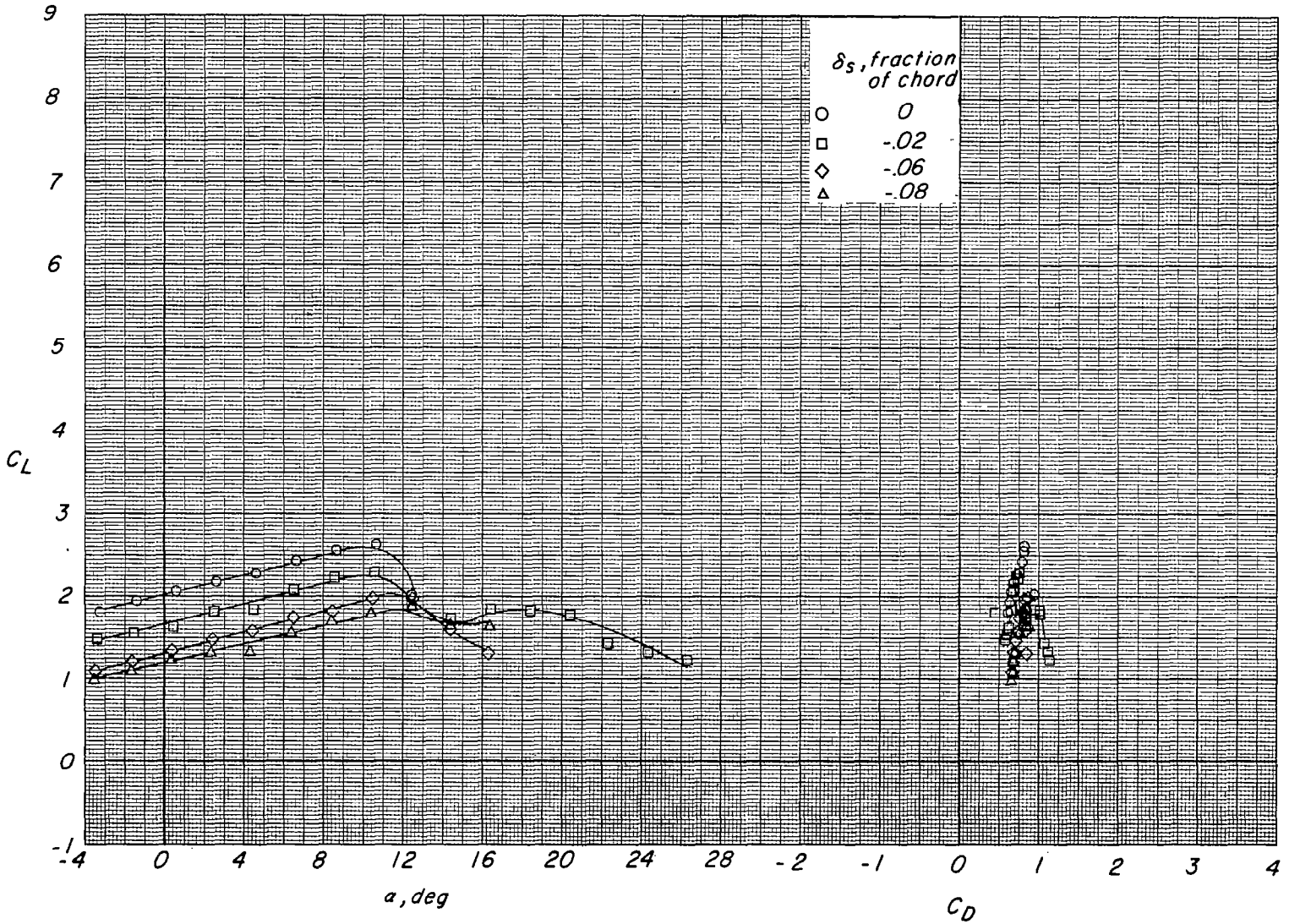

(a) $C_T = 0$ (propeller off).

Figure 20.- Effect of spoiler projection for configuration D (long span, $\delta_f = 75^\circ$).

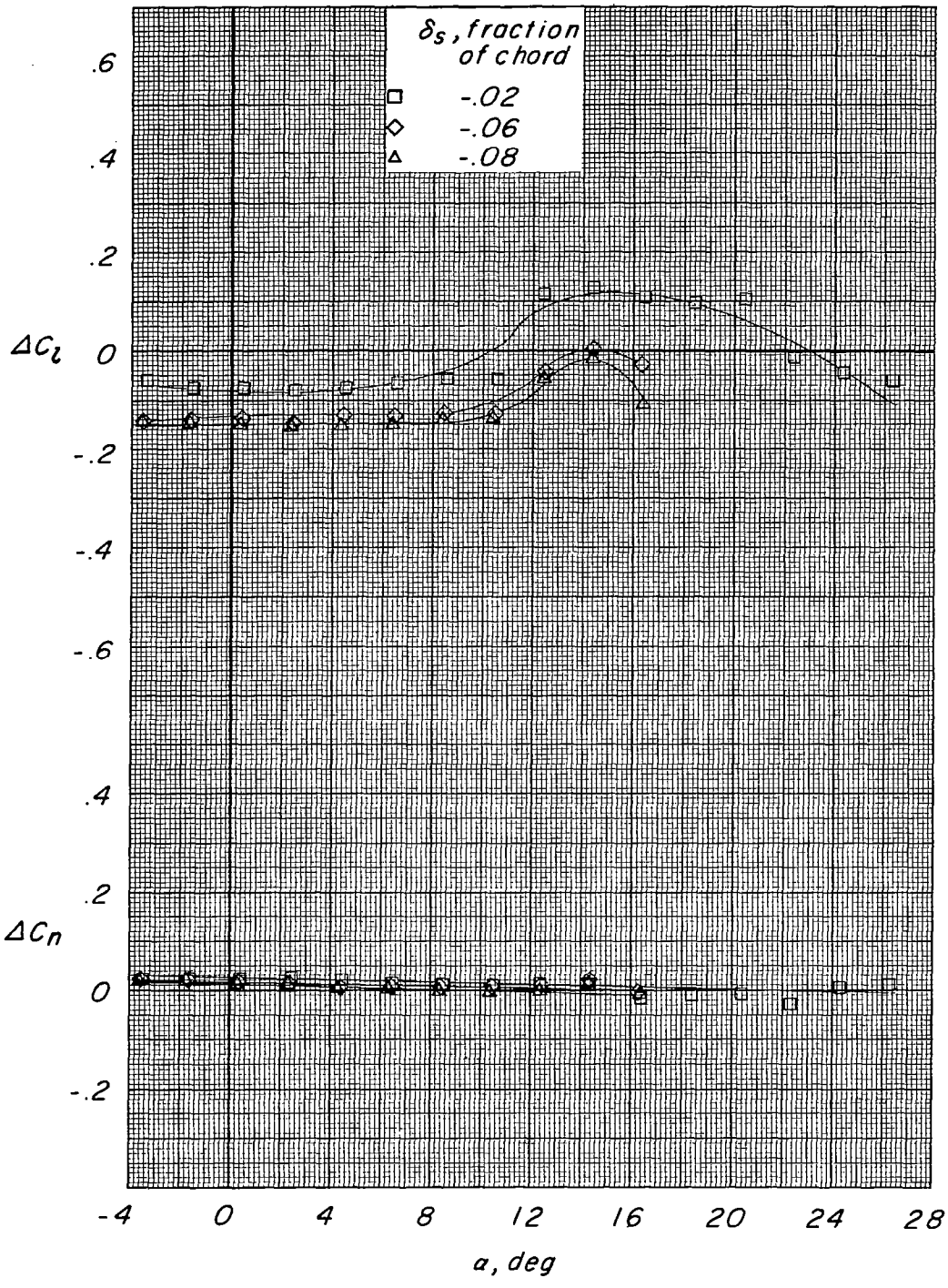

(a) Concluded.

Figure 20.- Continued.

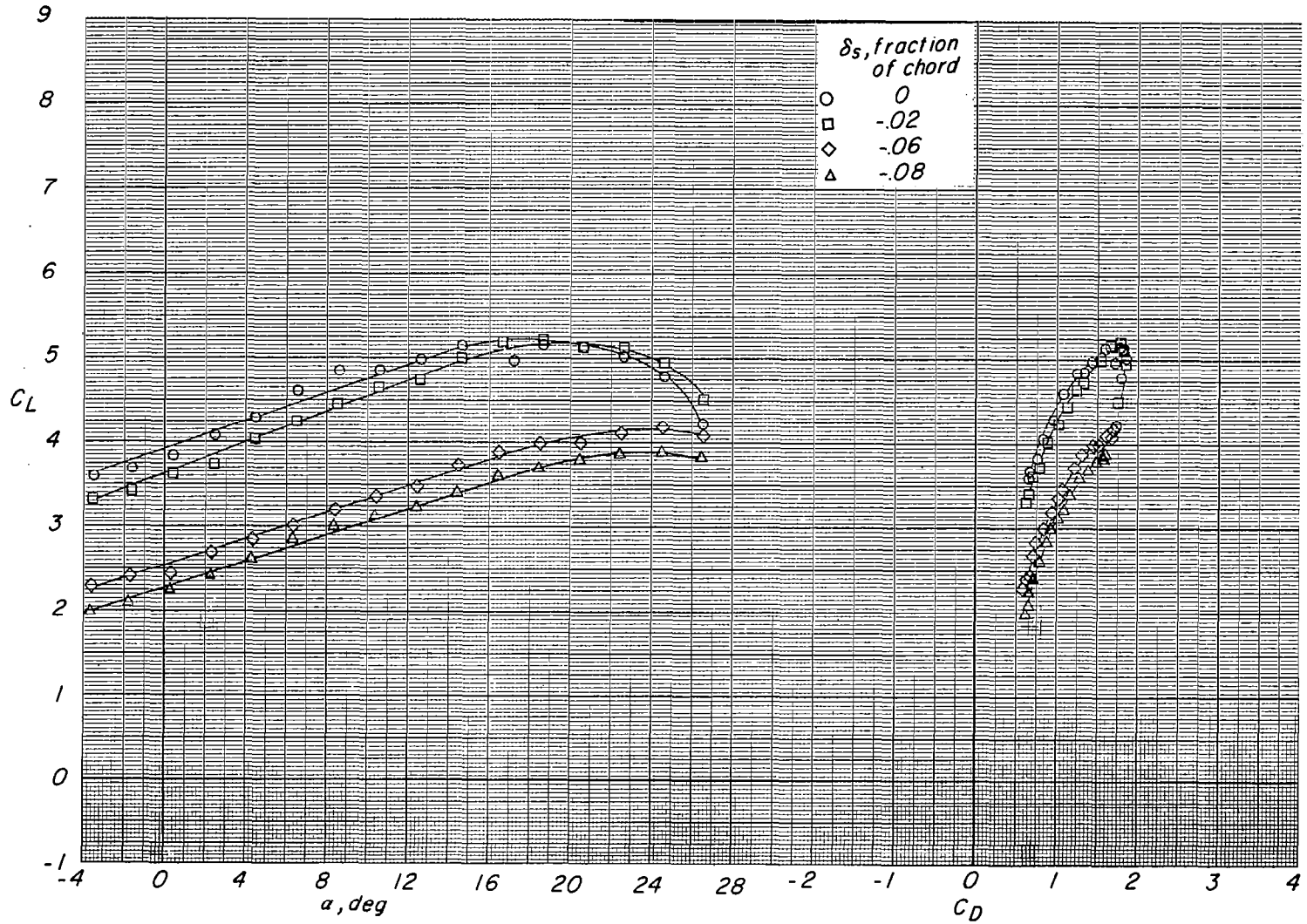

(b) $C_T \approx 0.9$.

Figure 20.- Continued.

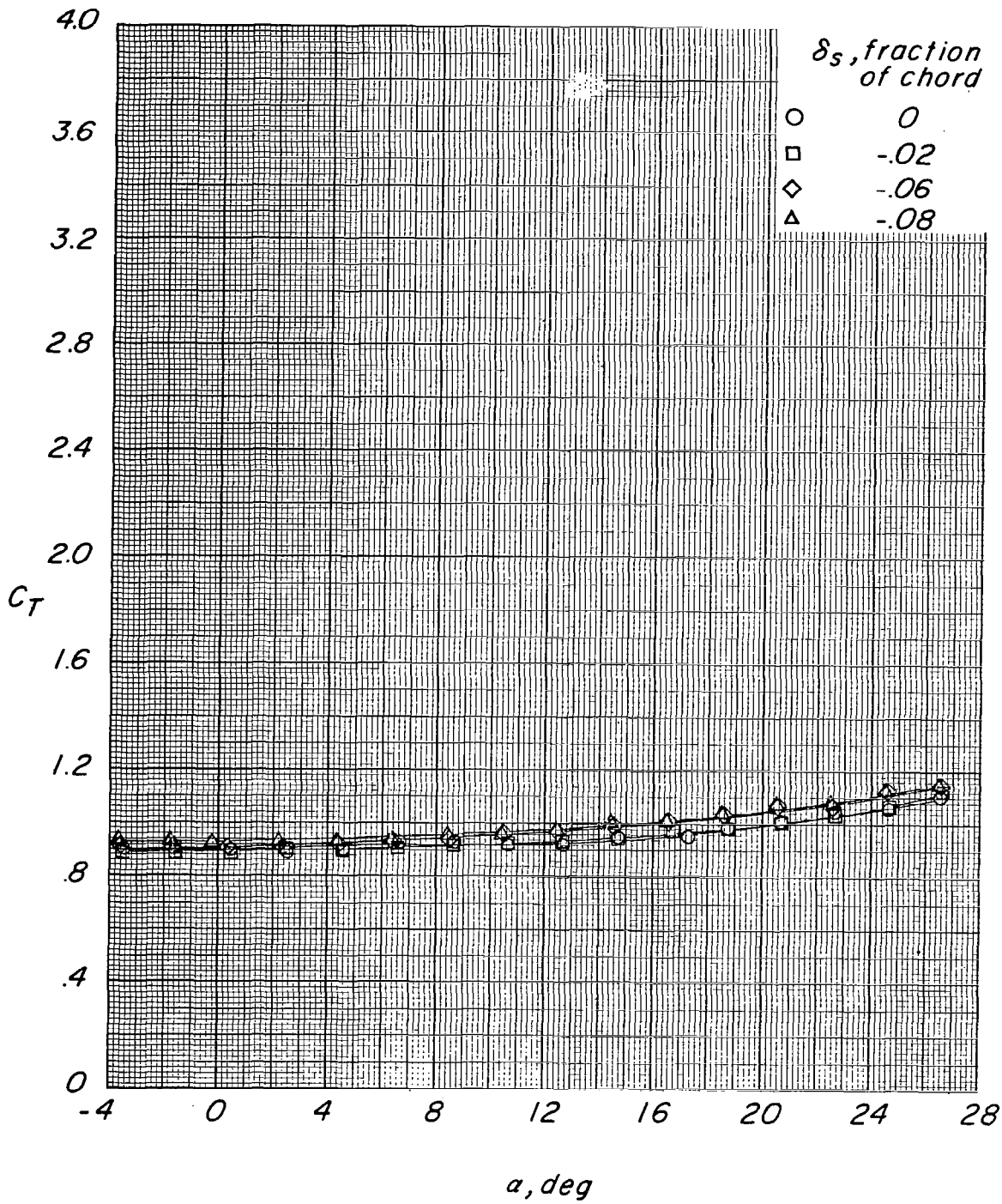

(b) Continued.

Figure 20.- Continued.

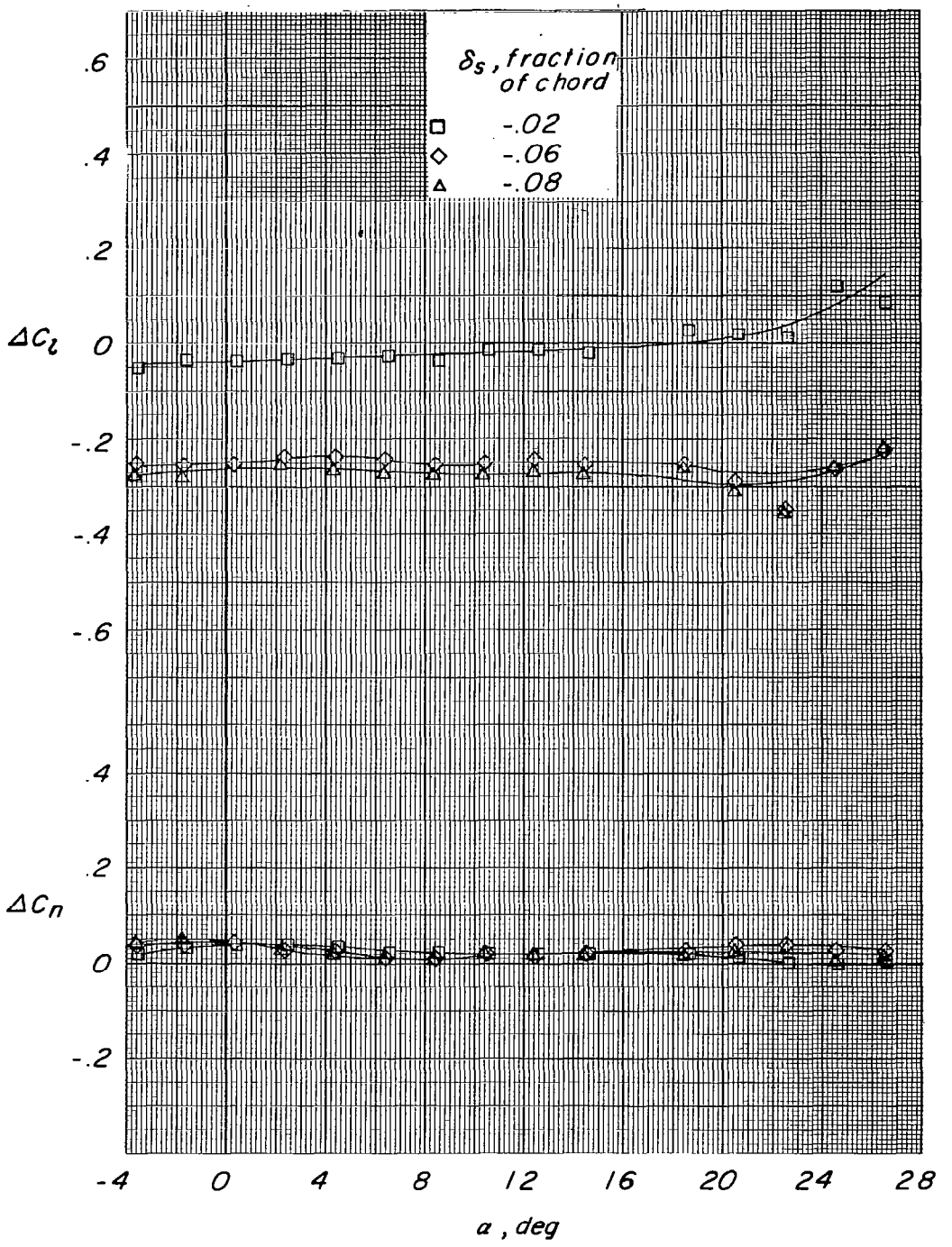

(b) Concluded.

Figure 20.- Continued.

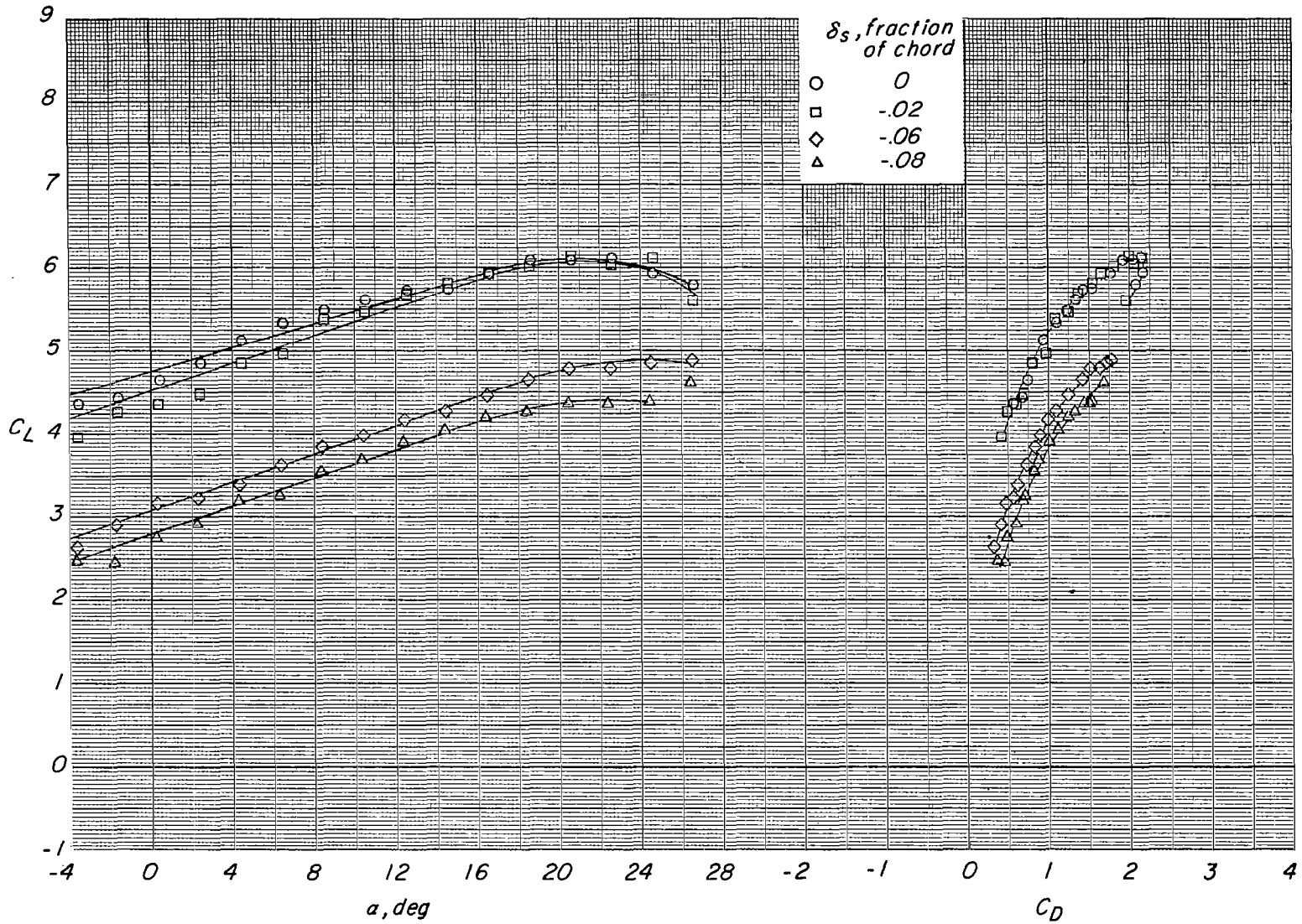

(c) $C_T \approx 1.6$.

Figure 20.- Continued.

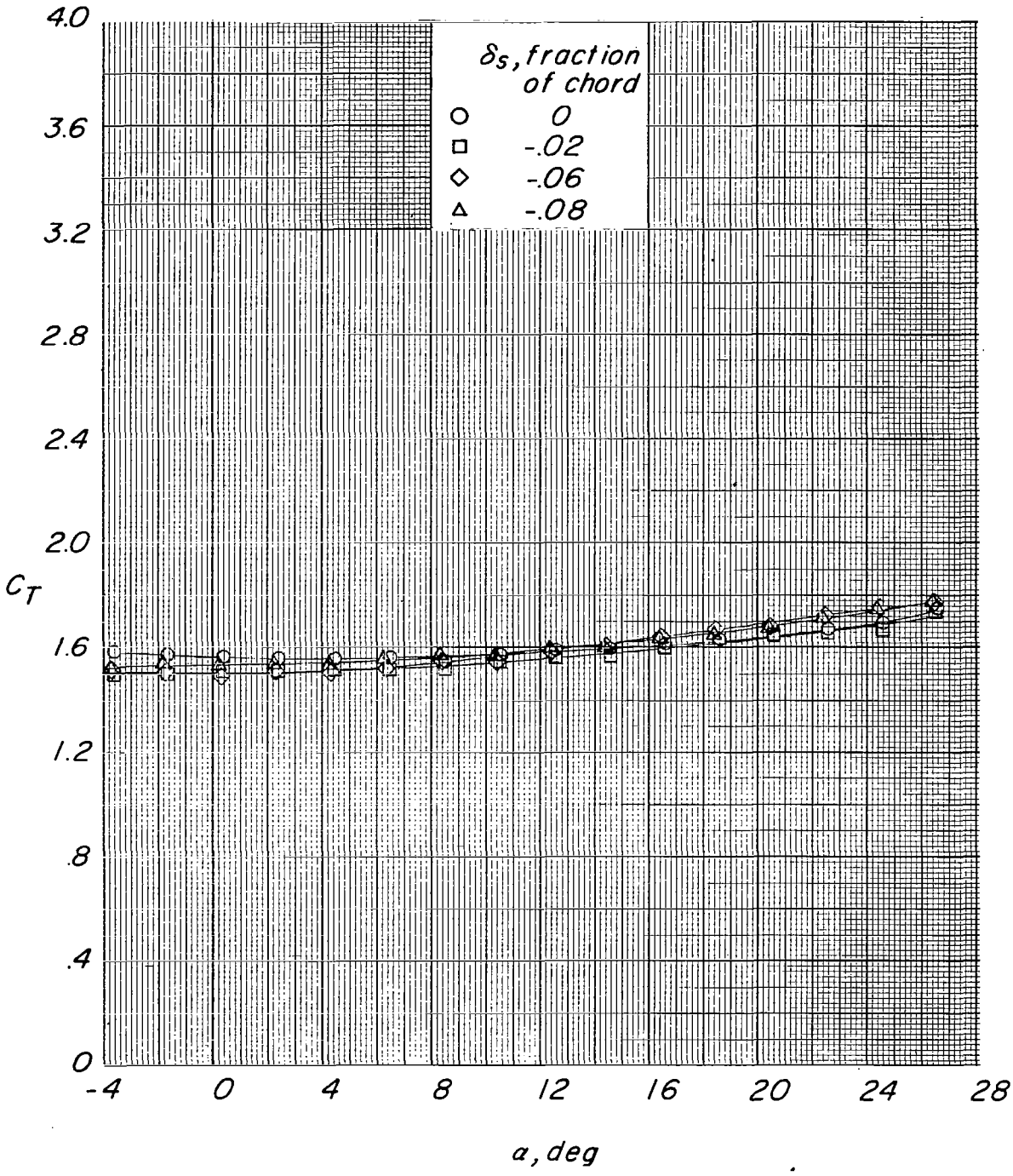

(c) Continued.

Figure 20.- Continued.

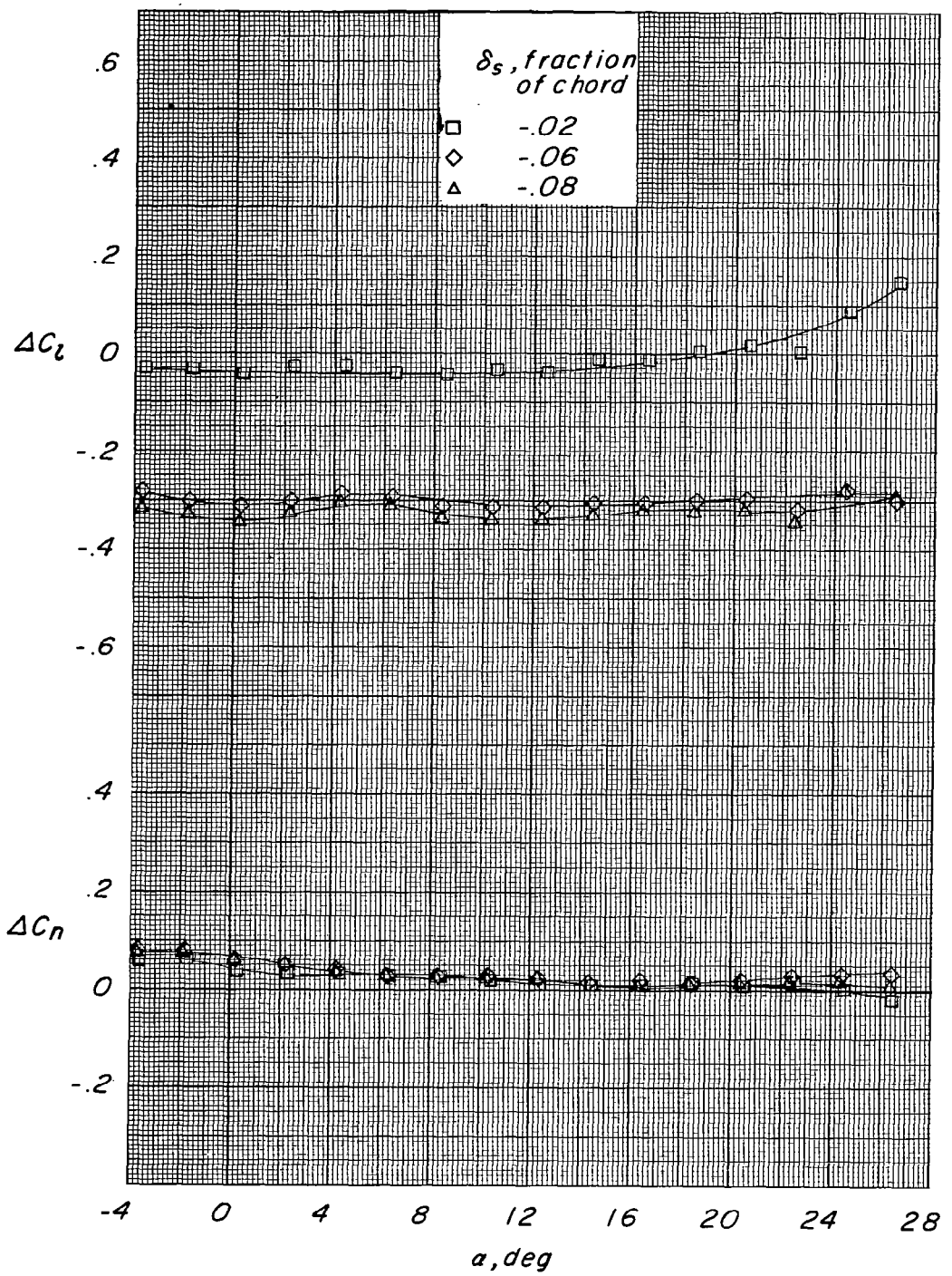

(c) Concluded.

Figure 20.- Continued.

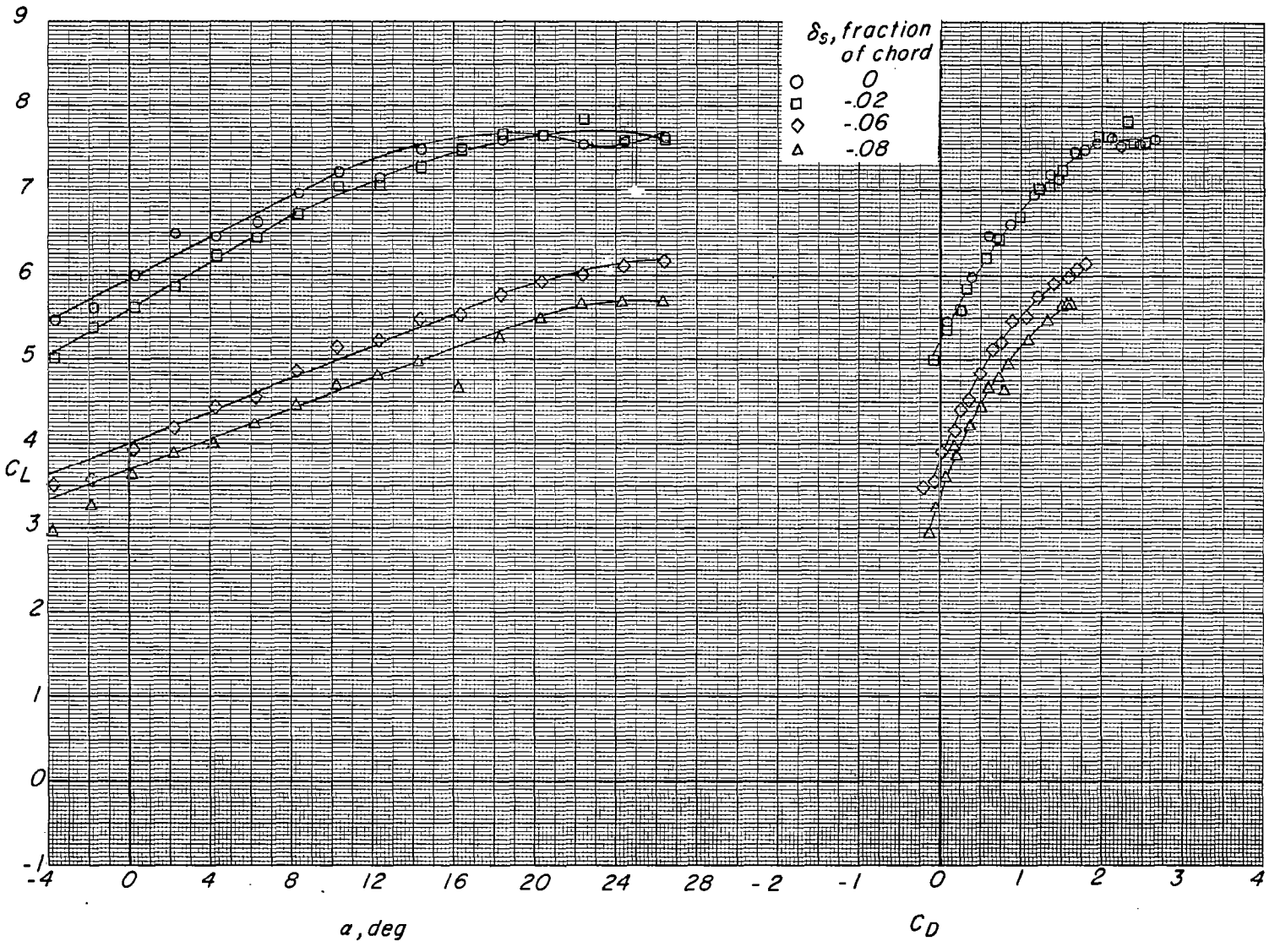

(d) $C_T \approx 2.7$.

Figure 20.- Continued.

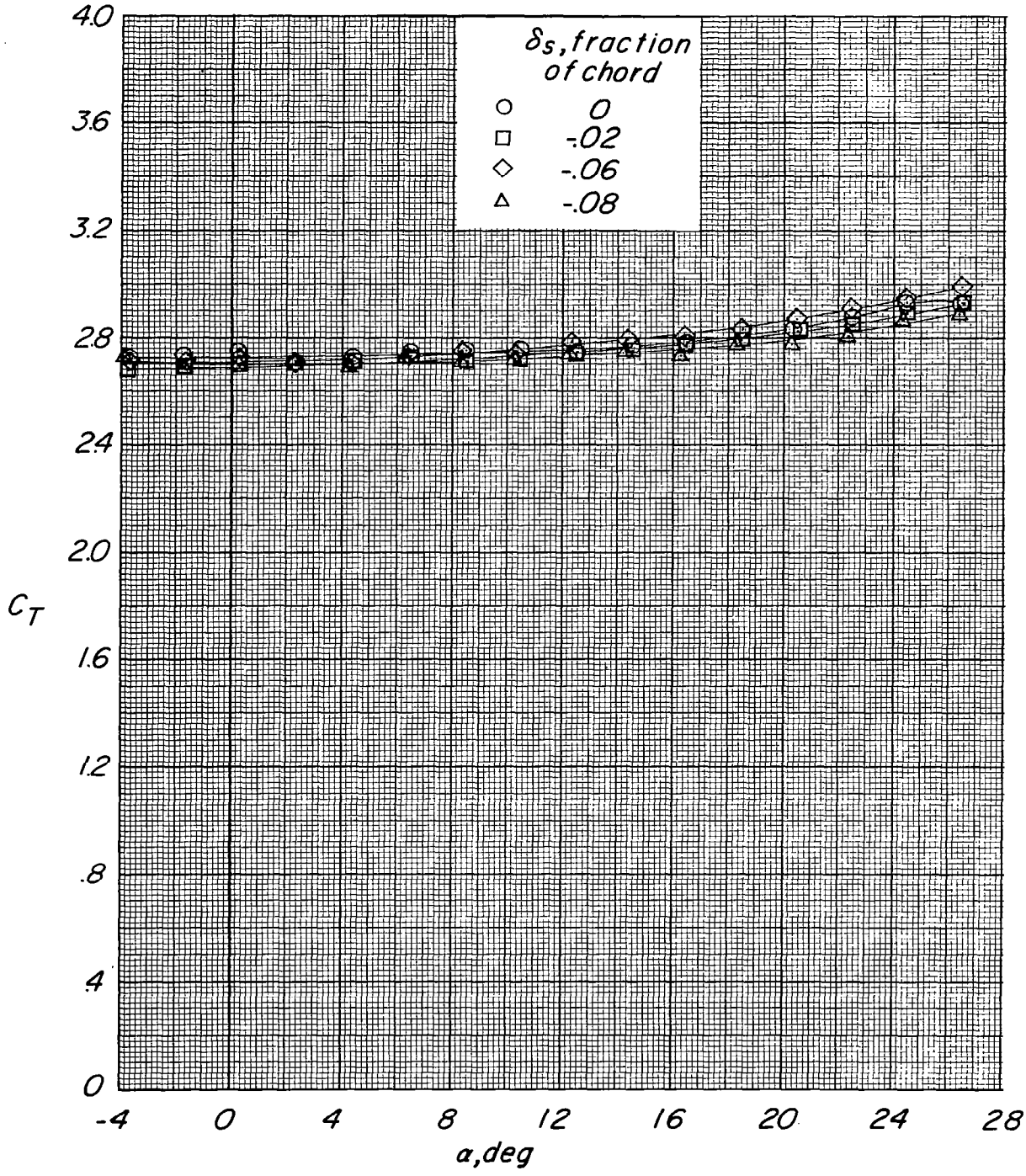

(d) Continued.

Figure 20.- Continued.

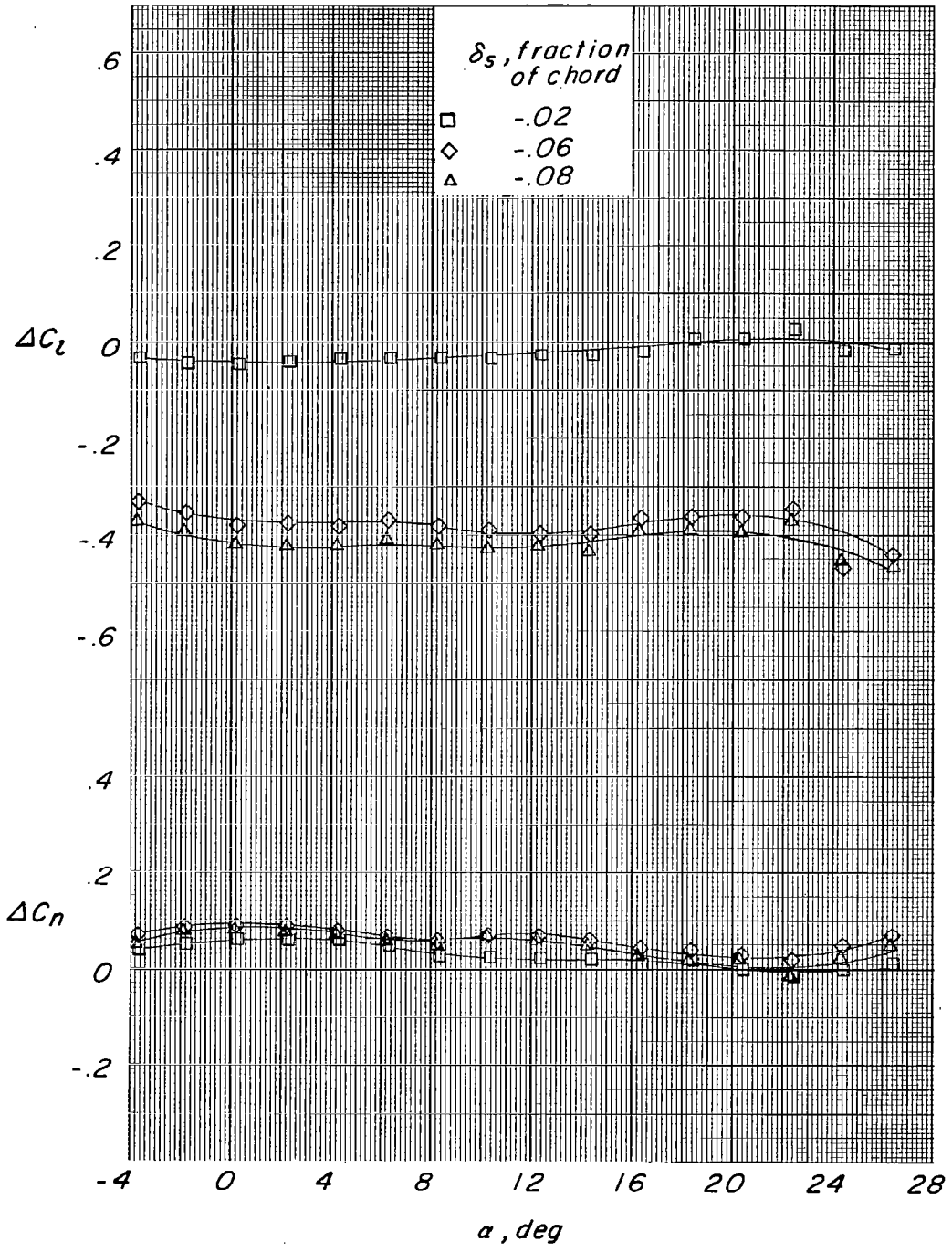

(d) Concluded.

Figure 20.- Concluded.

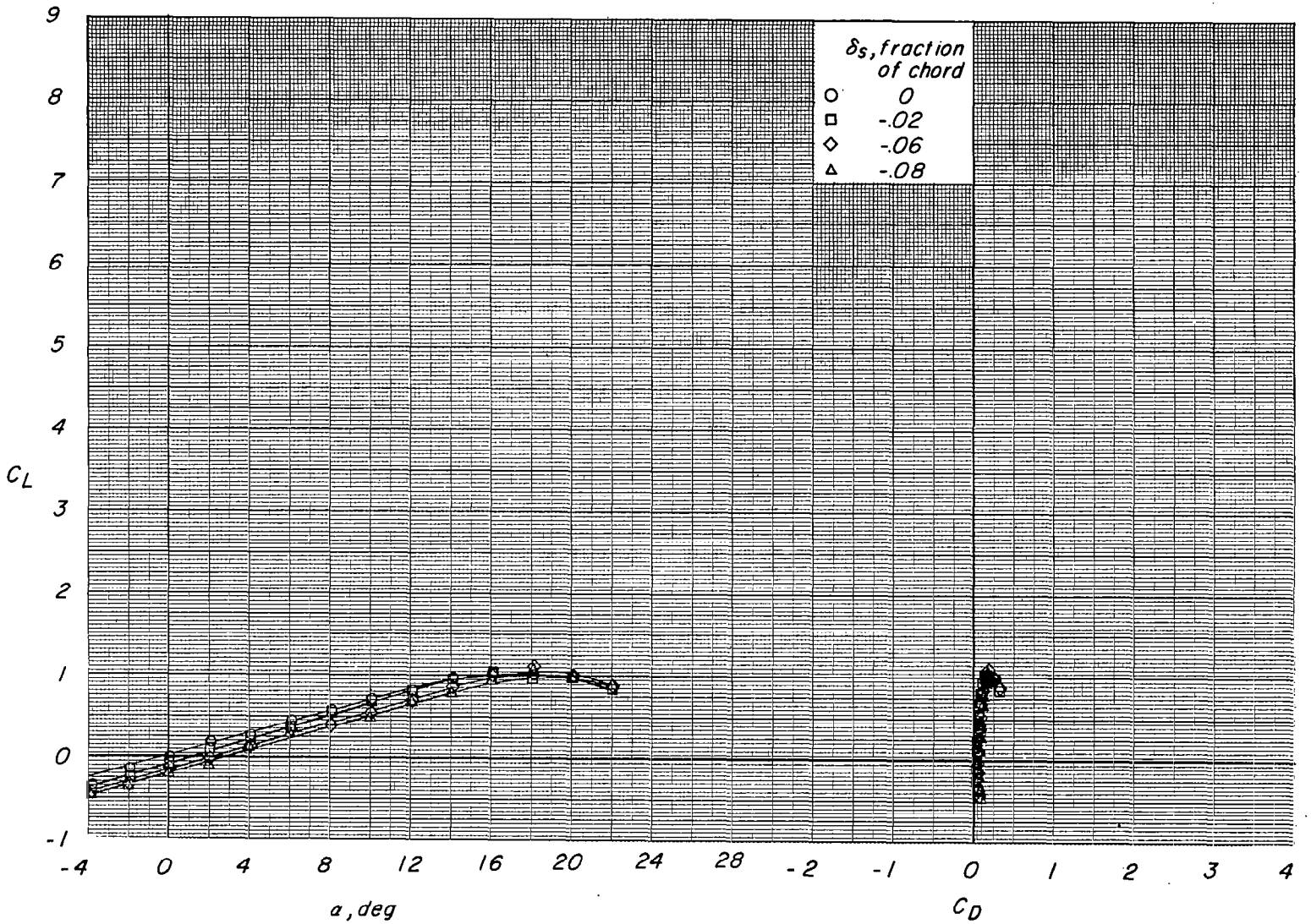

(a) $C_T = 0$ (propeller off).

Figure 21.- Effect of spoiler projection for configuration E (short span, $\delta_f = 0^o$).

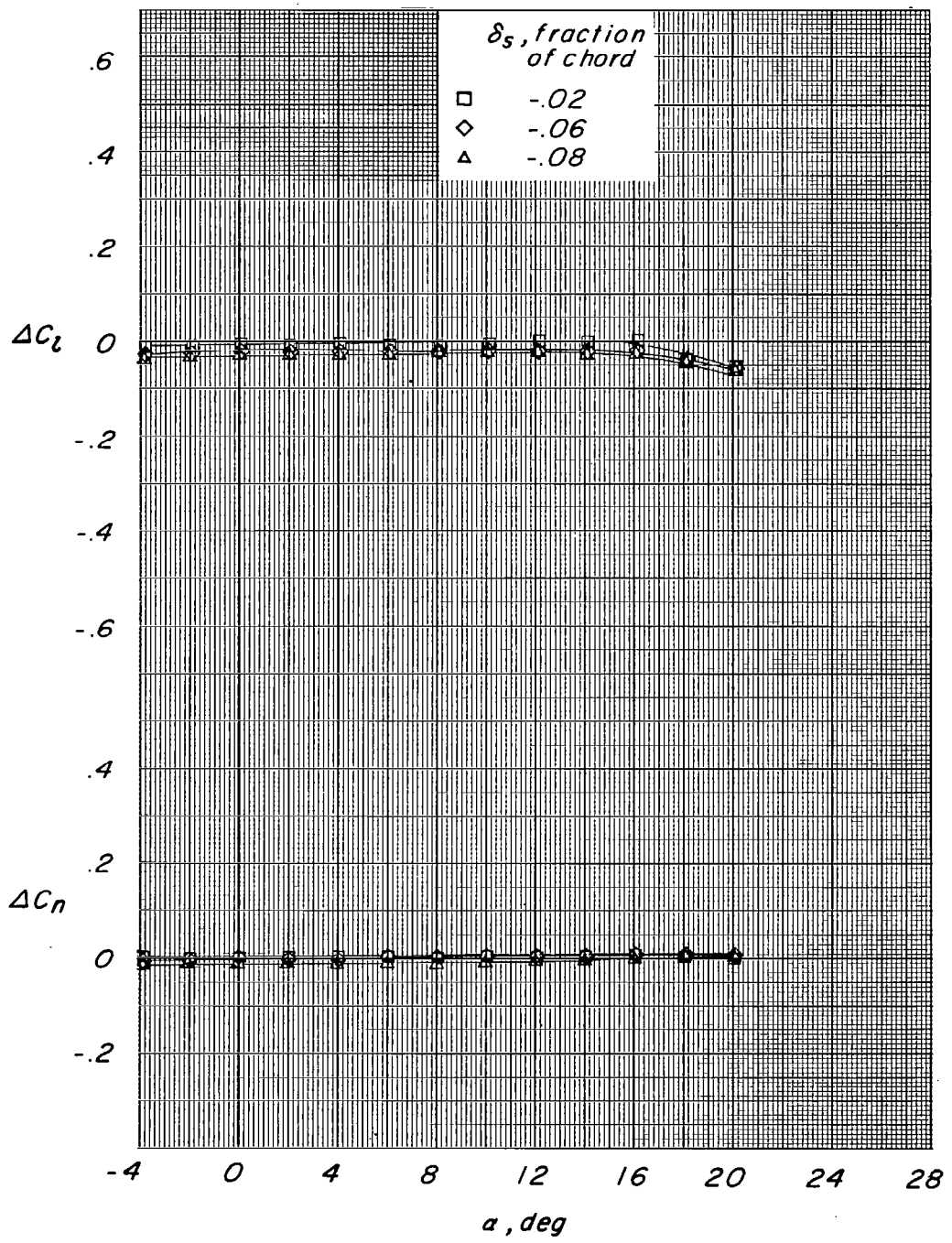

(a) Concluded.

Figure 21.- Continued.

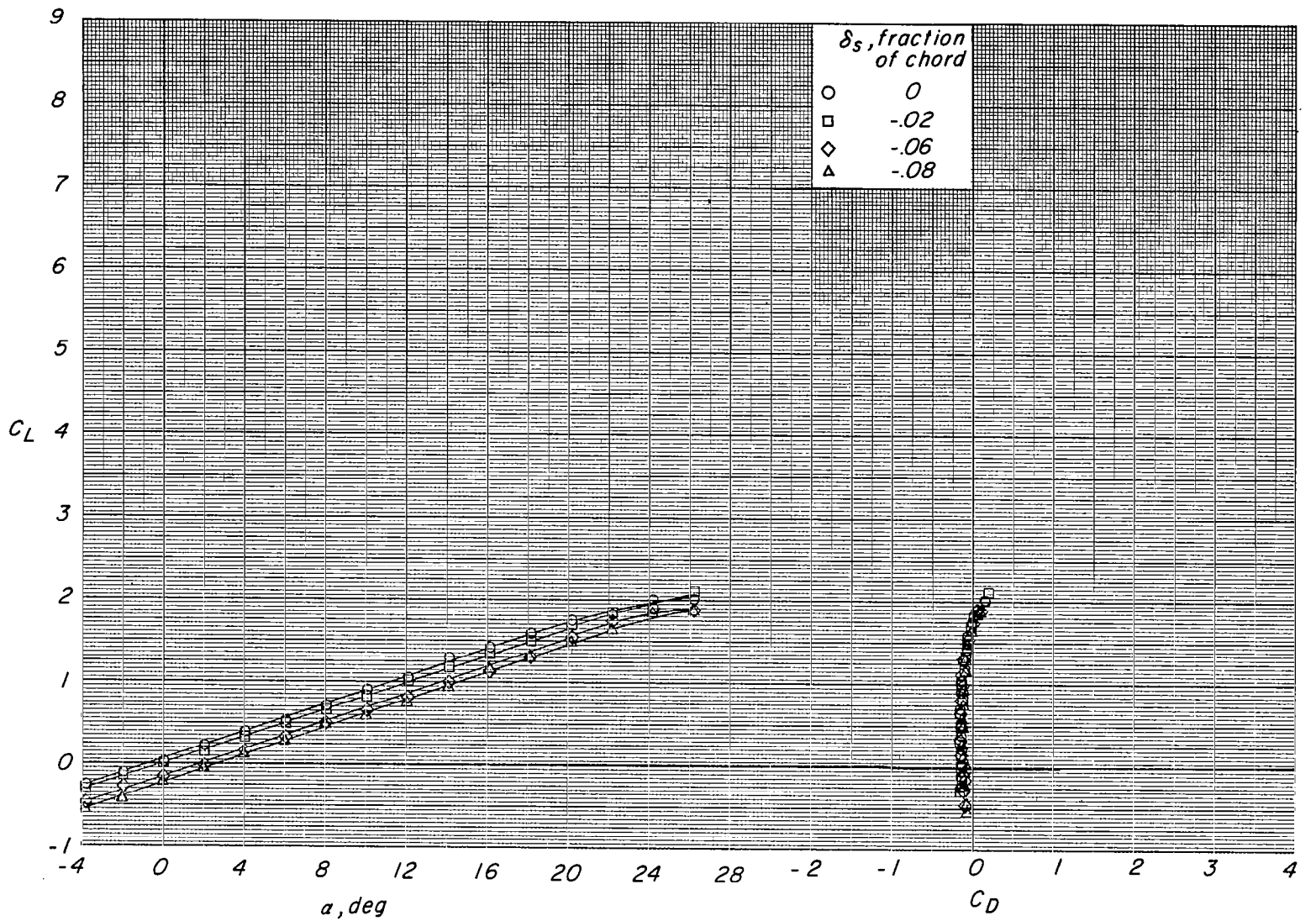

(b) $C_T \approx 0.25$.

Figure 21.- Continued.

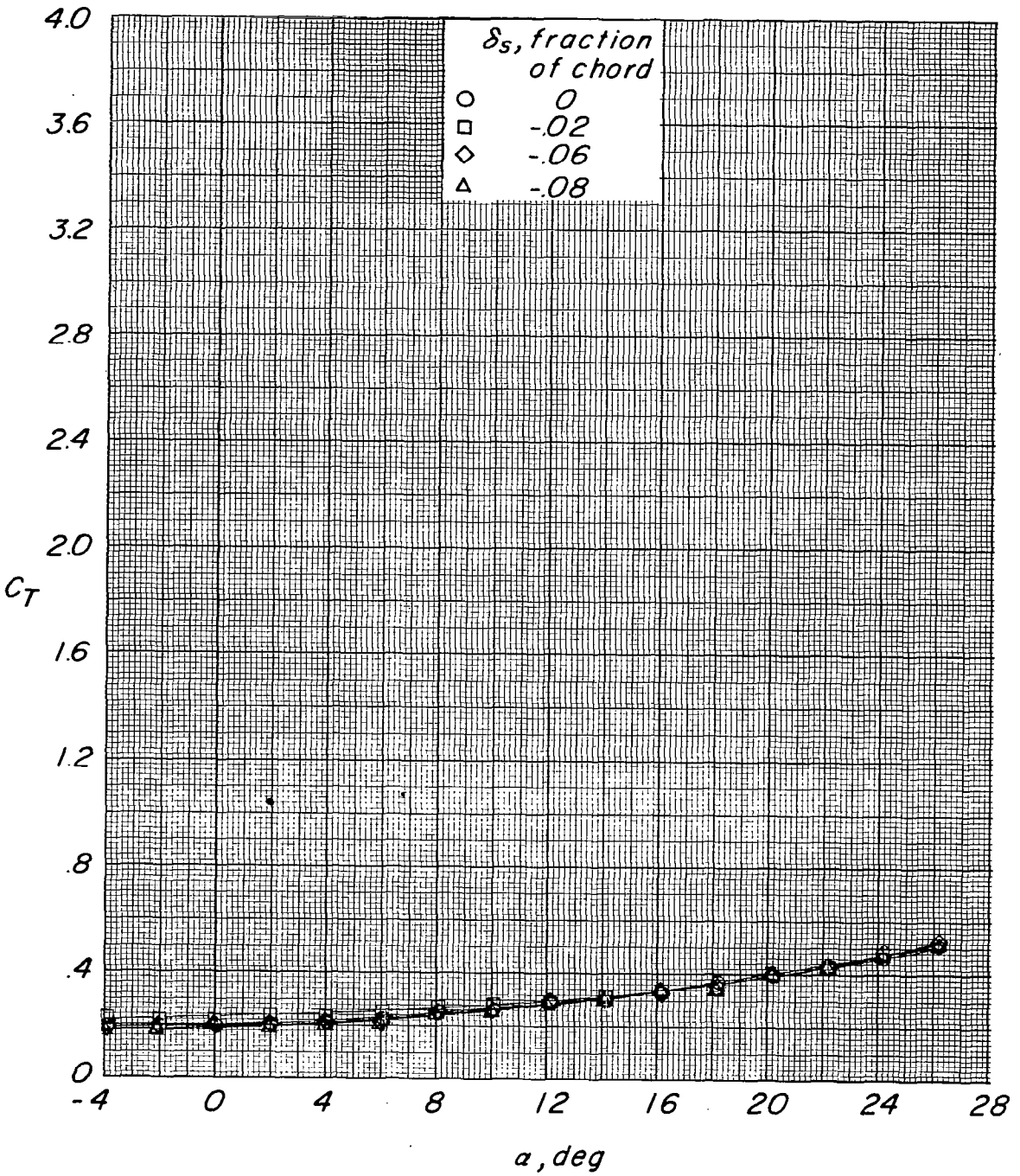

(b) Continued.

Figure 21.- Continued.

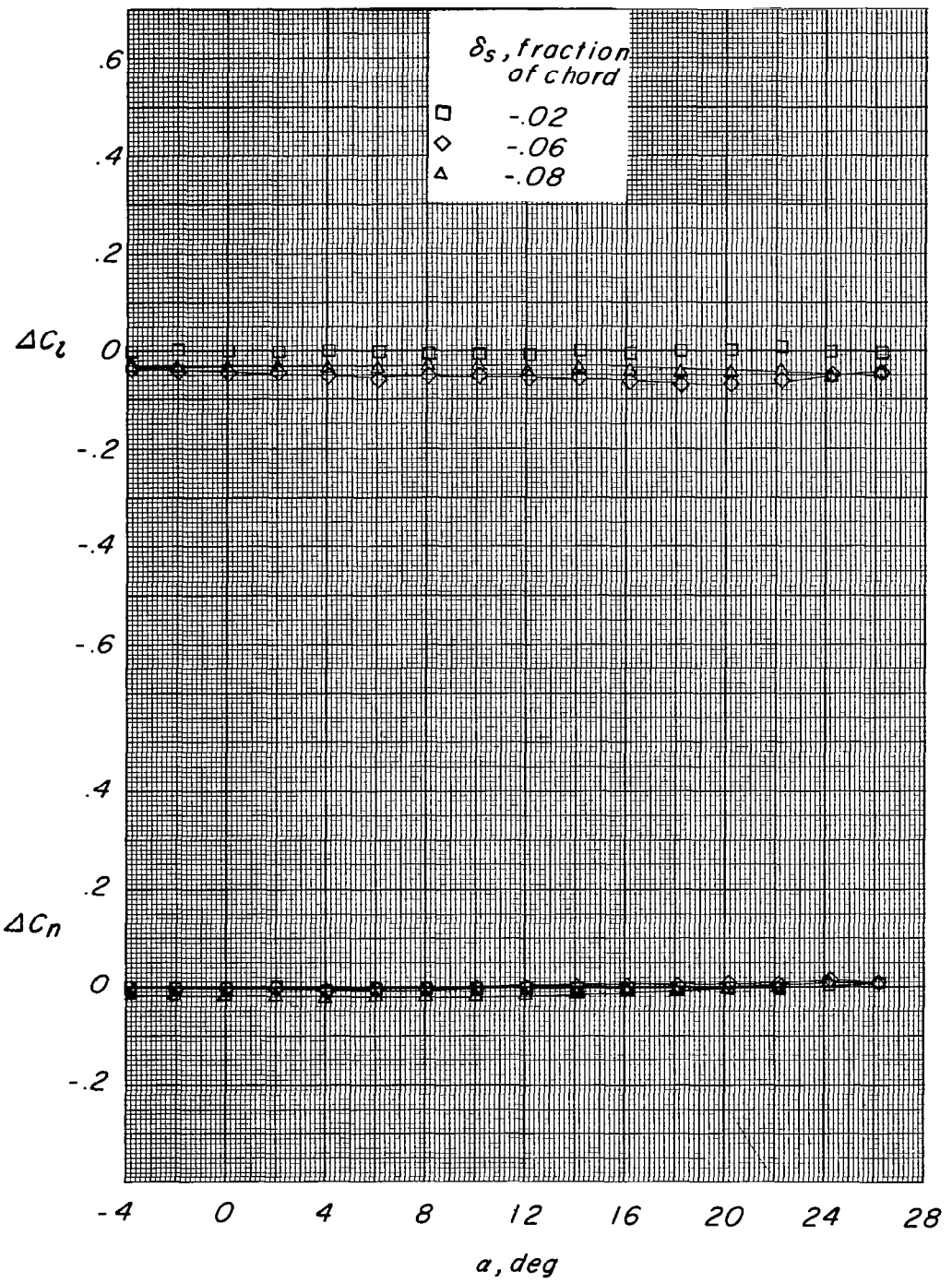

(b) Concluded.

Figure 21.- Continued.

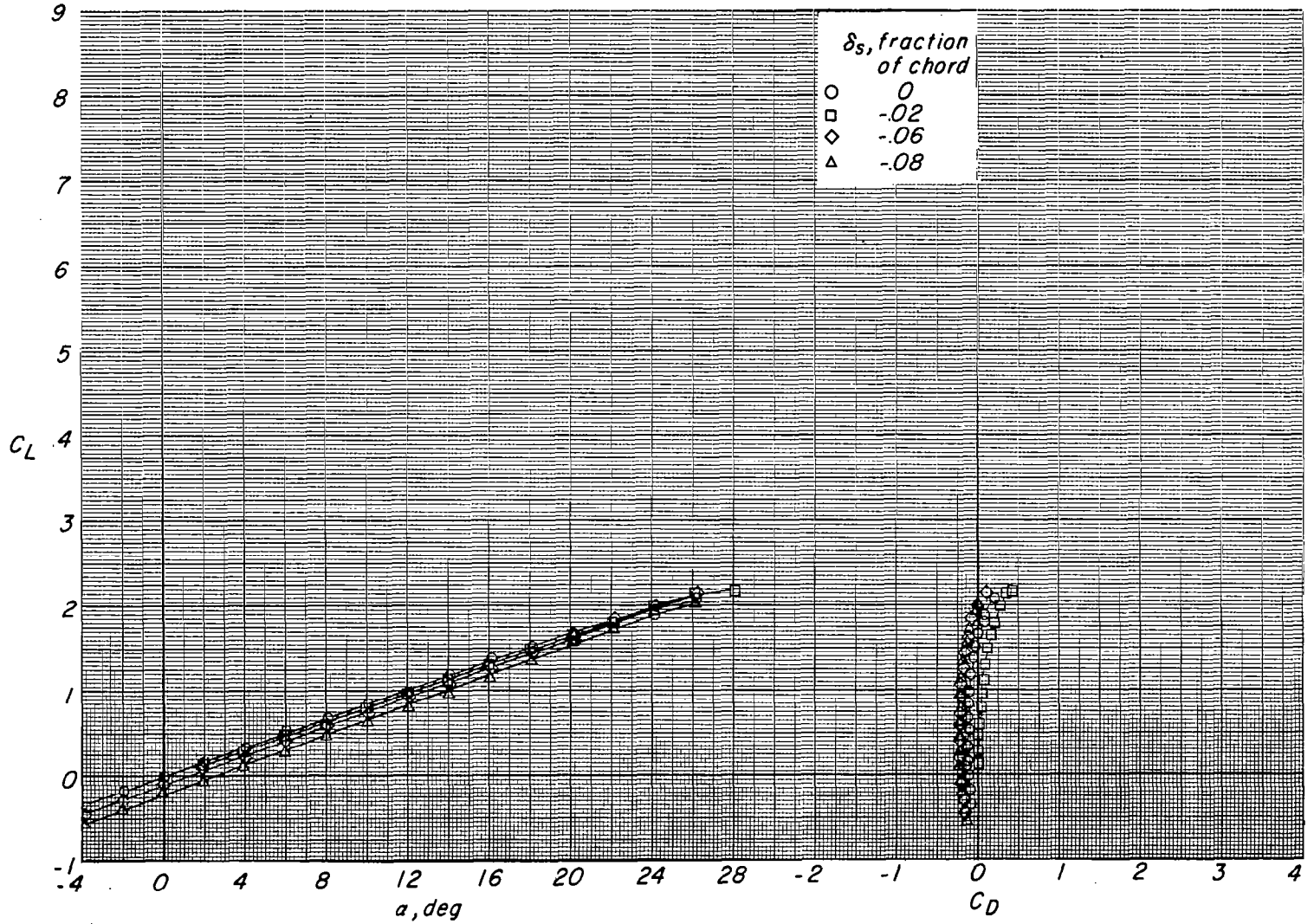

(c) $C_T \approx 0.45$.

Figure 21.- Continued.

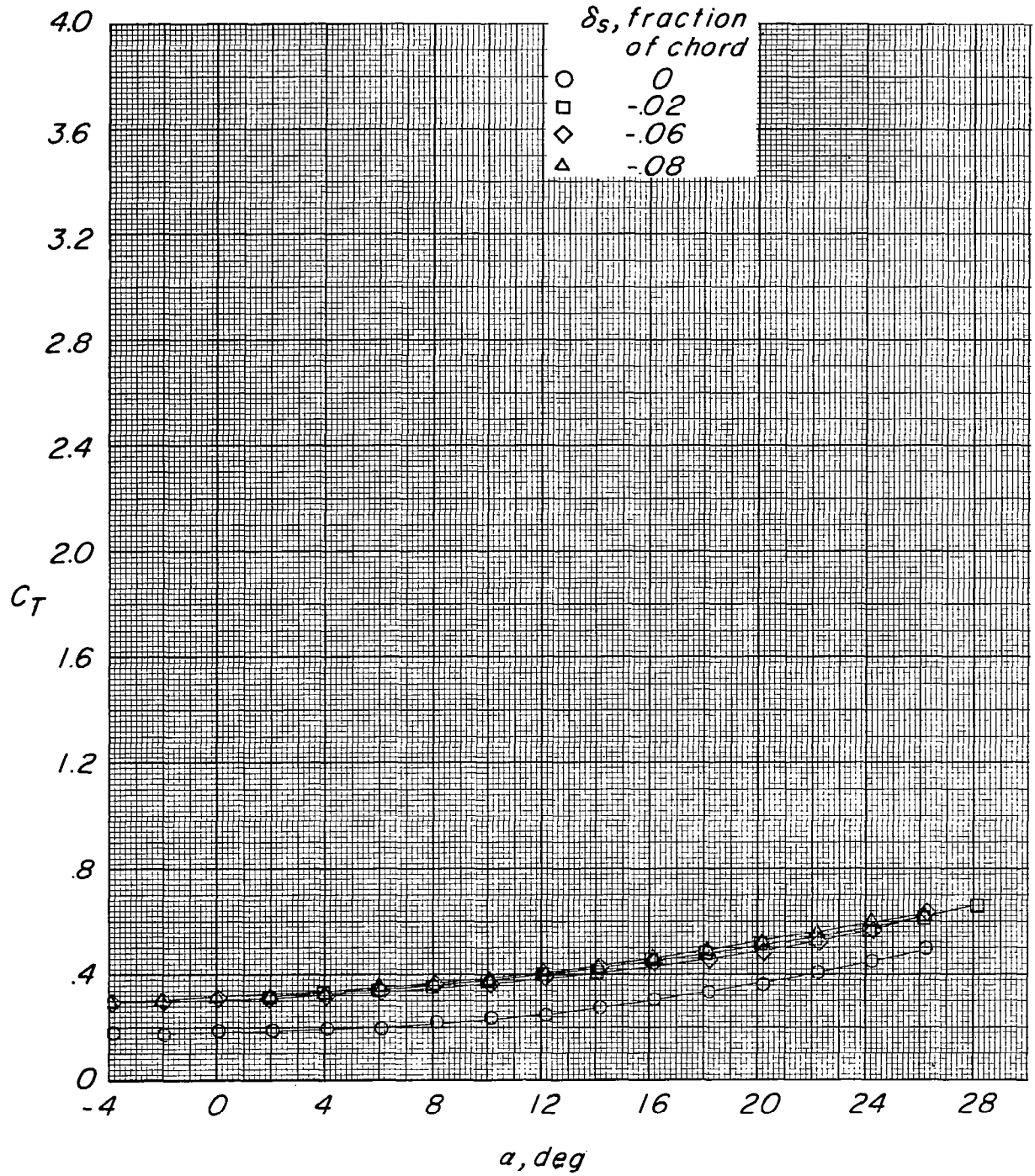

(c) Continued.

Figure 21.- Continued.

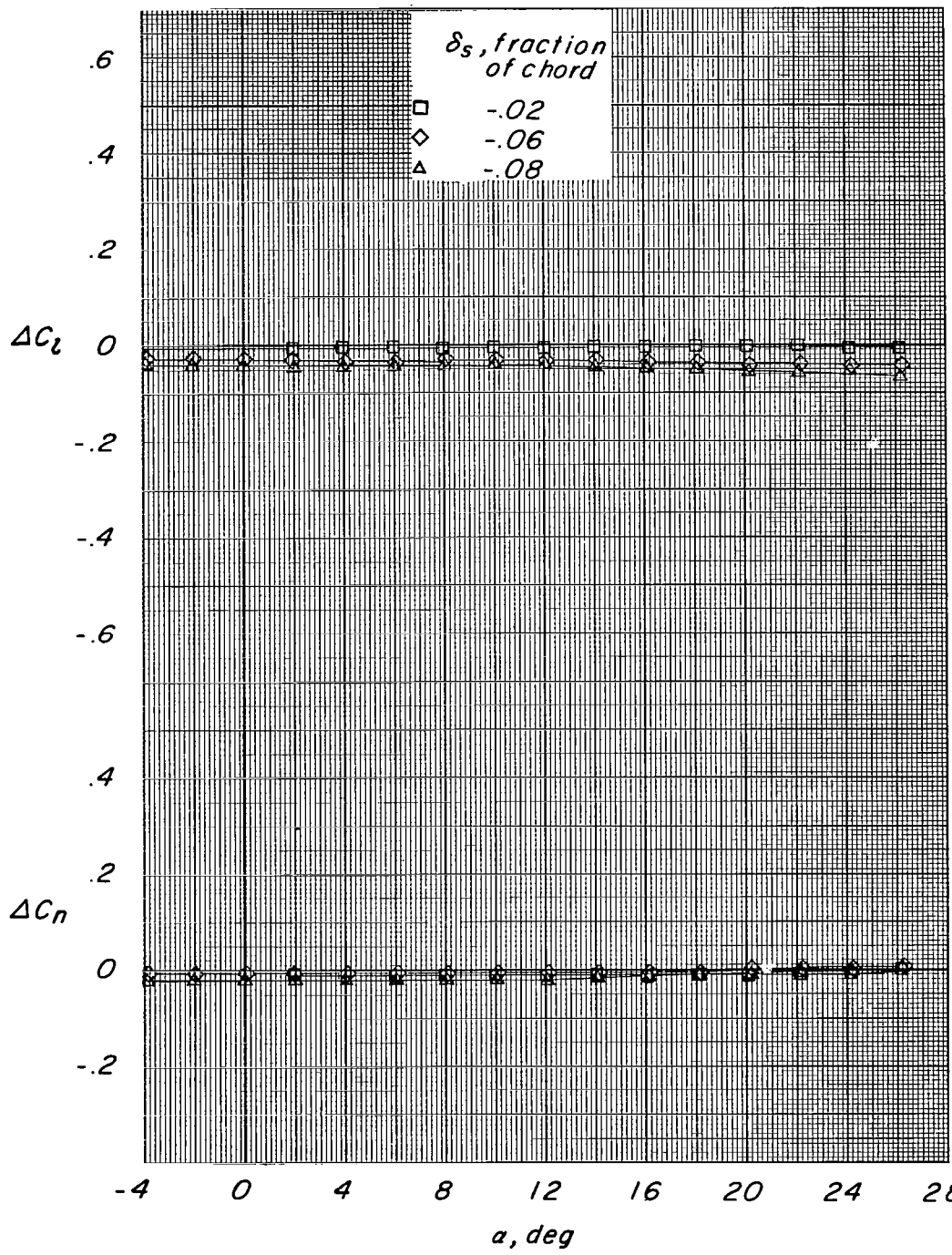

(c) Concluded.

Figure 21.- Concluded.

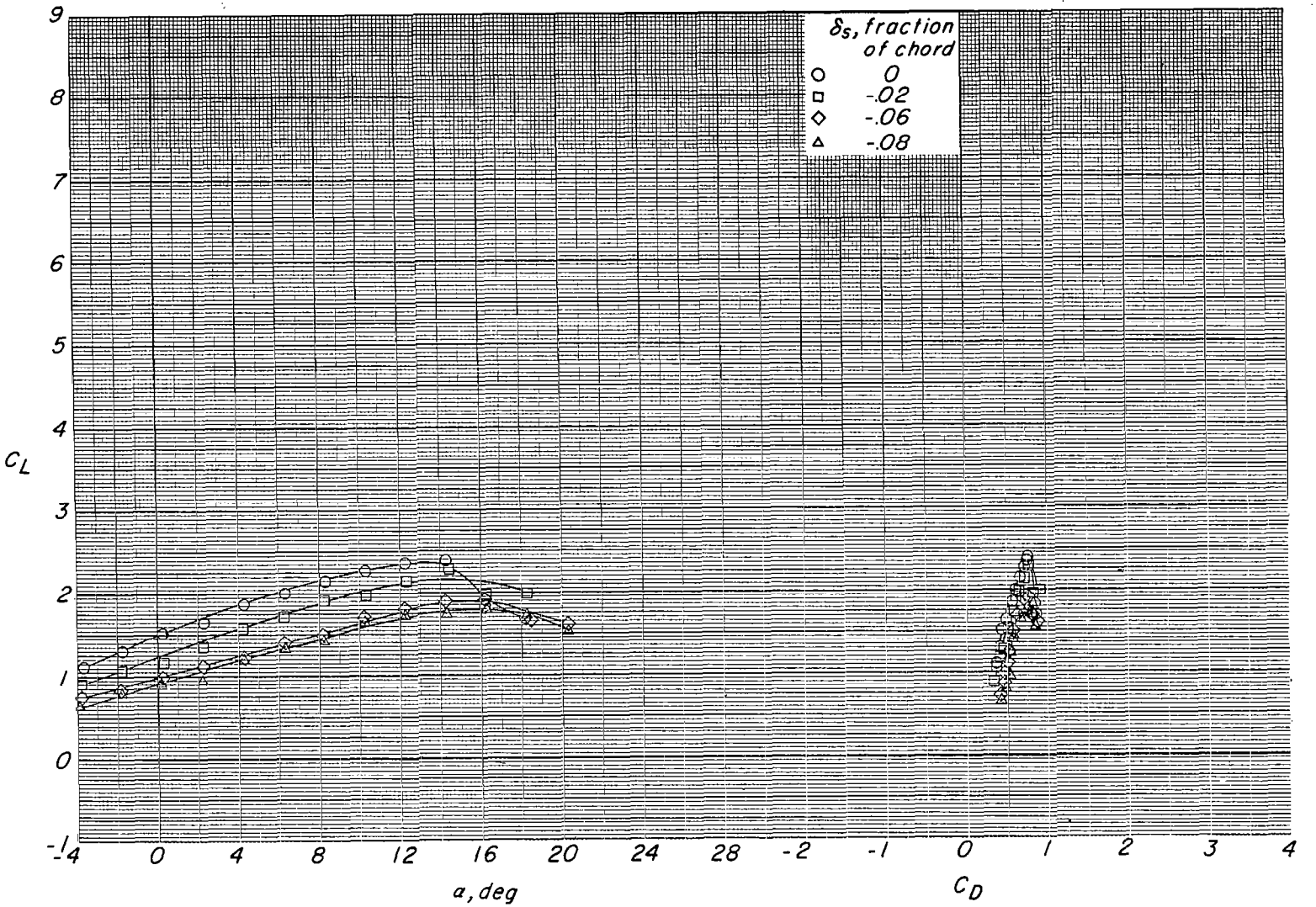

(a) $C_T = 0$ (propeller off).

Figure 22.- Effect of spoiler projection for configuration F (short span, $\delta_f = 45°$).

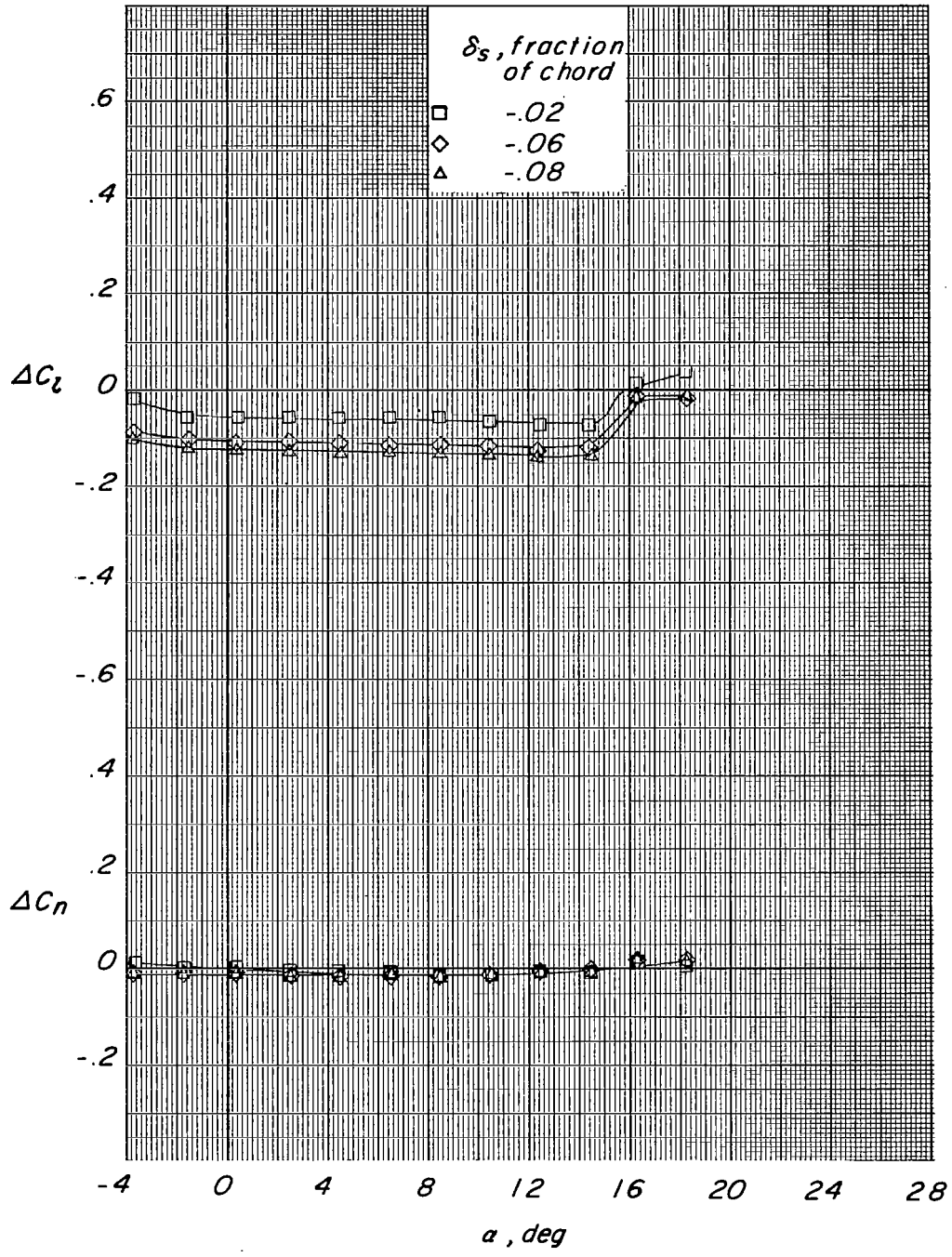

(a) Concluded.

Figure 22.- Continued.

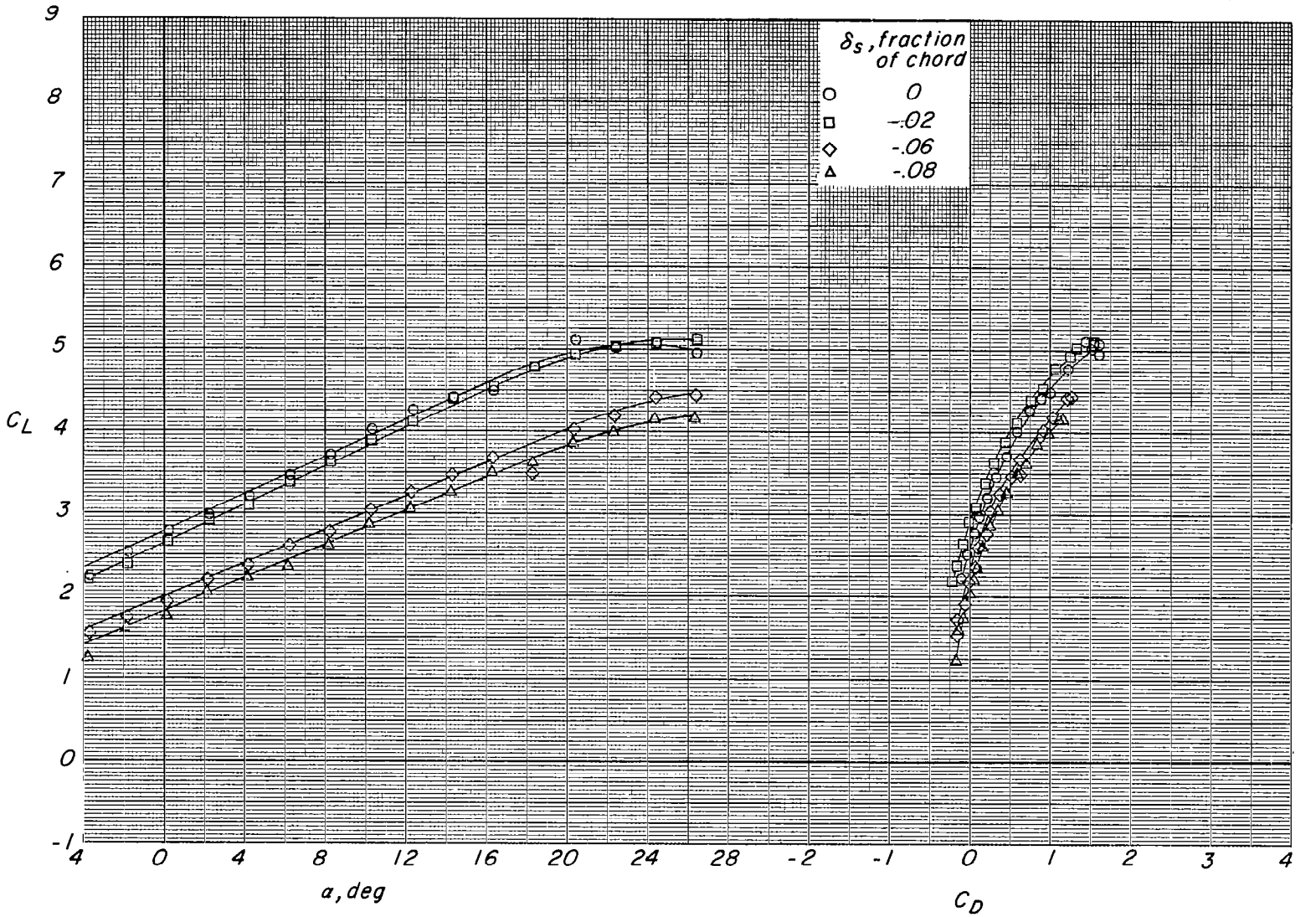

(b) $C_T \approx 1.3$.

Figure 22.- Continued.

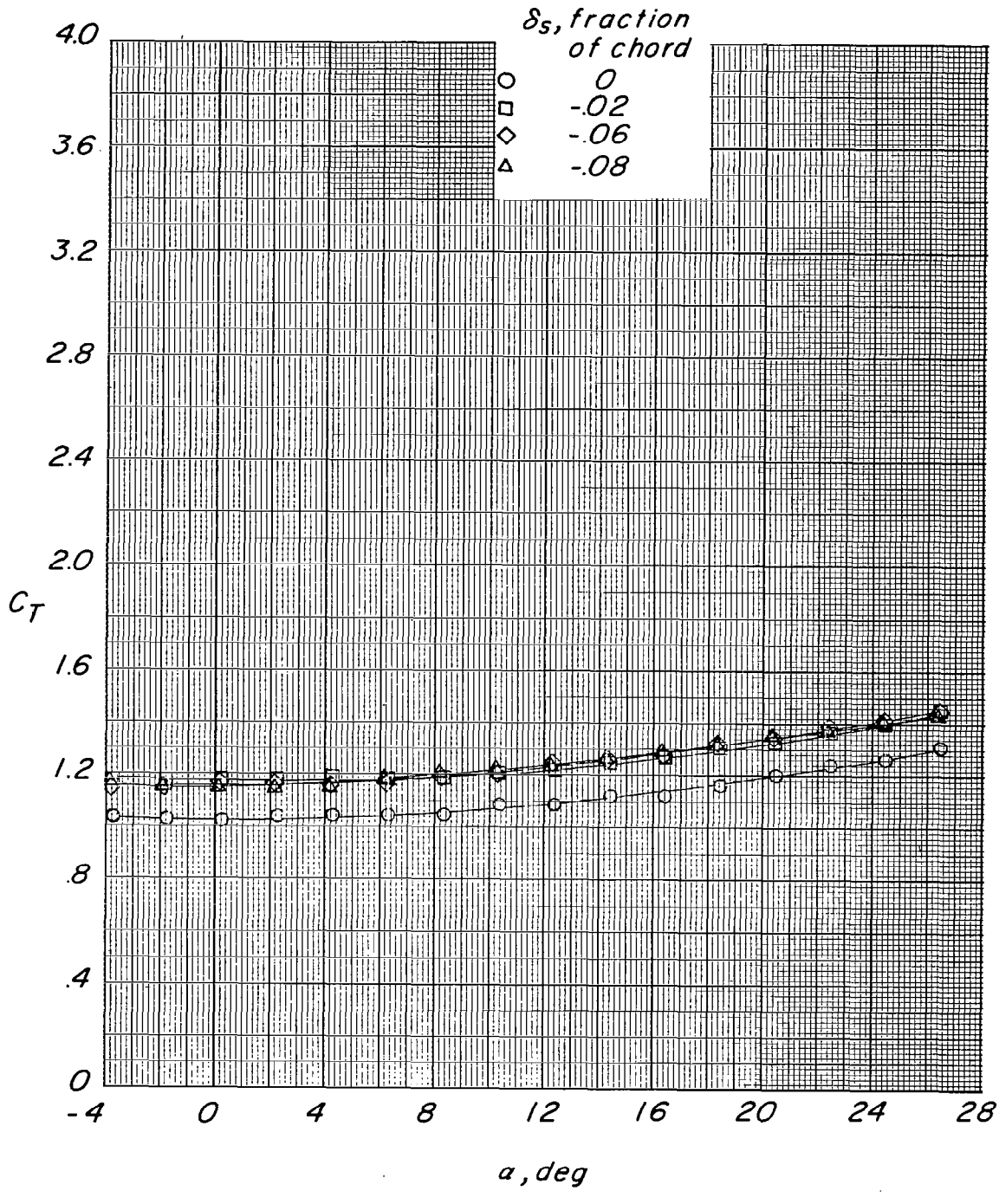

(b) Continued.

Figure 22.- Continued.

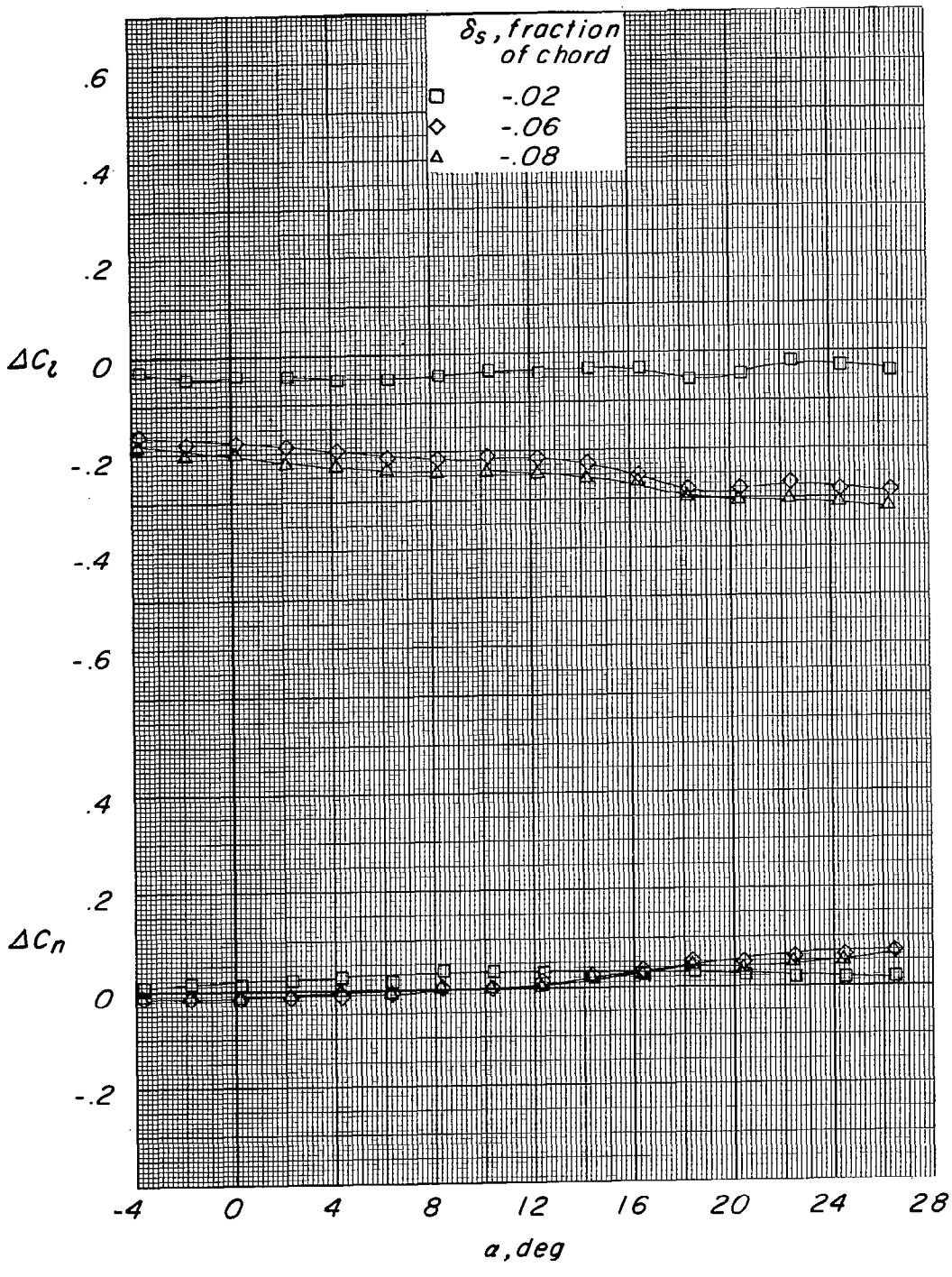

(b) Concluded.

Figure 22.- Continued.

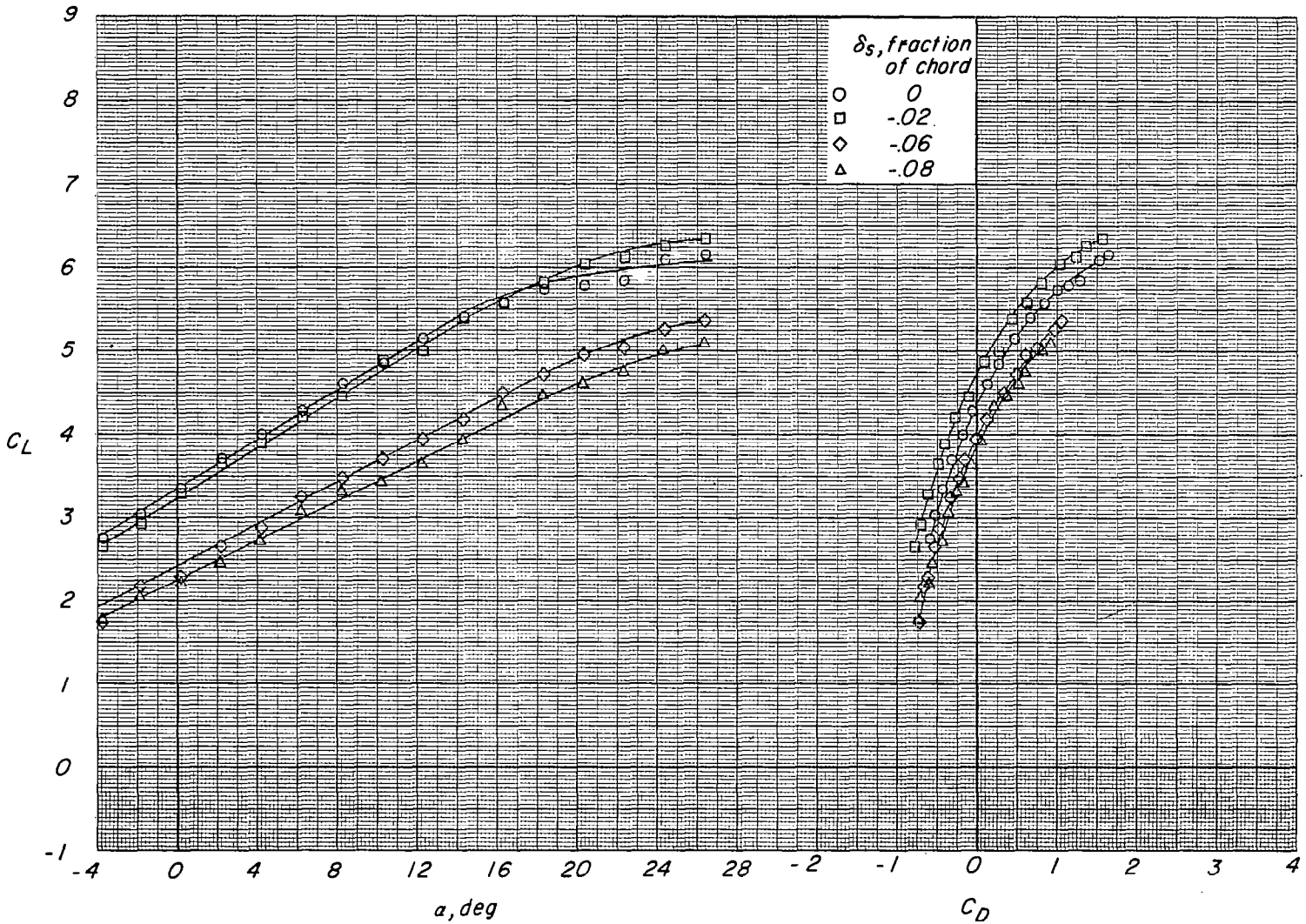

(c) $C_T \approx 2.2$.

Figure 22.- Continued.

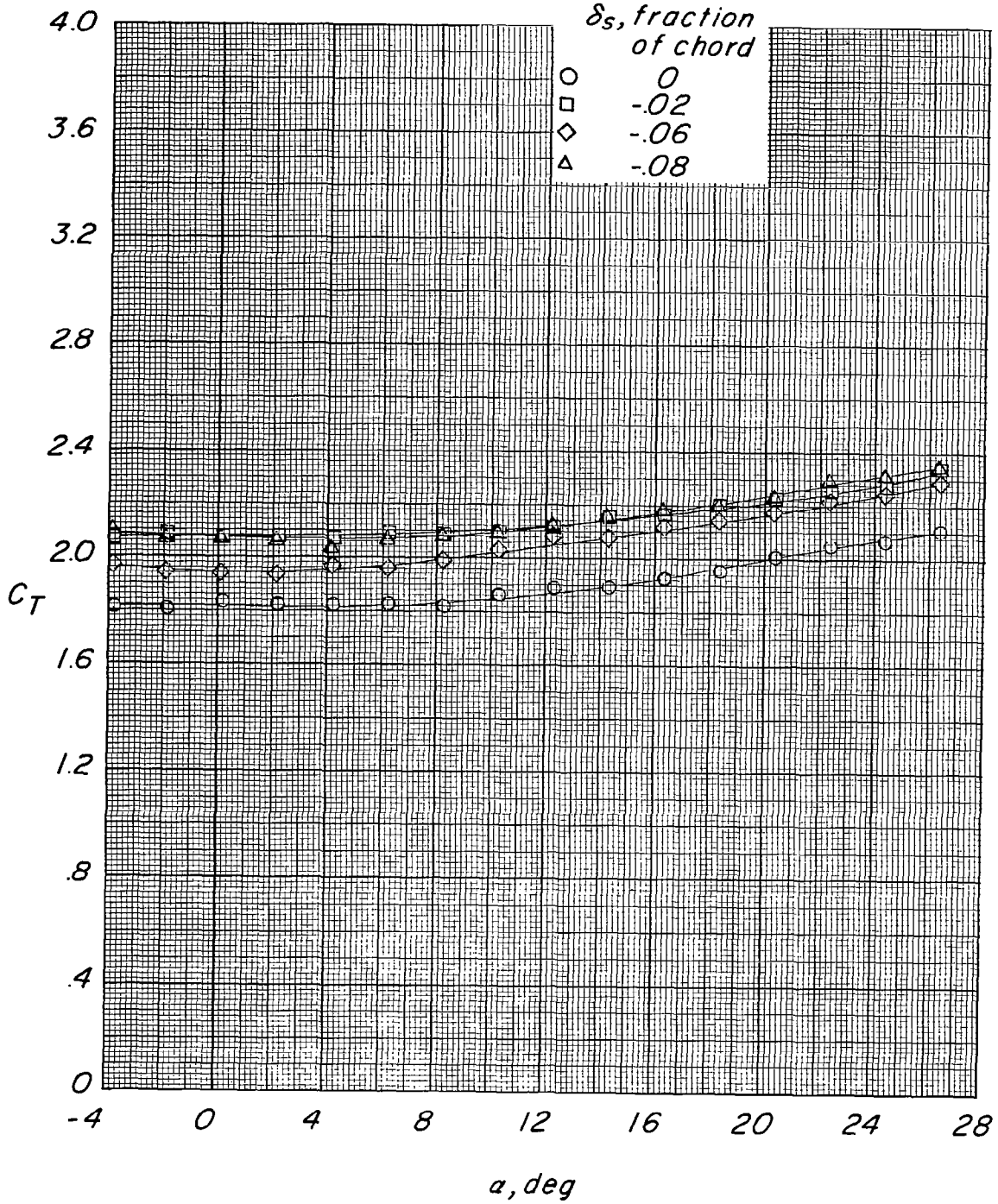

(c) Continued.

Figure 22.- Continued.

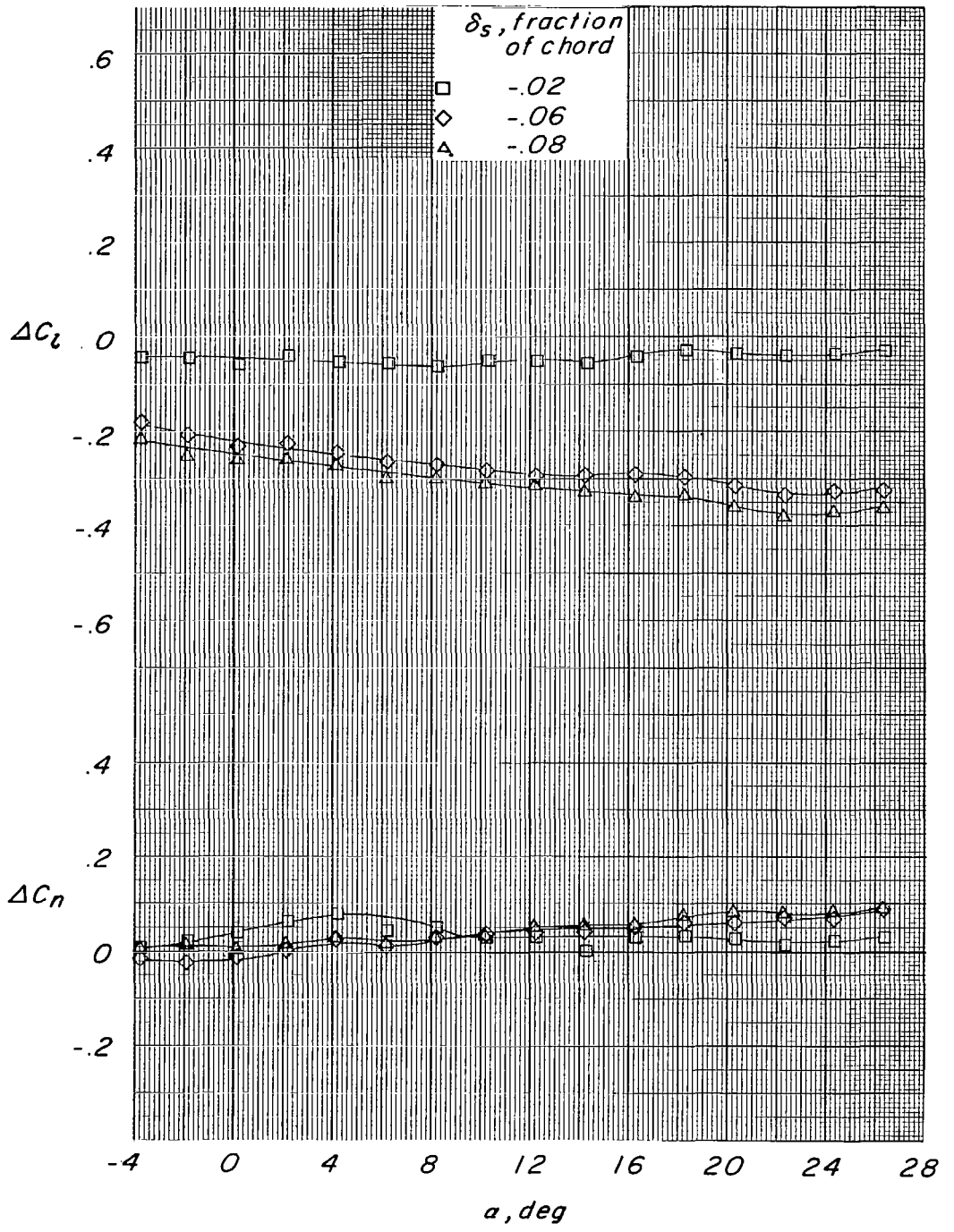

(c) Concluded.

Figure 22.- Continued.

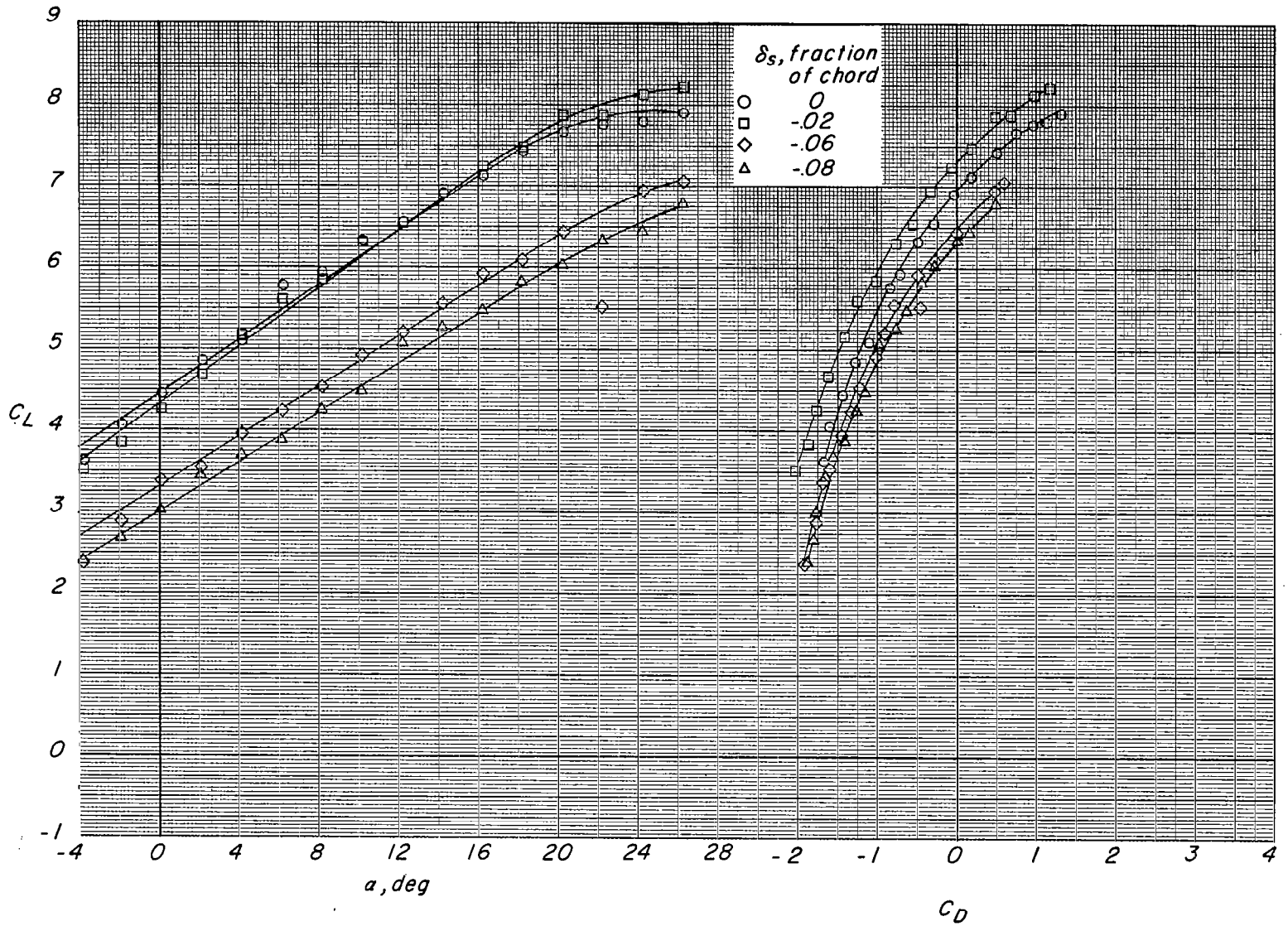

(d) $C_T \approx 3.8$.

Figure 22.- Continued.

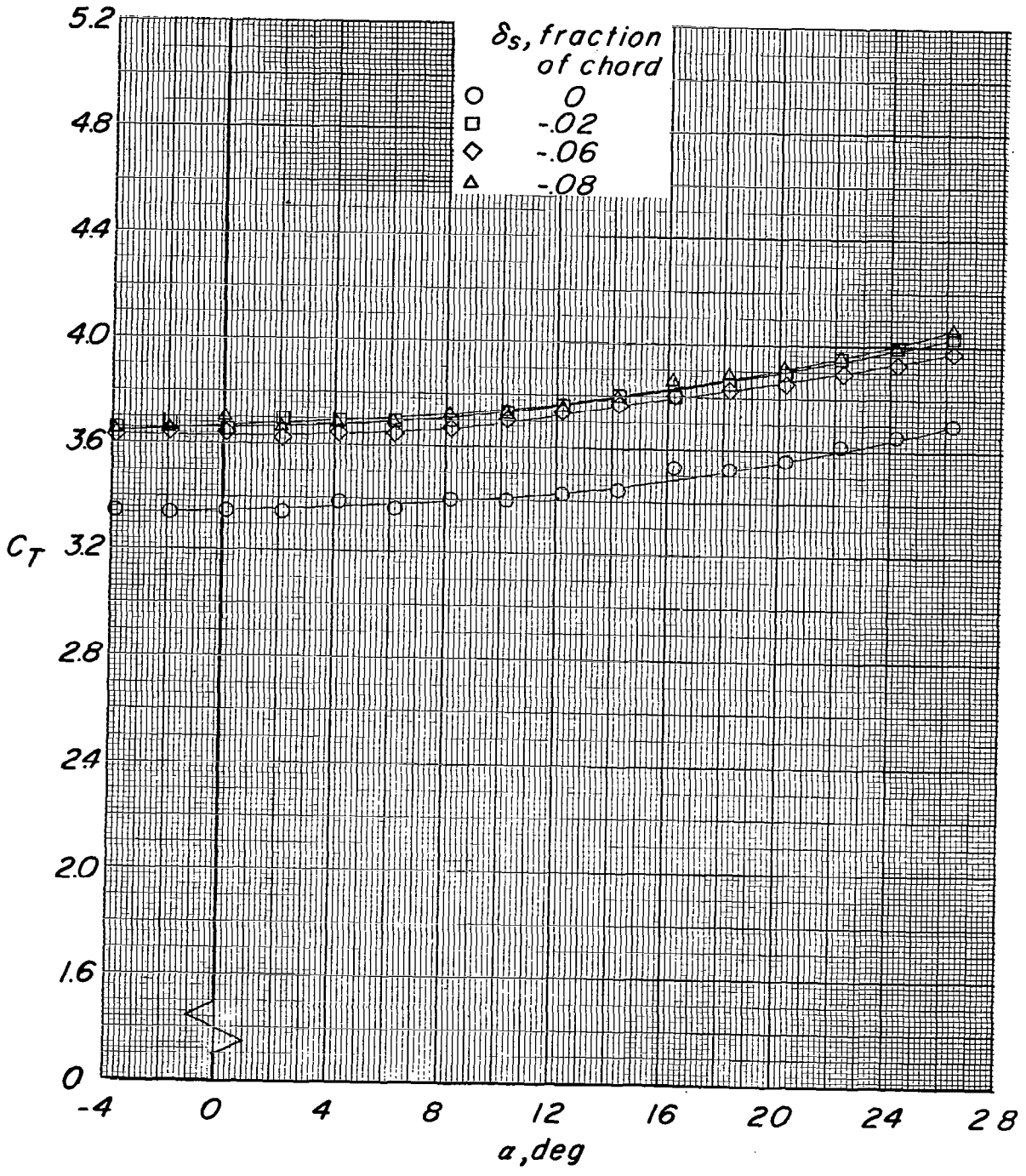

(d) Continued.

Figure 22.- Continued.

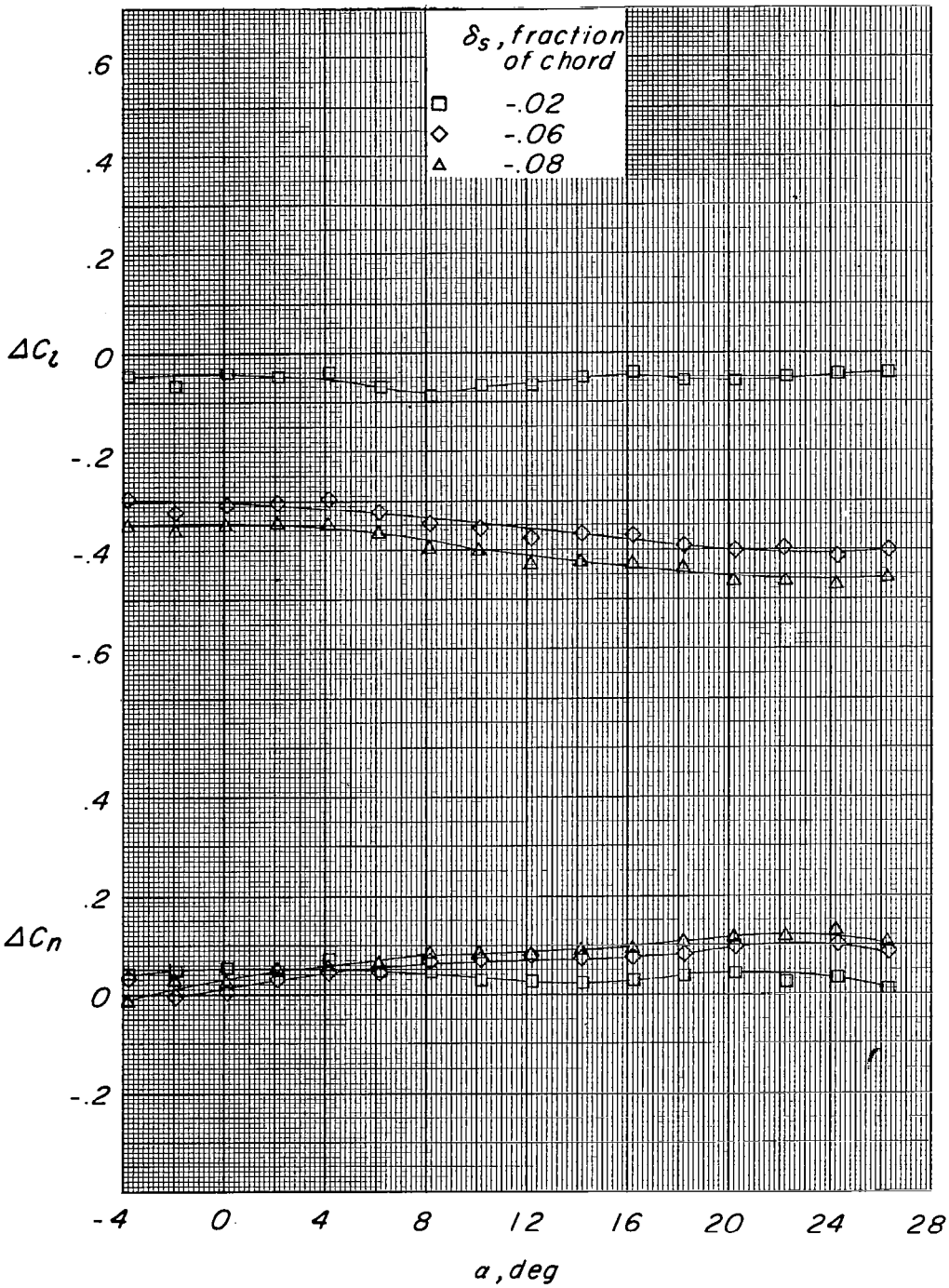

(d) Concluded.

Figure 22.- Concluded.

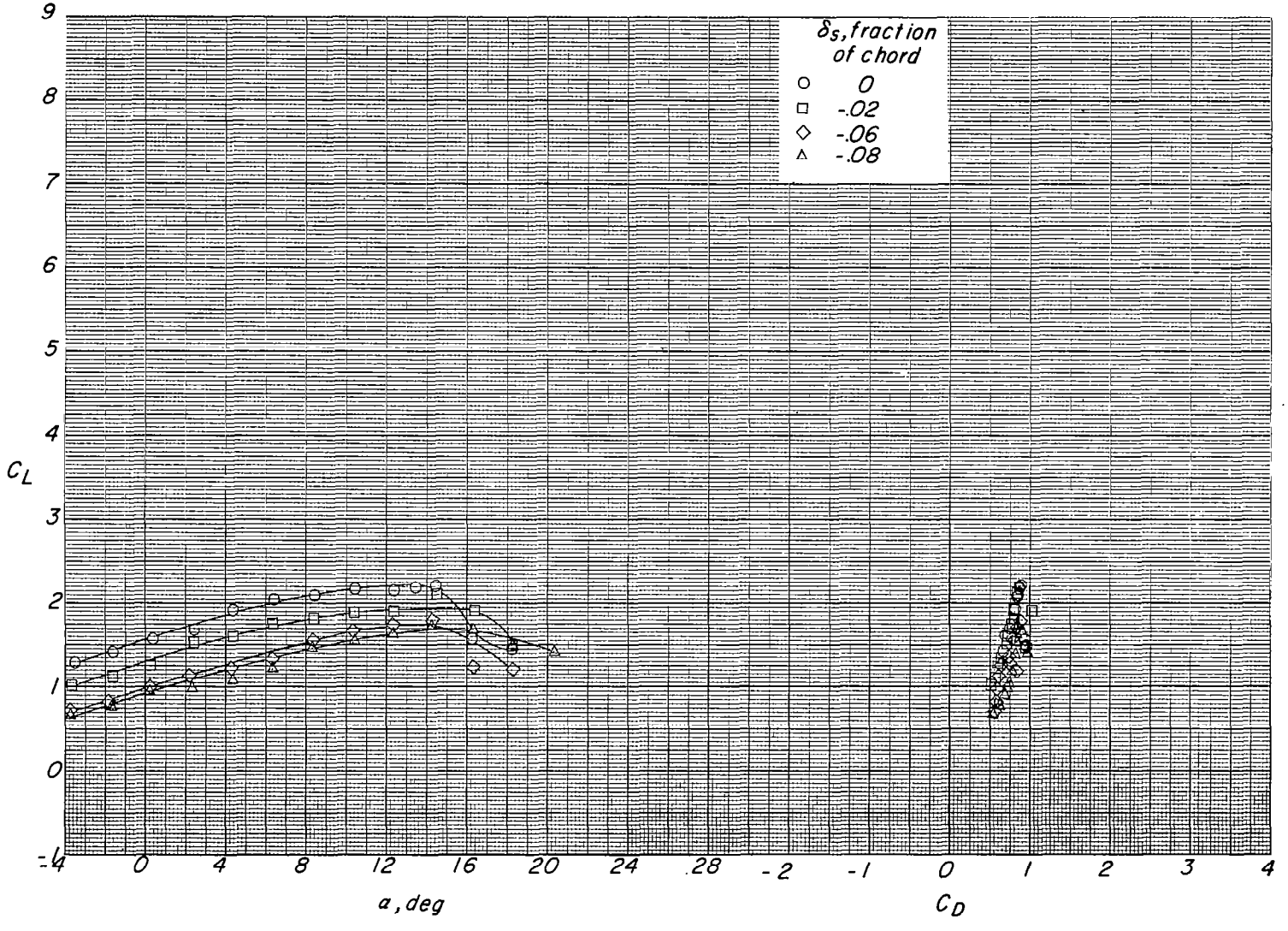

(a) $C_T = 0$ (propeller off).

Figure 23.- Effect of spoiler projection for configuration G (short span, $\delta_f = 75^\circ$).

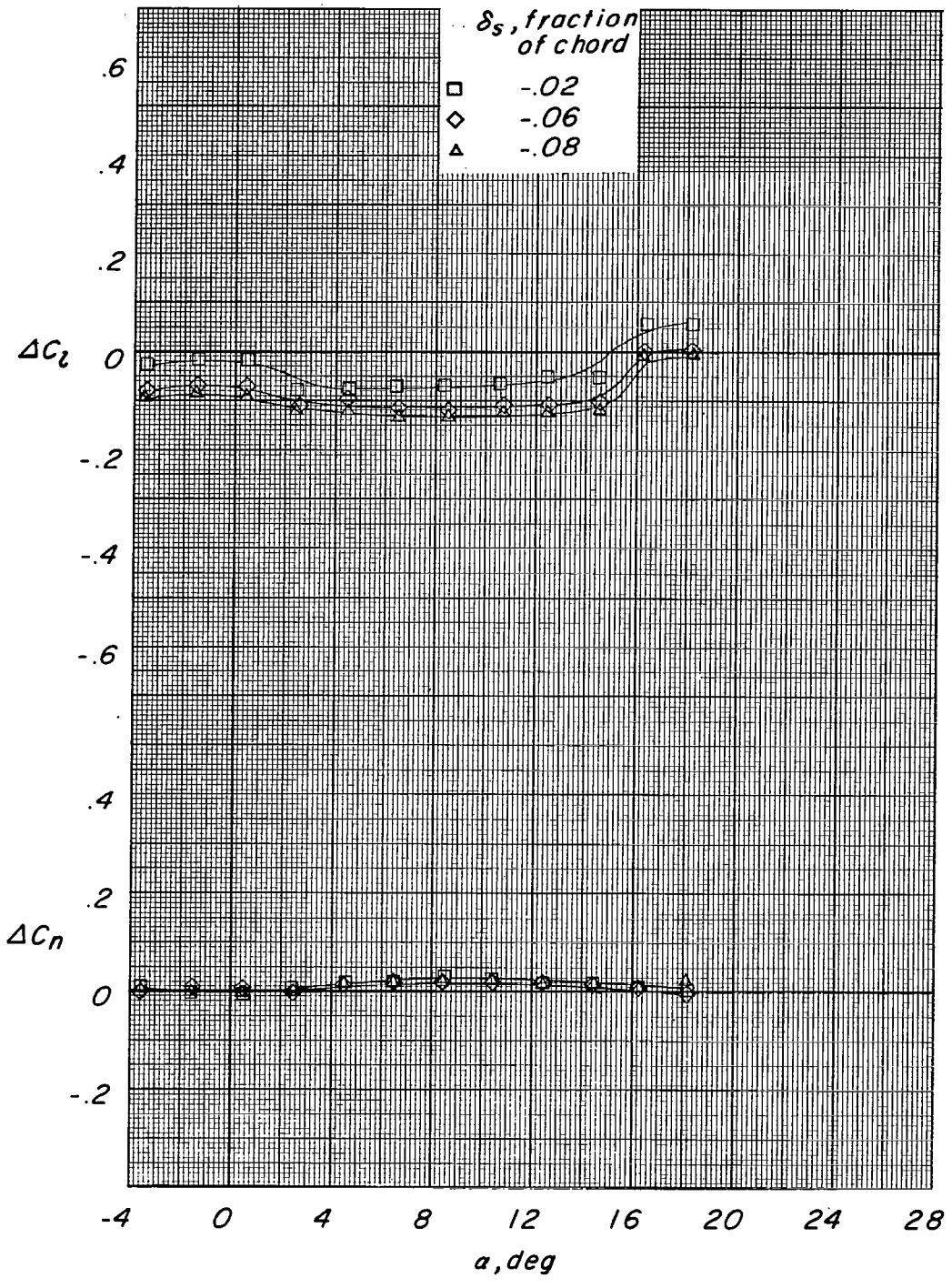

(a) Concluded.

Figure 23.- Continued.

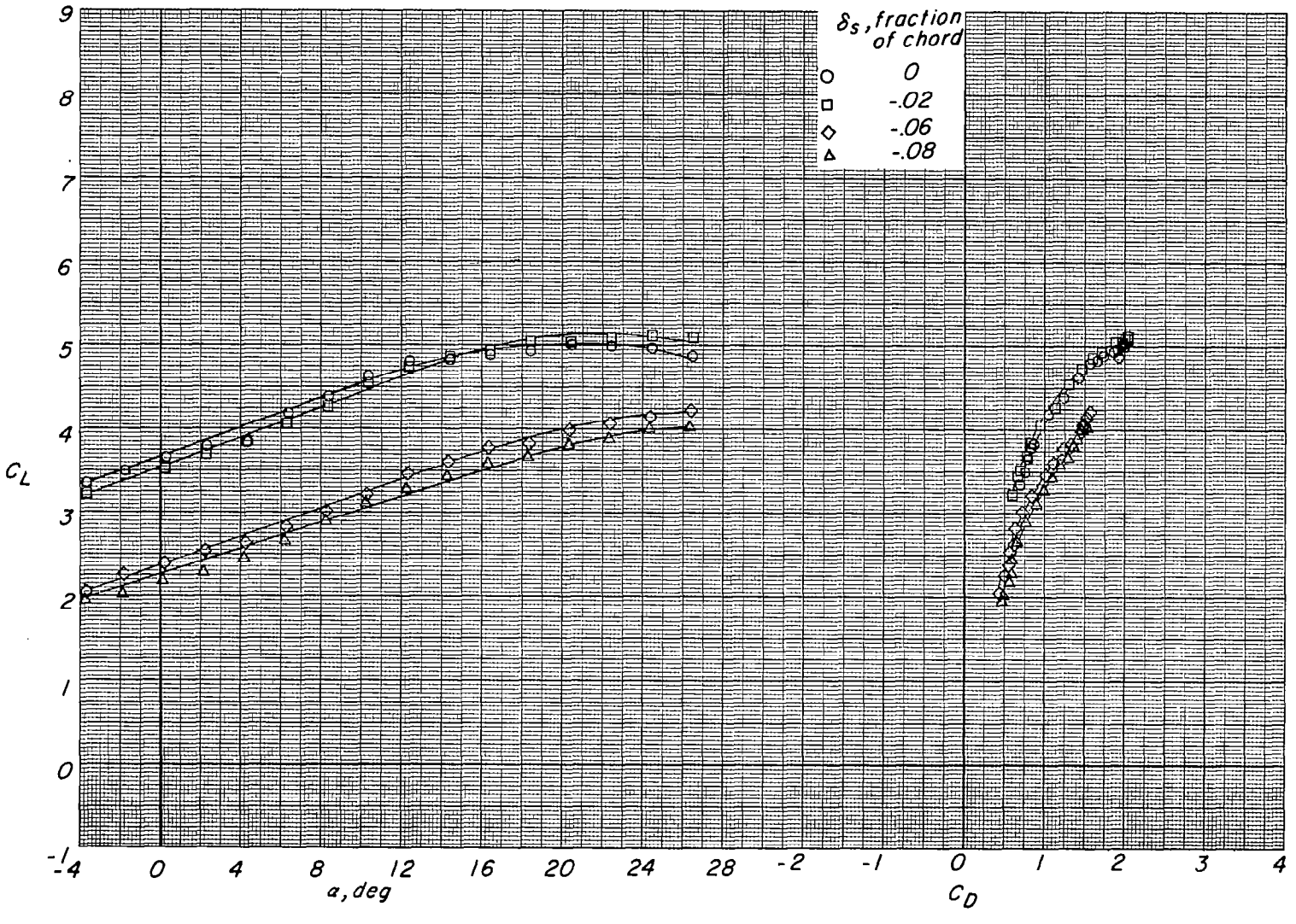

(b) $C_T \approx 1.3$.

Figure 23.- Continued.

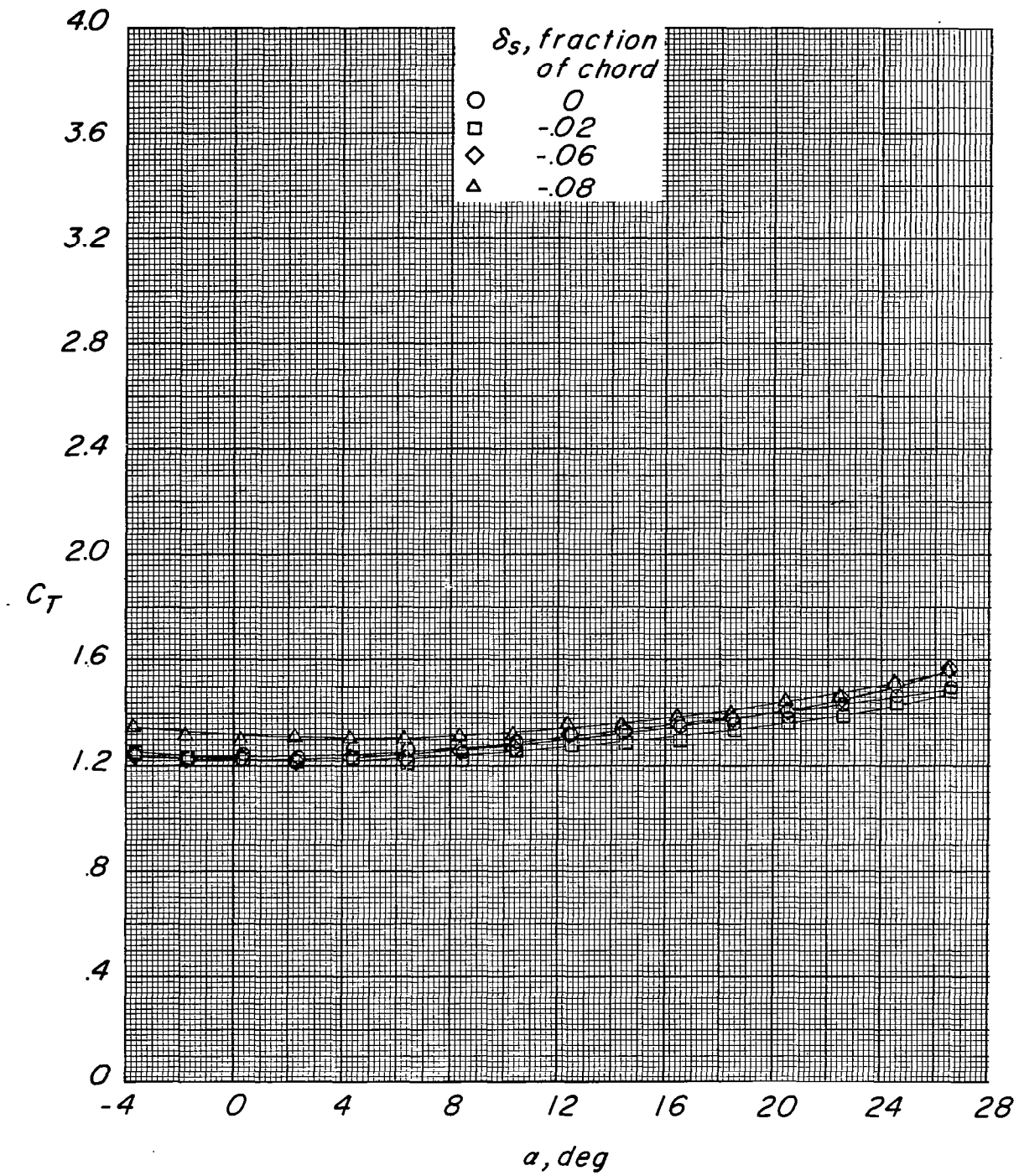

(b) Continued.

Figure 23.- Continued.

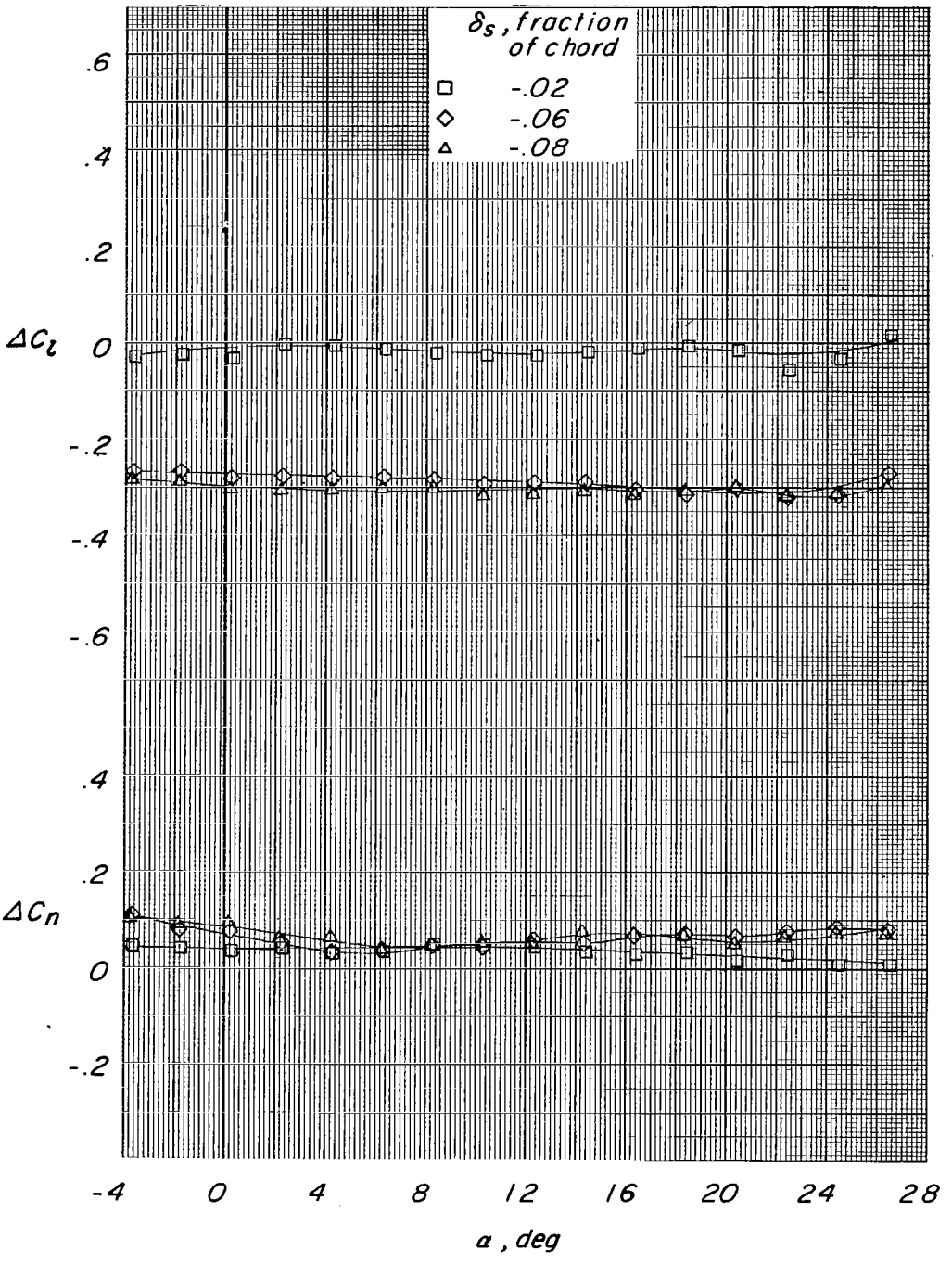

(b) Concluded.

Figure 23.- Continued.

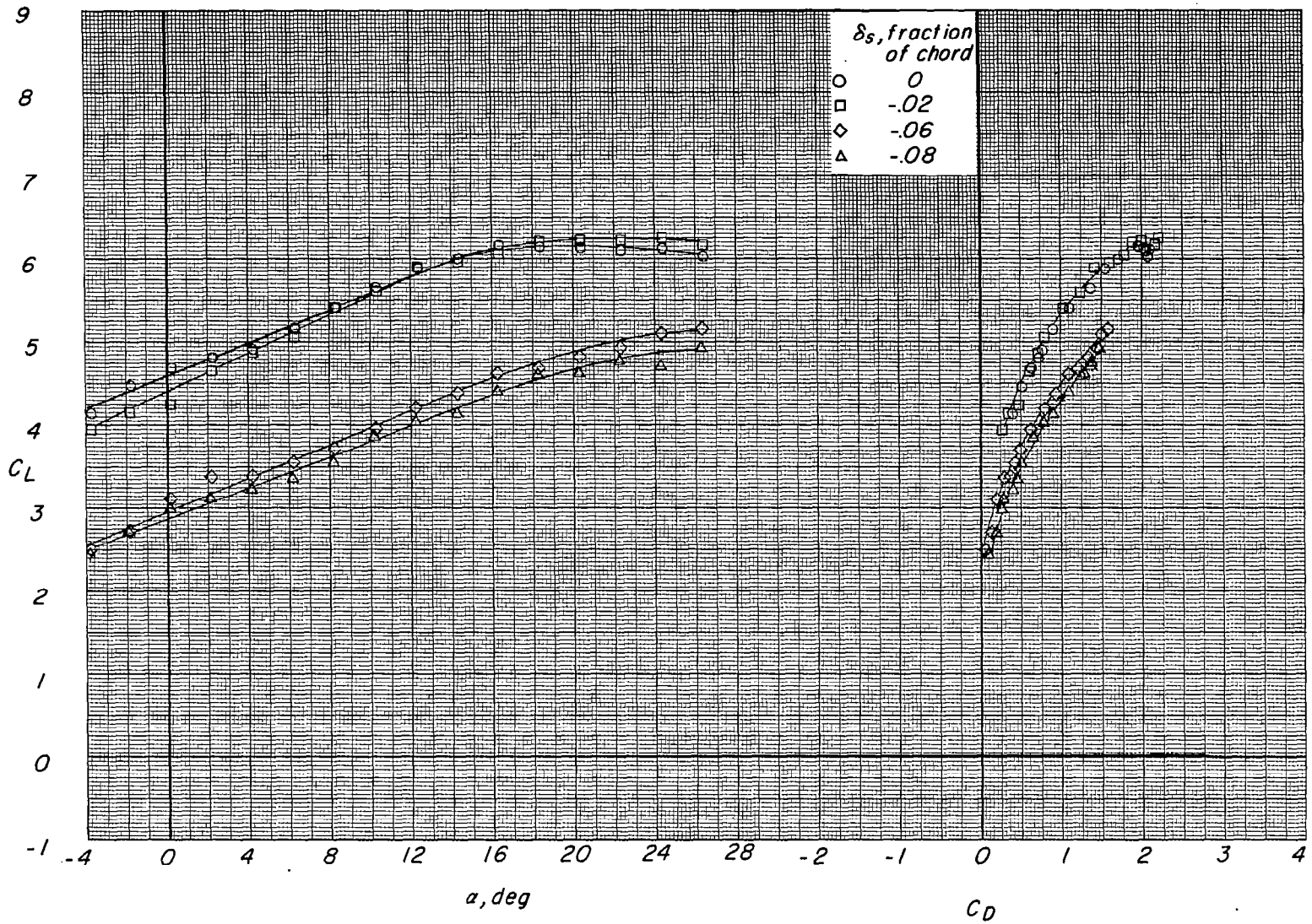

(c) $C_T \approx 2.2$.

Figure 23.- Continued.

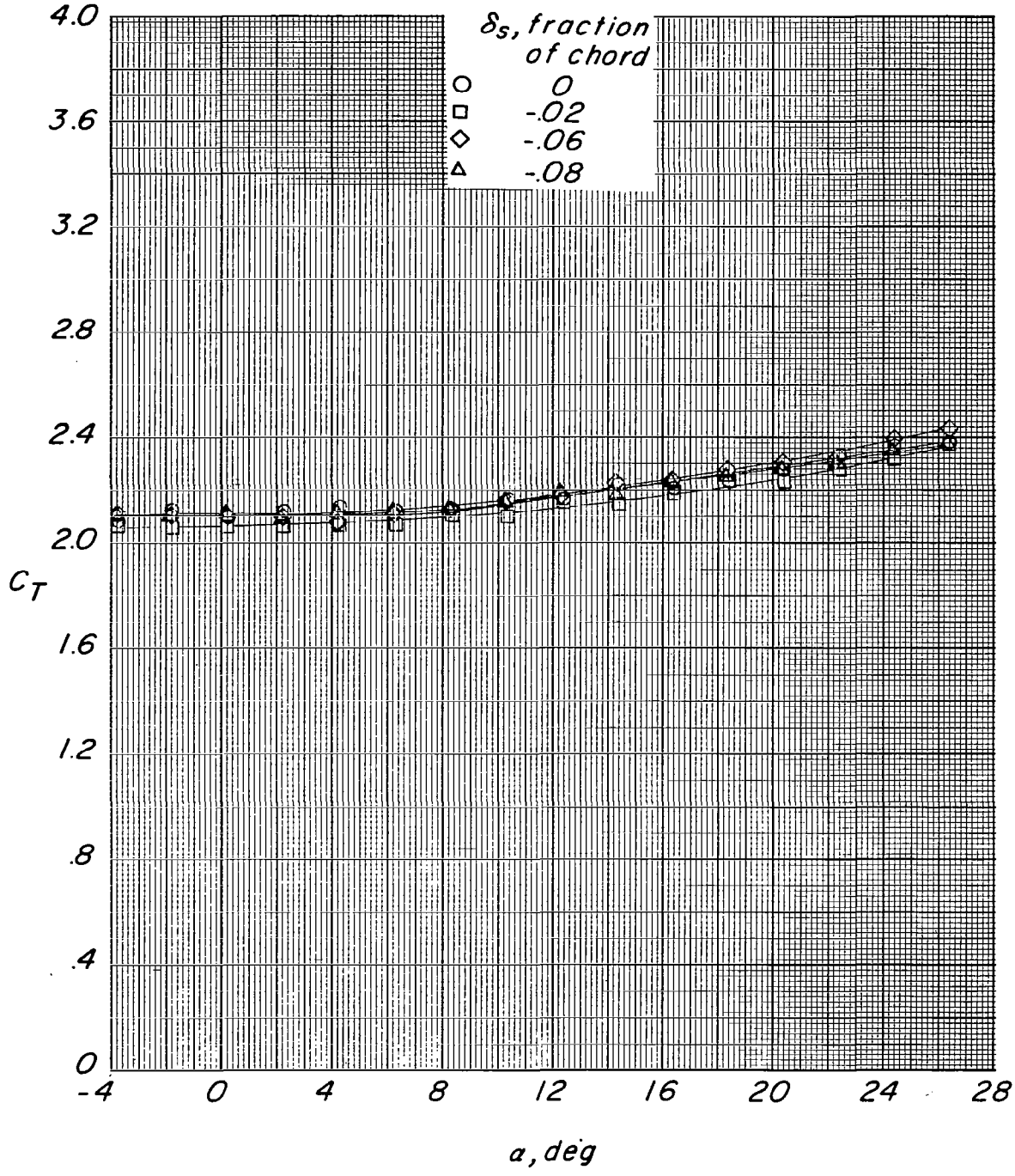

(c) Continued.

Figure 23.- Continued.

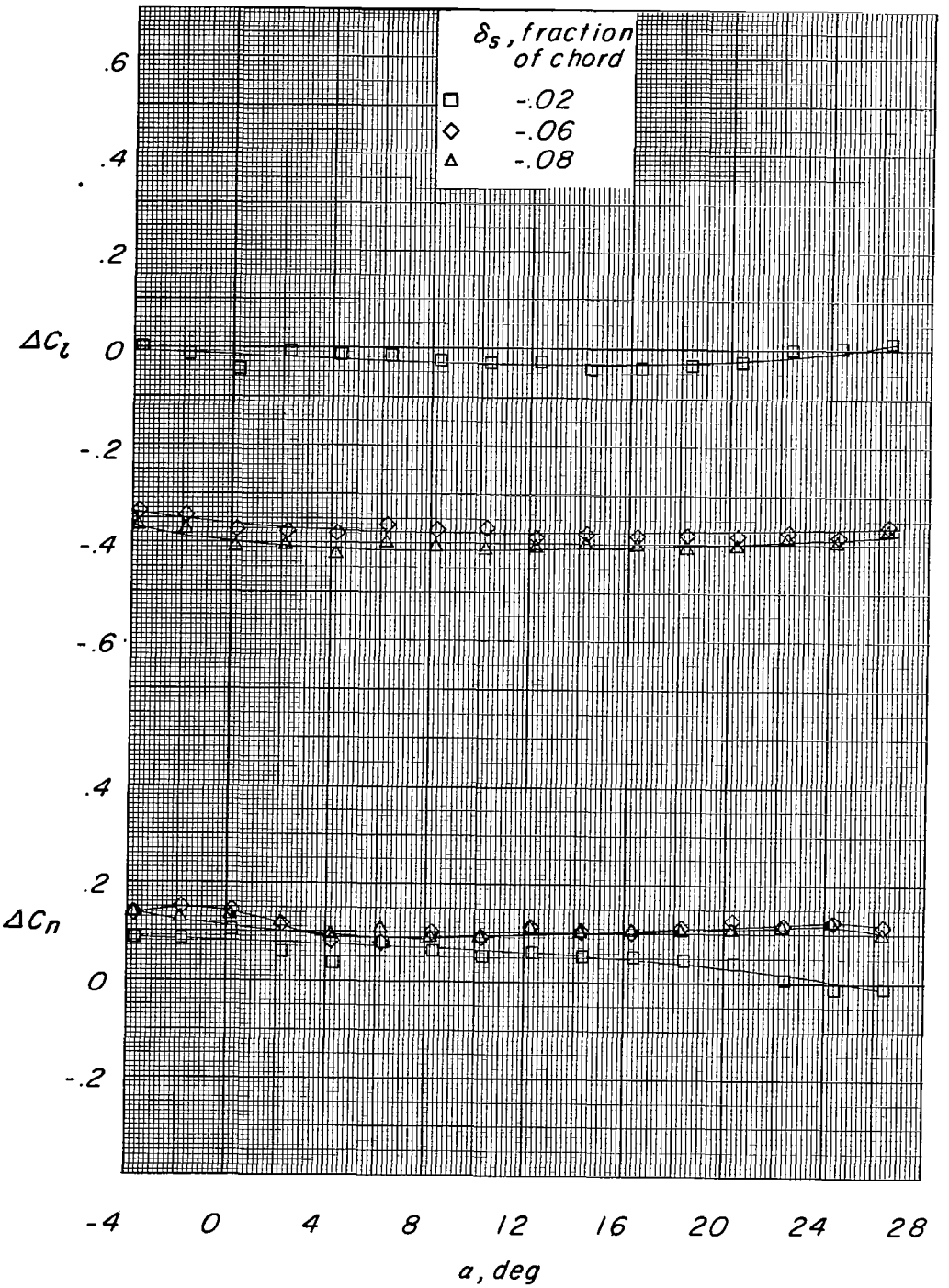

(c) Concluded.

Figure 23.- Continued.

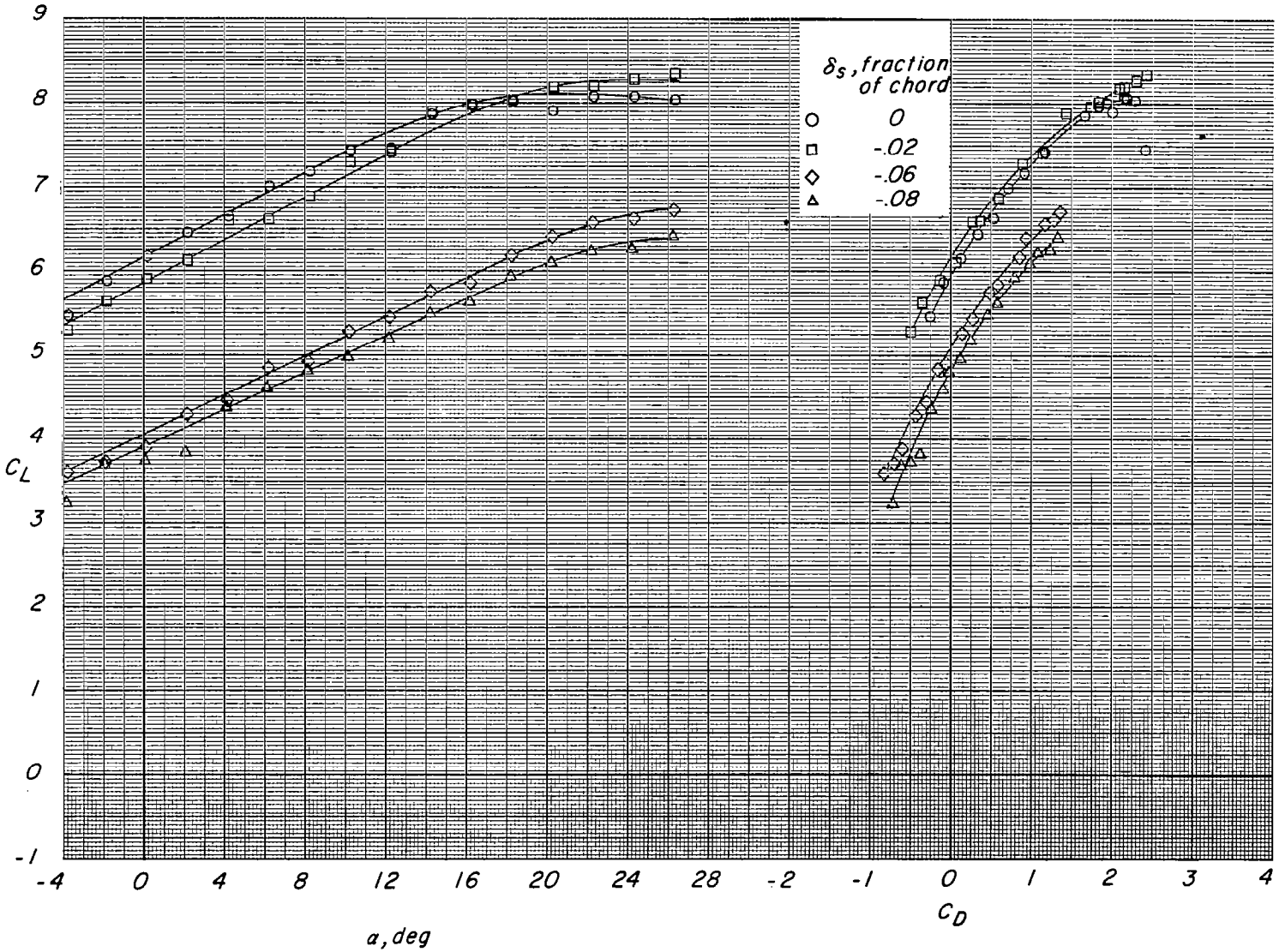

(d) $C_T \approx 3.8$.

Figure 23.- Continued.

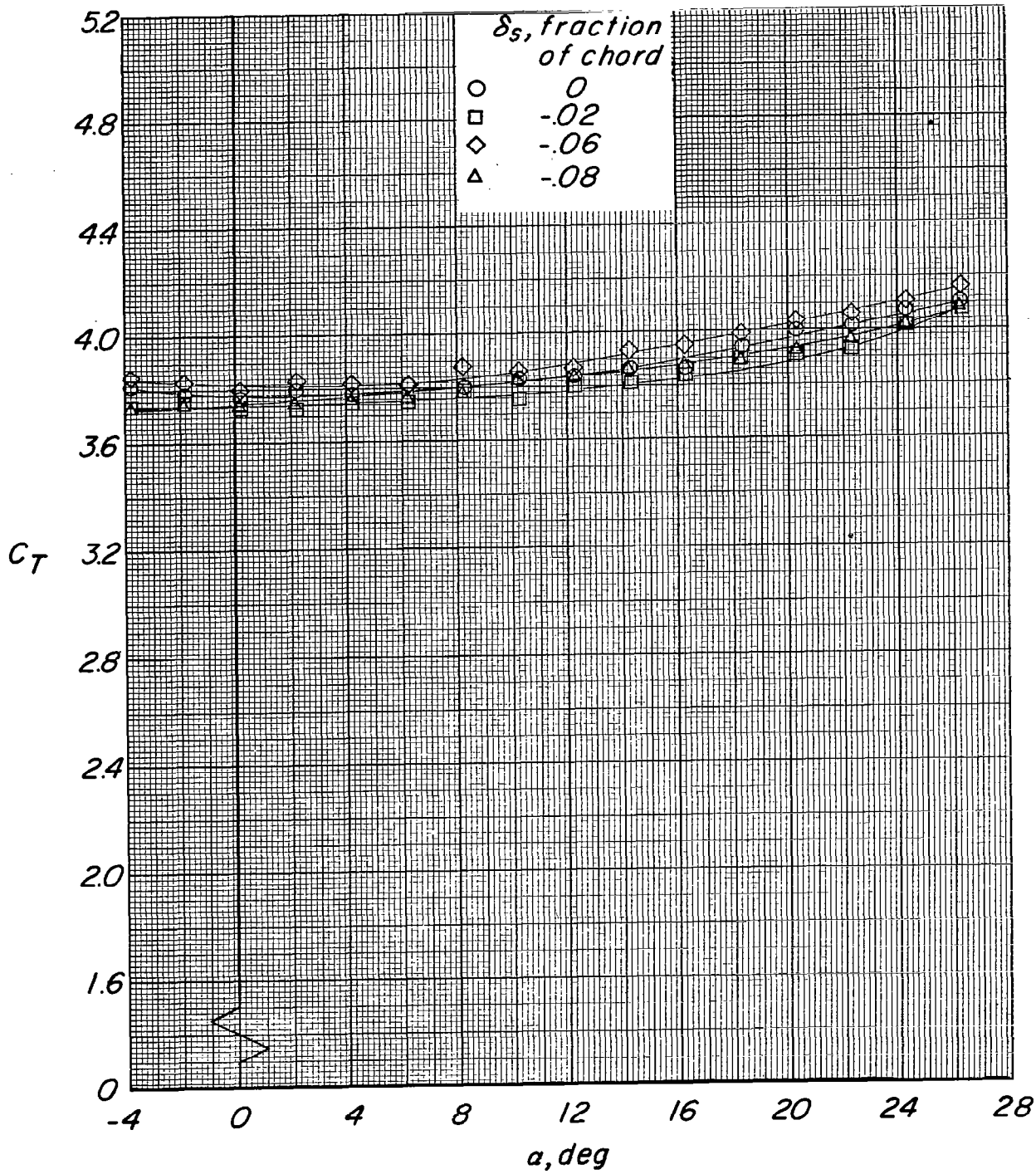

(d) Continued.

Figure 23.- Continued.

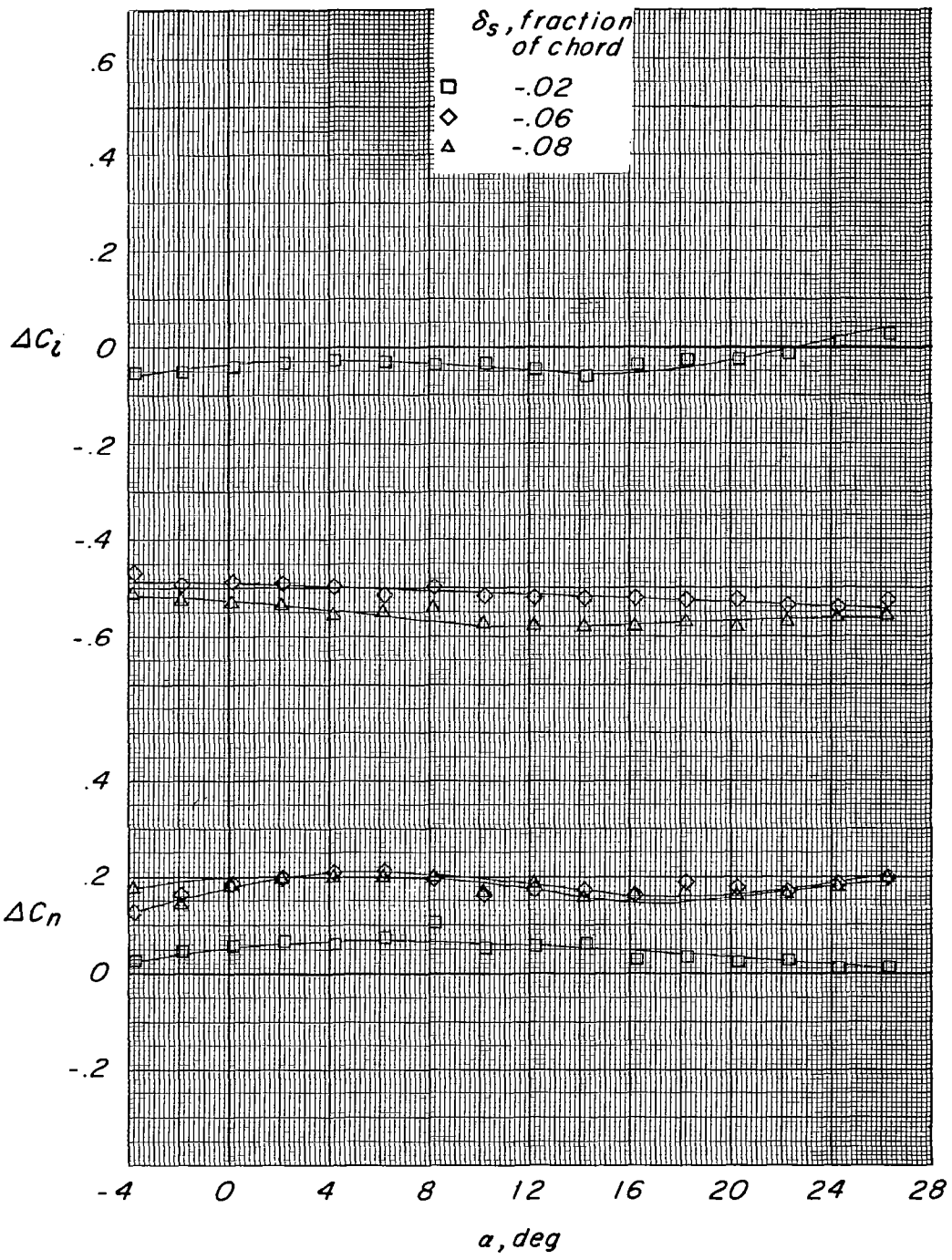

(d) Concluded.

Figure 23.- Concluded.

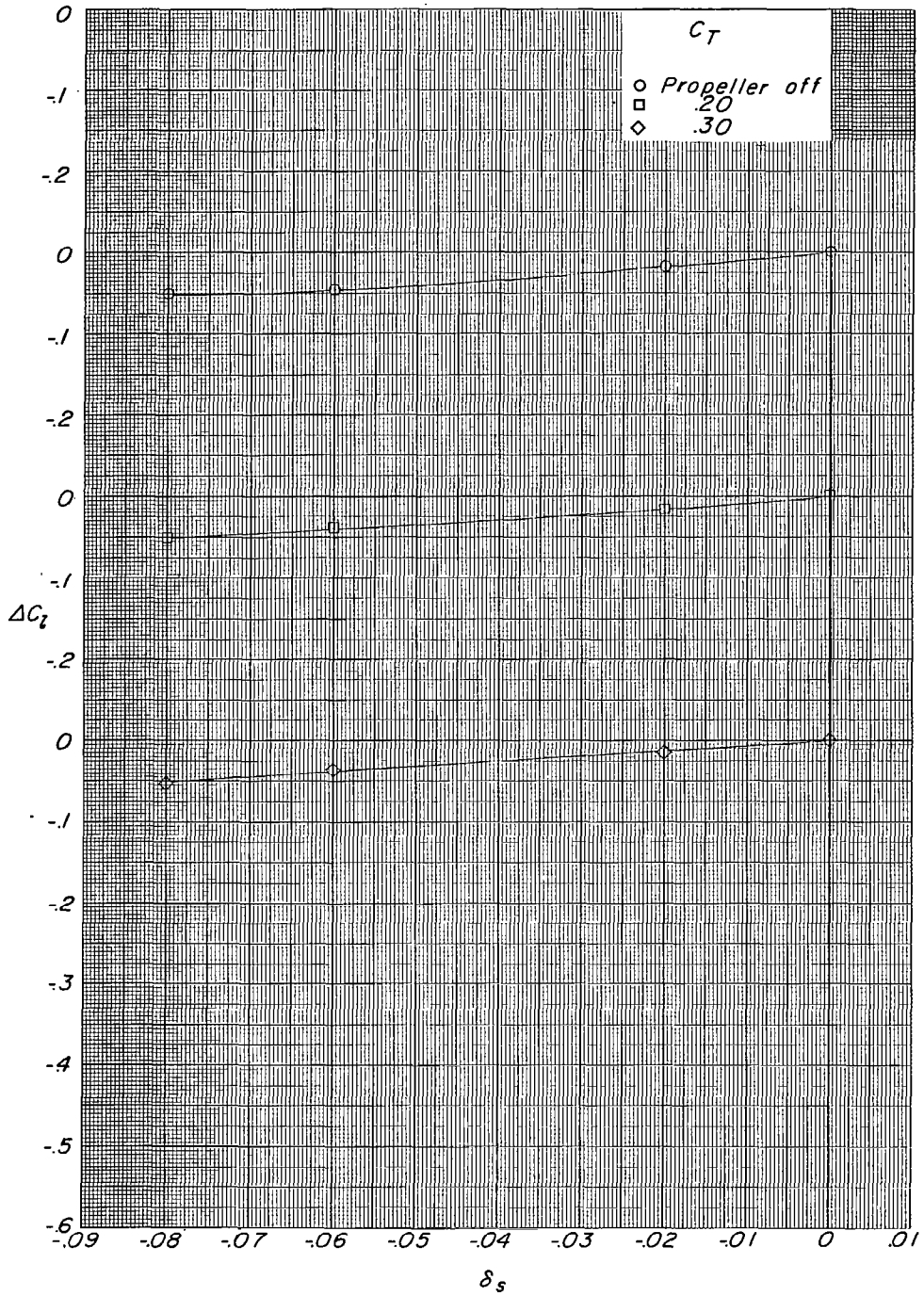

(a) Rolling-moment coefficient.

Figure 24.- Summary of lateral-directional moments due to spoiler projection for configuration A (long span, $\delta_f = 0^\circ$) at several thrust coefficients.

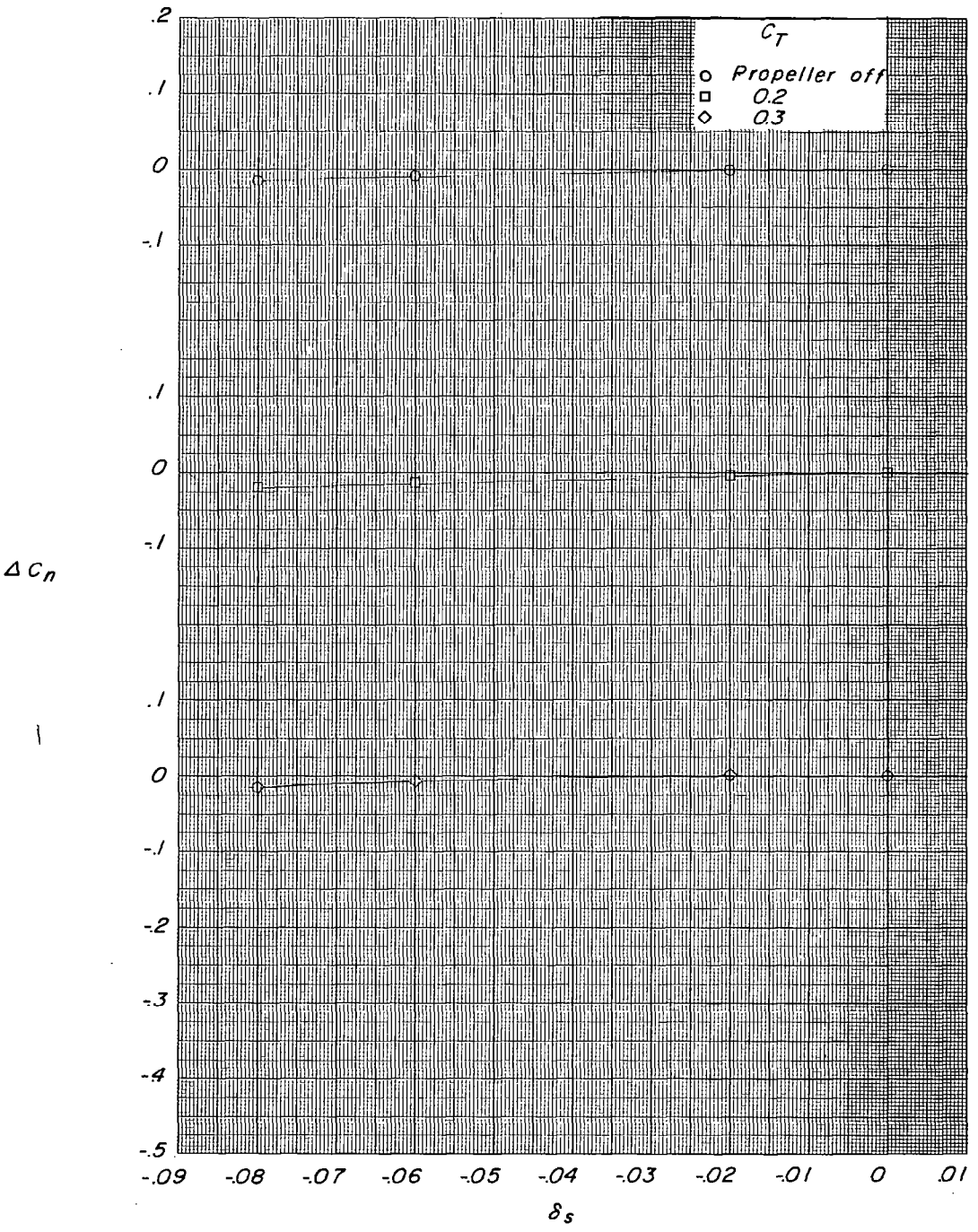

(b) Yawing-moment coefficient.

Figure 24.- Concluded.

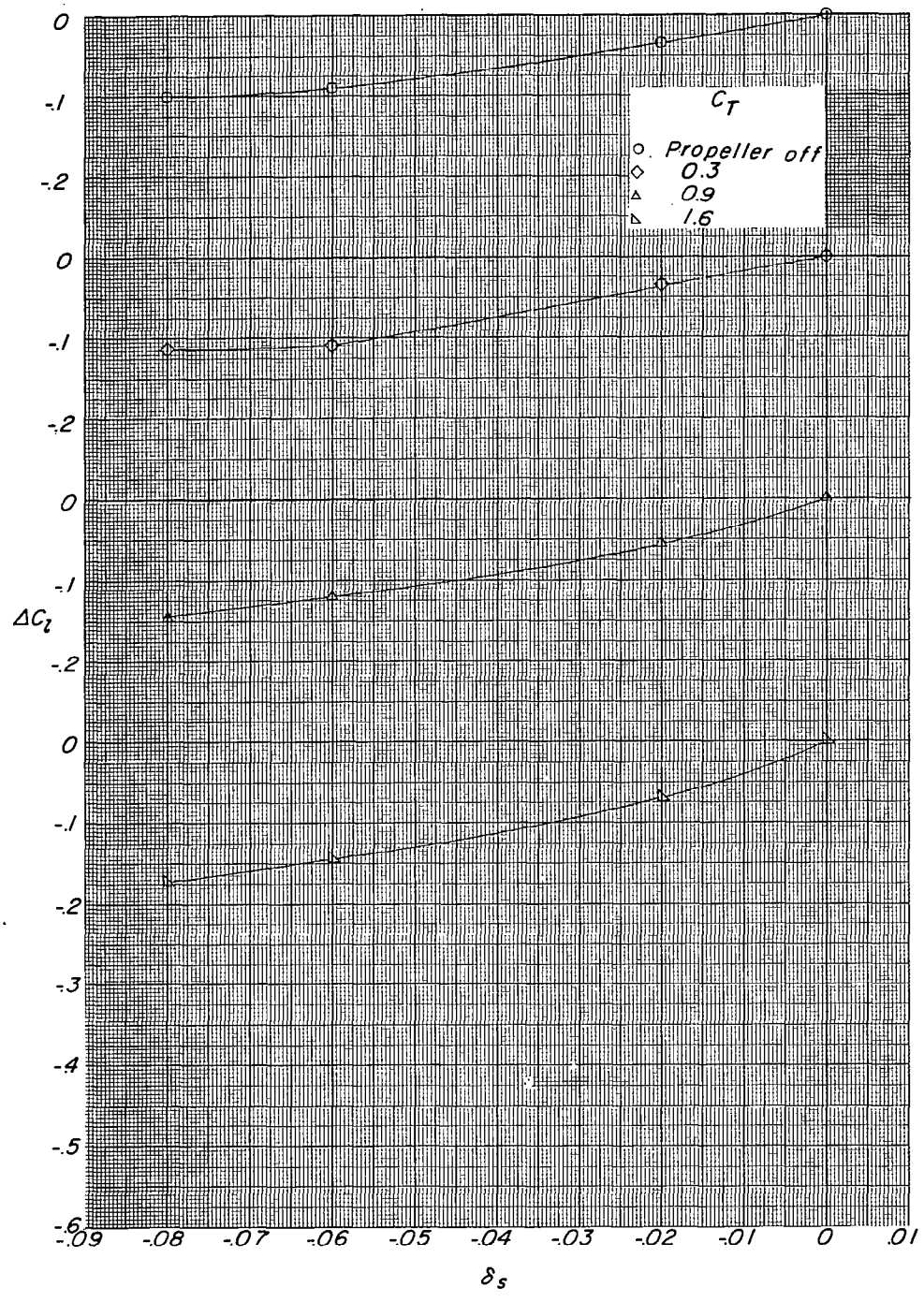

(a) Rolling-moment coefficient.

Figure 25.- Summary of lateral-directional moments due to spoiler projection for configuration B (long span, $\delta_f \approx 32.5^\circ$).

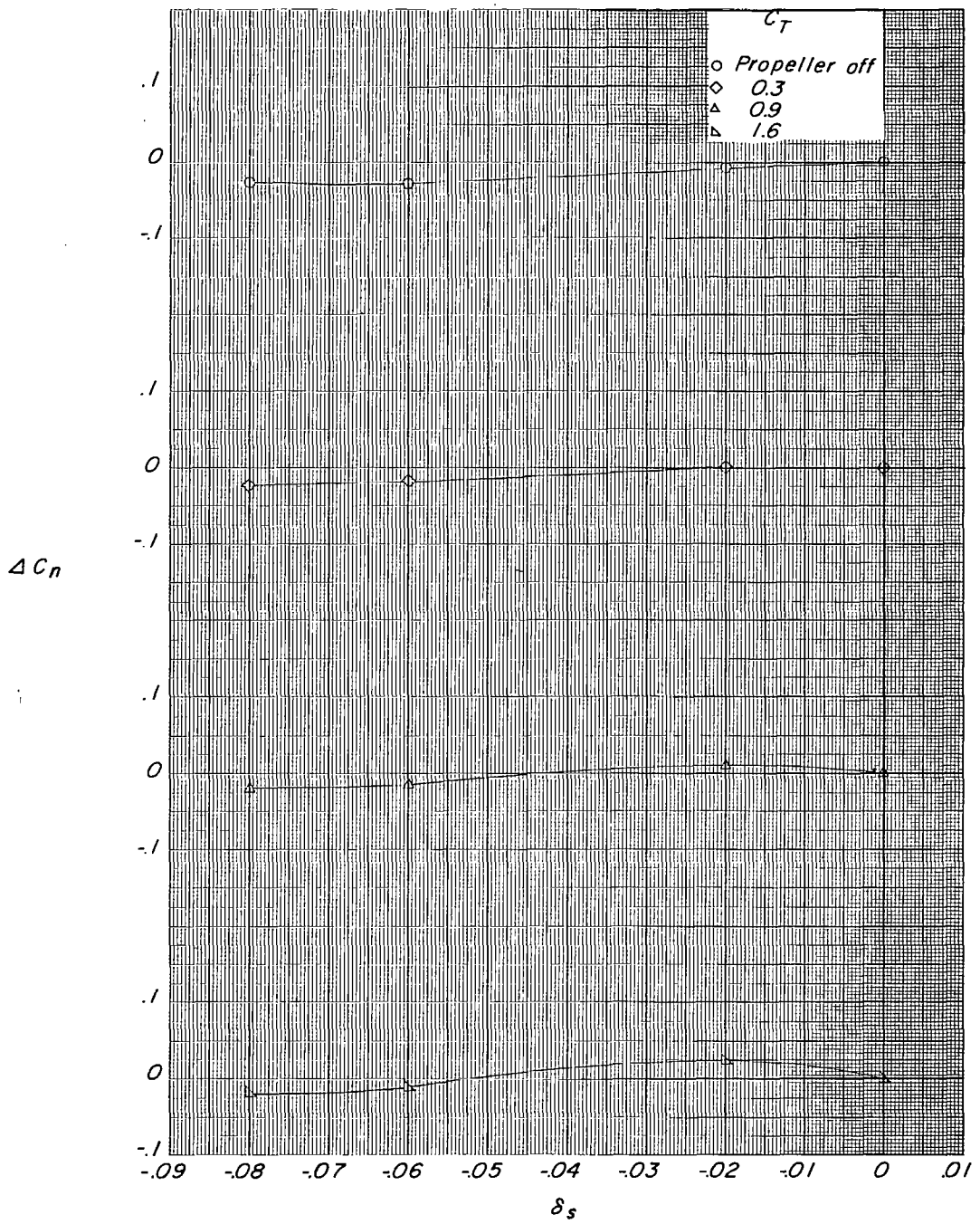

(b) Yawing-moment coefficient.

Figure 25.- Concluded.

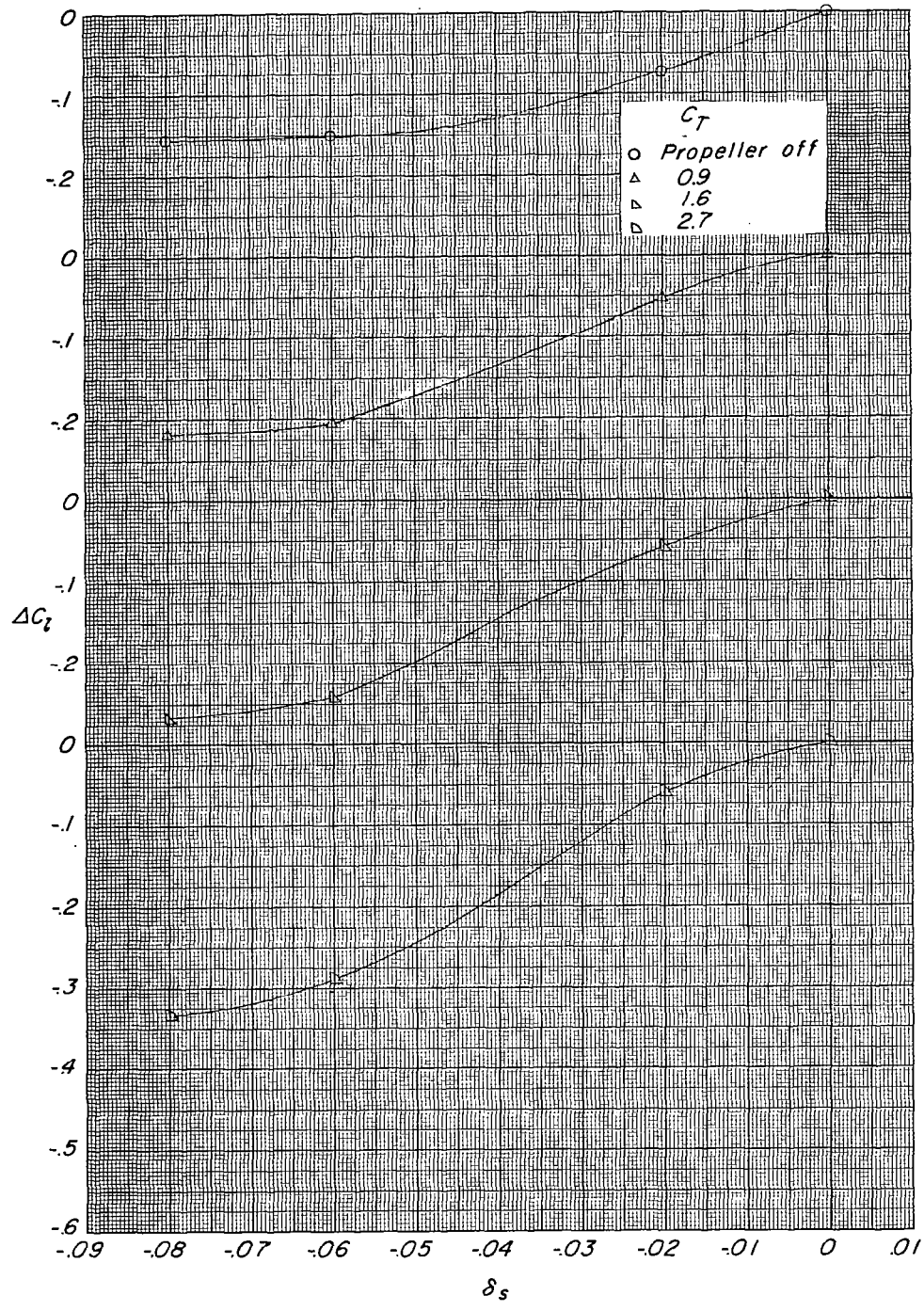

(a) Rolling-moment coefficient.

Figure 26.- Summary of lateral-directional moments due to spoiler projection for configuration C (long span, $\delta_f = 45°$).

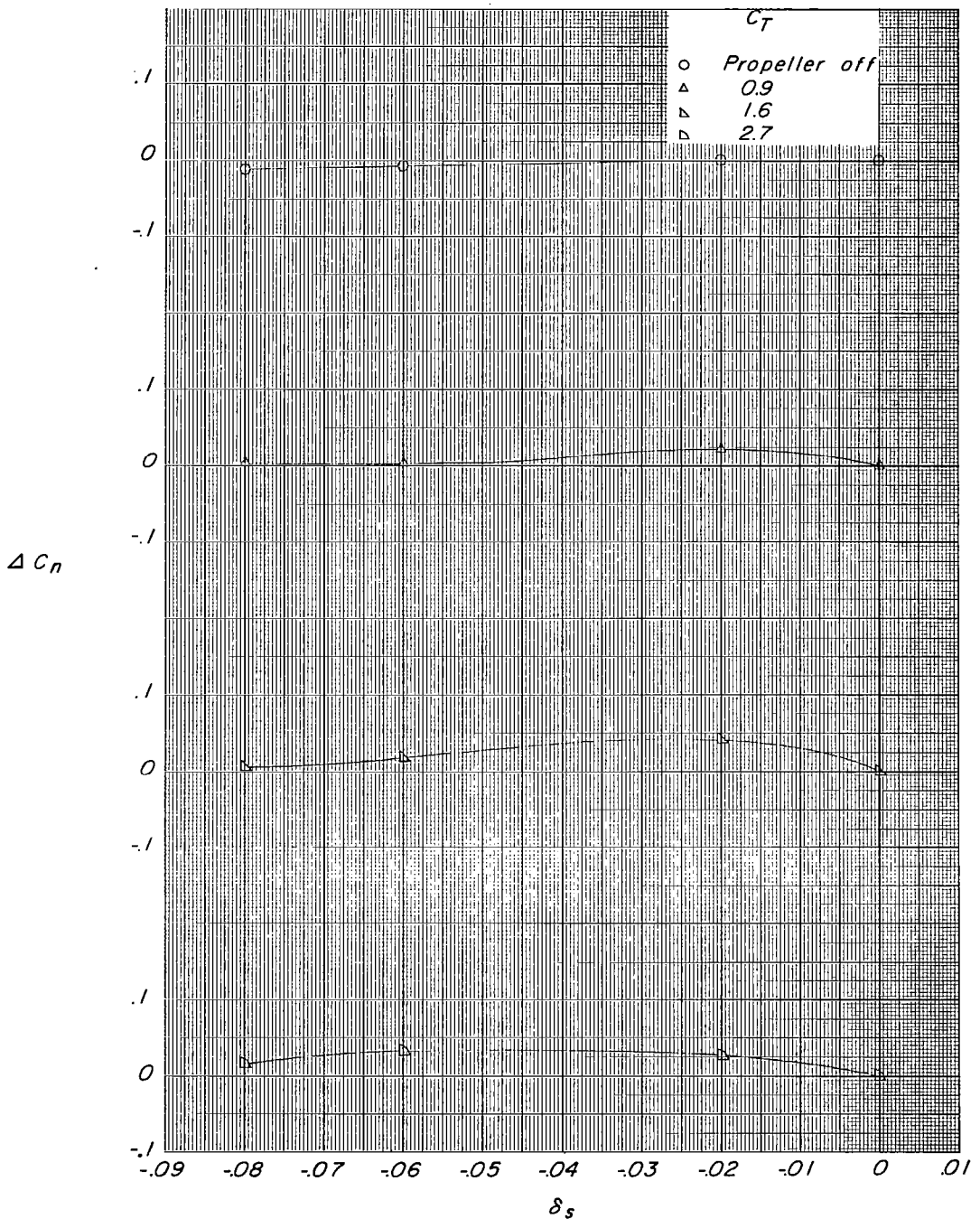

(b) Yawing-moment coefficient.

Figure 26.- Concluded.

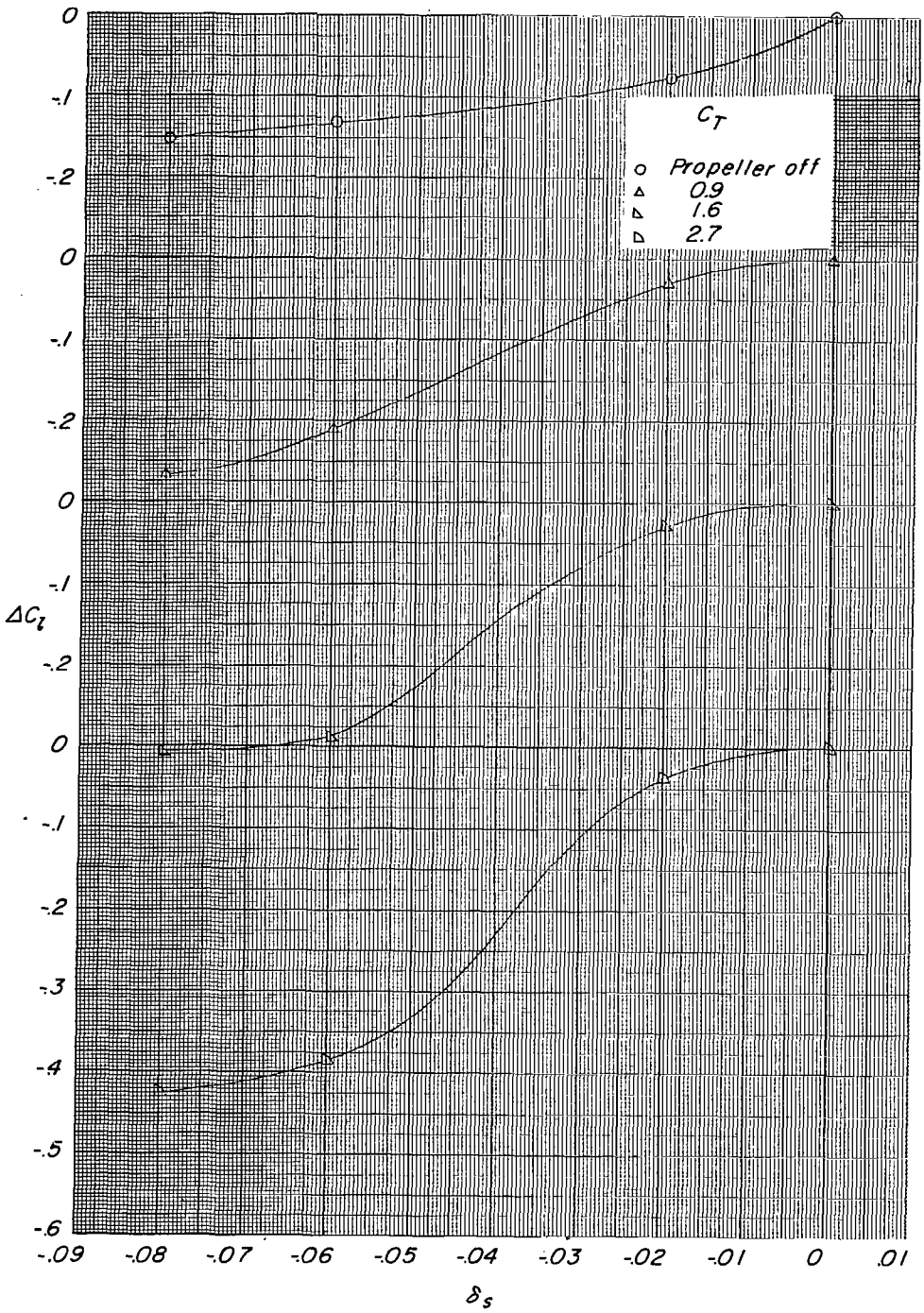

(a) Rolling-moment coefficient.

Figure 27.- Summary of lateral-directional moments due to spoiler projection for configuration D (long span, $\delta_f = 75^\circ$).

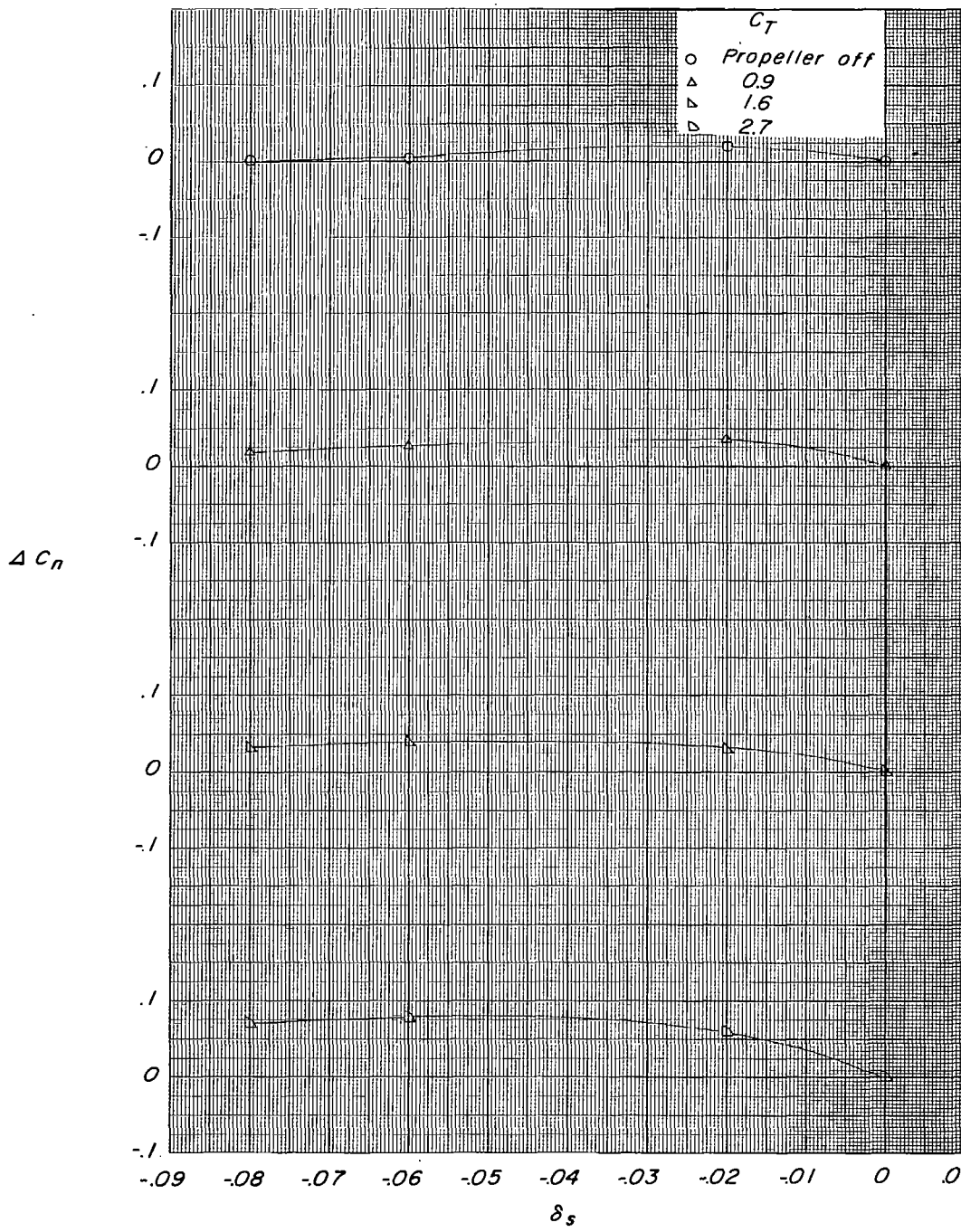

(b) Yawing-moment coefficient.

Figure 27.- Concluded.

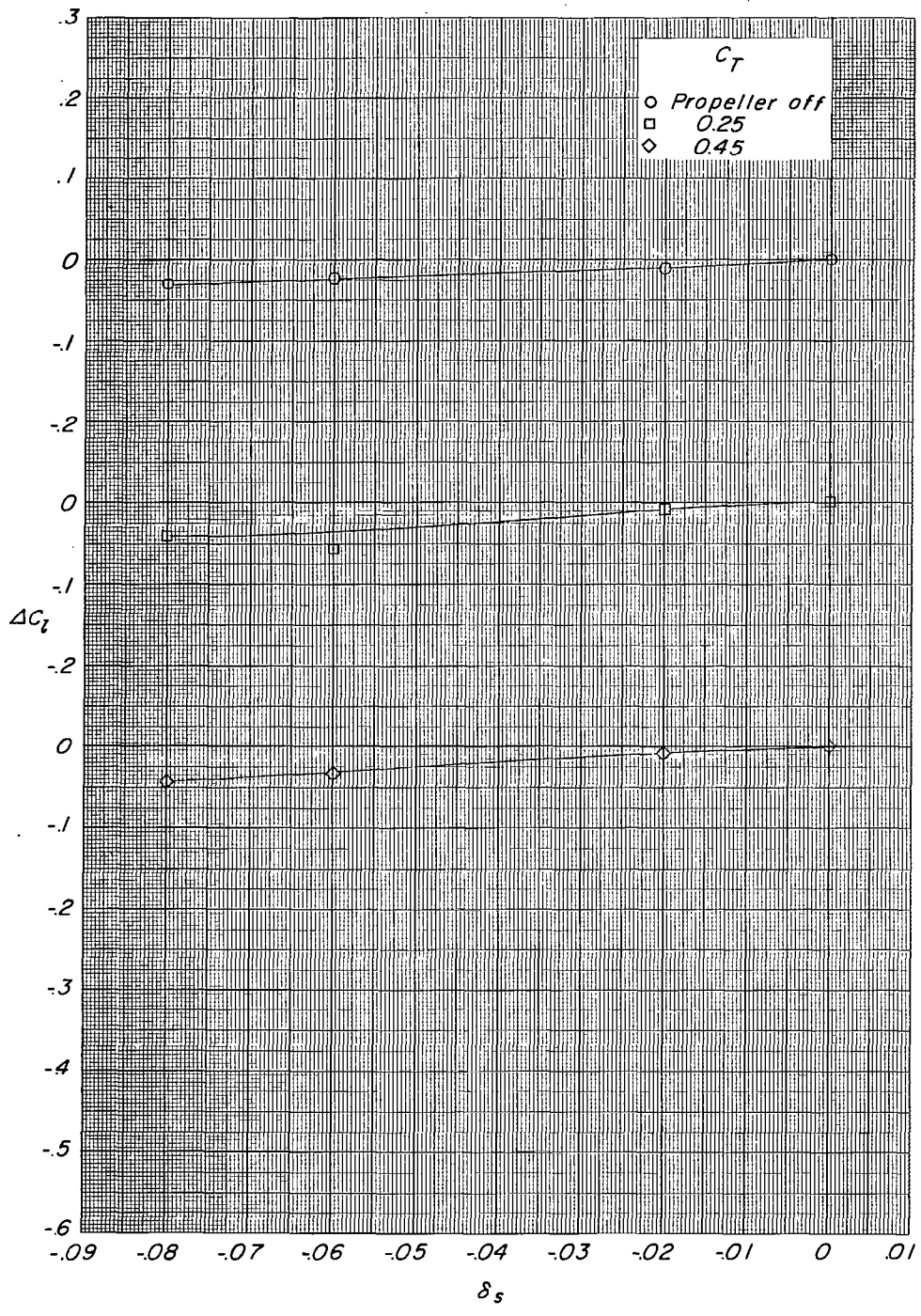

(a) Rolling-moment coefficient.

Figure 28.- Summary of lateral-directional moments due to spoiler projection for configuration E (short span, $\delta_f = 0^o$).

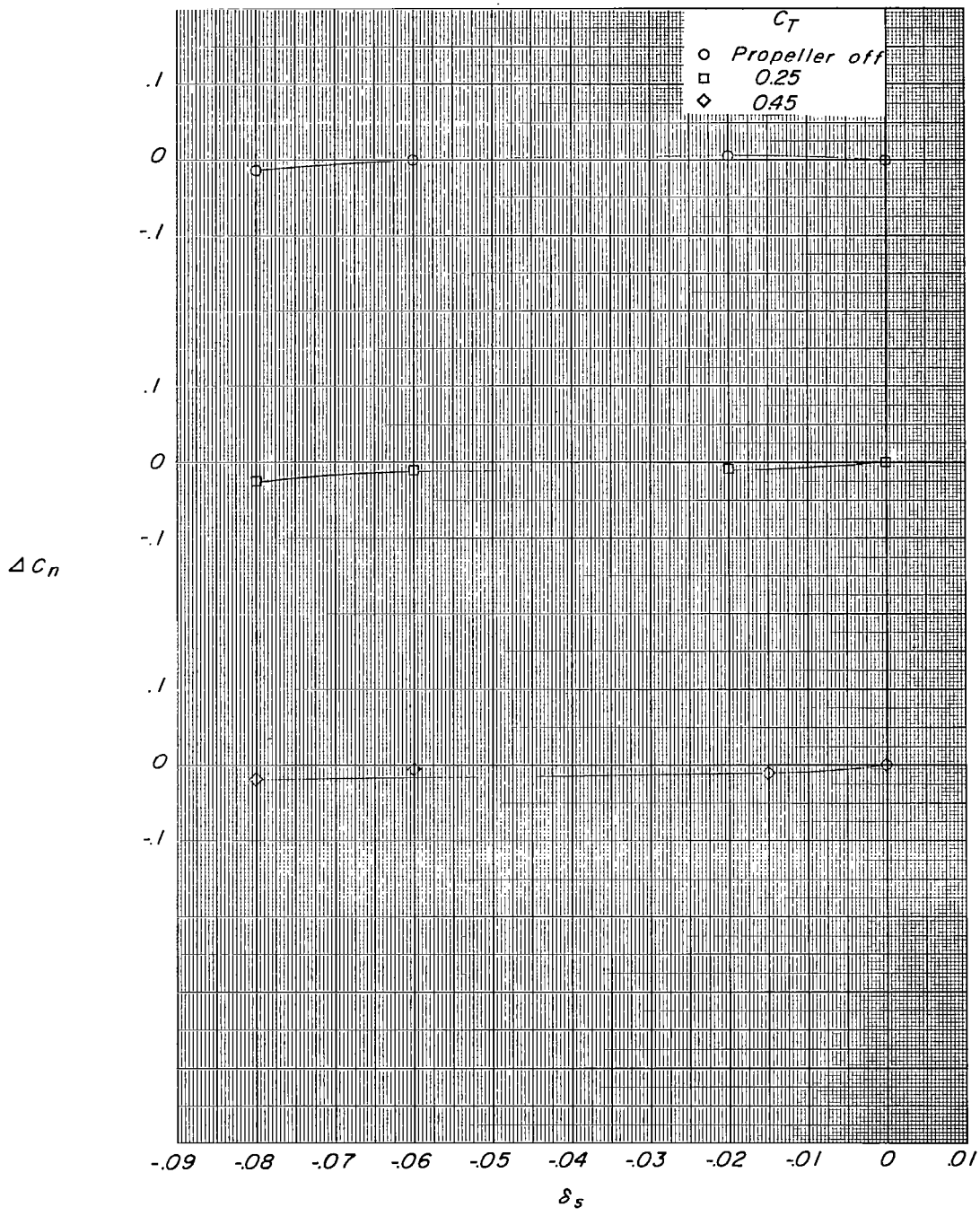

(b) Yawing-moment coefficient.

Figure 28.- Concluded.

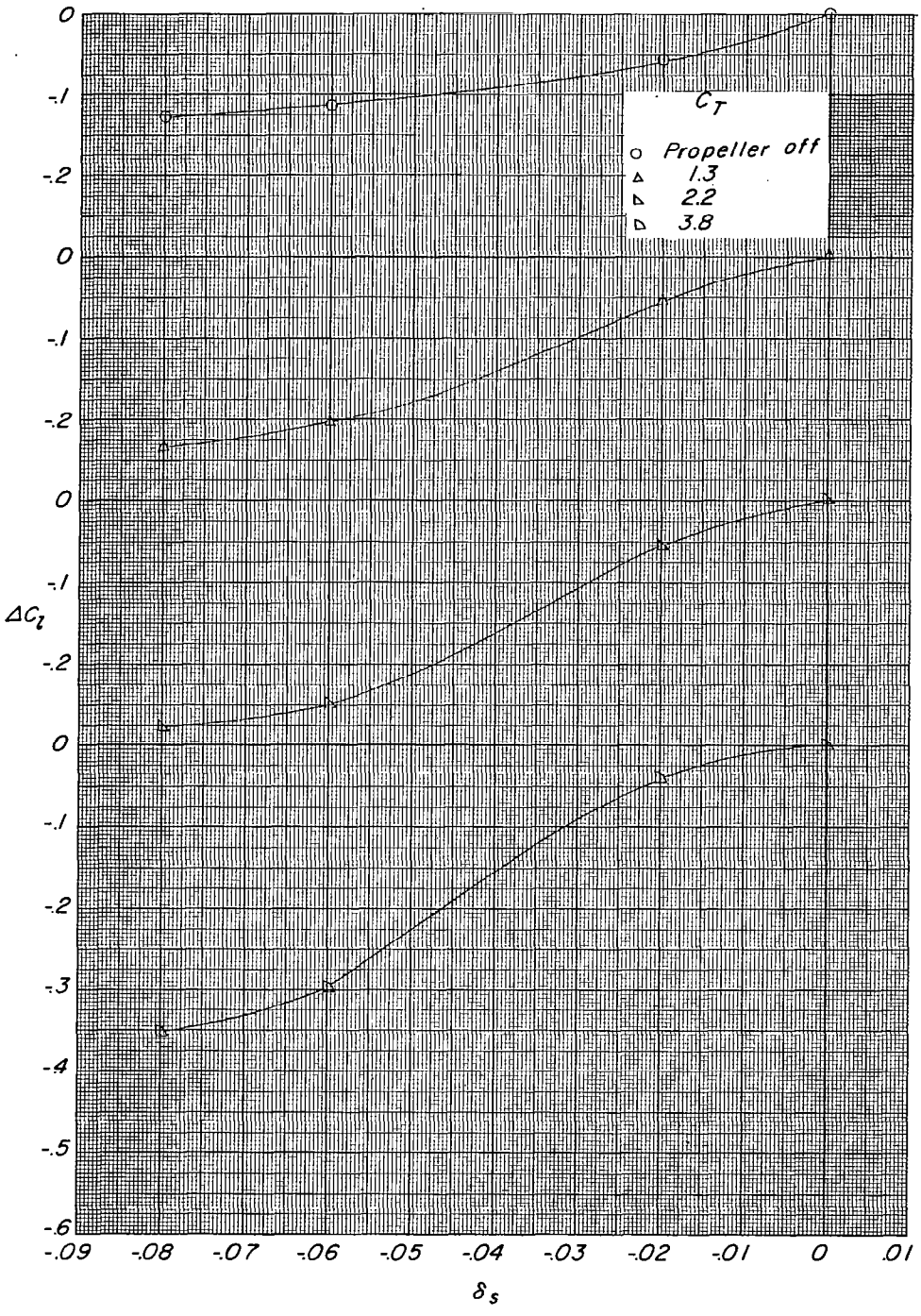

(a) Rolling-moment coefficient.

Figure 29.- Summary of lateral-directional moments due to spoiler projection for configuration F (short span, $\delta_f = 45^\circ$).

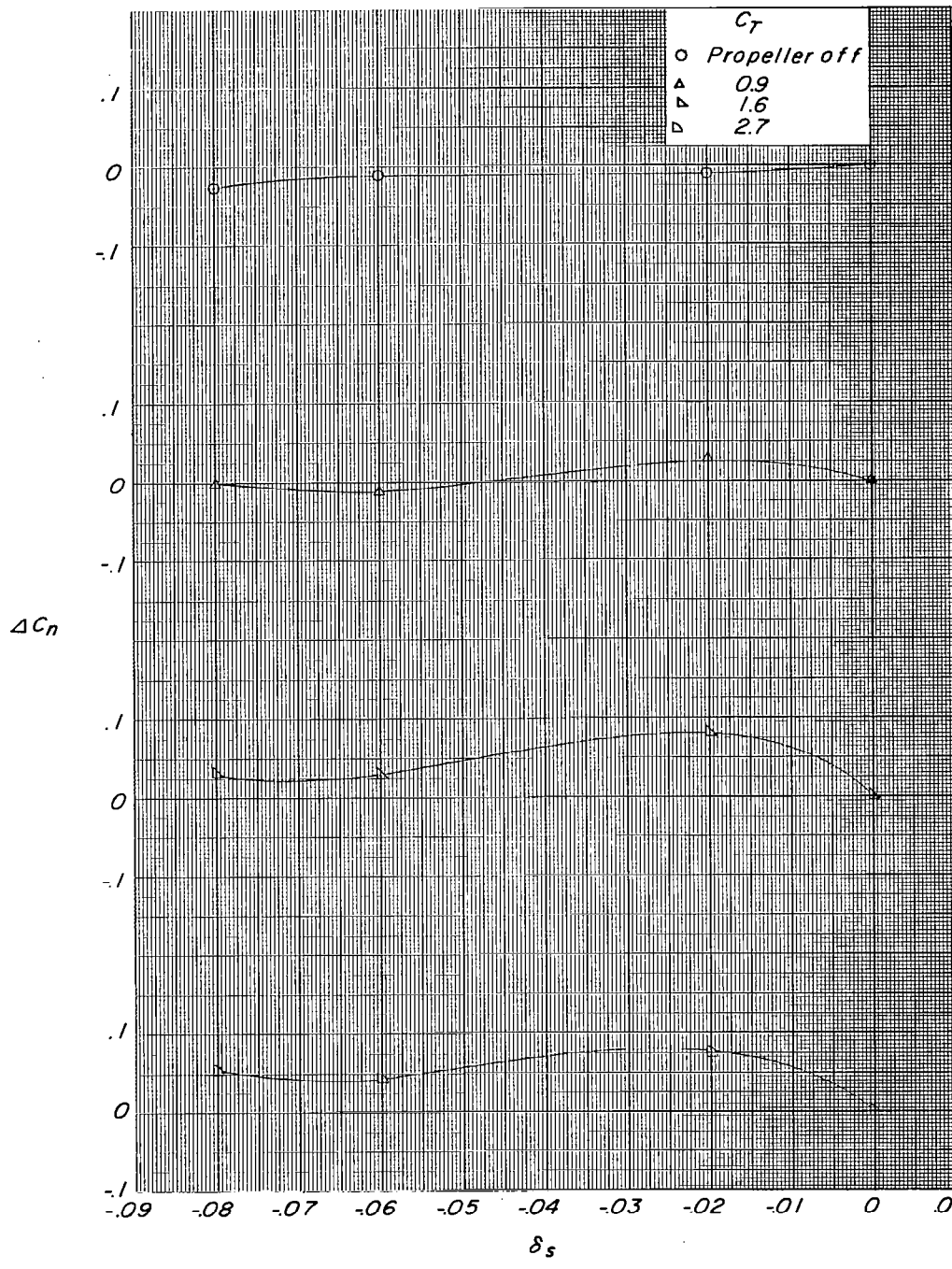

(b) Yawing-moment coefficient.

Figure 29.- Concluded.

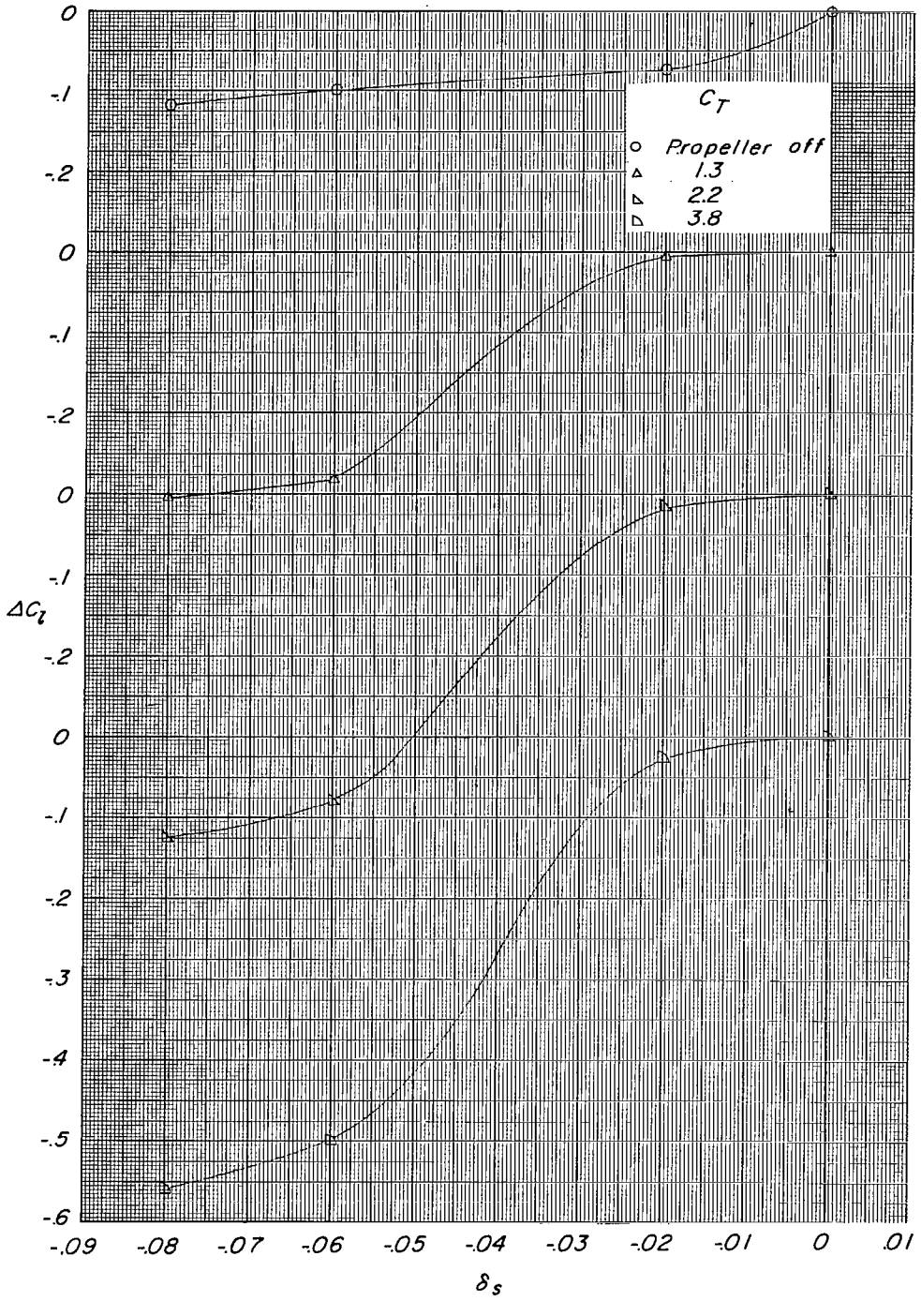

(a) Rolling-moment coefficient.

Figure 30.- Summary of lateral-directional moments due to spoiler projection for configuration G (short span, $\delta_f = 75^\circ$).

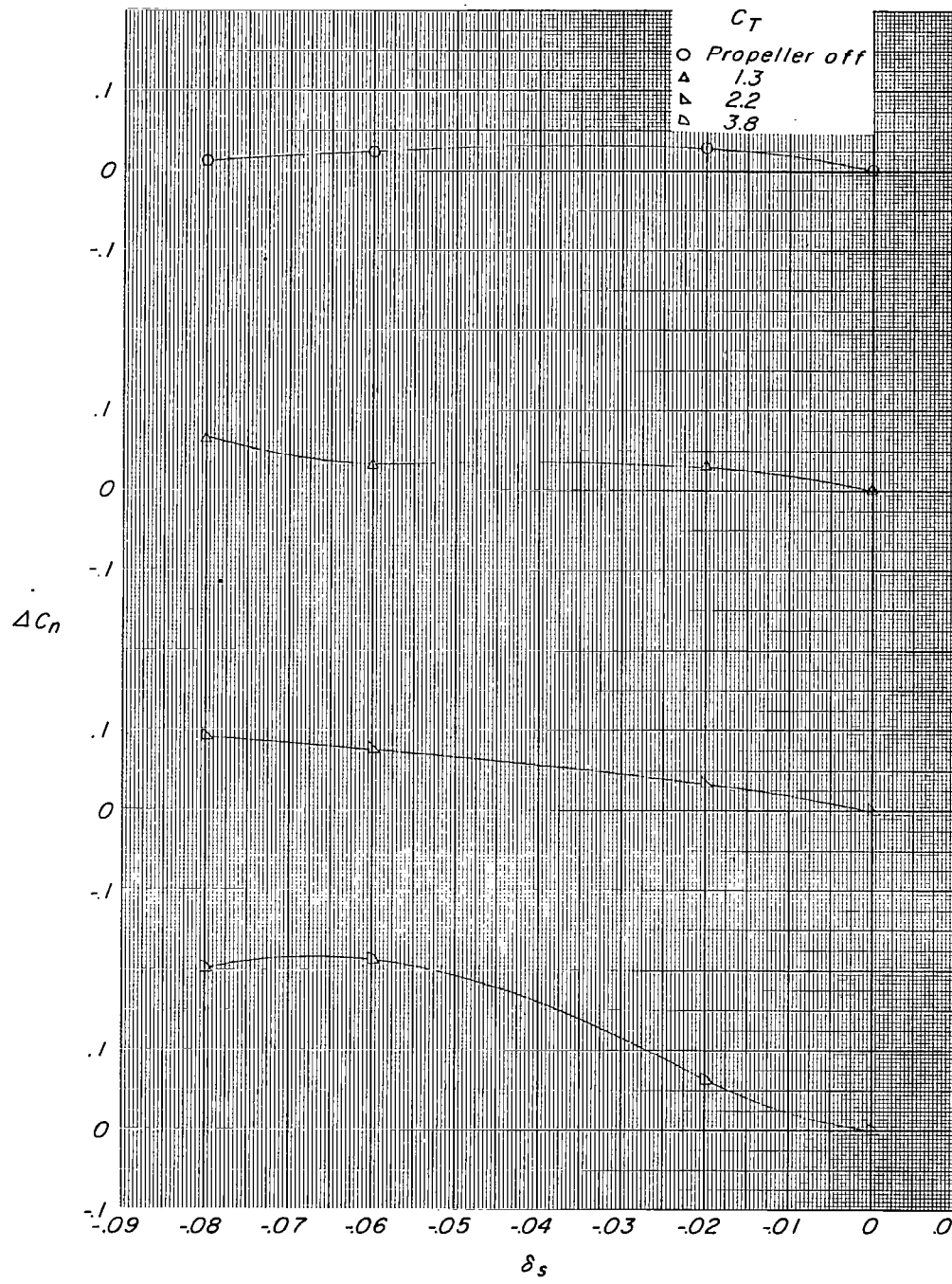

(b) Yawing-moment coefficient.

Figure 30.- Concluded.

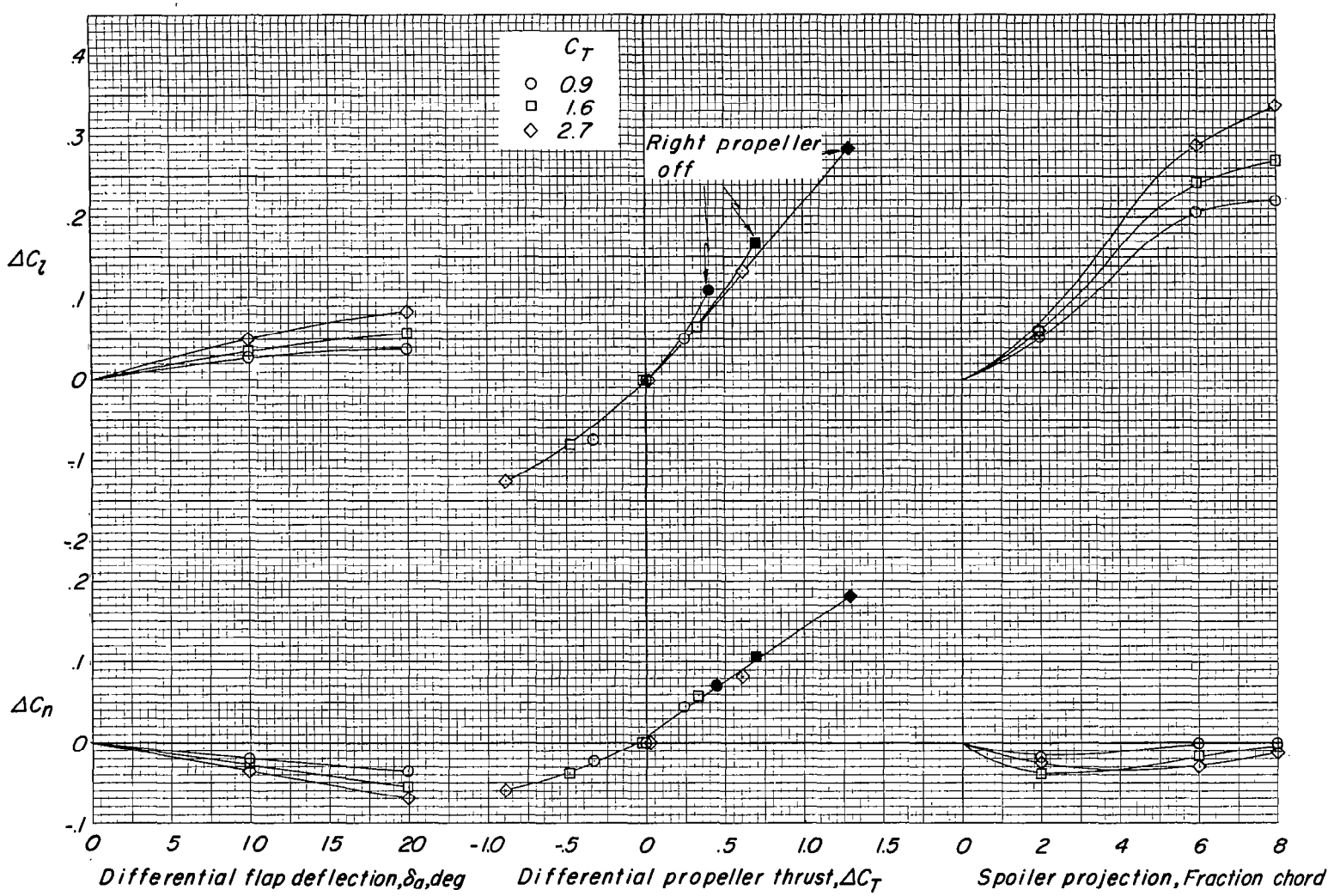

(a) Configuration C: $\delta_f = 45°$; long span; $\alpha = 4°$.

Figure 31.- Summary of the effect of the tests of control devices.

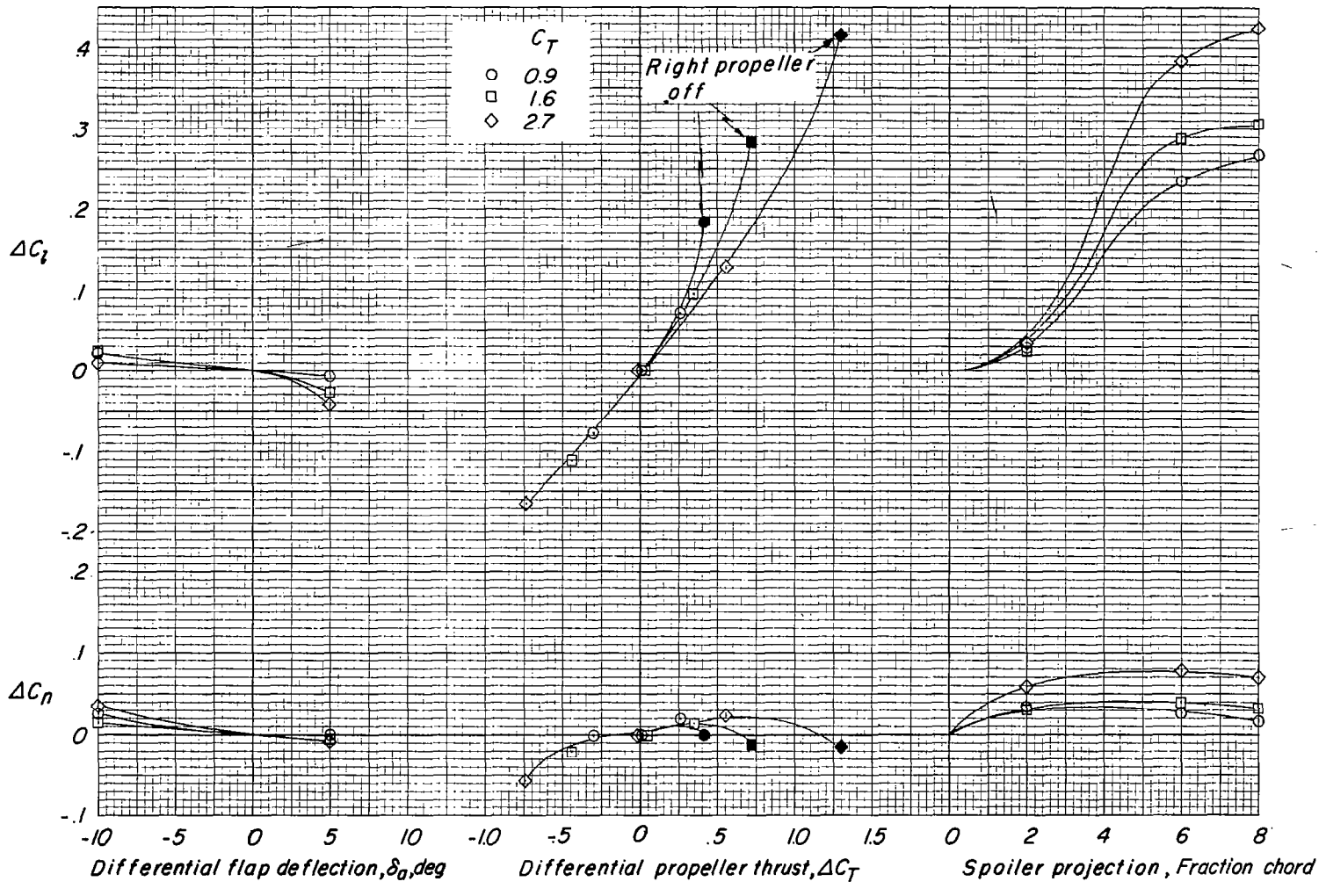

(b) Configuration D: $\delta_F = 75^\circ$; long span; $\alpha = 4^\circ$.

Figure 31.- Concluded.